

PREDICTIONS OF TURBULENT BOUNDARY-LAYER DEVELOPMENTS  
USING A TWO-EQUATION MODEL OF TURBULENCE

by

Kam Hong Ng M.Sc., B.Sc.(Eng.), D.I.C.

Thesis submitted for the degree of  
Doctor of Philosophy  
in the Faculty of Engineering  
University of London

November, 1971

Abstract

A turbulence model is proposed for the prediction of two-dimensional boundary-layer flows near walls. Two differential equations are solved: one for the turbulent kinetic energy and one for the turbulence-energy-length-scale product. The constants appearing in the equations are determined by reference to experimental data of self-similar boundary layers.

The calculations by the model for both incompressible and compressible wall boundary layers, with or without heat transfer, are found to compare favourable with the experimental data. Both qualitative and statistical comparisons of some of the predictions with those by other methods of calculation reveal that, the two-equation model predicts the main features of the boundary-layer flows as accurately as other simpler or more complex models. Moreover, the two-equation model is found to be more general in its application than the simpler models.

The experimental investigation of radial wall jets yields both the mean and turbulent quantities of the flow. The data are used to compare with the predictions of the two-equation model.

Acknowledgements

The author wishes to acknowledge with gratitude the advice, guidance and assistance of his supervisor, Professor D.B. Spalding of Imperial College, who suggested the work and provided many original ideas described in this thesis.

The author is also indebted to the members of his thesis committee, Mr. E.H. Cole and Dr. J.H. Whitelaw for their constant interest, advice and suggestion.

Thanks are also due to many other colleagues who have contributed to the successful completion of this work, in particular, Mr. W. Rodi for his assistance in the free shear flow calculations and Dr. S. Sivasesaram for his assistance in the compressible flow calculations.

Thanks are also extended to the technical staff of the Thermal-Fluid Section, Imperial College, for their kind assistance during the period of experimental work.

<u>Contents</u>	<u>Page</u>
<b>Chapter 1 <u>Introduction</u></b>	<b>7</b>
1.1 Background of problem considered	7
1.2 Purpose of the present investigation	10
1.3 Limitation of the present investigation	11
1.4 Outline of the thesis	11
<b>Chapter 2 <u>The equations of motion and the problem of closure</u></b>	<b>13</b>
2.1 Introduction	13
2.2 The mean-momentum equation and the mean-continuity equation	13
2.3 Equations for the transport of second-order turbulence-correlations	15
2.4 The equations for the transport of a conservative property	17
2.5 The transport equations for axisymmetric flows	18
2.6 Effects of compressibility on the transport equations	19
2.7 The closure problem	20
2.8 Classification of the turbulence models	21
2.9 A survey of the existing turbulence models	22
2.10 Concluding remarks from the survey	27
<b>Chapter 3 <u>A two-equation model of turbulence</u></b>	<b>30</b>
3.1 Introduction	30
3.2 The two-equation turbulence model	30
3.3 Some remarks on the two-equation model	37
<b>Chapter 4 <u>Determination of the constants in the turbulence model</u></b>	<b>43</b>
4.1 Introduction	43

4.2	Evaluation of the constants by reference to some simple flows	43
4.3	Procedure of optimisation of the constants	47
Chapter 5	<u>Method of solution and details of boundary conditions for the turbulence model</u>	55
5.1	Method of solution	55
5.2	Boundary conditions for the turbulence-model equations	55
Chapter 6	<u>Comparison of predictions with experimental data and predictions by other models of turbulence</u>	60
6.1	Introductory remarks	60
6.2	Comparison of the calculations of the two-equation model with experimental data	61
6.3	Some comparisons of the present calculations with similar calculations from other methods	81
Chapter 7	<u>Experimental investigation of radial wall jets</u>	89
7.1	Introductory remarks	89
7.2	A survey of the previous investigations	90
7.3	Object of the experimental investigation	95
7.4	Methods of measurements and data reduction	96
7.5	Experimental apparatus	96
7.6	Operating procedure	100
7.7	Presentation and discussion of results	102
7.8	Conclusion from the experimental investigation	109

<b>Chapter 8 <u>Conclusion</u></b>	<b>110</b>
<b>8.1 Principal results of the present investigation</b>	<b>110</b>
<b>8.2 Recommendation for further research</b>	<b>112</b>
<b>References</b>	<b>115</b>
<b>Nomenclature</b>	<b>127</b>
<b>Appendices</b>	<b>133</b>
<b>Figures</b>	<b>187</b>

CHAPTER 1.INTRODUCTION1.1 Background of problem considered

The calculation of turbulent boundary layers is an extensive subject of which the present investigation is concerned with the prediction of their properties by use of turbulence models. The motion of a turbulent Newtonian fluid can be divided into two modes: a primary mode which is the ensemble average or mean motion; and, superimposed on it, the secondary mode which is the random fluctuating motion we call turbulence. Theoretically, since such a fluid is governed by the Navier-Stokes equations, direct solution for the motion of the turbulent fluid should be possible. However, because of the random and complex nature of the motion, such an exact solution is quite impracticable even with the aid of existing computers, due to the enormous amount of computing time that would be required. Faced with such a difficulty, we have to seek approximate solutions of these equations which are compatible with our computing capability.

One way to tackle the problem of turbulent motion is to obtain the statistical correlations of the turbulence within the flow field. However, because of the non-linear nature of the Navier-Stokes equations, the correlation equations always include terms of higher-order correlations. Thus an infinite number of correlation equations have to be chosen and such a set of equations

is made determinate by means of additional information which may either be based on intuitive assumptions or on experimental evidence. The choice of the set of equations and the provision of hypotheses in addition to the hydrodynamic equations, so as to obtain a closed solution, constitute the approach of turbulence modelling.

Prior to 1965, attempts to calculate fluid motions through turbulence models were hampered by two main difficulties. The first was the lack of computational facilities and of general numerical techniques which could handle a large number of simultaneous partial differential equations. The requirement springs from the aforementioned fact that the complete specification of the flow field requires an infinite number of equations; therefore, we can expect that a model of reasonable universality (i.e. one which can be used to calculate a large number of flow situations without having to make any change in the governing equations) will in general require a large number of differential equations.

Secondly, there was a dearth of information upon which one could build the complete picture of a turbulent fluid. The information on the structure of turbulence is useful as a guide to the correct physical hypotheses. However, despite a number of informative treatises on the subject of turbulent motion e.g., Batchelor (1953), Townsend (1956) and Hinze (1959), the picture of the

mechanism of turbulent flow was, and still remains, far from complete.

Because of these obstacles, understandably, calculations of turbulent recirculating flows were non-existent; and the use of turbulence models was confined to two-dimensional boundary layers. These models consisted of no more than one differential equation in addition to momentum and continuity equations. Models which proposed the use of more differential equations, such as those of Kolmogorov (1942), Rotta (1951), Chou (1945), and Davydov (1961), had either not been tested at all or tested only over a limited number of classes of flow. However, this situation has been changed in recent years with the availability of general numerical techniques for the solution of parabolic and elliptic partial differential equations, like those of Patankar and Spalding (1970) and Gosman et al (1969). Furthermore, improved measuring techniques and equipment yield more reliable turbulence measurements.

The object of the present investigation is to make use of some of our present-day knowledge to develop a two-equation turbulence model applicable for boundary-layer flows near walls; the model has two equations which specify the local turbulence intensity and its length scale of the flow. Although the model has a potential application in recirculating flows, the present

investigation is limited to two-dimensional boundary layers. By restricting ourselves to the calculation of boundary layers rather than more complex flows, the mathematical task of devising a solution is reduced. This will in turn reduce the amount of computing time required in the process of developing the model. Moreover, the calculation of turbulent boundary layers is of great importance because such phenomena are frequently encountered in engineering thermal-fluid equipment as well as in Nature.

### 1.2 Purposes of the present investigation

The main object of the investigation has been indicated in the above Section. It may be stated more precisely as follows:

- (1) to survey existing turbulence models.
- (2) to develop a two-equation turbulence model based on the local turbulence intensity and its length scale for the calculation of two-dimensional boundary layers near walls.
- (3) to assess the accuracy of the model by comparing calculations with experimental data; the data include measurements of the hydrodynamics and heat transfer of incompressible and compressible boundary layers.
- (4) to compare some of the present predictions with those from other models of turbulence.
- (5) to carry out new measurements of the mean

and turbulent velocities of radial wall jets; these results are used in the development of the model.

### 1.3 Limitation of the present investigation

The present investigation is limited to two-dimensional boundary layers generated by smooth impermeable walls only. The development of the same model for free-shear flows (i.e. boundary layers without walls) is reported by Rodi (1971).

### 1.4 Outline of the thesis

The main body of the thesis is divided into eight Chapters headed by the Introduction.

Chapter 2 first presents the mathematical problem by the introduction of equations for momentum and scalar transport and for the second order correlations of these properties. The closure problem of these equations is then posed in Section 2.7. This is followed by a review of the existing turbulence models which are classified according to the number of equations in the closed system.

The development of the two-equation model is outlined in Chapter 3.

The constants in the model are determined with reference to a selected set of experimental data; the procedure is described in Chapter 4. The influence of each of these constants on the accuracy of the boundary-layer calculations is also investigated.

Chapter 5 presents the method of solutions for these equations by the finite-difference method of

Patankar and Spalding (1970). The boundary conditions for the model are given in Section 5.2.

Comparisons of predictions with experimental data are given in Chapter 6. The comparisons include both the hydrodynamic and heat-transfer properties of boundary-layer flows near walls; the data chosen for the comparisons include compressible and incompressible wall boundary layers, plane wall jets, radial wall jets, pipe flows, and channel flows. The reasons for the discrepancies between experiments and calculations which occur in some circumstances are discussed. The predicted results are also compared with similar predictions of other models, both of lower and higher order, in Section 6.3.

Chapter 7 reports the mean-velocity and turbulence measurements in two cases of radial wall jets; some of these data have been used in Chapter 6 for the development of the present model.

Finally, Chapter 8 summarises the work of the previous Chapters and suggests paths for further research of the proposed turbulence model.

CHAPTER 2THE EQUATIONS OF MOTION AND THE PROBLEM OF CLOSURE2.1 Introduction

Using the Navier-Stokes equations as a starting point, we can derive the transport equations for the correlation of the fluctuating velocities. The resulting mean-velocity and second-order turbulence-correlation equations applicable to steady two-dimensional boundary layers are listed in Sections 2.2 and 2.3 respectively. However, these equations contain more unknowns than the number of equations. Thus, to achieve closure, it is required to resort to additional physical hypotheses. The same difficulty also applies to the transfer of scalar properties; the relevant equations are presented in Section 2.4.

All the equations discussed above hold for a fluid of constant density; the effect of compressibility on the equations is discussed in Section 2.6.

A critical survey of the turbulence models is found in Section 2.9, in which these models are classified according to the number of differential equations required in the closed system.

2.2 The mean-momentum equation and the mean-continuity equation

The equations of mean motion governing the motion of a steady two-dimensional boundary layer are as follows:

the continuity equation,

$$\rho \frac{\partial U}{\partial x} + \rho \frac{\partial V}{\partial y} = 0, \quad (2.2-1)$$

the mean-momentum transport equation,

$$\rho \frac{DU}{Dt} = \frac{\partial}{\partial y} (\mu \frac{\partial U}{\partial y} - \rho \bar{u}\bar{v}) - \frac{dP}{dx} - \rho \frac{\partial}{\partial x} (\bar{u}^2 - \bar{v}^2). \quad (2.2-2)$$

The meanings of the symbols are defined in Nomenclature.

For a highly turbulent boundary layer, two simplifications can be made to the above equation:

(a) when the Reynolds number of turbulence (defined as  $e^{1/2}l/\nu$ ) is large, the laminar shear-stress is much smaller than its turbulent counterpart; thus the first term on the RHS of equation (2.2-2) can be neglected. The exception to this is in the sublayer close to the wall where the effect of the laminar viscosity plays the dominant role in momentum diffusion.

(b) the experimental evidence from boundary layers shows that the turbulence intensities  $\bar{u}^2$  and  $\bar{v}^2$  are often small. Thus the normal stresses terms in

Equation (2.2-2) can also be neglected.

### 2.3 Equations for the transport of second-order turbulence-correlations

All the transport equations of the second-order turbulence-correlations are listed below in the form applicable to two-dimensional boundary layers.

They entail:

(a) equation for the transport of  $\bar{u}^2$ :

$$\rho \frac{D\bar{u}^2}{Dt} = - 2 \frac{\partial}{\partial y} (\rho \bar{u} \bar{v}) + \mu \frac{\partial^2 \bar{u}^2}{\partial y^2} - 2\rho \bar{u} \bar{v} \frac{\partial U}{\partial y} + 2p \frac{\partial \bar{u}}{\partial x} - 2\mu \sum_{i=1}^3 \left( \frac{\partial \bar{u}}{\partial x_i} \right)^2, \quad (2.3-1)$$

I            II            III            IV            V            VI

(b) equation for the transport of  $\bar{v}^2$ :

$$\rho \frac{D\bar{v}^2}{Dt} = - 2 \frac{\partial}{\partial y} (p \bar{v} + \rho \frac{\bar{v}^3}{2}) + \mu \frac{\partial^2 \bar{v}^2}{\partial y^2} + 2p \frac{\partial \bar{v}}{\partial y} - 2\mu \sum_{i=1}^3 \left( \frac{\partial \bar{v}}{\partial x_i} \right)^2, \quad (2.3-2)$$

I            II            III            V            VI

(c) equation for the transport of  $\bar{w}^2$ :

$$\rho \frac{D\bar{w}^2}{Dt} = - 2 \frac{\partial}{\partial y} (\rho \bar{v} \bar{w}^2) + \mu \frac{\partial^2 \bar{w}^2}{\partial y^2} + 2p \frac{\partial \bar{w}}{\partial z} - 2\mu \sum_{i=1}^3 \left( \frac{\partial \bar{w}}{\partial x_i} \right)^2 \quad (2.3-3)$$

I            II            III            V            VI

(d) equation for the transport of  $\bar{uv}$ :

$$\rho \frac{D\bar{u}\bar{v}}{Dt} = - \frac{\partial}{\partial y} (p \bar{u} + \rho \bar{u} \bar{v}^2) + \mu \frac{\partial^2 \bar{u}\bar{v}}{\partial y^2} + p \left( \frac{\partial \bar{u}}{\partial y} + \frac{\partial \bar{v}}{\partial x} \right) - 2\mu \sum_{i=1}^3 \frac{\partial \bar{u} \partial \bar{v}}{\partial x_i \partial x_i} \quad (2.3-4)$$

I            II            III            V            VI

(e) equation for the transport of turbulent kinetic energy,  $e(\equiv(\bar{u}^2 + \bar{v}^2 + \bar{w}^2)/2)$ , which results from the summation of Equations (2.3-1, 2.3-2, 2.3-3) and the

elimination of  $\overline{p \frac{\partial u_i}{\partial x_i}}$  terms through the condition of mass conservation:

$$\rho \frac{D e}{Dt} = \frac{\partial}{\partial y} \left( \overline{p v + \frac{\rho}{2} (u^2 + v^2 + w^2) v} \right) + \mu \frac{\partial^2 e}{\partial y^2} - \rho \overline{u v} \frac{\partial U}{\partial y} - \mu \sum_{i=1}^3 \sum_{j=1}^3 \left( \frac{\partial u_i}{\partial x_j} \right)^2 \quad (2.3-5)$$

These equations represent the transport of Reynolds stresses in a boundary-layer flow and have been known for a long time. A discussion of these equations can be found in Townsend (1956) or Rotta (1964). The equations are similar to each other in form. The convection of a particular Reynolds stress (I), is determined by the turbulent diffusion (II), the molecular diffusion (III), the production due to the interaction of other Reynolds stresses with the mean strain (IV), the interactions between pressure fluctuation and velocity fluctuations (V), and the dissipative effects due to the presence of viscosity (VI). It must be borne in mind here that apart from the last term in Equations (2.3-1, 2.3-2, 2.3-3, 2.3-5) which is always negative, the other terms can either be positive or negative depending on the inhomogeneity of the flow.

For highly turbulent flow we can again neglect the molecular diffusion term (III) in Equations (2.3-1 to 2.3-5).

#### The pressure-velocity correlations.

As can be seen in Equations (2.3-1 to 2.3-5), the

---

<sup>+</sup> see Corrsin (1953), Hinze (1956) p.65.

pressure fluctuation appears as correlations with the fluctuating velocities. The instantaneous variation of  $p$  is governed by a Poisson equation (see for example, Rotta 1951, Kolovandin and Vatutin 1969):

$$\frac{1}{\rho} \nabla^2 p = - \sum_{i=1}^3 \sum_{j=1}^3 2 \frac{\partial U_i}{\partial x_j} \frac{\partial u_j}{\partial x_i} - \sum_{i=1}^3 \sum_{j=1}^3 \left( \frac{\partial^2 u_j u_i}{\partial x_j \partial x_i} - \frac{\partial^2 \bar{u}_j \bar{u}_i}{\partial x_j \partial x_i} \right). \quad (2.3-6)$$

This equation shows that  $p$  and the pressure-velocity correlations are completely determined by the velocity field. A number of investigators (Chou, Rotta, Kolovandin and Vatutin) have proposed formulations for modelling the pressure-velocity correlations in Equations (2.3-1 to 2.3-5).

#### 2.4 The equations for the transport of a conservative property

The equation for the transport of a conservative property  $\Phi$  reads:

$$\rho \frac{D\Phi}{Dt} = - \frac{\partial}{\partial y} \rho v \bar{\Phi} + \frac{\mu}{\sigma} \frac{\partial^2 \Phi}{\partial y^2} + S_\Phi \quad (2.4-1)$$

and the equation for the turbulent  $\Phi$ -transport flux reads:

$$\rho \frac{Dv\bar{\Phi}}{Dt} = - \frac{\partial}{\partial y} \rho v^2 \bar{\Phi} + \frac{\partial}{\partial y} \left( \frac{\mu \partial \bar{v}\bar{\Phi}}{\sigma \partial y} \right) + \rho v^2 \frac{\partial \bar{\Phi}}{\partial y} - \bar{\Phi} \frac{\partial p}{\partial y} + \bar{s}_{\Phi} \quad (2.4-2)$$

+ viscous terms.

The last term in Equation (2.4-1) represents the source or other additional transport properties of  $\Phi$ .

For the equation of stagnation enthalpy <sup>†</sup> transport,  $S$  is given by,

$$S_{H^*} = \frac{\partial}{\partial y} \left[ \mu \left( 1 - \frac{1}{\sigma} \right) \frac{\partial}{\partial y} \left( \frac{U^2}{2} + e \right) \right]. \quad (2.4-3)$$

## 2.5 The transport equations for axisymmetric flows

Flows in pipes, boundary layers developing along the surface of a cylinder with axis parallel to the main stream, and radial wall jets are just a few of the cases of two-dimensional boundary-layer flows which can be more conveniently analysed in cylindrical coordinates. All the second-order turbulence correlation equations in these coordinates have been derived by Rodi (1970). Comparison of these equations with Equations (2.3-1 to 5) reveals that additional terms are present in the equations for axisymmetric flow. These terms represent production due to, Coriolis forces, centrifugal forces, and additional pressure-velocity correlations. However, for an axisymmetrical boundary layer in the absence of axial swirl, these additional terms can be neglected.

<sup>†</sup> The stagnation enthalpy,  $H^*$ , is defined as,

$$H^* \equiv H + \frac{U^2}{2} + e.$$

Here, the kinetic energy of the mean motion in  $y$ -direction has been neglected.

## 2.6 Effect of compressibility on the transport equations

In supersonic flow and in boundary layers with large density variation due to the presence of large temperature difference across the layer, we can no longer assume  $\rho$  to be a constant. Furthermore, if the flow is turbulent there will appear in the transport equations correlations involving  $\tilde{\rho}$ , the fluctuating component of density. However, provided that the intensity of the fluctuation  $\sqrt{\tilde{\rho}^2}/\rho$  is the same order of magnitude as  $\overline{u^2}/U^2$ , all the density-correlation terms are small compared with the generation term IV in Equations (2.3-1 to 5) and therefore can be neglected from these equations. Some justification of this assumption comes from the data of Harvey et al (1969), who showed that up to a free-stream Mach number of 9, for a flat-plate flow,  $\sqrt{\tilde{\rho}^2}/\rho$  is nowhere greater than 0.1; their result is reproduced in Fig. 2.1.

The current assumption concerning the magnitude of density fluctuations is more restrictive than Morkovin's hypothesis (1964) which is based on the assumption that  $\tilde{\rho}^2/\rho^2$  is the same order of magnitude as  $\overline{u^2}/U^2$ . However, the resulting equations of mean momentum and turbulent kinetic energy based on this assumption (see Bradshaw and Ferriss 1971) and those based on the present assumption are almost identical. Therefore, in the present compressible-flow calculations, it is sufficient to replace  $\rho$  in the transport equations by its local mean

value which is calculated from the equation of state of the fluid. For an ideal gas, the equation of state is:

$$P = \rho R T, \quad (2.6-1)$$

where the mean temperature  $T$  is to be calculated from the enthalpy-transport equation.

Temperature fluctuations may also induce fluctuation of  $\mu$ . However, for air, correlation terms associated with  $\tilde{\mu}$  should be small as  $\mu$  varies only as a 0.76 power of temperature.

## 2.7 The closure problem

Because of the non-linear nature of the Navier-Stokes equations from which the set of Equations (2.3-1 to 6) is derived, this set contains more unknowns than the number of equations. Additional equations for higher-order correlations can of course be derived from the Navier-Stokes equations but no determinate (closed) set can be found. Thus, in order to close the equations, additional information about the behaviour of the turbulence needs to be introduced. Such information is usually formulated from the observation of the characteristics of the turbulence structure in simpler flows such as flows behind grid wires and from other physical hypotheses. With these additional formulations, the resulting equations will form a determinate set with a number of universal constants or functions; these can then be determined from the comparison of the solution from the

equations with a number of reliable experiments.

In the past, various workers have proposed different turbulence models composed of different closed sets of equations. They differ not only in the transport equations used and the physical hypotheses employed, but also in the degree of difficulty with which the solution can be obtained. A review and a classification of these models are found in Sections 2.8 and 2.9 respectively.

## 2.8 Classification of the turbulence models

Turbulence modelling is essentially a problem of approximation through closing the exact equation by semi-empirical formulae; therefore, in principle at least, the larger the number of differential equations employed to describe the turbulent correlations in a model, the more "realistic" it will be. Such a model is likely to fit a larger number of flows without having to make any change in the model. However, a model which requires more differential equations will need not only bigger efforts in devising a solution but also more computing time even if such a solution is possible at all. For this reason, we shall follow the approach of Rodi and Spalding (1969, 1970) who classified the models according to the number of differential equations required, in addition to the Navier-Stokes equations, to calculate the hydrodynamic developments of a two-dimensional turbulent flow.

## 2.9 A survey of the existing turbulence models

With the proliferation of proposals for turbulence models in recent years, it is helpful to make an up-to-date survey of all of them before attempting any new proposals. Furthermore, such a review will be useful in documenting the current state of the art in turbulence modelling.

A summary of the models known to the present author is tabulated in Appendix 1. These models are discussed in Sections 2.9-1 to 4 in which they are classified into zero-, one-, two- and multi-equation families respectively. The proposal of Deardorff (1970) is discussed in Section 2.9-5.

### 2.9-1 Zero-equation models

The name implies that no differential equation is employed apart from the mean-momentum and continuity equations. This is also known as the mean-field method (see Reynolds 1968, 1970) because the apparent shear-stress in the momentum equation is assumed to be proportional to the product of the mean-strain-rate and the mixing length or eddy viscosity; these in turn are functions of local parameters of the flow. Examples of this approach are found in Patankar and Spalding (1970) and Mellor and Gibson (1966). Despite the development of more sophisticated turbulence models, Prandtl's mixing-length method remains one of the most thoroughly tested and best documented methods for calculating boundary layers.

However, like the eddy-viscosity methods, it is well known that different functions are required to calculate the correct mixing length for different flow conditions.

#### 2.9-2 One-equation models

For one-equation models, an additional transport-equation of a turbulence property is employed. The transported property can either be the eddy viscosity itself as proposed by Nee and Kovazsnay (1969) or the turbulent kinetic energy as proposed by Prandtl (1945), Emmons (1954), Glushko (1965), Spalding (1967), Wolfshtein (1969), Saffman (1970), Gavain and Pritchett (1970), and Lundgren (1971). However, rather than use the eddy viscosity to calculate the turbulent shear stress, Bradshaw et al (1967) proposed that the shear stress is proportional to the local turbulent kinetic energy. But as will be shown in Section 4.2-2, the gradient-diffusion assumption and Bradshaw's assumption are identical in the absence of convection and diffusion of turbulent kinetic energy.

As for the zero-equation models, a length scale has to be prescribed for all the one-equation models.

#### 2.9-3 Two-equation model

All the two-equation models proposed so far are similar in two respects: firstly, they all have an equation for turbulence-energy transport and, secondly the length scale, which is prescribed algebraically in the one-

equation model, is determined from another transport equation. Kolmogorov (1942) was the first to propose the use of a "frequency"-transport equation in the calculation of turbulent boundary layers; the length scale is inversely proportional to the "frequency". This was followed by proposals for other length-scale equations by Harlow and Nakayama (1967, 1968), Spalding (1969a) and Wolfshtein (1970). Recently, Jones and Launder (1970) also proposed an equation for the transport of "isotropic dissipation rate" of the turbulence which was successfully applied to the calculation of boundary-layer re-laminarisation. Spalding (1971) calculated the fluctuating quantities in a free circular jet from a model containing an equation for the "square of vorticity fluctuation".

#### 2.9-4 Three-equation and higher-order models

In all two-equation models discussed in the foregoing Section, shear stress is calculated from the product of the mean strain, the square root of the turbulent kinetic energy and the length scale. This relation may be applied to equilibrium or near-equilibrium flows where the convection and diffusion of the shear stress are small compared to its generation and dissipation. However, diffusion of shear stress becomes important in the near-wall zone of a wall jet, and in asymmetric channels, as in the experiments of Hanjalic (1970). Accordingly the author introduced a transport equation in addition to the turbulent-kinetic-energy and

dissipation-rate equations, to account for the effects of convection and diffusion of the shear stress. A similar approach had been proposed earlier by Rotta (1969), who advocated the use of the energy-length equation instead of the dissipation equation.

Donaldson (1969) employed a four-equation model for the calculation of boundary-layer transition; instead of using the turbulent kinetic energy as dependent variable, he calculated  $\bar{u}^2$ ,  $\bar{v}^2$ ,  $\bar{w}^2$ , and  $\bar{uv}$  from the four differential equations but used a prescribed length scale. A similar method has also been employed by Kolovandin (1970) to investigate the scalar transport of turbulent boundary layers. Rotta (1951) and Daly and Harlow (1970) have separately proposed models possessing not only equations for the three components of turbulence intensity and shear stress but also a transport equation to calculate the length.

Higher-order models can of course be obtained by providing transport equations for the third-order correlations. Such models have been proposed by Chou (1945a), Davydov (1959, 1961) and Kolovandin and Vatutin (1969). Chou proposed to calculate both the second-and third-order correlations through a closed set of integral-differential equations while Davydov (1961) proposed to calculate the energy-dissipation rate through four differential equations. Kolovandin and Vatutin, on the other hand, chose to calculate six length scales from differential equations. One interesting aspect of these models is

that the fourth-order correlations which account for the turbulent diffusion of the third-order correlations are not assumed to be of the gradient-diffusion type; instead the fourth-order correlations are either neglected as in Chou (1945b) or decomposed into second-order correlations through the hypothesis of Millionschtchikov(1941), namely,

$$\overline{u_i u_j u_k u_l} = \overline{u_i u_j} \cdot \overline{u_k u_l} + \overline{u_i u_k} \cdot \overline{u_j u_l} + \overline{u_i u_l} \cdot \overline{u_j u_k} . \quad (2.10-1)$$

Use of this hypothesis serves to reduce the number of unknown constants required in the model, but there is physical ground for objection in the use of Millionschtchikov's hypothesis: it is strictly only applicable in turbulence where the probability-density of the fluctuation is Gaussian; however, Gaussianity of the turbulence is only observed in the final stage of decay of isotropic turbulence or at the axis of symmetry of a boundary layer.

#### 2.9-5 Turbulence model for the calculation of large eddies

The calculation method of Deardorff (1970, 1971) cannot be suitably classified according to the number of equations required, as in this method, the time-dependent equations are solved for the large eddies which encompass the grid distribution used in the calculation, while a generalised form of eddy-viscosity hypothesis (Smagorinsky et al 1965) is used in the calculation of subgrid-scale

turbulence; the size of the grid of course represents the length scale of the subgrid turbulence.

Although some useful turbulence characteristics of a channel flow have been predicted by this method a large amount of storage and computing time is required for a solution (over  $10^4$ s of CDC6600 running time for a rectangular-channel-flow problem); thus, the method is likely to remain as a guide to the future development in turbulent flow calculations rather than a general method for immediate use in the calculation of general turbulent flows.

## 2.10 Concluding remarks of the survey

### 2.10-1 The length-scale equation of the turbulence model

Examination of Appendix 1 reveals that all the turbulence models proposed so far are similar in one respect: they all require one or more length scales to specify the representative size of the eddies in the turbulent fluid. These length scales can present themselves in a model under different disguises, e.g. they can be calculated from the rate of energy dissipation as in the model proposed by Daly and Harlow (1970) or they can be retrieved from the vorticity-squared-fluctuation as in the model of Spalding (1971). Moreover, the length scale may either be an algebraic function as proposed by Prandtl (1925, 1945) and Bradshaw et al (1967), or it may be calculated from a differential equation, which is derived in one of the

following ways:

(a) it is constructed through intuition.

Examples of this approach are Harlow and Nakayama's (1967) length-scale equation and Kolmogorov's (1942) "frequency"-transport equation.

(b) it can be derived semi-empirically from the Navier-Stokes equations such as the "vorticity-decay" equation of Chou (1945), the energy-length equation of Rotta (1951), the dissipation equation of Daly and Harlow (1970) and the "vorticity-fluctuation-square" equation of Spalding (1971).

#### 2.10-2 The applicability of the turbulence models

The basis of assessment for the validity of the turbulence models is by comparison between observation and theory. However, from Appendix 1, one notes that not many of the proposed turbulence models have been compared with a large number of observations. In principle, those models which employ a large number of differential equations like those of Chou (1945a), Davydov (1961); and Kolovandin and Vatutin (1969) should be more universal in their applications; but their use as general calculation procedures is at present hampered by the difficulty of obtaining a solution from a large set of coupled differential equations and, by the unknown constants in these models, which remain to be determined. These problems are less acute in simpler models, for these have smaller

number of equations and constants.

Another reason for the popularity in the use of simpler models is that, in flows usually encountered in engineering equipment, there is a need to calculate not only the hydrodynamics of the flow but also other properties, like heat and mass transfer within the flow. Thus, in addition to the equations already in the turbulence model, one has to solve the transport equations for relevant transport properties like those of Equations (2.4-1, 2.4-2).

On the other hand, simple models usually lack universality. For example, Prandtl's mixing length works quite well in both free-jet flows and wall-boundary-layer flows but one needs to take a different constant of proportionality between the length and the layer thickness for these flows.

In Chapter 3, a turbulence model which requires the solution of only 2 equations is proposed; the dependent variables being the turbulent kinetic energy and a length scale of turbulence. It is shown later that such a model predicts satisfactorily the developments of a large number of boundary-layer flows.

CHAPTER 3A TWO-EQUATION MODEL OF TURBULENCE3.1 Introduction

The turbulence model to be proposed in Section 3.2 requires the solution of two differential transport equations, one for the turbulent kinetic energy and one for the kinetic-energy-length-scale product. The exact form of both Equations (3.2-3 and 3.2-5) is first derived from the Navier-Stokes equations. However, in order to close these exact equations, the unknown terms in the equations have to be related to other determinate variables; the proposed expressions are given in Section 3.2-3.

The closed form of the turbulent kinetic energy and energy-length product equations is given in Section 3.2-4. A consequence of the closure is the appearance of a number of universal constants in these equations. The values of these constants are to be determined by reference to experimental data; the procedure of which will be given in Chapter 4.

Finally, some remarks on the characteristics of the proposed model is given in Section 3.3.

3.2 The two-equation turbulence model

One measure of the turbulence field is the joint

correlation of the fluctuating velocities between two points in the flow field. Rotta (1951) has shown that the energy spectrum  $E$ , which is defined as the Fourier-transform of the two-point joint correlation  $R_i^i$ ,

$$E(k) = \frac{k^2}{4\pi^2} \int_{Vol} R_i^i(\vec{r}) dVol, \quad (3.2-1)$$

is governed by a transport equation. The derivation is presented in Appendix 2. For a two-dimensional constant-property boundary layer the  $E$  equation entails:

$$\rho \frac{DE}{Dt} = \frac{\partial \rho F_2}{\partial y} - \rho G_{12} \frac{\partial U}{\partial y} - 2\mu k^2 E - \rho T_1 - \rho T_2 \quad (3.2-2)$$

I	II	III	IV	V	VI
..	..	..	..	..	..

In this equation, terms (I to VI) represent convection, diffusion, generation, dissipation, inertial transfer and mean-motion-turbulence-interaction transfer, of  $E$  respectively. The meanings of each of these terms are explained in Appendix 2. Also in the Appendix are given the definitions of the functions  $F_2$ ,  $G_{12}$ ,  $T_1$ , and  $T_2$ .

### 3.2-1 The exact turbulent kinetic energy equation

The integration of Equation (3.2-2) with respect to  $k$  from 0 to  $\infty$  of course yields a turbulent-kinetic-energy transport equation,

$$\rho \frac{De}{Dt} = \frac{\partial \tilde{f}_e}{\partial y} + \tau \frac{\partial U}{\partial y} - D, \quad (3.2-3)$$

I	II	III	IV
---	----	-----	----

$$\text{where } \mathfrak{F}_e = (\frac{\rho v}{2}(u^2 + v^2 + w^2) + pv)$$

$$\text{and, } \mathfrak{D} = \mu \int_0^\infty k^2 dk = \mu \sum_{i=1}^3 \sum_{j=1}^3 \overline{(\frac{\partial u_i}{\partial x_j})^2}$$

at high Reynolds number of turbulence.

Equation (3.2-3) becomes identical to Equation(2.3-5) when laminar diffusion can be neglected.

### 3.2-2 The exact turbulent-kinetic-energy-length-scale-product equation

We define a length scale  $\ell$  as,

$$\ell = \frac{1}{e} \int_0^\infty E \frac{dk}{k} \quad (3.2-4)$$

Multiplication of Equation (3.2-2) by  $1/k$  and integration with respect to  $k$  from 0 to  $\infty$  yields a transport equation for the product of  $e\ell$ . For a boundary-layer flow, it entails:

$$\begin{array}{llllll} \rho \frac{De\ell}{Dt} & = & - \frac{\partial F_e}{\partial y} e\ell & + \rho \frac{\partial U}{\partial y} \int_0^\infty G_{12} \frac{dk}{k} & - 2\mu \int_0^\infty E k dk & - \rho \int_0^\infty \frac{T_1}{k} dk & - \rho \int_0^\infty \frac{T_2}{k} dk \\ \text{I} & \text{II} & \text{III} & & \text{IV} & \text{V} & \text{VI} \end{array} \quad (3.2-5)$$

$$\text{where } F_{e\ell} = \rho \int_0^\infty \frac{E^2}{k} dk$$

### 3.2-3 Physical hypotheses of the turbulence model

The Equations (3.2-3 and 3.2-5) are in the exact form. However, before these equations can be employed for the calculation of the dependent variables  $e$  and  $\ell$ , a number of physical hypotheses need first to be introduced.

(i) The eddy-viscosity hypothesis

It has been suggested that the turbulent diffusional flux  $\bar{v}\phi$  of a transportable property  $\phi$  is proportional to the local turbulence intensity, the length scale of the turbulence and the mean gradient of the property (Prandtl 1945, Hinze p.285). Accordingly, we have,

$$-\bar{v}\phi = \frac{1}{\sigma_\phi} e^{\frac{1}{2}} \ell \frac{\partial \phi}{\partial y} \quad (3.2-6)$$

where  $\phi$  is any transportable property,  $\ell$  is the length scale defined by Equation (3.2-4) and  $\sigma_\phi$  is a constant. Thus according to Equation (3.2-6),  $\mathcal{F}_e$  and  $\mathcal{F}_{el}$  in Equations (3.2-3) and (3.2-5) can be expressed as follows;

$$\mathcal{F}_e = \frac{1}{\sigma_e} \rho e^{\frac{1}{2}} \ell \frac{\partial e}{\partial y}, \quad (3.2-7)$$

$$\mathcal{F}_{el} = \frac{1}{\sigma_{el}} \rho e^{\frac{1}{2}} \ell \frac{\partial (e^\ell)}{\partial y} \quad (3.2-8)$$

Similarly, the turbulent shear stress is given by,

$$-\bar{\rho u v} = \frac{1}{\sigma_U} \rho e^{\frac{1}{2}} \ell \frac{\partial U}{\partial y} \quad (3.2-9)$$

If the diffusion of enthalpy,  $\bar{vh}$ , also obeys Equation (3.2-6), the diffusion of the stagnation enthalpy  $\bar{vh}^*$  entails

$$\bar{vh}^* = \bar{vh} + U \bar{uv} + \frac{1}{2} \bar{v} (u^2 + v^2 + w^2) = e^{\frac{1}{2}} \ell [ \frac{1}{\sigma_H} \frac{\partial H}{\partial y} + \frac{1}{\sigma_U} \frac{\partial}{\partial y} (\frac{U^2}{2}) + \frac{1}{\sigma_e} \frac{\partial e}{\partial y} ] \quad (3.2-10)$$

In Equations (3.2-7 to 10),  $\sigma_e$ ,  $\sigma_{el}$ ,  $\sigma_U$  and  $\sigma_H$  are assumed constants. The effect of diffusion due to pressure fluctuation has been neglected in the expressions for  $\mathcal{F}_e$  and  $\mathcal{F}_{el}$ . However, these pressure-diffusion effects are usually small in boundary-layer flows and in any case, their effects can be partially accounted for in the appropriate choice of  $\sigma_e$  and  $\sigma_{el}$ .

(ii) Physical hypotheses for the source terms in Equations (3.2-3 and 3.2-5)

Apart from the diffusion term in the e-transport equation (3.2-3), the viscous dissipation rate (VI) has to be expressed in terms of other dependent variables also. One can of course derive an exact equation for the transport of the dissipation rate as has been done by Davydov (1961) and Daly and Harlow (1970) but this equation has four more source terms which need to be modelled before the equation can be closed. However, the mechanism of the turbulent dissipation is well understood. Dissipation of turbulence occurs mainly in small-scale isotropic fluctuations; the dissipated energy is supplied from the larger-scale turbulence which in turn receives its energy from the interaction of the turbulent shear stress and the mean-velocity gradient. When the local Reynolds number of turbulence ( $= e^{1/2} \ell / v$ ) is large, Kolmogorov (1942) suggested that the dissipation rate is independent of the laminar viscosity but depends on the turbulence intensity and the length scale of the larger eddies only. Thus,

$$\mathcal{D} = \mu \sum_{i=1}^3 \sum_{j=1}^3 \left( \frac{\partial u_i}{\partial x_j} \right)^2 = C_1 \rho e^{3/2} / \ell , \quad (3.2-11)$$

where  $C_1$  is taken to be a constant.

In the  $\epsilon\ell$ -equation (3.2-5), four source terms (III to VI), which represent the generation or destruction of the  $\epsilon\ell$ -entity due to turbulence interactions, need to be modelled.

The integral in (III) represents the spectral distribution of  $\bar{uv}$  weighted by  $k^{-1}$ . It is assumed that the shape of this function is characterised by the product of  $\bar{uv}$  and  $\ell$ ; thus,

$$(III) = C_2 \tau \ell \frac{\partial U}{\partial y} , \quad (3.2-12)$$

where  $C_2$  is a constant.

Likewise, term (IV) represents the dissipation spectrum weighted by  $k^{-1}$ , therefore, it is assumed,

$$(IV) = C_3' \rho e^{3/2} , \quad (3.2-13)$$

where  $C_3'$  is a constant.

As mentioned earlier in Appendix 2, the function  $T_1$  represents the inertial transfer of energy from large eddies to smaller ones due to the self-stretching motion of the turbulence, therefore, it is assumed that term (V) obeys the following relation;

$$(V) = C_3'' \rho e^{3/2} , \quad (3.2-14)$$

where  $C_3''$  is a constant.

Term (VI) proves to be more difficult to model. The function  $T_2$  represents the transfer of energy from one wave number to another through the interaction of the mean flow with the turbulent motion. Near a wall, this interaction may be strong. Therefore, it is assumed that,

$$(VI) = f \tau \ell \frac{\partial U}{\partial y} \quad . \quad (3.2-15)$$

In this equation,  $f$  is an empirical function defined as,

$$f = (C_4 \frac{\ell}{y})^q , \quad (3.2-16)$$

where  $C_4$  and  $q$  are taken as constants,  $q$  being greater than unity.

It must be said that the above assumption for  $f$  is based mainly on intuition and on the requirement for the model to satisfy some well known conditions near a wall. The latter will be discussed in Section 4.2-2. The justification will be the good agreement obtained in our subsequent predictions with the model.

### 3.2-4 The final form of the $e$ - and $e\ell$ -equations

Finally, substitution of Equations (3.2-7, 8, 9, 11, 12, 13, 14, 15) into Equations (3.2-3 and 3.2-5), with one of the arbitrary constants  $\sigma_U$  set at unity, yields the desired  $e$ - and  $e\ell$ -equations:

$$\rho \frac{De}{Dt} = \frac{1}{\sigma_e} \frac{\partial}{\partial y} (\rho e^{\frac{1}{2}\ell} \frac{\partial e}{\partial y}) + \tau \frac{\partial U}{\partial y} - C_1 \rho e^{3/2} / \ell , \quad (3.2-17)$$

$$\rho \frac{D\ell}{Dt} = \frac{1}{\sigma_{el}} \frac{\partial}{\partial y} (\rho e^{\frac{1}{2}\ell} \frac{\partial \ell}{\partial y}) + C_2 \tau \ell \frac{\partial U}{\partial y} - C_3 \rho e^{3/2} - f \tau \ell \frac{\partial U}{\partial y}, \quad (3.2-18)$$

where  $C_3 = C_3' + C_3''$ .

The quantities  $C_1$ ,  $C_2$ ,  $C_3$ ,  $\sigma_e$  and  $\sigma_{el}$ , in Equations (3.2-17 and 3.2-18) are taken as constants whereas  $f$  is an algebraic function defined by Equation (3.2-16).

Before we can make use of the two-equation model, the constants appearing in the equations (3.2-17, (3.2-18) have to be first determined. The procedure of determining the values of these constants is given in Chapter 4.

### 3.3 Some remarks on the two-equation model

#### 3.3-1 Other ways of modelling the mean-motion-transfer term in Equation (3.2-2)

In an earlier attempt, Ng and Spalding (1971) assumed that term(VI) in Equation (3.2-6)

$$\rho \int_0^\infty \frac{T_2}{k} dk = C_4' \left(\frac{\ell}{y}\right)^q \rho e^{3/2} \quad (3.3-1)$$

But Equation (3.2-16) appears to be more plausible on physical grounds because, according to the definition of Equation (A.2-7),  $T_2$  must vanish everywhere in flows with no mean-velocity gradient. This occurs in homogenous grid-turbulence flows (Batchelor 1953) or when the wall is moving at the same velocity of the turbulent fluid (Uzkan and Reynolds 1967). However the choice between Equations (3.3-1) and (3.2-15) makes little difference in

the predicted results of a boundary layer if  $C_4$  and  $C_4'$  are correctly chosen because, with negligible convection and diffusion of  $e$ ,  $\ell \frac{\partial U}{\partial y}$  is proportional to  $\rho e^{3/2}$ , as can be seen from the manipulation of Equation (3.2-17), when the diffusion and convection terms are neglected.

However, it was found that the use of the expression in Equation (3.3-1) in the prediction of wall jets gave inferior results compared with those using Equation (3.2-15).

Rotta (1969, 1971) on the other hand has assumed that

$$f \propto \ell^2 \frac{\partial^3 U}{\partial y^3} \left( \frac{\partial U}{\partial y} \right)^{-1} \quad . \quad (3.3-2)$$

As for equation (3.2-16), the above expression reduces to a constant value near the wall where both  $\frac{\partial U}{\partial y}$  and  $\ell$  are proportional to the distance from the wall.

### 3.3-2 Predictions by the model in free shear flows

For free shear flows where the boundary layer is remote from any solid surface, the last term in Equation (3.2-18) vanishes. Whereas, the present investigation is concerned with calculation of near-wall flows, the application of almost the same model for free shear flows is reported by Rodi (1971).

### 3.3-3 Comparison of the present $\epsilon\ell$ -equation with the length-scale equation of other models of turbulence

It may be illustrative to compare the characteristics

of Equation (3.2-18) with the length-scale equation of some other models of turbulence.

Apart from the near-wall term discussed earlier in this Section and the diffusion term, the present  $\epsilon\ell$ -equation (3.2-18) closely resembles that proposed by Roata (1951, 1969). In his earlier proposal, Rotta neglected the near-wall term but in both proposals he assumed that the diffusion flux of  $\epsilon\ell$  is governed by the following expression,

$$\mathcal{F}_{e\ell} = \rho e^{\frac{1}{2}\ell} \left( \frac{\ell \partial e}{\sigma_1 \partial y} + \frac{e}{\sigma_2} \frac{\partial \ell}{\partial y} \right), \quad (3.3-3)$$

where  $\sigma_1$  and  $\sigma_2$  take different values. The above expression becomes identical to Equation (3.2-8) when,

$$\sigma_1 = \sigma_2 = \sigma_{e\ell}. \quad (3.3-4)$$

Instead of using an equation of the  $e\ell$ -product, we can calculate the length-scale from a dissipation equation. An exact dissipation ~~can~~ can be derived from the Navier-Stokes equation or by integration of Equation (3.2-2) with respect to  $k$  after it has been multiplied by  $k^2$ . (Since dissipation  $\equiv \mu \int_0^\infty k^2 E dk$ ) In the dissipation equation, the same number of terms as in the  $e\ell$ -equation (3.2-5) occurs and they have to be either neglected or modelled. Use of the dissipation equation has been proposed by Chou (1945a) and Davydov (1961) and more recently by Daly and Harlow (1970), and Hanjalic (1970).

Spalding (1971), on the other hand, proposed the use of a "vorticity-fluctuation-squared" ( $\equiv e/\ell^2$ ) equation for the calculation of the length scale. This equation can also be derived semi-empirically from the Navier-Stokes equation. However, at present, no measurement of the individual terms in each of the above equations is available to justify the preference of one equation to the other. But when the diffusion term in each of these equations is neglected, the present  $\epsilon\ell$ -equation, Spalding's vorticity-fluctuation-squared equation, and Hanjalic's version of dissipation equation become identical.

### 3.3-4 Implication of the eddy-viscosity hypothesis(Equation3.2-9)

Another feature of the proposed two-equation model is the use of the eddy-viscosity equation (3.2-9) to calculate the shear stress from local mean-velocity gradient, local turbulent kinetic energy and length scale. Although it will be shown in Section 6.2-5 that in some of the calculations, the use of this hypothesis is not correct and, the local shear stress has to be calculated from an additional equation, it is nevertheless interesting to note the implication of the eddy-viscosity expression of Equation (3.2-9).

One way of deriving a semi-empirical equation for the transport of shear stress was proposed by Rotta (1951, 1969).

It reads:

$$\rho \frac{D\bar{U}\bar{V}}{Dt} = \frac{1}{\sigma} \frac{\partial}{\partial y} (\rho e^{\frac{1}{2}(\frac{\partial \bar{U}\bar{V}}{\partial y})} - C_5 \rho e^{\frac{1}{2}\bar{U}\bar{V}/\ell} - C_6 \rho e^{\frac{1}{2}\bar{U}\bar{V}/\ell}) \quad (3.3-5)$$

When the convection and diffusion terms are neglected from Equation (3.3-5), we have the following expression for the shear stress  $\tau$ .

$$\frac{\tau}{\rho} = \frac{C_5}{C_6} e^{\frac{1}{2}\ell \frac{\partial U}{\partial y}} \quad (3.3-6)$$

The reader may recognise that this equation is identical to the eddy-viscosity relation of Equation (3.2-9)  $\sigma_U$  equals to  $C_5/C_6$ . Thus, the use of either the eddy-viscosity expression of Equation (3.2-9) or the shear-stress equation (3.3-5) should produce the same results of prediction when the convection and diffusion of shear stress can be neglected; this condition indeed exists over much of the boundary-layer thickness in flows which are far downstream of any disturbance or obstacle and are not close to separation.

### 3.3-5 Effects of Reynolds numbers on the constants

The physical hypotheses discussed in Section 3.2-3 imply that the viscosity plays no direct part in the turbulent motion. Therefore, the constants in Equations (3.2-17 to 18) are independent of the viscosity. This is probably correct when the Reynolds number of turbulence is large. But when the Reynolds number of turbulence is low such as in the final stage of decay of grid turbulence or in the viscous sublayer of a boundary layer near the

wall, the constants in Equations (3.2-17) and (3.3-18) will no longer have unique values but will be functions of the Reynolds number of turbulence. The determination of these functions lies outside the field of the present enquiry. Nevertheless, to bypass this problem in the boundary-layer calculations, the detail solution using the model is only calculated up to a point close to the viscous sublayer next to the wall. The detail procedure is given in Section 5.2.

### 3.3-6 Effect of compressibility

Equations (3.2-17 and 3.2-18) have been derived for constant property fluid only. One can of course derive these equations incorporating the effect of density fluctuations; these equations will include additional terms of density-fluctuation correlations. However, in view of the dearth of experimental data regarding these density-fluctuation correlations and the level of approximations used in obtaining Equations (3.2-17 and 3.2-18), such a move is felt not justified at present. Following the argument in Section 2.6, it is assumed a priori that both the equations and constants are unchanged provided that the density  $\rho$  in these equations is replaced by its local mean value.

CHAPTER 4DETERMINATION OF THE CONSTANTS IN THE TURBULENCE MODEL4.1 Introduction

The closure scheme of the turbulence-model equations (3.2-17 and 3.2-18) proposed in Section 3.2 produces a number of unknown universal constants in these equations. The values of these constants must be fixed by comparison with a number of experimental data and their solutions using the turbulence model.

In determining the constants, there are some cases of flow which allow analytical solution of the equations and, comparison with experiments for these flows yields direct information about some of the constants. The remaining constants must then be deduced from data for more complex flows; the solutions of the equation with which these data must be compared have to be obtained by numerical integration.

The validity of the model will then be measured by its success in predicting other cases of turbulent flows using the same set of constants in the turbulence-model equations. These comparisons will be given in Chapter 6.

4.2 Evaluation of constants by reference to some simple flows

#### 4.2-1 Homogeneous turbulence behind grids

When a uniform stream of fluid passes through a grid of bars, turbulence is generated downstream of the grid. For this flow, Equations (3.2-17 and 3.2-18) reduce to:

$$U \frac{de}{dx} = - C_1 e^{3/2} / \ell , \quad (4.2-1)$$

and

$$U \frac{d(e\ell)}{dx} = - C_3 e^{3/2} . \quad (4.2-2)$$

Combination of these equations yields,

$$\frac{e}{\ell} \frac{d\ell}{de} = \frac{C_3}{C_1} - 1 = - a . \quad (4.2-3)$$

According to the experimental data of Batchelor and Townsend (1948a, b),  $a$  is between 0.5 and 0.8 depending on the stage of the turbulence decay; this gives  $C_3/C_1$  between 0.5 and 0.2. However, some more recent experiments by Uberoi (1963) suggested that for the initial period of decay of grid turbulence,  $a$  may be as low as 0.33, resulting  $C_3/C_1$  to be 0.67. In any case,  $C_3/C_1$  should lie between 0.67 and 0.2.

#### 4.2-2 Flows in local equilibrium

The domain of a fluid is said to be in local equilibrium when the rate of convection and diffusion of turbulent kinetic energy is negligible compared with the rate of generation and dissipation. For this situation,

Equation (3.2-17) reduces to:

$$\circ = \tau \frac{\partial U}{\partial y} - C_1 \rho e^{3/2} / \ell . \quad (4.2-4)$$

Elimination of the mean-velocity gradient from the above equation using Equation (3.2-9) leads to

$$\tau / (\rho e) = C_1^{1/2} . \quad (4.2-5)$$

The reader may recognise that this relation is one of the assumptions used in the one-equation model of Bradshaw et al (1967) (see Appendix 1) first proposed by Townsend (1961), albeit on different grounds.

The value of  $C_1$  can be determined from experiments. Flows in pipes and along flat plates are in a state of local equilibrium as can be seen from the turbulent kinetic energy balance in Figs. 6.3 and 6.28. The variation of  $\tau / (\rho e)$  for pipe flow and wall-boundary-layer flow are displayed in Fig. 4.1 ; the data are those of Laufer (1954) and Klebanoff (1955). Both sets of data show that  $\tau / (\rho e)$  is about 0.3 under local equilibrium conditions. Substitution of this value for  $\tau / (\rho e)$  into Equation (4.2-5) leads to a value of 0.09 for  $C_1$ . Earlier a value of 0.1 for  $C_1$  has been used by Ng and Spalding (1971) in the same model but the use of such a value resulted in an underestimation of the turbulence level in the boundary layer.

#### Equilibrium flows close to a wall

One of the outcomes of the condition of local equilibrium is Prandtl's mixing-length hypothesis. To

show this, the value of  $\epsilon$  from Equation (4.2-5) is substituted into Equation (4.2-4) to yield,

$$\tau = \rho \frac{\ell^2}{C_1^2} \left( \frac{\partial U}{\partial y} \right)^2 \quad (4.2-6)$$

The above relationship is identical to Prandtl's mixing-length hypothesis if the mixing length  $\ell_m$  is related to  $\ell$  as,

$$\ell_m = \ell / C_1^{1/4} \quad (4.2-7)$$

Experiments show that in the fully turbulent "logarithmic" region near a wall, the mixing length is proportional to the distance from the wall  $y$ . Thus,

$$\ell_m = \kappa y \quad , \quad (4.2-8)$$

where  $\kappa$  is a constant of the order of 0.4, a value concluded from the survey of a large number of wall boundary layer flow data by Escudier (1967) and recently given support by the theoretical analysis of Goldshtik and Kutateladze (1969). Substitution of Equation (4.2-8) into Equation (4.2-7) yields the distribution of  $\ell$  near a wall namely,

$$\ell = C_1^{1/4} \kappa y \quad . \quad (4.2-9)$$

Furthermore,  $\tau$  approaches a constant value as can be derived from Equation (2.2-2) when the convection, mean-pressure gradient, and laminar diffusion terms are neglected. Finally, substitution of Equations (4.2-4),

4.2-5 and 4.2-9) into Equation (3.2-17), after neglecting the convection term of  $\ell$ , yields,

$$\circ = C_1^{\frac{1}{2}} \kappa^2 \sigma_{el}^{-1} + C_2 C_1 - C_3 - C_4 q C_1^{(1+q/4)} \kappa^q . \quad (4.2-10)$$

It is found that, when  $C_1$ ,  $C_2$ ,  $C_3$ ,  $\sigma_{el}$ , and  $q$  are given values appropriate to experimental data remote from walls, and  $\kappa$  has a value near to 0.4, Equation (4.2-10) can be satisfied only by a non-zero value of  $C_4$ ; it is this fact that has necessitated the introduction of the final term in Equation (3.2-18). The above relation can be used for fixing the value of  $C_4$  when all the other quantities are known.

#### 4.3 Procedure of optimisation of the constants

The simple solutions of the turbulence-model equations described in the foregoing Section have resulted in a number of constraints and relations for some of the constants in the model. However, the exact values of the constants have to be determined by the best predictions these constants give for some simple boundary-layer flows. Such a procedure for the determination of the constants is termed optimisation.

##### 4.3-1 Choice of experimental data for the optimisation

Apart from  $C_1$ , for which we take the value of 0.09 and,  $C_4$  which is determined from Equation (4.2-10), the remainder of the constants in Equations (3.2-16, 3.2-17 and 3.2-18) are chosen so as to obtain the best agreement

between predictions and experiments for a number of well known characteristic quantities in the following self-similar boundary-layer flows, namely:

(i) boundary layer on a semi-infinite flat

plate with  $\tau_s / (\rho U_G^2) = \text{constant}$ ;

(ii) flow in a pipe of uniform circular

cross-section with  $\tau_s / (\rho U_m^2) = \text{constant}$ ;

(iii) flow between wide parallel plates with

$\tau_s / (\rho U_m^2) = \text{constant}$ ;

(iv) plane wall jet in stagnation surroundings

with  $\tau_s / (\rho U_{\max}^2) = \text{constant}$ ;

(v) plane mixing layer between a uniform

moving stream and a stagnation stream.

(vi) plane free jet in a stagnation surrounding;

(vii) radial fan jet in a stagnation surrounding;

The characteristic quantities of these flows chosen for comparison are tabulated in Table 4.1. The flows are calculated from the numerical integration of the turbulence-model equations (2.2-1, 2.2-2, 3.2-17, 3.2-18) using different values for the constants during each calculation of the flows; the integration procedure is described in Section 5.1. The constants are then optimised until the predicted characteristics agree with those listed in Table 4.1. In the wall flows listed from

<u>case</u>	<u>characteristic quantities</u>	<u>experimental value</u>	<u>references</u>	<u>predicted value</u>
(i)	$(1 - H_{12}^{-1}) \frac{U_G}{U_\tau}$	6.1 6.8	Hama(54) Coles(30)	6.53
(ii)	$\frac{U_{max} - U_m}{U_\tau}$	3.75 3.50	Schlichting(126) Nunner(105)	3.76
(iii)	$\frac{U_{max} - U_m}{U_\tau}$	2.32	Clark(28)	2.3
(iv)	$\frac{dy_{\frac{1}{2}}}{dx}$	0.078 0.075	Myers(97) Tailland(139)	0.073
(v)	$\frac{d(y_{*9} - y_{*1})}{dx}$	0.16	Liepmann & Laufer(80)	0.159
(vi)	$\frac{dy_{\frac{1}{2}}}{dx}$	0.08 0.11	Bradbury(8) Heskestad(62)	0.106
(vii)	$\frac{dy_{\frac{1}{2}}}{dx}$	0.11	Heskestad(63)	0.11

Table 4.1. Comparison between the measured values of the characteristic quantities of the self-similar boundary layers and the values calculated from the two-equation model.

(i) to (iv), the constant friction-coefficient is supplied as a boundary condition. This ensures that the predicted results are independent of laminar viscosity. Doing so does not invalidate comparison with the experiments because the characteristic quantities chosen for comparison are either completely or only slightly dependent on the Reynolds number of the flow. Thus, with the friction coefficient specified and with the boundary conditions for  $e$  and  $\ell$  as those given in Section 5.2, the set of differential Equations (2.2-1, 2.2-2, 3.2-17 and 3.2-18) can be integrated.

A value of  $2.5 \times 10^{-3}$  for the friction coefficient for flow cases (i) to (iii), has been chosen for the present calculations. The predicted characteristic quantities for these flows were found to be little influenced by the choice of friction coefficient. This was confirmed by predicting the characteristic quantities using half and twice the chosen friction coefficient. However, the predicted growth rate,  $dy_1/dx$ , of the plane wall jet (case iv) is more sensitive to the choice of the friction coefficient, therefore we have chosen a value of  $2.8 \times 10^{-3}$  for the friction coefficient, a value which is the average of all experimental data.

#### 4.3-2 Optimisation procedure

An earlier attempt in optimising the constants was reported by Ng and Spalding (1971). The authors optimised the constants to give the best predictions

for five characteristic quantities of the near-wall self-similar flows only. Not surprisingly, it was found that the constants thus obtained do not give the best predictions for free shear flows due to such a limited field of enquiry. These constants have been re-optimised through "numerical experiments" to give the best agreements with the target quantities for both wall and free shear flows. The resultant constants are tabulated in Table 4.2; the calculated characteristic quantities using these constants are tabulated in the last column of Table 4.1.

$c_1$	$c_2$	$c_3$	$c_4$	$\sigma_e$	$\sigma_{e\ell}$	$q$
0.09	0.98	0.058	4.3	1.0	1.0	6

Table 4.2. The optimised constants for Equations (2.2-16 to 18).

#### 4.3-3 Influence of the constants on predicted characteristic quantities

Examination of the constants in Table 4.2 shows that they agree with the constraints discussed in Section 4.2. In particular, the ratio of  $c_3$  to  $c_1$  is 0.65, which agrees with the experimental data of Uberoi (1963). The sensitivity of the predicted characteristic quantities to change of each individual constant is tabulated in Table 4.3. In the Table, the

percentage change in each characteristic quantity due to 5% change of each constant in Equations (3.2-17, 3.2-18) is displayed. It is clear that some constants exert a bigger influence on the predicted results than others. In particular, the change of the predicted characteristic quantities due to 5% increase of  $\sigma_e$  or  $\sigma_{el}$  is less than 1% whereas the corresponding percentage increase in  $C_1$ ,  $C_2$ , or  $C_3$  results in change of over 2.9% in each selected target. The result is not unexpected: the diffusion of  $e$  is negligible compared with the generation and dissipation in these self-similar boundary layers; thus the predicted quantities are much less sensitive to the choice of  $\sigma_e$  and  $\sigma_{el}$  than  $C_1$ ,  $C_2$ , and  $C_3$ .

#### 4.3-4 Other predicted properties of the self-similar flows and their comparison with experimental data.

The predicted mean-velocity profiles for all self-similar flows are plotted in Figs. 4.2-4.8.

In each case of flow, the relevant experimental data are also presented. Discussion on the comparison of predictions with experiments for free shear flows can be found in Rodi(1971).

We shall refrain from discussing in detail the comparison between the predictions and experiments. This is because many of the features appearing in Figs (4.2 to 4.8) will subsequently be covered in the predictions for non-similar flows in Chapter 6. It may suffice to mention

Table 4.3 Percentage variation of the predicted characteristic quantities at 5% increase of the individual constants in Equation (3.2-17 and 3.2-18).

Case	i	ii	iii	iv	v	vi	vii
% con- stants	$(1 - H_{12}^{-1}) \frac{U_G}{U_\tau}$	$\frac{U_{max} - U_m}{U_\tau}$	$\frac{U_{max} - U_m}{U_\tau}$	$\frac{dy_1}{dx}$	$\frac{d(y_{*9} - y_{*1})}{dx}$	$\frac{dy_1}{dx}$	$\frac{dy_1}{dx}$
$C_1$	- 3.1	- 3.7	- 3.0	+ 5.7	+ 2.9	+ 3.6	+ 3.7
$C_2$	- 4.2	- 3.7	- 3.6	+ 7.4	+ 19.6	+ 27.6	+ 27.0
$C_3$	+ 2.9	+ 3.8	+ 3.7	- 5.4	- 5.8	- 7.1	- 7.3
$n$	- 1.7	- 2.2	- 2.4	+ 2.8	-	-	-
$\sigma_e$	- 0.4	- 0.6	- 0.9	+ 0.2	+ 0.1	+ 0.2	+ 0.3
$\sigma_e$	- 0.3	- 0.7	- 0.6	+ 0.9	+ 0.7	+ 0.4	+ 0.4
$q$	- 0.5	- 0.8	- 0.8	+ 0.8	-	-	-

that indeed, self-similarity is attained in these flows as can be seen from the asymptotic behaviour of the parameters shown in the figure a's in Figs. 4.2 to 4.8.

CHAPTER 5METHOD OF SOLUTION AND DETAILS OF BOUNDARYCONDITIONS FOR THE TURBULENCE MODEL5.1 Method of solution

Apart from a number of special cases, a general analytical solution for a closed set of Equations (2.2-1, 2.2-2, 3.2-17, 3.2-18) is unlikely to be found. Therefore solution of these coupled equations is only possible by numerical methods using computers. The implicit finite-difference procedure of Patankar and Spalding (1970) was used for the numerical integration of the turbulence-model equations throughout the present investigation. So much has been reported about the Patankar and Spalding (1970) procedure (see Ng et al 1968, Patankar and Spalding 1970), that further discussion here is unnecessary. It is sufficient to mention that the independent variables of the integration are the streamwise distance and a dimensionless streamfunction across the boundary layer. The integration marches stepwise downstream of the boundary layer. A listing of the program adopted for the present calculations is displayed in Appendix 6.

5.2 Boundary conditions for the turbulence-model equations

The calculation of the boundary layer using Equations (2.2-1, 2.2-2, 3.2-17, 3.2-18) requires the details

of the boundary conditions to be specified. The boundary conditions can be classified into two types:

(i) the boundary conditions at the edges of the boundary layer and (ii) the initial profiles of the dependent variables at the starting point of the integration. The former will be referred to as lateral boundary conditions and, the latter as starting profiles.

### 5.2-1 The lateral boundary conditions

(a) In the free-stream edge of a boundary layer, one-dimensional flow prevails. Thus Equations (2.2-2, 3.2-17, 3.3-18) degenerate into

$$\left[ \frac{\rho dU}{2dx} \right]_G = - \frac{dP}{dx}, \quad (5.2-1)$$

$$U_G \frac{de_G}{dx} = - C_1 e_G^{3/2} / \ell_G, \quad (5.2-2)$$

$$\text{and} \quad U_G \frac{d(e\ell)_G}{dx} = - C_3 e_G^{3/2}. \quad (5.2-3)$$

Other conservative properties are assumed to be given at the free stream.

The value of  $U_G$ ,  $e_G$ , and  $(e\ell)_G$  can be calculated from Equations (5.2-1 to 3). In the absence of any free-stream turbulence,

$$e_G = 0 \quad (5.2-4)$$

$$(e\ell)_G = 0 \quad (5.2-5)$$

(b) For an axisymmetric or plane-symmetric flow, the integration proceeds from one outside edge to the line of symmetry only. At the symmetry line,

$$\left(\frac{\partial \Phi}{\partial Y}\right)_C = 0 \quad (5.2-6)$$

where  $\Phi$  can be  $U$ ,  $e$ ,  $\ell$ , or other transport properties.

(c) The boundary condition along a solid impermeable surface is less straightforward. As mentioned in Section 3.3-5 the present model with a fixed set of universal constants is strictly valid only in regions of the flow where the Reynolds number of turbulence is high. Thus the model is not expected to be applicable within the viscous sublayer near the wall where the Reynolds number of turbulence approaches to zero at the wall. To bypass this difficulty, we carry out the numerical integration up to a point B just outside the sublayer as shown in Fig. 5.1. The boundary conditions at the point B are then supplied from a number of well known semi-empirical relationships based on the couette-flow solutions of the transport equations. The boundary conditions at B are:

$$U_B \left( \frac{\rho}{\tau_S} \right)^{\frac{1}{2}} = \frac{1}{\kappa} \ln \left[ \frac{E Y_B (\tau_S \rho)^{\frac{1}{2}}}{\mu} \right] , \quad (5.2-11)$$

$$\left( \frac{\tau_S}{\rho e} \right)_B = C_1^{\frac{1}{2}} , \quad (5.2-12)$$

$$(\ell/Y)_B = C_1^{\frac{1}{4}} \kappa . \quad (5.2-13)$$

Equation (5.2-11) is the "logarithmic law of the wall" where  $\kappa$  is 0.41 and  $E$  is 7.8 according to the data survey of Coles (1968). Equations (5.2-12 and 5.2-13) are identical to Equations (4.2-5 and 4.2-9).

The boundary condition at B for any other conservative property  $\Phi$  is,

$$\frac{(\Phi_S - \Phi_B)(\rho \tau_S)^{\frac{1}{2}}}{J_S} = U_B \left( \frac{\rho}{\tau_S} \right)^{\frac{1}{2}} + \rho + Q . \quad (5.2-14)$$

where  $\rho$  is a semi-empirical function which accounts for the resistance to the transfer of  $\Phi$  across the viscous sublayer (see Spalding 1964); according to Patankar and Spalding (1970),  $\rho$  obeys the following relationship:

$$\rho \left( \sigma / \sigma_{\Phi} \right) = 9.24 \left[ \left( \sigma / \sigma_{\Phi} \right)^{\frac{1}{4}} - 1 \right] \left[ 1 - 0.28 \exp(-0.007 \frac{\sigma}{\sigma_{\Phi}}) \right], \quad (5.2-15)$$

where  $\sigma$  and  $\sigma_{\Phi}$  are the laminar and turbulent Prandtl/Schmidt number of  $\Phi$  respectively; the latter is taken as 0.89.

In the absence of any source of generation or other additional transport effects, the function  $Q$  in Equation (5.2-14) vanishes. For stagnation enthalpy,  $Q$  is given by,

$$Q = (\sigma_H - 1) \frac{U_B^2 (\tau_S \rho)^{\frac{1}{2}}}{2 J_S} . \quad (5.2-16)$$

In the case of calculating flows with large

density variations as in the case of supersonic flows, the density  $\rho$  in Equations (5.2-11) and (5.2-14) are taken to be the arithmetic mean between the wall  $S$ , and B. Sivasegaram (1969) has found that the use of mean density retains the validity of the "log-law" (Equation 5.2-11) in supersonic flows.

### 5.2-2 Starting profiles for the calculation of boundary layers

In order to calculate the downstream development of a boundary layer, we require to specify the starting profiles of all dependent variables of the two-equation turbulence model,  $U$ ,  $e$ , and  $\ell$ . In practice,  $\ell$  is not a directly measurable quantity but it can be deduced from  $U$ -,  $e$ -, and  $\tau$ - profiles according to Equation (3.2-9), if these quantities are given. In the absence of any information about the starting profiles they have to be invented. The procedure to calculate these quantities is shown in Appendix 3 whereby the profile of  $\ell$  is assumed to be a ramp-type and  $e$  is a cubic function depending on the local pressure-gradient and the wall shear-stress. This procedure has been employed successfully by Ng and Spalding (1970) for wall-boundary-layer calculations.

If the initial  $U$ - profile is not given, it is assumed to obey the 1/7th-power law. For heat-transfer calculations, Crodo's temperature profile is employed as the starting profile. c/

Discussions on the influence of the starting profiles on predictions will be found in Section 6.2-1.

CHAPTER 6COMPARISONS OF PREDICTIONS WITH EXPERIMENTAL DATA  
AND PREDICTIONS BY OTHER MODELS OF TURBULENCE6.1. Introductory remarks

In Chapter 4, a set of constants were selected for the two-equation turbulence model so that it calculates correctly the characteristics of a number of self-similar flows. Although satisfactory predictions were obtained for these flows, they nevertheless represent only a limited type of two-dimensional boundary layers that are common occurrence in engineering equipment. Many other important parameters which affect the development of boundary layers are absent from these self-similar flows; for example, they are independent of laminar viscosity and that there is no streamwise pressure-gradient variation, both of which are important parameters in real boundary-layer flow.

Furthermore, only the hydrodynamic properties of the self-similar boundary layers were compared; no calculation of heat transfer using the two-equation model has been made. The present Chapter presents the comparisons of predictions with experiments which include not only the hydrodynamics but also the heat transfer for both incompressible and compressible wall boundary layers. The main purpose of the comparisons is to assess the accuracy of the predictions by the two-equation model. Moreover, through these comparisons, modifications to the model, so as to increase its accuracy of prediction and range of

applicability, can be formulated.

The assessment would not be complete without the comparison of the calculations of the present model with those of other models of turbulence. Through the comparison, the merits and demerits of using the two-equation turbulence model can be realised.

## 6.2 Comparison of the calculations of the two-equation model with experimental data

All the comparison will be restricted to steady boundary-layer flows developing along smooth and impermeable walls.

### 6.2-1 Hydrodynamics of the constant-property wall boundary layers

#### Hydrodynamic properties of a flat plate

The calculation of a constant-shear-stress-coefficient boundary layer has already been presented in Fig. 4.2. Fig. 6.1 presents the comparison of the calculated friction coefficient,  $s_S$  and shape factor,  $H_{12}$ , of a flat plate with Coles' correlation (1962). In this figure, the friction coefficient and the shape factor are plotted against the momentum-deficit-thickness Reynolds number,  $R_2$ . The agreement between the calculation and the correlation is found to be satisfactory. As a further comparison, both the mean-velocity and the turbulence quantities of a flat plate, measured by Klebanoff (1955), and the corresponding

calculated values are displayed in Fig. 6.2. Whereas the mean-velocity and the shear-stress profiles have been correctly predicted by the two-equation model, the turbulent kinetic energy is under-predicted close to the wall. Fig. 6.2 (c) displays the calculated eddy-viscosity and mixing-length profiles; the former has been normalised by  $U_G \delta_1$  and the latter by  $y_G$ . The mixing length,  $l_m$ , was calculated from the following equation:

$$l_m^2 = e^{\frac{1}{2} \ell} \left| \frac{\partial U}{\partial y} \right|^{-1} \quad (6.2-1)$$

As shown in the figure, the predicted eddy-viscosity profile agrees well with the data. The interesting feature of the predicted mixing-length profile is that near the wall it is proportional to  $y$  and having a constant of proportionality of 0.41. Furthermore, the mixing length attains a maximum of 0.09 of  $y_G$ , a value which was used in the mixing-length model of Patankar and Spalding (1970).

A comparison of predicted contributions of the various terms in the turbulent-kinetic-energy equation with experimental measurements is displayed in Fig. 6.3. Considering the difficulty of obtaining accurate measurements of dissipation and total diffusion rates, the predictions appear to be satisfactory.

#### Hydrodynamics of boundary layers developing under varying streamwise pressure gradients

The wall-boundary-layer experimental data collected

by Coles and Hirst (1968) forms the bulk of the data used in this comparison. Fig. 6.4 presents the comparison of the predictions with the 32 sets of boundary-layer measurements which were subjected to different free streamwise pressure-gradient variations. Each flow shown in the diagram is denoted by an identity number (IDENT); the nature of the experiment and the name of the investigator(s) can be obtained from the accompanying table. For each flow, the predicted variation of  $H_{12}$ ,  $s_s$ , and  $R_2$  with  $x$  is compared with the experimental data; the lines represent the predictions, and the circles represent the data. To facilitate more detailed inspection and discussion, six representative cases of flow (IDENT = 1500, 2400, 2500, 2800, 3300, and 4800 in Fig. 6.4) are replotted to a larger scale in Figs. 6.5 to 6.10. For IDENT = 2400, 2500, 2800 and 3300, the calculated  $U$ ,  $\tau$ , and  $e$  are also compared with the available data at the last station of the relevant experiments, which are displayed in Figs. 6.12 to 6.15.

From Fig. 6.4, one can infer that the predictions agree tolerably with the experimental data. Inspection of the predictions made by other methods for the same conditions, reported in the Proceedings of the Stanford Conference, shows that where the present method fails, e.g. IDENT = 1200, 2900, and 5300, most of the other methods fail also; there is reason to believe that our predictions are in as good agreement with the data as the experimental accuracy warrants. Ng and Spalding (1970) have discussed in some detail about the accuracy of the set of data

collected by Coles and Hirst (1968). In particular they found that the accuracy of each individual experiment is affected by the following factors:

(a) The procedure used for the evaluation of skin-friction. The "experimental" values of  $s_S$  are based not on direct measurements, but on the deduction from velocity-profile measurements by the "Clauser-plot" method. Differences as much as 10% in the evaluated  $s_S$  under the same experimental conditions were found between this method of evaluation and other methods of measurement such as that of the Preston-tube.

(b) The lateral convergence or divergence of the boundary layer. In wind-tunnel measurements, boundary-layer growth along the side walls can cause lateral convergence or divergence of the boundary layer under investigation; it then ceases to obey Equations (2.2-1, 2.2-2). This breakdown is shown by the lack of momentum-balance of the boundary layer in question. Insofar as this is not due to incorrect values of  $s_S$  or the breakdown of other boundary-layer assumptions (e.g. the neglect of the normal-turbulent-stresses terms in Equation 2.2-2), the cause can be attributed to the lateral convergence or divergence of the boundary layer.

Inspection of the Stanford data reveals that flow convergence is present in most of the experiments under strong adverse-pressure gradients.

(c) Inadequate number of points to specify the mean-velocity profile. The integral parameters  $H_{12}$  and  $R_2$  can be wrongly ascribed when there are too few cross-stream points close to the wall to allow correct determination of the velocity profile. This is probably the cause of disagreement in  $H_{12}$  between experiment and prediction of flows of IDENT = 3100, 3600, 3700, and 4100 in Fig. 6.4.

#### Possible sources of errors in predictions

Of course, the failure to obtain agreement between predictions and experiments is not necessarily due to the inaccuracies of the latter. There are also a number of possible sources of error in the predictions namely;

(a) The "wall-law" assumptions (Equations 5.2-11 to 13) close to the wall. In the present prediction, the logarithmic law of the wall (Equation 5.2-11 has been employed for the calculation of  $\tau_s$  from  $U$  and  $y$  at point B (see Fig. 5.1). This practice is relatively simple, and in reasonable agreement with experimental data over a wide range of flow conditions. In reality however,  $\tau_s$  must depend upon other variables like the pressure gradient and turbulence level etc. The effect of the former has been accounted for in the "wall-law" developed by Townsend (1961), McDonald (1969a,b) and Patankar and Spalding (1970, 1971), and the latter influence appears in the formulae developed by Spalding (1967a, b), Wolfshtein (1969), and Runchal (1969). Therefore it may be valuable to establish later, whether any of these proposals can improve agreement with reliable experimental data.

(b) The neglect of the normal-stresses terms in the momentum equation (2.2-2). In the calculations, we have neglected the contribution of the normal-stresses terms in Equation (2.2-2). Although they are usually negligible compared with other terms in the equation, they may nevertheless be significant when the turbulence level in a boundary layer is high as it occurs when the flow is near separation ( see for example, Spangenberg et al 1967). Therefore, the result of neglecting the normal-stress terms in flows under this situation may lead to discrepancies. Corrections for these terms can of course be made in the calculations, but the variations of the turbulence quantities are not given with the data.

(c) The assumption concerning the starting profiles  
For all the predictions shown in Fig.6.4, the initial profiles of  $e$  and  $\ell$  have to be invented according to the procedure in Appendix 3. In order to test the influence of the starting profiles on the predictions, flows IDENT = 2400, 2600 and 3300 were re-calculated with the initial profiles of  $e$  and  $\ell$  identical to those which, in these cases, were reported by the experimenters, ( $\ell$  is deduced from  $\tau$ ,  $e$ , and  $U$  profiles according to Equation 3.2-9). The new predictions show little difference from the earlier ones, indicating that the assumed profiles for  $e$  and  $\ell$  (Equations A.3-2 and A.3-3) are adequate for these flows whose immediate upstream conditions are near a state of equilibrium. However, for boundary layers downstream of a re-attachment, our assumed

starting profiles of  $e$  and  $\ell$  are likely to be in error. The effects of using the correct starting profiles for re-attaching flows can be seen in Fig 6.11. It shows the comparison of predictions with some recent measurements of Bradshaw and Wong (1971). The calculations were started first with the given starting profiles, and then with profiles of  $e$  and  $\ell$  as given in Appendix 3; the poor prediction of the latter is evident. Indeed, the poor agreement of Tillmann's ledge flow (1945) displayed in Fig. 6.5, may be attributed to the same cause also.

Comparison of the predicted  $U$ ,  $e$ , and  $\tau$  profiles with experiments

Figs. 6.12 to 15 display the predicted profiles of  $U/U_G$ ,  $\tau/(\rho U_G^2)$  and  $e^{1/2}/U_G$  at the last station of flows IDENT = 2400, 2500, 2800 and 3300, and compare with the available data. Mindful of the possible inaccuracies of the experimental data and the possible errors in the calculation discussed above, we see that the mean-velocity profiles are well predicted for all four cases.

A more rigorous test of the turbulence model is its ability to predict the shear-stress profiles accurately. The comparisons of these profiles with data are shown in figure b's in Figs. 6.12 to 6.15. It is noted that for all cases, the  $\tau$  profile has been well predicted except near the free stream where however, the value of  $\tau$  is small compared with its local maximum.

Mixing-length distributions in flows with varying pressure-gradient

Fig. 6.16 presents the predicted mixing-length distributions of Bradshaw's relaxing boundary layer (IDENT = 2400). In this flow, the boundary layer is accelerated by the sudden removal of the adverse pressure-gradient. The predicted mixing-length distributions at three streamwise stations are displayed in the figure. It is interesting to note that in the outerlayer, the ratio of mixing-length to boundary-layer-thickness ( $\ell_m/y_G$ ) is predicted to be a constant, but the value increases with the diminish of the adverse pressure-gradient. This is also evident from the mixing-length profiles deduced from the experiment, which are displayed in Fig. 6.16 also.

6.2-2 Heat transfer across constant-property boundary layers

The prediction of heat transfer in a turbulent boundary layer requires the solution of an additional transport equation for enthalpy (Equation 2.4-1) where the diffusion flux term is modelled according to Equation (3.2-6) with  $\sigma_H$  equal to 0.89. The data of Moretti and Kays (1965) were chosen for the comparison, from which three cases of flow are presented in Figs. 6.17 to 19. The heat-transfer rate is plotted as the local Stanton number ST vs x. The predictions are shown in

solid lines in Figs. 6.17 to 6.19. The first two figures show the heat transfer of a wall boundary layer in zero and adverse pressure gradients respectively and the predictions agree reasonably well with the data. Fig. 6.19 shows the Stanton number variation of a suddenly accelerated boundary layer downstream of a flat-plate flow; the prediction starts to deviate from the measurements in the region where the sudden acceleration was imposed on the boundary layer. Here we encounter a deficiency of our turbulence model. The acceleration of the fluid diminishes the turbulence level, which subsequently causes "laminarisation" resulting in a large reduction of the local Stanton number; the prediction fails because of the reduction of the Reynolds number of turbulence. It has been pointed out in Section 3.3-5 that, when the Reynolds number of turbulence is small, the constants appearing in Equations (3.2-16 to 18) will no longer have unique values as proposed but become functions of laminar viscosity. Some of these functions have been incorporated in other calculation procedures such as those of Graham and Deissler (1967), Jones and Launder (1970). Later, it may be interesting to establish the correct functions for the constants in the present two-equation model.

### 6.2-3 Supersonic turbulent boundary layers

A logical extension of the calculation of heat transfer in constant-property flows is the calculation of compressible supersonic boundary layers.

Based on the available experimental evidence of density fluctuations in a supersonic boundary layer, it has been suggested in Section 3.3-6, that supersonic boundary layers can be calculated from the same turbulence-model equations for constant-property flows if the density,  $\rho$ , appearing in these equations is replaced by its local value in the calculation. Some predictions of supersonic flows have already been reported by Ng and Sivasegaram (1970) who made use of an earlier version of the present two-equation model. Fig. 6.20 presents the comparison of the calculated velocity profile with experimental data for an adiabatic flat-plate flow at different free-stream Mach numbers,  $M_G$ , from 2.0 to 4.5. The measurements are those of Coles (1953). The agreement of the prediction with data is well within the accuracy of the experiments when we note that the uncertainties of measurements in compressible flows are likely to be greater than those of incompressible flows. It may be relevant to compare the calculated skin-friction coefficient of a flat-plate flow with other existing empirical or semi-empirical correlations such as those of Coles or Spalding and Chi, but recent measurements of skin-friction as reported by Hopkins et al (1969) showed that none of these correlations gives accurate estimation of the skin-friction coefficient within the complete range of Mach number from 0.0 to 8.0.

Figs. 6.21 and 6.22 display the comparisons of predictions with experiment for two cases of adiabatic compressible boundary layer under favourable and adverse pressure gradients respectively; the measurements are those of Sivasegaram (1969). The comparison of the predicted and experimental mean-velocity profiles for these two flows are shown in Figs. 6.23 and 6.24 respectively and the agreement is considered satisfactory. Furthermore for both cases of flow,  $\delta_2$  and  $H_{12}$  are well predicted as shown in Figs. 6.21 and 6.22, showing that not only have we calculated the velocity profiles accurately but we have also predicted the local density variations correctly. The value of  $s_S$ , however, is on the average over-predicted, but it is worth noting that Sivasegaram (1969) has suggested the possibility of the measured  $s_S$  being 5% too low. In the first third of the adverse pressure-gradient flow, shown in Fig. 6.22, the value of  $s_S$  is over-predicted by up to 25%. This is suspected to be due to the relaminarisation of the boundary layer which has been subjected to strong acceleration in the upstream region of the flow.

#### Heat transfer in supersonic boundary layers

As a test case for the ability of the present model to predict supersonic flow with heat transfer, four of the measured temperature profiles of Lobb et al (1955), obtained in zero pressure gradient with heat transfer, are compared with their predictions. The

comparisons are shown in Fig 6.25 and are found to be satisfactory.

#### Prediction of the mixing-length distribution

Lastly, Fig. 6.26 shows comparison of a different kind. It presents the mixing-length distribution across the compressible boundary layer on a flat plate as predicted by the present two-equation model. Comparison with the distributions proposed by Maise and McDonald (1968) and Sivasegaram and Whitelaw (1971) suggests that they all agree reasonably well with each other.

#### 6.2-4 Developed flows in circular pipes and channels<sup>f</sup>

Unlike external wall boundary layers, the flow in ducts requires different boundary conditions for the transport equations as given in Section 5.2. The calculation procedure of Patankar and Spalding (1970) is capable of calculation of internal flows. Some of the results of calculations of internal flows using the present model have already been presented in Figs. 4.3 and 4.4, in which the calculated mean-velocity-defect profiles for a pipe and a channel are plotted. Fig. 6.27 displays a more detailed comparison between prediction and experimental data for a pipe flow. The data are those measured by Laufer (1954); the Reynolds number of the flow,  $\frac{U_{max}D}{\nu}$ , is equal to 500,000. The calculated

---

<sup>f</sup> The term "channel flow" is taken to mean flows between two large parallel plates or flows in a rectangular duct with large aspect ratio.

mean-velocity profile shown in Fig.6.27(a) is in good agreement with the experimental data. As expected,  $\tau$  is predicted to be proportional to the radial distance from the axis of the pipe, as shown in Fig.6.27(b). Also displayed in the same figure is the prediction and data of the variation of  $e$ ; although the turbulence intensity is underpredicted near the wall, the prediction nevertheless agrees reasonably well near the centre of the pipe, where both prediction and experiment attain a minimum.

The calculated distributions of  $\ell_m$  and  $\ell$  are displayed in Fig.6.27(d). Although the predicted mixing length becomes infinite at the centre, it remains proportional to  $\ell$  over most part across the pipe, at a constant ratio of approximately 0.54, as revealed from the plot of  $\ell/\ell_m$ . This is identical to the outcome of Equation (4.2-7) for  $C_1$  equal to 0.09, implying that the flow is in local equilibrium over much across the pipe. As a further comparison, the predicted turbulent-kinetic-energy balance and the relevant experimental data of Laufer(1954) and Lawn (1971) are presented together in Fig.6.28. The agreement is considered satisfactory.

The comparison of prediction with experiments for a channel flow is displayed in Fig.6.29. The data to be compared are those of Laufer (1951). The comments for the comparison of the pipe flow are applicable to the channel flow also. However, inspection of Fig.6.29(b) reveals that the skin-friction is over predicted by about 10%. Examination of Laufer's data reveals that while the mean-velocity profile conforms with the log-law

(Equation 5.2-11), the constant  $E$ , obtained from these data takes a value much greater than 7.8, which is used in the calculations. That this disagreement is the main cause for over-prediction of the skin-friction is revealed by the good agreement in the velocity-defect plot shown in Fig.4.4, where the calculation is independent of Equation (5.2-11). There is reason to believe that Laufer's skin-friction measurement is in error. Nevertheless the important point to learn from the result of the comparisons shown in Figs.6.27 and 6.29 is that both the pipe and the channel flows are calculated correctly using the same set of constants as found applicable to external boundary layers.

#### 6.2-5 Wall-jet type boundary layers

When a stream of fluid is injected tangentially to a main stream, which is moving either at a higher or lower velocity than the injected fluid, a wall-jet flow is developed downstream of the injection slot. The comparison of the calculation with experiments to be presented will be restricted to constant - property fluids only.

##### Plane two-dimensional wall-jet flows

A detailed comparison of the measurements of Tailland (1970), for a plane wall jet in a stagnation surrounding, with the corresponding predictions is displayed in Figs.6.30 and 6.31. The streamwise variation of friction coefficient,  $\tau_s / (\rho U_{\max}^2)$ , is

plotted in Fig.6.30(b). Although both the growth rate and the velocity decay have been correctly predicted, the friction coefficient has been over-predicted by about 3%. Examination of the mean-velocity and shear-stress profiles displayed in Fig.6.31 reveals that the predicted positions of velocity maximum and vanishing shear are coincident while the measurements indicate that the latter lies closer to the wall than the former. The failure to predict the different positions of the velocity maximum and the vanishing shear lies in the use of the eddy-viscosity hypothesis of Equation (3.2-9); it implies that the mean-velocity gradient and the shear stress must vanish together. As has already been pointed out in Section 3.4-5, the use of Equation (3.2-9) implies the negligibility of shear-stress diffusion. However, near the point of zero shear in a wall jet, the diffusion of shear stress is no longer negligible compared to the generation of the shear stress..

Predictions by the incorporation of the shear-stress equation

One of the possible ways of accounting for the diffusion of turbulent shear is to solve the shear-stress transport Equation (3.3-5) in place of the eddy-viscosity hypothesis (3.2-9). A computer program for the two-equation model was modified to solve this additional transport equation. The constants  $\sigma_t$  and  $C_5$  in Equation (3.3-5) are taken as 0.9 and 0.235 respectively according

to the proposal of Hanjalic (1970);  $C_6$  is assumed equal to  $C_5$  according to the requirement that the shear-stress equation should reduce to the eddy-viscosity Equation (3.2-9) when the convection and diffusion of shear stress are neglected, as discussed in Section 3.3-4.

The results of calculation for the plane wall jet are plotted in dotted lines in Fig.6.31. Comparison of the earlier predictions reveals that the mean-velocity profile is in better agreement with the experiments in the near-wall region of the wall jet. A higher value of  $\tau_{\max}$ , however, is predicted as shown in Fig.6.31b, but this may be diminished by making more careful choice of the constants in the shear-stress equation.

#### Wall jets in a moving main stream

Fig.6.32 compares the predicted result with the semi-empirical correlation of Patel (1971) for a constant-property wall jet in a slower moving stream. The development of the flow proceeds from left to right in the diagram. As shown in these figures, the predictions agree well with Patel's correlation over most part of the flow but deviate progressively from the correlation at the right-hand side of the diagrams.

Fig. 6.33 presents the comparison of the predicted streamwise variation of the hydrodynamic as well as the heat transfer properties with the experimental

data of Kacker and Whitelaw (1968, 1971). Two cases of wall-jet flow are presented for comparison; one in which the injected fluid is at a higher velocity than the main stream ( $U_{\max,SL}/U_G = 2.3$ ) and the other in which the injected fluid is at a lower velocity than the main stream ( $U_{\max,SL}/U_G = 0.75$ ). For both cases, the prediction starts at ten slot heights from the jet exit. As revealed in Fig.6.33, all the hydrodynamic properties for the former case are well predicted. For the latter case, although the variation of the shape factor is reasonably well predicted, the agreement for  $R_2$  and  $s_S$  is rather poor. This may be due to the presence of lateral convergence in the flow. This can be seen far downstream of the injection slot where our calculations underpredict the skin-friction coefficient but overestimate the rate of increase of the momentum-deficit-thickness; since our calculations satisfy the integral momentum equation, the data must have suffered from the presence of lateral convergence.

Fig.6.33e presents the heat-transfer property of the wall jet in the form of the film-cooling-effectiveness, defined as the ratio of the temperature difference between the main-stream fluid and the wall to the temperature difference between the main-stream and the injected fluids. The agreement between predictions and data for both cases of flow is very good.

A detailed comparison of the predicted  $U$ ,  $\tau$  and  $e$  profiles with experiments for the case of

$U_{\max,SL}/U_G = 2.3$  are displayed in Fig.6.34. The profiles at 50 slot heights and 150 slot heights are compared. For both stations, the mean-velocity profile is well predicted, but the predicted  $\tau$  and  $e$  profiles deviate considerably from the experimental data. However, the calculations do predict a gradual decay of the turbulence quantities as the flow proceeds downstream.

#### Radial wall jets

Two cases of measurements of radial wall jets in a stagnation surrounding have been obtained in the experimental investigation described in the next Chapter. When the present two-equation model with the same constants were used to calculate the development of these flows, the growth rate  $y_1/\frac{r}{2}$  was found to be underestimated by as much as 40%; the predictions are shown in dotted lines, in Fig.6.35 where the relevant measurements are also displayed. Here, we encounter another defect in our turbulence model. It may be recalled that the last term in Equation (3.2-18) is modelled empirically as proportional to  $f$ , which is assumed to vary as a function of  $\ell/y$  according to Equation(3.2-16). However, it can be shown from the condition of self-similarity that, if a radial wall jet is to grow at the same rate as a plane wall jet, the length scale of the former should be about  $\sqrt{2}$  times that of the latter. But this increase in  $\ell$  in a radial

wall jet will also increase the magnitude of the last term in Equation (3.2-18) compared to the other terms, thus preventing the correct prediction of the radial wall-jet flow. To allow the two-equation model to predict the behaviour of radial wall jets correctly, it is required to modify the algebraic expression of  $f$ . Thus, the following formula is proposed;

$$f = \left[ C_4 \left( \frac{\ell}{y} \right) \left( 1 + C_7 \frac{\ell}{r} \frac{dr}{dx} \right)^{-1} \right]^q \quad (6.2-2)$$

$dr/dx = 1$  in radial flow

where  $C_7$  is a constant. It is chosen so that the turbulence model with the modified expression for  $f$  gives the correct prediction of the growth rate of self-similar radial wall jet ( $y_{1/2}/r = 0.085$ ): a value of 150.0 was found to be suitable.

The expression for  $f$  shown in Equation (6.2-2) possesses the following properties:

(i) for a plane flow,  $dr/dx$  vanishes and Equation (6.2-2) reduces to Equation (3.2-16),

(ii) as  $y$  approaches to zero,  $\ell$  becomes proportional to  $y$  according to Equation (4.2- 9); thus,

$$f = \left( \frac{C_4 \ell^q}{y} \right)$$

which is independent of  $r$ .

Although other forms of expressions for  $f$  have been tried,<sup>†</sup> the functional relationship of Equation (6.2-2) was found to be the most satisfactory.

The resulting predictions for two cases of radial wall-jet flows (cases a and b), shown by solid lines in Fig.6.35, are compared also with the relevant experimental data. As can be seen from the growth rates of the two flows, case (b) represents a wall-jet flow which is close to the state of self-similarity, while case (a) represents a developing radial wall jet. The predicted growth rate and velocity decay for both cases agree reasonably well with experimental data as shown in the figure. Comparisons for the mean-velocity, shear-stress, and turbulent kinetic energy profiles for case (b) are displayed in Fig.6.36. Examination of the mean-velocity and energy profiles reveals that, the height of the velocity maximum from the surface and the turbulence level were not correctly predicted, but, on the whole, the

<sup>†</sup> (i)  $f = \left[ C_4 C_1 y \left( \frac{\rho_e}{\tau_s} \right)^2 \right]^q$ ; the expression gives satisfactory prediction for radial wall jets but fails to predict correctly the developments of the wall boundary layers strong adverse pressure gradients.

(ii)  $f = \left[ \frac{C_4}{K C_1^2} \left( \frac{\partial \ell}{\partial y} \right)^2 \frac{\ell}{y} \right]^q$ ; the expression neither predicts the wall-jet flows nor the flat-plate flows correctly.

agreement between calculation and data is satisfactory. The agreement is perhaps the best justification for the proposed modification of the model.

### 6.3 Some comparisons of the present calculations with similar calculations from other methods

In the foregoing Section, we have compared qualitatively some of our calculations with a large variety of wall-boundary-layer measurements; in some cases our calculations agree well with the experimental data while in others there are disagreements between our predictions and measurements. Therefore, it is useful to compare some of those predictions with the predictions of other methods.

Calculations from a number of methods have been chosen for these comparisons. They entail the zero-equation mixing-length model of Patankar and Spalding (1970), the one-equation model of Bradshaw et al (1967), the three-equation model of Hanjalić (1970), and the five-equation model of Daly and Harlow(1970).

#### 6.3-1 Comparisons with simpler models

##### Statistical comparison for external wall boundary layers

The Stanford Conference on turbulent boundary layers stimulated interest in discrimination between various available procedures by comparison with a standard set of data. However, no quantitative measure

as to the accuracy of prediction of each individual procedure has been reported. Since the accuracy of each set of these experimental data varies to a considerable degree, a statistical comparison of the deviation of each procedure from the data should be more desirable.

Such a comparison between the Patankar-Spalding model, Bradshaw's model, and the two-equation model has been undertaken first by Ng and Spalding (1970b). The result of such an investigation is presented in Table 6.1.

model average value of the 18 runs	Patankar- Spalding	Bradshaw et al	two equ. model	two-equ. model proposed by Ng and Spalding (1971)
$\Delta H_{12}$	0.06	0.05	0.06	0.05
$\Delta s_S \times 10^3$	0.12	0.11	0.11	0.10
$\Delta R_2$	0.11	0.09	0.09	0.10

Table 6.1 Mean deviations of predictions from the data for three models of turbulence.

Table 6.1 lists the average value of  $\Delta H_{12}$ ,  $\Delta s_S$ , and  $\Delta R_2$ , calculated by the three models, for all the mandatory and optional-requested runs<sup>f</sup> of the Stanford Conference. The results calculated from the Patankar-Spalding model, Bradshaw's model, and the present two-equation model, are displayed in Columns 2 to 4 respectively. The entry in the fourth column contains

---

<sup>f</sup> exceptions are IDENT = 5000, 5300

the results calculated by an earlier version of the two-equation model (Ng and Spalding 1971), whose constants have been optimised with reference to wall-boundary-layer flow only.<sup>+</sup> The quantities  $\Delta H_{12}$ ,  $\Delta s_S$ ,  $\Delta R_2$  for each flow are defined by,

$$\Delta H_{12} = \frac{1}{N} \sum_{i=1}^N /_1 - \frac{H_{12,p}}{H_{12,ex}} /_i , \quad (6.3-1)$$

$$\Delta s_S = \frac{1}{N} \sum_{i=1}^N /s_{S,p} - s_{S,ex}/_i , \quad (6.3-2)$$

and,

$$\Delta R_2 = \frac{1}{N} \sum_{i=1}^N /1 - \frac{R_{2,p}}{R_{2,ex}} /_i . \quad (6.3-3)$$

Here N is the number of x-station values for which experimental values are available for  $H_{12}$ ,  $s_S$ , and  $R_2$  downstream of the starting point of the calculation; subscripts p and ex denote "predicted" and "experimental" respectively.

Mindful of the degree of accuracy of the Stanford data, which has been discussed in Section 6.2-1 inspection of the entries in Table 6.1 reveals that the three methods give about the same degree of accuracy

---

<sup>+</sup> constants proposed by Ng and Spalding (1971):

$C_1$	$C_2$	$C_3$	$C_4$	$\sigma_e$	$\sigma_1$	$\sigma_2$	q
0.1	0.84	0.55	2.16	2.0	1.2	2.0	4

statistically in the calculation of external wall boundary layers. The result is perhaps not surprising: most of the data collected are very near to the state of local equilibrium; as it may be recalled in Section 4.2 that, when local equilibrium prevails, these three models show many identical features.

#### Comparison for supersonic flows

Unlike incompressible flows, the absence of a large set of accurate supersonic boundary-layer measurements makes a statistical comparison less satisfactory. Therefore, the same three methods of calculation were compared quantitatively only for the two cases of supersonic flows measured by Sivasegaram (1969). In Figs. 6.21 and 6.22, curves showing the fractional deviation of the two other predictions from the predictions of the two-equation model are plotted under each sub-diagram. Inspection of these curves reveals that the predicted  $s_S$  and  $\delta_2$  by the three models differ by less than 5%. However, the predicted  $H_{12}$  by Bradshaw's model is about 20% larger than that by the two-equation model. Nevertheless, the difference is within the degree of uncertainty of the experiments. This can be seen from the data of  $H_{12}$  displayed in Figs. 6.21 and 6.22, in which more than 20% change in  $H_{12}$  due to a 10% change of the recovery factor used in the evaluation of the experimental  $H_{12}$ , is observed.

### 6.3-2 Comparisons with higher-order models

A statistical comparison of the Stanford data for Hanjalić (1970) and the Daly-Harlow (1970) models is being undertaken by the present writer and will be reported separately. The comparison of predictions from the two-equation model and some other higher-order models will be restricted to the hydrodynamic properties of developed channel flows and wall-jet flows only. The former flows are capable of prediction by most of the higher-order models as well as by some simpler models but the latter flows are unlikely to be predicted accurately by simpler models.

#### Developed flow in a channel

Fig. 6.29 also reproduces the prediction by Daly and Harlow (1970) for Laufer's channel flow experiment. Inspection of both the predicted velocity profile and turbulence quantities displayed in the figure reveals that the two-equation model give predictions which are no worse than and in many respects closer to the measurements than the higher-order model of Daly and Harlow. Although higher-order models should offer closer approximation to the actual turbulence motion by the use of a larger number of transport equations, they do not however, always give more accurate results; this is because in general, they require a larger number of constants than simpler models, all of which have to

be optimised accurately to give the correct predictions.

#### Plane wall jet in a moving main stream

Fig. 6.34 also displays the  $U$ ,  $\tau$ , and  $e$  profiles predicted by Hanjalic (1970), for the film-cooling measurements of Kacker and Whitelaw (1971). Comparison of the accuracies of prediction by the two-equation model and by Hanjalic's model shows that, the general features of the flow are predicted to the same degree of accuracy by both methods. However, the use of the shear-stress-transport equation in the latter model to account for the diffusion of turbulent shear, results in more accurate prediction near the region of velocity maximum and zero shear. The implication of the use of the shear-stress equation has been discussed in Sections 3.3-4 and 6.2-5.

#### 6.3-3 Concluding remarks from the comparisons with other models of turbulence

Although it is limited to the hydrodynamic behaviour of wall boundary layers, the comparison of the predictions by the two-equation model with those by other simpler models shows that the former are as accurate as the latter.

However, the greatest merit of using the two equation model is that there are boundary-layer flows for which the two-equation model is capable of correct

predictions, while simpler models would fail. Two examples will suffice to emphasize this point. The mixing-length hypothesis allows all the free-jet flows to be predicted quite well, but only if the ratio of the mixing length to the layer thickness has a different value for each flow. The present model, on the other hand, allows all the flows to be predicted with a single set of constants. The second example concerns the wall-jet flow. We have calculated satisfactorily the main features with the present model; whereas the simpler model of Bradshaw et al provides no predictions in which the shear stress exhibits both positive and negative values.

However, when the two-equation model is compared with higher-order models, it must be expected that the latter possess a greater ability to fit a larger range of experimental data. For example, models which use a shear-stress equation instead of the eddy-viscosity hypothesis should be better equipped to predict wall-jet flows.

Higher-order models, however, take longer time to develop; and as a result, it is not possible to put to any solid conclusion from this limited demonstration that there are greater merits in using higher-order models than the two-equation models for the prediction of boundary layers. Furthermore from the user's point of view, higher-order models will require more computer

time to solve the larger number of differential equations. The two-equation model appears to be a satisfactory compromise between accuracy of the solution and economy of execution.

CHAPTER 7EXPERIMENTAL INVESTIGATION OF RADIAL WALL JETS7.1 Introductory remarks

The calculation procedure for two-dimensional turbulent boundary layers developed in CHAPTERS 3 and 4 rests on the assumption that a number of terms in the exact equations are reducible to universal functions which include a number of empirical constants. Although the equations and their constants had been shown to work favourably in plane boundary layers and pipe flows, it was nevertheless found that modification to the model was required in order to predict radial wall-jet flow correctly. The essence of this Chapter is to report the measurements of radial wall jets used for the comparison with the two-equation model predictions.

A radial wall jet is resulted from one of the two cases of flow (a and b) shown in Fig. 7.1. In case(a), the impinging jet is close to the wall and the jet is deflected by both the wall and the circular flange fixed at the jet exit. In case (b) the distance between the jet exit and the wall is large compared with the jet diameter such that the jet is deflected by the presence of the wall only. Radial wall jets are common occurrence in process engineering and in aerospace engineering. Therefore, the understanding of the radial wall-jet

<sup>on</sup>phenomenon is of great practical importance. There is another welcoming aspect to the study of radial wall-jet flows, i.e. side-wall effects, which very often interfere with the wind-tunnel experiments, are absent in such flows, allowing a truly two-dimensional flow. The measurement of the development of radial wall jet in a stagnation surrounding forms the basis of the present investigation. Both the mean velocity and the turbulence correlations are reported in Section 7.7.

## 7.2 A survey of previous investigations

To the best of the writer's knowledge, the first experimental investigation of radial wall jet was performed by Bakke (1957) whose work was stimulated by the earlier theoretical investigation of Glauert (1956). Other experimental investigations of the hydrodynamic aspects of radial wall jets were reported by Bradshaw and Love (1959), Hodgson (1962), Poreh et al (1967), Jayatelleke (1969), and Baker (1969). All these investigations are summarised in Table 7.1. It is obvious from the Table that, although all the data show that the wall jet grows proportionally to the radius from the axis of symmetry, there is lack of general agreement as to the rate of growth reported by different investigators. For example, the reported growth rate varies from 0.046 as reported by Jayatelleke to 0.093 by Poreh et al and only recently, Nakatogawa et al (1970)

Investigator/s	Geometry of jet exit	Range of experiment	velocity transducer used	measurements taken	$\frac{Y_1}{r}$ deduced from measurements
Bakke (Ref.3)	$Z_1 = 1.5 \text{ cm}$ $r_1 = 6.3 \text{ cm}$	$14.3 \text{ cm} \leq r \leq 30.3 \text{ cm}$	Pitot-tube	$U$	0.077
Bradshaw and Love (Ref.16)	$Z_2 = 50 \text{ cm}$ $r_2 = 2.54 \text{ cm}$	$12.6 \text{ cm} \leq r \leq 51 \text{ cm}$	Yaw-meter	$U$	0.085
Hodgson (Ref.65)	$Z_1 = 1.91 \text{ cm}$ $r_1 = 7.62 \text{ cm}$	$11.4 \text{ cm} \leq r \leq 30.5 \text{ cm}$	hot wire	$U, \overline{u^2}, \overline{v^2}$	0.085
Poreh et al (Ref.112)	$Z_2 = 61 \text{ cm}$ $r_2 = 2.54, 7.62, 5.08 \text{ cm}$	$45.7 \text{ cm} \leq r \leq 168 \text{ cm}$	hot wire	$U, \overline{u^2}, \overline{v^2}, \overline{w^2}, \overline{uv}, \text{skin friction by friction balance}$	$= 0.098 \left( \frac{r}{r_2} \right)^{-1}$ $\approx 0.093 \text{ at } \frac{r}{r_2} \text{ equal to } 1.75$

Table 7.1 continued.

Jayatelleke (Ref.67)	$Z_1 = 0.165$ $0.508$ $0.567 \text{ cm}$ $r_1 = 7.5 \text{ cm}$	$7.5 \text{ cm}$ $< r <$ $31.8 \text{ cm}$	Pitot-tube	U	0.046
Baker (Ref.1)	$Z_1 = 0.254 \text{ cm}$ $r_1 = 7.6 \text{ cm}$	$7.6 \text{ cm}$ $< r <$ $35.5 \text{ cm}$	Pitot-tube	U	0.054

Table 7.1

Survey of experimental data of radial wall jet;  $r_1$  = radius of wall jet exit slot;  $Z_1$  = slot height;  $r_2$  = radius of the impinging jet;  $Z_2$  = height of the impinging jet.

reported that the growth rate of a radial wall jet should be 0.0683. Far downstream, the radial wall jet should attain a self-similar form, and therefore, should be independent of its inlet conditions. However, some of the disagreement of the results listed in Table 7.1 may be the result of measurements not far enough downstream of the exit. To illustrate this point, the data of Jayatelleke (1969) are plotted as  $\frac{Y_1}{2}$  vs  $r$  in Fig. 7.6. This figure shows that,  $\frac{Y_1}{2}$  is only proportional to  $r$  near the downstream end of the region of experiment. If the wall jet is self-similar, then, according to the boundary-layer equations, not only the mean-velocity, but also the turbulence quantities should exhibit self-similarity also. However none of the investigators listed in Table 7.1 have made enough detailed turbulence measurements as to aid such a clarification. Although some turbulence intensity measurements have been reported by Hodgson (1962) and Poreh et al (1967), only the latter provided some shear-stress distribution profiles. But, they show such a large scatter (see Fig. 7.16) that it is difficult to draw any complete conclusion as to whether the wall-jet data reported attained self-similarity or not.

Another possible cause for the difference in the reported growth rate may be due to the different velocity transducers used in each investigation. As shown in Table 7.1 the measurements are made with either total head Pitot-tube (including yaw-meters) or constant-temperature hot wires. Their different characteristic

response in low speed flows with a high turbulence level, as those existing in radial wall jets, may result in different measured velocity profiles. In particular, the Pitot-tube is likely to underestimate the mean-velocity profiles of flows with high turbulence levels due to the presence of large instantaneous yawing angles (see Fig. 7.7). This effect will contribute a large error in radial wall-jet measurements, where the local turbulence level,  $e^2/U^1$ , is greater than 40% over most part of the wall jet as displayed in Figs. 7.12(f) and 7.13(f). Another important influence in pitot-tube measurements is its response at low-speed flows. MacMillan (1954) has reported that corrections have to be made for Pitot-tube measurements at low speed flows, depending on the size of the pitot. As the range of velocities in a radial wall jet spans from its local maximum to zero at the stagnation surroundings and at the non-slip wall, large corrections may be required in part of the measurements.

On the other hand, both the mean-velocity and turbulence levels can be calculated from the output signals of the hot wire as shown in Appendix 4. Furthermore, an indirect check on the accuracy of the hot-wire measurements can be provided from the comparison of the measured shear stress with that deduced from the integration of the momentum equation.

An example of the difference in measurements of a radial wall-jet profile by Pitot-tubes and hot wires is displayed in Fig. 7.8. In this figure, the same

velocity profile, measured by two Pitot-tubes of different configuration, is compared with that measured by a constant-temperature hot wire. One of the Pitot-tubes was a 0.82 mm diameter tubular probe and the other was a flattened pitot with 0.10 mm by 1.01 mm rectangular opening; the latter is identical to that used by Jayatelleke. During the course of the pitot measurements, negative total heads were measured on the outer edge of the wall jet, but these readings have not been displayed in the figure. This phenomenon<sup>6n</sup> has formerly been observed by Bradshaw and Gee (1960), Heskestad (1965), and Jayatelleke (1969) and is due to the severe yawing of the total velocity vector in the presence of entrainment at the outer edge. Fig. 7.8 shows that the resulted  $\frac{Y_1}{2}$ 's from the three measurements differ by as much as 15%.

### 7.3 Object of the experimental investigation

In the light of the findings discussed in the foregoing section, it was decided to carry out new measurements for radial wall jets in stagnation surroundings. The area of enquiry will be restricted to the mean-velocity profiles and all other second-order turbulence quantities, specifically,  $\overline{u^2}$ ,  $\overline{v^2}$ ,  $\overline{w^2}$ , and  $\overline{uv}$ . Through these measurements, we hope (a) to establish the asymptotic growth rate of the radial wall jet, and (b) to provide suitable experimental data for the basis of assessment of the two-equation turbulence model.

#### 7.4 Methods of measurements and data reduction

The difficulties of obtaining reliable velocity data of radial wall jet from Pitot-tube measurements have been discussed in Section 7.2. Hence it was decided to employ constant-temperature hot wires for both mean-velocity and turbulence measurements in the present investigation. Many previous investigators have proposed ways of calculating the mean velocity and turbulence correlations from the output of hot-wire signals. An examination of these methods in Appendix 4 leads to the proposal of interpreting the mean and turbulence quantities from signals generated when a single wire was placed at four different angles relative to the direction of flow. The values of  $U$ ,  $\overline{u^2}$ ,  $\overline{v^2}$ ,  $\overline{w^2}$ , and  $\overline{uv}$ , were calculated from Equation (A.4-7 to A.4-11) when the d.c. and a.c. components of the hot-wire signals were measured. In practice, it is difficult to repeat measurements at the identical position for each traverse of the hot-wire at one of the four inclinations to the flow, so interpolations are required. The interpolations and the solutions of Equations (A.4-7 to A.4-11) were calculated in a data-reduction program, by a CDC6600 computer.

#### 7.5 Experimental apparatus

##### 7.5-1 The test plate and nozzle assembly

The experiments reported below were carried out with two types of nozzles blowing normally on to a

test plate, the general arrangements of which are shown in Fig. 7.2 and are designated as case(a) and case (b) respectively; the dimensions of these nozzles and test plate are also displayed.

The test plate was a 0.91 m square by 0.95 cm thick aluminium plate, mounted vertically on a steel frame, which was separated from the mounting frames of the nozzle and the traversing mechanism of the hot wire. This was to prevent the transmission of any possible mechanical vibrations. The test-plate mounting has three foot screws and a screw jack, which permitted adjustments of the "square-ness" of the plate with respect to the impinging nozzle. Three identical Pitot-tubes were mounted on the plate, at  $120^{\circ}$  pitch, and at 43 cm radius from the centre of the plate. Furthermore, the height of these pitots was fixed at 1 cm so that symmetrical flow was assured when the three pitots showed identical readings.

For the nozzle assembly in case (a), air was delivered from a centrifugal fan through a plenum box and a 7.6 cm bore PVC pipe of 3.05 m long (see Fig.7.3a) The length of the pipe was necessary to eliminate any presence of swirl in the jet. The compressed air was regulated to within  $\pm 1$  deg. C of the ambient temperature at exit by an automobile radiator fitted inside the plenum box. Before entering the fan, air was passed through an electronic air cleaner to remove dust particles larger than 0.03 microns.

The nozzle and plate assembly of case (b) was set up after it had been realised that it was not possible to obtain a self-similar wall jet within the range of measurements in case(a), due to the limited size of the test plate. However, instead of changing to another larger test plate, further measurements were carried out using a smaller size nozzle as shown in Fig.7.2(b). The air supply system is shown in Fig.7.3(b). In this case, no air cooler was necessary as it was found that within the required range of flow rate, the compressed air was at the same temperature as the ambient surroundings. The optimum height of 2.54 cm of the nozzle from the test plate surface was chosen after a preliminary investigation. By traversing a single wire at a fixed radius of 27 cm from the axis of symmetry each time the impinging distance  $Z_2$  is increased, it was found that, when  $Z_2$  was greater than 1.9 cm, the height of the wire at which its mean d.c. signal equals to half the maximum value remained unchanged. In this investigation the mass flow rate of the compressed air was kept nearly constant at 0.03 kg/min, but the increase of flow rate by 50% was found to give very much the same result.

#### 7.5-2 Instrumentation

The items of the measuring instruments are listed below:

1. A probe traversing mechanism mounted on a GRIMSTON

No.1 compound table as shown in Fig.7.4. The combined span of the traverse is 65 cm by 15 cm.

2. A cathetometer, mounted on another compound table fitted with a dial gauge, as shown in Fig.7.4 to locate the exact distance of the hot wire from the test plate.

3. A DISA 55A01 constant-temperature hot-wire anemometer, DISA 55D10 lineariser, DISA 52B30 true integrator, DISA 55D35 rms voltmeter, FENLOW 301-A digital voltmeter, TELEQUIPMENT D53 oscilloscope. These instruments are shown in Fig. 7.5. A TEKTRONIC 564 storage oscilloscope was used in taking photographs of the hot-wire traces shown in Fig. 7.17.

4. DISA 55F04 gold-plated boundary-layer probe, DISA 55F02 gold-plated 45° slanting probe used in all the measurements.

5. A low turbulence level ( $\sqrt{u^2}/U \approx 0.4\%$ ) hot-wire calibration wind tunnel with adjustable flow rates from 0 to 50 m/s; the tunnel and its accessories have been described by Melling (1970).

6. A verticle U-tube manometer, with 90 cm long columns filled with paraffin (s.g. 0.787), was used to measure mean velocities above 40 m/s. For velocities below 40 m/s, a micro-manometer capable of reading an accuracy of a head of 0.02 mm of paraffin was used; the micromanometer has been described by Baker (1971).

## 7.6 Operating procedure

### 7.6-1 Setting up of the test plate and the nozzles

Before the test plate was placed against each of the nozzles, Pitot-tube traverses across the nozzle exit were made to ensure that the impinging jets were indeed axisymmetrical. At the start of each run, the nozzle was first located centrally and perpendicular to the test plate. The correct height of the nozzle from the plate was checked by means of slip gauges. When the air supply was turned on, finer adjustments of the plate were made, when necessary, to obtain identical readings from the three fixed Pitot-tubes mounted on the plate.

### 7.6-2 Hot-wire calibration

The linearised hot wire was calibrated before and after each set of runs, which normally lasted about four to five hours. A typical calibration curve is shown in Fig. 7.9. If the slope of the two calibration curves differed by more than 5%, the set of runs would be rejected. Otherwise, the calibration curve for each run was linearly interpolated between the two curves.

### 7.6-3 Method of measurements

In accordance with the results of the analysis in Appendix 4, each experimental station was traversed by single wires placed at four different

inclinations to the main stream. The boundary-layer probe (55F04) was first traversed over all the experimental stations. It was then replaced by the 45° slanting probe (55F02), and the procedure was repeated with the probe in each of the three inclinations.

For case (a), the first station of the measurements is at the exit of the nozzle, but for case (b), the first station is 7.3 cm from the nozzle exit; no measurements were taken closer to the nozzle because the thickness of the wall jet in this region was no longer large compared with the length of the hot wire.

#### Determination of the distance of the hot wire from the wall

Each traverse was always started at the farthermost point from the test plate. At three different positions, the distance between the hot wire and its optical image was measured by the cathetometer, mounted on a compound table which traversed at right angle to the plate as shown in Fig. 7.10. Since both the object and its image remained at the same distance from the cathetometer, no re-focusing of the cathetometer was required during the measurement.

#### The constant-temperature hot-wire circuitry

The block diagram of the hot-wire circuitry is displayed in Fig. 7.11. During each traverse of the hot wire, both the mean and r.m.s. voltage were recorded. The rms-meter was operated at the maximum

integration time-constant of 30 seconds, and the mean voltage was taken over a period of 200 seconds throughout the experiments. However, for case (a) the mean voltage was read direct from the digital voltmeter because the integrator was not available at the time of the experiment. In all the measurements, the hot wire was operated at an overheat ratio of 1.8 and with a high frequency cutoff at 10 kHz.

### 7.7 Presentation and discussion of results

The readings taken for cases (a) and (b) were processed in a CDC 6600 digital computer to obtain the profiles of  $U$ ,  $\overline{u^2}$ ,  $\overline{v^2}$ ,  $\overline{w^2}$ ,  $e$ , and  $\overline{uv}$  according to Equations (A.4-7 to A.4-11). These profiles for each station were tabulated in Appendix 5.

#### 7.7-1 Mean velocity and turbulence quantities of the wall jets

The mean velocity, the turbulent shear stress, the three components of turbulence, and the turbulent kinetic energy of each station, for both cases (a) and (b), are displayed in Figs. 7.12 and 7.13 respectively. Each of these profiles is nondimensionalised by its local  $U_{max}$  and  $y_{\frac{1}{2}}$ . The reader may notice that the scatter of the mean-velocity profiles for case (a) is greater than the corresponding profiles of case (b); this is entirely the result of the much shorter averaging time of output hot-wire bridge voltage in case (a) compared with case (b),

where each signal was integrated over a period of 200 seconds. The intermittent character of the turbulence of the radial wall jet can be seen from the traces of the hot-wire signal shown in Fig. 7.17. Four traces at different distance from the wall were taken with a straight wire placed normal to the flow, the duration of the trace being one second. It can be seen that long integration period is necessary, especially near the outer edge of the wall jet.

Examination of Fig. 7.13 reveals that while the mean-velocity profile attains its self-similar form much more readily, the turbulence quantities do not become self-similar until much further downstream. However, the shear-stress and  $\overline{u^2}$  profiles tend to become self-similar earlier than the  $\overline{v^2}$  and  $\overline{w^2}$  profiles. This can be seen from the measurements displayed in Figs. 7.13(b) to (e); both the  $\overline{uv}$  and  $\overline{u^2}$  profiles are found to attain their self-similar shape at the second station, but  $\overline{v^2}$  and  $\overline{w^2}$  do not become self-similar until the third station. This is in agreement with the Navier-Stokes equations because in a two-dimensional boundary layer, energy taken from the mean motion of the fluid is first converted into  $\overline{u^2}$ , which is then transferred to the other two components of fluctuation through the action of pressure fluctuations, as shown in Equations (2.3-1 to 3). The phenomenon discussed above has been observed in many free shear flow experiments like those of Wygnanski and Fiedler (1969) and Champagne et al (1970).

For case (a), the turbulence quantities do not exhibit a self-similar state within the range of the measurements.

#### 7.7-2 The rates of growth and mean velocity decay of the radial wall jets

The measured development of  $y_{\frac{1}{2}}$  and  $U_{max}$  for both cases (a) and (b) are displayed in Figs. 7.14 and 7.15 respectively. For case (b),  $y_{\frac{1}{2}}$  is found to be proportional to  $r$ , the constant of proportionality, i.e. the growth rate, being 0.085. However, the decay of  $U_{max}$  is found to vary as  $r^{-1.15}$ , as shown in Fig. 7.15. The exponent is smaller than -1, which is the value found in the decay of a fan jet (Heskestad 1966), and which is also the value should perfect similarity prevail in a wall jet; the departure of the exponent from unity, albeit small, shows the slight Reynolds number dependence of the flow.

For case (a), the growth rate does not attain a constant value; this and the lack of self-similarity of the turbulence quantities displayed in Fig. 7.12 show that the radial wall jet of case (a) was not yet fully developed within the range of measurements.

#### 7.7-3 Positions of vanishing shear stress and velocity maximum

Examination of the mean velocity and  $\bar{uv}$  profiles in Fig. 7.12 and 7.13 reveals that the position of zero shear and the position of velocity maximum do not

coincide. In particular, the heights at the point of velocity maximum and at the point where  $\bar{uv}$  vanishes are 0.2 and 0.075 of  $y_{\frac{1}{2}}$  respectively as shown in Figs. 7.13(a) and (b). The non-coincidence of these two points in wall jets has previously been confirmed by Bradshaw and Gee (1960). Poreh et al (1967), Tailland and Mathieu (1967, 1970), Manian and Besant (1969) and Kacker and Whitelaw (1971).

#### 7.7-4 Accuracy of the measurements

The accuracy of the results presented is affected by two factors: the accuracy of the measuring equipment and the correctness of the method used in the data reduction.

The accuracy of the hot-wire anemometer and the other electronic equipments used depends to a very large extent on frequency of the turbulence to be measured. As this differs at different parts of a radial wall jet, it is therefore not possible to quote an absolute figure on the accuracy of the instruments.

Three factors contribute to the data-reduction inaccuracies.

(i) The most important factor is the accuracy of the hot-wire calibrations. As shown in Fig.7.9, the calibration curve is indeed linear and the variation of the constant of proportionality  $K$  in Equation (A.4-2) is under 2% within the range of velocity encountered in the experiments.

(ii) The accuracy of the method of calculation of the mean and turbulent quantities from Equations (A.4-7 to A.4-11) is difficult to estimate without the knowledge of the other higher-order correlations, which we have neglected in the analysis. However, these higher-order correlations must be small compared with the second-order correlations in low or moderate turbulence level.

We have also neglected the V - component of the mean velocity in the calculations. However, this should not cause large error in the results. As can be seen from the V - profile displayed in Fig. 7.13a, V is less than 2% of  $U_{max}$  over most of the wall-jet thickness. Nevertheless, near the outer edge of the flow, V/U should approach infinity, implying that the neglect of V in this region can cause large error in the results.

(iii) The last factor is the determination of the effective centre of the hot wire. In our measurements this was treated as the geometrical centre. In places where the scale of turbulence is small compared with the length of the wire or where there is a large mean-velocity gradient, the effective centre of the wire may deviate from its geometrical centre. The former effect has been investigated by Wyngaard (1968) and the latter by Gessner and Moller (1971); the results of these investigations showed that these effects can cause error in the estimation of the turbulence quantities.

Clearly, with all the uncertainties discussed above, the accuracy of the measurements differs at different

parts of the wall jet. Therefore, instead of estimating the possible errors quantitatively, we shall demonstrate the accuracy of the measurements through qualitative means.

Comparison of the measured turbulent shear stress with that deduced from the momentum equation

A comparison of the measured shear stress with that calculated from the momentum equation and continuity equation for case(b) is shown in Fig. 7.13(b). The calculated shear stress was determined from the integration of the following equations for radial flows;

$$\frac{\partial U}{\partial r} + \frac{U}{r} + \frac{\partial V}{\partial y} = 0 \quad , \quad (7.7-1)$$

$$U \frac{\partial U}{\partial r} + V \frac{\partial U}{\partial y} + \frac{\partial}{\partial r} (U^2 - V^2) + \frac{(U^2 - V^2)}{r} + \frac{\partial \bar{U}\bar{V}}{\partial y} - \nu \frac{\partial^2 U}{\partial y^2} = 0 \quad , \quad (7.7-2)$$

where the mean velocity,  $U$ , is given by the measured profiles of the last two stations of case (b). The wall shear stress,  $\left[ \frac{\partial U}{\partial Y} \right]_{Y=0}$ , is calculated from the parabolic fit from the wall to the nearest two points of measurement close to the wall.

From Fig. 7.13 (b), it can be seen that the shear stress measured directly by the hot wire is less than that deduced from Equations (7.7-1 and 2). In particular the difference is about 12% at  $y_2$ . This may be due to some of the uncertainties discussed previously. In particular, the underestimation of the measured shear stress may be due to the special characteristics of the rms meter used in the measurements, which has a low

frequency cutoff of 1 Hz<sup>f</sup>. Wygnanski and Fiedler (1969) have reported that, in jet measurements as large as 10% of the turbulent shear lies below the frequency of 1Hz. If the same is true in radial wall jets, the 1 Hz cutoff will result in the underestimation of the shear stress.

The effect of the normal turbulent stresses and centrifugal stresses in the estimation of shear stress from Equation (7.7-2)

If the centrifugal-stress (fourth) term in Equation (7.7-2) is neglected in the calculation of the shear stress, a shear-stress profile, as shown in the chain-dotted line in Fig.. 7.13(b) is obtained. The shear stress in this case is underestimated by as much as 12%. However, when both the centrifugal-stress term and the normal-stress (third) term are neglected, the shear-stress profile is underestimated by about 7%. Thus it is shown that the centrifugal and normal stresses are by no means negligible compared with the shear-stress diffusion in a radial wall jet. Nevertheless, their contributions to the transfer of momentum are opposite to each other.

Comparison of the measured shear-stress profiles with those measured by Poreh et al (1967)

The  $\tau$  profiles for a radial wall jet were measured by Poreh et al (1967). Fig. 7.16 displays the comparison between their measurements and those from

---

<sup>f</sup> DISA manual 55D35

case (b) of the present investigation. The comparison reveals that, apart from the smaller scatter of the present measurements, they also display a larger maximum of the shear-stress profile than those obtained by Poreh et al.

#### 7.8 Conclusion from the experimental investigation

Examination of the growth rates in Fig. 7.14, the velocity decays in Fig. 7.15, and the mean-velocity and turbulence profiles in Figs. 7.12 and 7.13, reveals that a nearly self-similar flow has been attained in the radial wall jet of case (b) but not in case (a). The growth of  $y_{\frac{1}{2}}$  in case (b) was found to be proportional to the radius and furthermore, the rate of growth is equal to 0.085, which agrees with the findings of Bradshaw and Love (1959) and Hodgson (1962) although each of these experiments had a different nozzle geometry at the exit, showing that the growth rate of a self-similar wall jet is independent of its inlet conditions. The rate of maximum velocity decay was found to vary as  $U_{\max} r^{-1.15}$  for case (b).

The difference in the position of velocity maximum and zero shear is further confirmed in the present measurements. In particular, the height of the point at maximum velocity and the point of zero shear are 0.2 and 0.075 of  $y_{\frac{1}{2}}$  respectively.

Comparisons of the two cases of radial wall jets with the predictions from the two-equation turbulence model have been given in Chapter 6.

CHAPTER 8CONCLUSION8.1 Principal results of the present investigation

The main conclusions resulted from the present study are listed below:

1. The review of the available literature on the prediction of turbulent boundary layers in Chapter 2 has pointed to the necessity of formulating turbulence models which calculate the turbulent kinetic energy and length scale distributions from transport equations.

2. A two-equation model, which solves the turbulent kinetic energy and a length scale from two differential equations, was developed in Chapters 3 to 5. These differential equations contain a number of empirical constants, the values of which were fixed with reference to some well known experimental data. It was found that the present model predicts accurately a large number of characteristics of both free and wall boundary layers with only a single set of the constants.

3. Close to the wall, in the viscous sublayer, where the Reynolds number is small, the constants in the model will no longer have a unique value but become functions of Reynolds number of turbulence. The problem of finding the correct functions has been bypassed in the present study by matching the integration of the

differential equations with a set of well known semi-empirical formulae near the wall. This was discussed in Chapter 5.

4. The model can be readily "upgraded" to a higher order models by the introduction of additional transport equations, e.g. equation for shear stress or equations for the three components of the turbulent kinetic energy. The inclusion of some of these equations in the turbulence model may be necessary wherever the diffusion or the convection of these properties are significant. The incorporation of the shear-stress equation in the two-equation model for the calculation of a plane wall jet has been demonstrated in Chapter 6.

Heat transfer in boundary layers was calculated from the enthalpy-transport equation, which was solved simultaneously with other differential equations of the turbulence model.

5. The comparison of the calculations for the present turbulence model with the experimental data revealed that the predictions agree with the data to the accuracy achievable in the measurements. The comparison which was discussed in Chapter 6, included both the hydrodynamics and heat transfer of incompressible and compressible boundary layers.

For the case of a radial wall jet, one of the constants in the model has to be modified in order to procure agreement between predictions and experiments.

6. The comparison of some of the above predictions with those calculated from other turbulence models revealed that wherever these models were applicable, they gave results very similar to the predictions of the present two-equation model. Moreover, multi-equation models available at present were not found to give much more accurate predictions than the present two-equation model.

7. The experimental investigation reported in Chapter 7 showed that a self-similar radial wall jet grows at a uniform rate with  $y_{\frac{1}{2}}$  equal to 0.085 of  $r$ . The self-similarity of the wall jet was confirmed by the self preserving nature of the measured shear-stress and turbulence-intensity profiles.

#### 8.2 Recommendation for further research

The two-equation model investigated in the present study has been shown to predict accurately a large variety of two-dimensional boundary layers. Nevertheless, there is still scope for further improvements and refinements, upon which even more promising predictions may result from the model.

Firstly, there still exist a number of boundary-layer flows in which the two-equation model will fail to predict correctly without some modifications of the model. The calculation of the radial wall jet discussed in Chapter 6, provides an example, in which one of the empirical constants has to be modified. Similar difficulty

is encountered in the calculation of round jets (see Rodi 1971). Of all the models known to the writer which have been applied to the prediction of round jets, at least one of the constants has to be changed in order to procure agreement. Perhaps, the change of constants may be avoided by solving higher-order transport equation at the expense of the economy of the calculation. On the other hand, the range of applicability for the two-equation model can be enlarged without the introduction of more differential equations, if suitable formulae for the variation of some of the constants are established. For lack of reliable data of higher-order correlation measurements, the latter approach may prove to be more fruitful at present.

Another problem is the dependence of the constants on Reynolds number. Although this has been bypassed in the present study as discussed in Chapter 5, the Reynolds number effect on the constants is critical in the correct predictions of the viscous sublayer near the wall, and the laminarisation of the flow when it is subjected to sudden and severe acceleration. Recent theoretical investigation of the laminarised boundary layers by Jones and Launder (1970) has yielded encouraging results when the constants in the energy-dissipation model were varied according to a set of semi-empirical functions of Reynolds number of turbulence. There should be no difficulty in employing a similar approach to the present two-equation model.

The two-equation model has only been applied to two-dimensional boundary layer flows; its validity in recirculating flows has still to be verified. With the availability of fast computer techniques for the solving of two-dimensional elliptic equations, e.g. the procedure reported by Gosman et al (1969), the test provides the next logical step of the research. The ultimate goal is the prediction of three-dimensional turbulent flows. For this, however, we have to await the development of a suitable solution procedure. Already, there are encouraging developments in this direction recently, which have been reported by Patankar and Spalding (1971).

At the time of writing, there are already a number of two-equation models which have been developed and tested against different types of boundary layer flows. As discussed in Chapter 3, these models differ essentially only in the way in which the diffusion of the length scale is modelled. Considering the degree of approximation involved in arriving at these equations, it is difficult to determine which of these formulations are more suitable. The ultimate choice will lie on the accuracy of the predictions and the universality of the model. We are making some comparisons of boundary layer calculations with other two-equations turbulence models, but further computations are required to complete the picture.

REFERENCES

1. Baker, E. "Influence of mass injection on turbulent flow near walls." in Progress in Heat and Mass Transfer (Edited by Grigull, U., and Hahne, E., Pergamon Press 1969) Vol.1, p.99.
2. Baker, R.J. "Transpired turbulent boundary layer with streamwise pressure gradient." Ph.D. Thesis, Lond. U. (1971).
3. Bakke, P. "An experimental investigation of a wall jet." J.Fluid Mech. 2, 467 (1957).
4. Batchelor, G.K. The Theory of Homogeneous Turbulence. (Cambridge University Press, 1953).
5. Batchelor, G.K., and Townsend, A.A. "Decay of isotropic turbulence in the initial period". Proc.Roy.Soc. 193A, 539(1948a).
6. Batchelor, G.K., and Townsend, A.A. "Decay of turbulence in the final period." Proc.Roy.Soc. 194A, 527 (1948b).
7. Beckwith, I.E. and Bushnell, D.M. "Detailed description and results of a method for computing mean and fluctuating quantities in turbulent boundary layers." NASA TN -D-4815, (1968).
8. Bradbury, L.J.S. "The structure of a self-preserving plane jet. J.Fluid Mech. 23, 31 (1965).
9. Bradshaw, P. "Prediction of the turbulent near-wake of a symmetrical aerofoil." AIAA J. 8, 1507 (1970).
10. Bradshaw, P. "Calculation of three-dimensional turbulent boundary layers." J.Fluid Mech. 46, 417 (1971).
11. Bradshaw, P. and Ferriss, D.H. "The response of a retarded equilibrium turbulent boundary layer to the sudden removal of pressure gradient." NPL Aero. Rep. 1145 (1965).
12. Bradshaw, P. and Ferriss, D.H. "Calculation of boundary layer development using turbulent energy equation VIII compressible heat transfer." NPL Aero. Rep. 1325 (1970).
13. Bradshaw, P. and Ferriss, D.H. "Calculation of boundary layer development using the turbulent energy equation - compressible flow on adiabatic walls." J.Fluid Mech. 46, 83 (1971).

14. Bradshaw, P., Ferriss, D.H. and Atwell, N.P. "Calculation of boundary-layer developments using the turbulent energy equation." *J.Fluid Mech.* 28, 593 (1967).
15. Bradshaw, P. and Gee, M.T. "Turbulent wall jets with and without an external stream" *A.R.C. R.& M.* 3252 (1960).
16. Bradshaw, P. and Love, E.M. "The normal impingement of a circular air jet on a flat surface." *A.R.C. R & M* 3205 (1959).
17. Bradshaw, P. and Wong, F.Y.F. "The relaxation of a turbulent shear layer after reattachment." *I.C. Aero Dept. Rep.* 71-05 (1971).
18. Bruun, H.H. "The performance of normal and yawed hot wires." *I.S.V.R. Rep. TR No.* 21 (1969).
19. Cebeci, T. "Calculation of compressible boundary layers with heat and mass transfer." *AIAA J.* 9, 1091 (1971).
20. Cebeci, T. and Smith, A.M.O. "A finite-difference solution of the incompressible turbulent boundary-layer equations by eddy-viscosity concept." *Douglas Aircraft Div. Rep.* DAC 67130 (1968).
21. Cebeci, T., Smith A.M.O. and Mosinskis, G. "Solution of the incompressible turbulent boundary layer with heat transfer." *J.Heat Transfer* 92, 133 (1970).
22. Champagne, F.H., Harris, V.G. and Corrsin, S. "Experiments on nearly homogeneous turbulent shear flow." *J.Fluid Mech.* 41, 81 (1970).
23. Champagne, F.H. and Sleicher, C.A. "Turbulence measurements with inclined hot wires. Part II: hot wire response equations." *J.Fluid Mech.* 28, 177 (1967).
24. Champagne, F.H., Sleicher, C.A. and Wehrmann, O.H. "Turbulence measurements with inclined hot-wire." *J.Fluid Mech.* 28, 153 (1967).
25. Chou, P.Y. "On velocity correlation and the solutions of the equation of turbulent fluctuation." *Quart.Appl.Math.* 3, 38 (1945a).
26. Chou, P.Y. "Pressure flow of a turbulent fluid between two infinite parallel planes." *Quart. Appl. Math.* 3, 198 (1945b).
27. Chou, P.Y. "The turbulent flow along a semi-infinite flat plate." *Quart. Appl. Math.* 5, 346 (1947).

28. Clark, J.A. "A study of incompressible turbulent boundary layer in channel flow." *J.Basic Eng.* 90, 455 (1968).
29. Coles, D.E. "Measurements in the boundary layers on a smooth flat plate in supersonic flow." *J.P.L. Reps.* 20-69, 20-70, 20-71 (1953).
30. Coles, D.E. "The turbulent boundary layer in a compressible fluid." *Rand Corporation Rep. R-403-PR* (1962).
31. Coles, D.E. and Hirst, E.A. (Editors) Proceedings on Computation of Turbulent Boundary Layers - 1968 Vol.2 (Stanford University, California, 1968).
32. Corrsin, S. "Interpretation of viscous term in the turbulent energy equation." *J.Aero.Sci.* 20, 853 (1953).
33. Daly, B.J. and Harlow, F.H. "Transport equations of turbulence." *Phys.Fluids* 13, 2634 (1970).
34. Davydov, B.I. "On the statistical theory of turbulence." *Dok.Akad.Nauk SSSR* 127, 980 (1959) [Soviet Physics - Doklady. 4, 779 (1960)].
35. Davydov, B.I. "On the statistical dynamics of an incompressible turbulent fluid." *Dok.Akad.Nauk SSSR* 136, 47 (1961) [Soviet Physics - Doklady 6, 10 (1961)].
36. Deardorff, J.W. "A numerical study of three-dimensional turbulent channel flow at large Reynolds numbers." *J. Fluid Mech.* 41, 453 (1970).
37. Deardorff, J.W. "On the magnitude of the subscale eddy coefficient." *J.Comp.Phys.* 7, 120 (1971).
38. Donaldson, C.du P. "A computer study of an analytical model of boundary layer transition." *AIAA J.* 7, 271 (1969).
39. Durst, F. and Whitelaw, J.H. "Evaluation of turbulence characteristics from amplitude probability density measurements of hot-wire anemometer output signals." *I.C. Mech. Eng. Dept. Rep. ET/TN/A/3* (1970).
40. Emmons, H.W. "Shear-flow turbulence." in Proceedings of the Second U.S. National Congress of Applied Mechanics. (America Society of Mechanical Engineers, New York. 1954), p.1.
41. Escudier, M.P. "The distribution of mixing length in the turbulent flows near walls." *I.C. Mech. Eng. Dept. Rep. TWF/TN/1* (1965).

42. Escudier, M.P. "The turbulent incompressible hydrodynamic boundary layer." Ph.D. Thesis, Lond. U. (1967).
43. Frenkiel, F.N. and Klebanoff, P.S. "Higher-order correlations in a turbulent field." Phys. Fluids 10, 507 (1967).
44. Gawain, R.H. and Pritchett, J.W. "A unified heuristic model of fluid turbulence." J. Comp. Phys. 5, 383 (1970).
45. Gebhart, B., Audunson, T. and Pera, L. "Forced, mixed and natural convection from long horizontal wires, experiments at various Prandtl numbers." Paper NC3.2 in Heat Transfer 1970 Vol. 4. (Edited by Grigull, U. and Hahne, E. VDI, Düsseldorf 9170).
46. Gessner, F.B. and Moller, G.L. "Response behaviour of hot-wire in shear flow." J. Fluid Mech. 47, 449 (1971).
47. Gibson, M.M. and Spalding, D.B. "Application of the k-W model of turbulence to boundary layers with streamwise pressure gradients, large temperature variations, and transpiration cooling." I.C.Mech. Eng. Dept. Rep. EHT/TN/A/32 (1971).
48. Glauert, M.B. "The wall jet." J. Fluid Mech. 1, 625 (1956).
49. Glushko, G.S. "Turbulent boundary layer on a flat plate in an incompressible fluid." Izv. Akad. Nauk SSSR, ser. Mekh. No. 4, p. 13 (1965) [NASA TTF - 10080 (1966)].
50. Goldshtik, M.A. and Kutateladze, S.S. "Calculation of the wall turbulence constant." Dok. Akad. Nauk SSSR 185, 535 (1969) [Soviet Phys. - Doklady 14, 194 (1969)].
51. Gosman, A.D. and Ng, K.H. "Heat transfer in falling liquid films." (to be published).
52. Gosman, A.D., Pun, W.M., Runchal, A.K., Spalding, D.B. and Wolfshtein, M. Heat and Mass Transfer in Recirculating Flows. (Academic Press, London 1969).
53. Graham, R.W. and Diessler, R.G. "Prediction of flow-acceleration effects on turbulent heat transfer." J. Heat Transfer 89, 371 (1967).
54. Hama, F.R., quoted in Rotta (1962), p. 105.
55. Hanjalić, K. "Two-dimensional asymmetric turbulent flow in ducts." Ph.D. Thesis, Lond.U. (1970).

56. Harlow, F.H. and Nakayama, P.I. "Turbulence transport equations." *Phys. Fluids* 10, 2323 (1967).
57. Harlow, F.H. and Nakayama, P.I. "Transport of turbulence energy decay rate." Los Alamos Scientific Laboratory Rep. LA - 3854 (1968).
58. Harlow, F.H. and Romero, N.C. "Turbulence distortion in a nonuniform tunnel." Los Alamos Scientific Laboratory Rep. LA - 4247 (1969).
59. Harsha, P.T. "Free turbulent mixing: a critical evaluation of theory and experiment." Arnold Engineering Development Center, Tenn., AEDC - TR - 71 - 36 (1971).
60. Harvey, W.D., Bushnell, D.M. and Beckwith, I.E., "Fluctuating properties of turbulent boundary layers for Mach Numbers up to 9." NASA TN D-5496 (1969).
61. Herring, H.T. and Mellor, G.L. "A method of calculating compressible turbulent boundary layers." NASA CR - 1144 (1968).
62. Heskestad, G. "Hot-wire measurements in a plane turbulent jet." *J.App. Mech.* 32, 1 (1965).
63. Heskestad, G. "Hot-wire measurements in a radial turbulent jet." *J.App.Mech.* 33, 417 (1966).
64. Hinze, J.O. Turbulence (McGraw-Hill, New York, 1959).
65. Hodgson, T.H. "Pressure fluctuations in flow turbulence." Ph.D. Thesis, Lond.U. (1962).
66. Hopkins, E.J. Rubesin, M.W., Inouye , M., Keener,E.R., Mateer, G.C. and Polek, T.E. "Summary and correlation of skin-friction and heat-transfer data for a hypersonic turbulent boundary layer on simple shapes." NASA TN-D-5089 (1969).
67. Jayatelleke, C.L.V. "The influence of Prandtl number and surface roughness on the resistance of the laminar sub-layer to momentum and heat transfer." in Progress in Heat and Mass Transfer Vol. 1. (Edited by Grigull, U. and Hahne, E., Pergamon Press, 1969) p.193.
68. Jerome, F.E., Guittot, D.E. and Patel, R.P. "Experimental study of the thermal wake interference between closely spaced wires of an X-type hot-wire probe." *Aero.Quart.* 22, 119 (1971).

69. Jones, W.P. and Launder, B.E. "The prediction of laminarisation with a two-equation model of turbulence" I.C. Mech. Dept. Rep. BL/TN/A/40 (1970).
70. Kacker, S.C. and Whitelaw, J.H. "An experimental investigation of the influence of slot-lip-thickness on the impervious-wall effectiveness of the uniform density, two-dimensional wall jet." I.C. Mech. Eng. Dept. Rep. EHT/TN/13(1968).
71. Kacker, S.C. and Whitelaw, J.H. "The turbulence characteristics of two-dimensional wall-jet and wall-wake flows." J.App.Mech. 38, 239 (1971).
72. Klebanoff, P.S. "Characteristics of turbulence in a boundary layer with zero pressure gradient." NACA Rep. 1247 (1955).
73. Kolmogorov, A.N. "Equations of turbulent motion in an incompressible fluid." Izv. Akad. Nauk. SSSR, ser. Fiz. 6, 56 (1942) [I.C. Mech. Eng. Dept. Rep. ON/6 (1968)].
74. Kolvandin, B.A. "Scalar substance transfer in non-homogeneous turbulence." in Heat Transfer 1970 (Edited by Grigull, U. and Hahne, E., VDI, Düsseldorf, 1970), Vol. 7, paper No. CT 2.6.
75. Kolvandin, B.A. and Vatutin, I.A. "On statistical theory of non-uniform turbulence." paper presented at the International Seminar on Heat and Mass Transfer, Herceg Novi, Yugoslavia, September, 1969.
76. Koosinlin, M.L. and Lockwood, F.C. "The prediction of turbulent boundary layers on rotating axially-symmetrical bodies." I.C. Mech. Eng. Dept. Rep. BL/TN/A/46 (1971).
77. Laufer, J. "Investigation of turbulent flow in a two-dimensional channel." NACA Rep. 1053 (1951).
78. Laufer, J. "The structure of turbulence in a fully developed pipe flow." NACA Rep. 1174 (1954).
79. Lawn, C.J. "The determination of the rate of dissipation in turbulent pipe flow." J.Fluid Mech. 48, 477 (1971).
80. Liepmann, H.P. and Laufer, J. "Investigation of free turbulent mixing." NACA TN 1257 (1957).
81. Lobb, R.K., Winkler, E.H., Persh, J. "Experimental investigation of turbulent boundary layers on hypersonic flow." Navord Rep. 3880 (1955).

82. Lumley, J.L. "Spectral energy budget in wall turbulence." *Phys. Fluids* 7, 190 (1964).
83. Lumley, J.L. and Panofsky, H.A. The Structure of Atmospheric Turbulence (Interscience, New York, 1964).
84. Lundgren, T.S. "Turbulent pipe and channel flow." *Phys. Fluids* 14, 225 (1971).
85. MacMillan, F.A. "Viscous effects on pitot-tubes at low speeds." *J. Roy. Aero. Soc.* 58, 570 (1954).
86. Manian, V.S. and Besant, R.W. "Turbulence measurements in a cylindrical wall jet." *App. Sci. Res.* 21, 194 (1969).
87. Maise, G. and McDonald, H. "Mixing length and kinematic eddy viscosity in a compressible boundary layer." *AIAA J.* 6, 73 (1968).
88. McDonald, H. "The effect of pressure gradient on the law of the wall in turbulent flow." *J. Fluid Mech.* 35, 311 (1969a).
89. McDonald, H. "Linear stress distribution and the turbulent boundary-layer equation of motion." *Phys. Fluids* 12, 2241 (1969b).
90. Melling, A. "The laser-doppler shift technique and hot wire anemometry: a comparison." M.Sc. Thesis, Lond.U. (1970).
91. Mellor, G.L. "Incompressible, turbulent, boundary layers with arbitrary pressure gradients and divergent or convergent cross flows." *AIAA J.* 5, 1537 (1967).
92. Mellor, G.L. and Gibson, D.M. "Equilibrium turbulent boundary layer." *J. Fluid Mech.* 24, 225 (1966).
93. Mellor, G.L. and Herring, H.J. "Two methods of calculating turbulent boundary layer behaviour based on numerical solutions of the equations of motion." in Proceedings of Computation of Turbulent Boundary Layers. Vol. 1. (Edited by Kline et al, Stanford U., California 1968), p.331.
94. Millionschlchikov, M.D. "On the theory of homogeneous isotropic turbulence." *Compt. Rend. Acad. Sci. USSR* 32, 65 (1941).
95. Moretti, P.M. and Kays, W.M. "Heat transfer to a turbulent boundary layer with varying free-stream velocity and varying surface temperature - an experimental study." *Int. J. Heat Mass Transfer* 8, 187 (1965).

96. Morkovin, M.V. "Effects of compressibility on turbulent flows." in the Mechanics of Turbulence (Edited by Farve, A., Gorden and Breach, New York, 1964), p.24.
97. Myers, G.E., Schauer, J.J. and Eustis, R.H. "The plane turbulent wall jet Pt. 1: Jet development and friction factor." J. Basic Eng. 1, 47 (1963).
98. Nakatogawa, T., Nishiwaki, N., Hirata, M. and Toru, K. "Heat transfer of round turbulent jet impinging normally on flat plate." in Heat Transfer 1970. Vol. 2 (Edited by Grigull, U. and Hahne, E., VDI, Düsseldorf, 1970), paper No. FC5.2.
99. Nee, V.W. and Kovasznay, L.S.G. "Simple phenomenological theory of turbulent shear flows." Phys. Fluids 12, 473 (1969).
100. Ng, K.H., Patankar, S.V. and Spalding, D.B. "The hydrodynamic turbulent boundary layer on a smooth wall, calculated by a finite-difference method." in Proceedings on Computation of Turbulent Boundary Layers. Vol. 2. (Edited by Kline et al, Stanford University, California 1968), p.356.
101. Ng, K.H. and Sivasegaram, S. "Predictions of two-dimensional compressible turbulent boundary layers on wall using a two-equation model of turbulence." A.R.C. 32048 HMT 248, also I.C. Mech. Eng. Dept. Rep. BL/TN/A/29 (1970).
102. Ng, K.H. and Spalding, D.B. "Predictions of two-dimensional boundary layers on smooth walls with a two-equation model of turbulence." I.C. Mech. Eng. Dept. Rep. BL/TN/A/25 (1970a).
103. Ng, K.H. and Spalding, D.B. "A comparison of three methods of predicting hydrodynamic behaviour of two-dimensional turbulent boundary layers on smooth walls." I.C. Mech. Eng. Dept. Rep. BL/TN/A/32 (1970b).
104. Ng, K.H. and Spalding, D.B. "Turbulence model for boundary layer near walls." (to be published in Phys. Fluids 1971).
105. Nunner, W. "Wärmenbergang und Druckabfall in rauhen Röhren." VDI - Forch. 455 (1956).
106. Patankar, S.V. and Spalding, D.B. Heat and Mass Transfer in Boundary Layers. (2nd Edition, Intertext, London, 1970).

107. Patankar, S.V. and Spalding, D.B. "A calculation procedure for heat, mass and momentum transfer in three-dimensional parabolic flows." I.C. Mech. Eng. Dept. Rep. BL/TN/A/45(1971)
108. Patel, R.P. "A study of two-dimensional symmetric and asymmetric turbulent shear flows." Ph.D. Thesis, McGill U. (1970).
109. Patel, R.P. "Turbulent jets and wall jets in uniform streaming flow." Aero. Quart. 22, 311 (1971).
110. Patel, V.C. and Head, M.R. "A simplified version of Bradshaw's method for calculating two-dimensional turbulent boundary layers." Aero. Quart. 21, 243 (1970).
111. Peerless, S.J. "Turbulent mixing of gas streams". Ph.D. Thesis, London U. (1971).
112. Poreh, M., Tsuei, Y.G. and Germak, J.E. "Investigation of a turbulent radial wall jet." J.App. Mech. 34 457 (1967).
113. Prandtl, L. "Über die ausgebildete Turbulenz." ZAMM 5, 136 (1925).
114. Prandtl, L. "Über ein neues Formelsystem der ausgebildeten Turbulenz." Nachr. Akad. Wiss. Göttingen, Math-Phys. Kl., p.6 (1945).
115. Reynolds, W.C. "A morphology of the prediction methods." in Proceedings on Computation of Turbulent Boundary Layers. Vol. 1. (Edited by Kline et al, Stanford U. California, 1968).
116. Reynolds, W.C. "Computation of turbulent flows-state-of-the-art, 1970." Stanford U. Thermoscience Div. Rep. MD - 27 (1970).
117. Rodi, W. "Basic equations for turbulent flow in cartesian and cylindrical coordinates." I.C. Mech. Dept. Rep. BL/TN/A/36(1970).
118. Rodi, W. "Prediction of free turbulent boundary layers by use of a two equation model of turbulence." Ph.D. Thesis (to be completed).
119. Rodi, W. and Spalding, D.B. "A two-parameter model of turbulence and its application to free jets." Wärme-und-Stoffübertragung 3, 85 (1970).
120. Rotta, J.C. "Statistische Theorie nichthomogener Turbulenz." Z.Phys. 129, 5471; 131, 51 (1951) [I.C.Mech. Eng. Dept. Reps. TWF/TN/38,39].

121. Rotta, J.C. "Turbulent boundary layers in incompressible flow." in Progress in Aeronautical Sciences. Vol.2 (Edited by Ferri et al, Macmillan, New York, 1962), p.1.
122. Rotta, J.C. "Über eine Methode zur berechnung Turbulenz Scherstromungsfelder." Aerodynamische Versuchsaustalt 69A14 (1969).
123. Rotta, J.C. "Recent attempts to develop a generally applicable calculation method for turbulent shear flow layers." paper delivered at AGARD Meeting, London, Sept. 1971.
124. Runchal, A.K. "Transfer process in steady two-dimensional separated flows." Ph.D. Thesis, London.U. (1969).
125. Saffman, P.G. "A model for inhomogeneous turbulent flow." Proc. Roy. Soc. 317A, 417 (1970).
126. Schlichting, H. Boundary Layer Theory. (Mcgraw-Hill, New York, 1960).
127. Smagorinsky, J., Manabe, S. and Holloway, J.L. "Numerical results from a nine-level general circulation model of the atmosphere." Mon.Weath.Rev. 93, 727 (1965).
128. Sivasegaram, S. "An experimental investigation of supersonic boundary-layer flows with pressure gradients." I.C. Mech. Eng. Dept. Rep.BL/TN/B/16 (1969).
129. Sivasegaram, S. and Whitelaw, J.H. "The prediction of turbulent, supersonic two-dimensional, boundary-layer flows." Aero.Quart. 22, 174 (1971).
130. Spalding, D.B. "Contribution to the theory of heat transfer across a turbulent boundary layer." Int. J. Heat and Mass Transfer 7, 743 (1964).
131. Spalding, D.B. "Heat transfer from turbulent separated flows." J. Fluid Mech. 27, 97 (1967a).
132. Spalding, D.B. "Monograph on turbulent boundary layers." I.C. Mech. Eng. Dept. Rep. TWF/TN/33(1967b).
133. Spalding, D. B. "The calculation of the length scale of turbulence in some turbulent boundary layers remote from walls." in Progress in Heat and Mass Transfer Vol.2 (Edited by Irvine et al, Pergamon Press, Oxford, 1969), p.255.

- 134. Spalding, D.B. "Turbulence models and the theory of the boundary layers." I.C. Mech. Eng. Dept. Rep. BL/TN/A/24(1969b).
- 135. Spalding, D.B. "Concentration fluctuations in a round turbulent free jet." Chem. Eng. Sci. 26, 95 (1971a).
- 136. Spalding, D.B. (in the WALL FUNCTION Routine of the GENMIX 5 program, 1971b).
- 137. Spalding, D.B. and Chi, S.W. "The drag of a compressible turbulent boundary layer on a smooth flat plate with and without heat transfer." J.Fluid Mech. 18, 117 (1964).
- 138. Spangenberg, W.G., Rowland, W.R. and Mease, N.E. "Measurements in a turbulent boundary layer maintained in nearly separated conditions." in Fluid Mechanics of Internal Flows. (Edited by Sovran, G., Elsevier Press, Amsterdam, 1967). p.110.
- 139. Tailland, A. "Contribution a l'etude d'un jet plan dirige tangentiellelement a une paroi plane." D.Sc. Thesis, Lyon U. (1970).
- 140. Tailland, A. and Mathieu, J. "Jet parietal." J. de Mecanique 6, 103 (1967).
- 141. Taylor, G.I. "Eddy motion in the atmosphere." Phil. Trans. Roy. Soc. 215A, 1 (1915).
- 142. Taylor, G.I. "The transport of vorticity and heat through fluids in turbulent motion." Proc. Roy. Soc. 135A, 685 (1932).
- 143. Tillmann, W. "Investigation of some particularities of turbulent boundary layers on plates." U. and M. 6627 (1945) [British Rep. and Transl. CGD-497, MAP)VG 34-T (1946)].
- 144. Townsend, A.A. The Structure of Turbulent Shear Flow. (Cambridge University Press, Cambridge, 1956).
- 145. Townsend, A.A. "Equilibrium layer and wall turbulence." J. Fluid Mech. 11, 97 (1961).
- 146. Tuve, G.L. "Air velocity in ventilating jets." Heating, Piping, and Air Conditioning Jan., p.181, 1953.
- 147. Uberoi, M.S. "Energy transfer in isotropic turbulence." Phys. Fluids 6, 1048 (1963).
- 148. Uzkan, T. and Reynolds, W.C. "A shear-free turbulent boundary layer." J. Fluid Mech. 28, 803 (1967).

149. Van Atta, C.W. and Chen, W.Y. "Correlation measurements in grid turbulence using digital harmonic analysis." *J. Fluid Mech.* 34, 497 (1968).
150. Wolfshtein, M. "The velocity and temperature distribution in one-dimensional flow with turbulence augmentation and pressure gradient." *Int. J. Heat Mass Transfer* 12, 301 (1969).
151. Wolfshtein, M. "On the length-scale-of turbulence equation." *Israel J. of Technology* 8, 87 (1970).
152. Wygnanski, I. and Fiedler, H.E. "Some measurements in the self-preserving jet." *J. Fluid Mech.* 38, 577 (1969).
153. Wygnanski, I. and Fiedler, H.E. "Two-dimensional mixing region." *J. Fluid Mech.* 41, 327 (1970).
154. Wyngaard, J.C. "Measurements of small-scale turbulence structure with hot wires." *J. Sci. Instruments Ser. 2*, 1, 1105 (1968).
155. Zarić, Z. "Statistical interpretation of the velocity measurements in high intensity turbulence." paper presented at the International Seminar on Heat and Mass Transfer, Herceg Novi, Yugoslavia. Sept., 1969.

NOMENCLATURE

<u>Symbol</u>	<u>Meaning</u>	<u>Equation of first occurrence</u>
A, B	constants of the hot-wire equation	A.4-1
$A_1, A_2 \dots$	empirical constants or functions in the turbulence models displayed in Appendix 1.	
a	constant	4.2-3
$C_i$	empirical constants	
$C_p$	specific heat at constant pressure	
c	tangential-cooling coefficient	A.4-1
D	diameter of pipe or width of channel	
d	slot-lip thickness	
$\frac{D}{Dt}$	$= U \frac{\partial}{\partial x} + V \frac{\partial}{\partial y}$	2.2-2
E	turbulence energy spectrum	3.2-1
e	$\equiv \frac{1}{2}(\bar{u^2} + \bar{v^2} + \bar{w^2})$ , turbulent kinetic energy	2.3-5
F	function defined by Equation (A.2-4)	A.2-2
f	empirical function	3.2-16
f	frequency	
G	function defined by Equation (A.2-5)	A.2-2
H	time-mean enthalpy	A.3-4
$H^*$	$\equiv H + \frac{U^2}{2} + e$ , stagnation enthalpy	
$H_{12}$	$\equiv \delta_1/\delta_2$ , shape factor	
h	fluctuating component of H	
$h^*$	fluctuating component of $H^*$	

$J_S$	wall flux of $\Phi$	5.2-14
K	constant of the hot-wire calibration curve	A.4-2
k	wave number of turbulence	3.1-1
L	length scale	
$l$	length scale	3.2-4
$l_m$	mixing length	4.2-7
M	Mach number	A.3-4
N	number of x-stations downstream of starting point	6.3-1
n	constant exponent of the hot-wire equation	A.4-1
P	mean pressure	2.2-2
p	fluctuating component of P	2.3-1
q	constant exponent	3.2-16
R	gas constant	
$R_2$	$\equiv \frac{U_G \delta_2}{v}$ , momentum-deficit-thickness Reynolds number	
$R_i^j$	$\equiv \sum_{i=1}^3 \overline{u_i u_j}$ , sum of the cross-diagonal components of the joint correlation	3.2-1
$R_i^n$	components of the second-order joint correlation	A.2-1
$R_{in}^j, R_i^{jn}$	components of the third-order joint correlation	A.2-1
r	radius	7.7-1
$r_1$	radius of the wall jet exit	
$r_2$	radius of the impinging jet	
S	additional terms in the $\Phi$ -transport equation	2.4-1
ST	$\equiv \frac{J_S}{\rho U_G (\Phi_S - \Phi_G)}$ , Stanton number	

$s$	fluctuating component of $S$	2.4-2
$s_S$	$\equiv \tau_S / (\rho U_G^2)$ , friction coefficient	
$T$	temperature	A.3-4
$T_1$	function defined by Equation (A.2-6)	3.2-2
$T_2$	function defined by Equation (A.2-7)	3.2-2
$t$	time	2.2-2
$U$	mean velocity in $x$ -direction	2.2-1
$U_i, U_j \dots$	mean velocities in $i, j \dots$ directions	
$U_{\text{eff}}$	effective velocity	A.4-1
$U_\tau$	$\equiv \frac{\tau_S}{\rho_S}$ , shear velocity	
$u$	fluctuating component of $U$	2.2-2
$u_i, u_j \dots$	fluctuating velocity components in $i, j \dots$ direction	
$v$	mean velocity in $y$ -direction	2.2-1
$V_{\text{ol}}$	volume	3.2-1
$v$	fluctuating component of $v$	2.2-2
$w$	fluctuating component of the velocity perpendicular to the $x-y$ plane	2.3-3
$x$	streamwise direction	2.2-1
$x_1, x_2, x_3$	three directions of the cartesian coordinates	
$y$	lateral direction measured from the wall	2.2-1
$y_n$	distance from wall or from axis/plane of symmetry where, $U = n(U_{\max} - U_G)$ .	
$z$	slot heights	

$z_1$	slot height of radial wall jet	
$z_2$	height of impinging jet	
$D$	turbulent kinetic energy dissipation rate	3.2-2
$F$	turbulent diffusion flux	3.2-3
$\rho$	function defined by Equation (5.2-15)	5.2-14
$Q$	function	5.2-14
$\alpha$	angle of inclination of the hot wire to the $x_2-x_3$ plane	A.4-3
$\beta$	angle of inclination of the hot wire to the instantaneous velocity	A.4-1
$F$	instantaneous hot-wire bridge voltage	A.4-1
$\gamma$	a.c. component of the bridge voltage	A.4-6
$\gamma$	$\equiv \frac{C_p}{C_v}$ , ratio of specific heats	A.3-4
$\Delta H_{12}, \Delta s_S, \Delta R_2$	mean deviations defined by Equations (6.3-1 to 3.)	6.3-1 to 3
$\delta_1$	$\equiv \int_0^\infty \frac{\rho}{\rho_G} (1 - \frac{U}{U_G}) dy$ , displacement thickness	
$\delta_2$	$\equiv \int_0^\infty \frac{\rho U}{\rho_G U_G} (1 - \frac{U}{U_G}) dy$ , momentum-deficit-thickness	
$E$	constant	5.2-11
$\epsilon$	$\equiv \frac{Y_G}{2\rho C_1} \frac{1}{2} \frac{dP}{dx}$	
$\zeta$	function	
$\eta$	$\equiv y/Y_G$ , dimensionless boundary-layer thickness	A.3-1

$\theta$	$\equiv \frac{T_G - T_S}{T_G - T_{SL}}$ , film-cooling-effectiveness	
$\kappa$	constant	4.2-8
$\lambda$	constant	
$\mu$	viscosity	2.2-2
$\nu$	$\equiv \frac{\mu}{\rho}$ , kinematic viscosity	
$\nu_t$	turbulent kinematic viscosity	
$\rho$	density	2.2-1
$\sigma$	Prandtl/Schmidt number	2.4-1
$\tau$	shear stress	3.2-11
$\Phi$	conservative property	2.4-1
$\phi$	fluctuating component of $\Phi$	2.4-1
$\omega$	fluctuating vorticity	

Superscripts                  Condition pertained to.

$\sim$	fluctuating component
$\rightarrow$	vector
'	at point o'
$\overline{\quad}$	time-mean

Subscripts

a	adiabatic
B	at a point outside the viscous sublayer
c	at the symmetry line
ex	experimental
G	at free stream
m	bulk-mean

max maximum  
o predicted by other models  
p predicted by the two-equation  
model  
S at the surface  
SL at slot exit  
 $\Phi$  of the  $\Phi$  - entity

Appendix 1. Summary of the turbulence models.

Proposer/s	Year	Ref/s	Particulars of the model	No. of differential eqns. reqd. in 2-D b.l.flows	Applicable to low Reynolds No. flow	Applications
Taylor	1915 (64, 141)		Vorticity transport: $\overline{u_2 w} = L_w \left  \frac{\partial U_1}{\partial x_2} \right  \left  \frac{\partial^2 U_1}{\partial x_2^2} \right $	0		jets and wakes (142)
Prandtl	1925 (113)		Momentum transport: $-\overline{u_1 u_2} = \ell_m \left  \frac{\partial U_1}{\partial x_2} \right  \left  \frac{\partial U_1}{\partial x_2} \right $	0		see Patankar- Spalding model
Mellor and Gibson	1966 (92)		Eddy-viscosity model: $-\overline{u_1 u_2} = v_t \frac{\partial U_1}{\partial x_2}$ where $v_t$ is a prescribed algebraic function	0		incompressible and compressible wall boundary layers (61, 91, 92, 93 )

Cebeci and Smith	1968 (20)	similar to Mellor-Gibson model but with a different formula for $v_t$ .	0	incompressible and compressible wall boundary layers. (19, 20, 21)
Patankar and Spalding	1970 (106)	similar to Prandtl's (1925) proposal but uses van Driest's formula near the wall.	0 ✓	incompressible and compressible boundary layers, liquid films, duct flows, wall jets, free jets. (2, 51, 59, 76, 100, 111, 129)
Turbulent kinetic energy equation:				
Prandtl	1945 (114)	$\frac{De}{Dt} + \frac{\bar{u}_1 \bar{u}_2 \frac{\partial U_1}{\partial x_2}}{v_t} + A_1 \frac{e^{\frac{3}{2}}}{\ell} - A_2 \frac{\partial}{\partial x_2} (v_t \frac{\partial e}{\partial x_2})$ $v_t \equiv e^{\frac{1}{2}} \ell$	1	boundary layers, free shear flows, recirculating flows. (52, 59)
Emmons	1954 (40)	similar to Prandtl's model (1945)	1	duct flows. (40)

---

Glushko	1965	(49)	similar to Prandtl's (1945) model	1	✓	boundary layers (7, 49)
---------	------	------	-----------------------------------	---	---	----------------------------

---

Bradshaw et al	1967	(14)	shear-stress equation:	1	incompressible and compressible wall boundary layers, 3-D boundary layers, wakes.
			$A \frac{D\bar{u}_1 \bar{u}_2}{Dt} - \bar{u}_1 \bar{u}_2 \frac{\partial \bar{u}_1}{\partial x_2} - (-\bar{u}_1 \bar{u}_2)_{\max}^{\frac{1}{2}} \frac{\partial}{\partial x_2} (A_2 \bar{u}_1 \bar{u}_2)$ $- (-\bar{u}_1 \bar{u}_2)^{\frac{3}{2}} / L = 0$		(9, 10, 12, 13, 14, 110)

L is a prescribed length scale

---

Mellor and Herring	1968	(93)	similar to Prandtl's (1945) model.	1	✓	wall boundary layers (93)
-----------------------	------	------	------------------------------------	---	---	---------------------------------

---

Nee and Kovasznay	1969	(99)	turbulent-viscosity equation:	1	wall boundary layers (99)
			$\frac{Dv_t}{Dt} - A_1 v_t \left  \frac{\partial \bar{u}_1}{\partial x_2} \right  + A_2 \frac{v_t^2}{\ell_m} - A_3 \frac{\partial}{\partial x_2} (v_t \frac{\partial v_t}{\partial x_2}) = 0.$		

---

---

Wolfshtein	1969 (150)	Similar to Prandtl's and Glushko's model	1	✓	channel flow (150)
------------	------------	--	---	---	--------------------

Gawain and Pritchett	1970 (44)	Turbulent kinetic energy equation:	1	pipe flow, round jet.
----------------------	-----------	------------------------------------	---	--------------------------

$$\begin{aligned} \frac{De}{Dt} - A_1 v_t \left( \frac{\partial U_1}{\partial x_2} \right)^2 + A_2 Z e^{\frac{v_t}{2}} \\ - \frac{\partial}{\partial x_2} \left( A_3 v_t \frac{\partial e}{\partial x_2} \right) = 0; \\ v_t \equiv A_4 e^{\frac{1}{2}L} \end{aligned} \quad (44)$$

L and Z are functions calculated from mean-velocity distributions.

---

Lundgren	1971 (84)	e-equation similar to Prandtl's but with $v_t$ defined as	1	duct flows
		$v_t \equiv e \left( \frac{e}{L} + \frac{De}{Dt} \right)^{-1}$		(84)

---

Kolmogorov	1942 (73)	e-equation similar to Prandtl's but with another equation for "frequency of fluctuation".	2	mixing-layers (111)
------------	-----------	---	---	---------------------

$$\frac{Df}{Dt} + \frac{7}{11} f^2 - A_1 \frac{\partial}{\partial x_2} \left( \frac{e \partial f}{f \partial x_2} \right) = 0;$$

$$v_t \equiv A_2 e/f$$

Harlow and Nakayama	1967 (56)	e-equation similar to Prandtl's equation for length scale L:	2	pipe flow (56)
		$\frac{DL}{Dt} - A_1 \frac{L}{e^2} \left( \frac{\partial U_1}{\partial x_2} \right)^2 + A_2 e^{\frac{1}{2}} - A_3 \frac{\partial}{\partial x_2} (v_t \frac{\partial L}{\partial x_2}) = 0;$ $v_t \equiv e^{\frac{1}{2}} L$		
Spalding	1969 (133)	similar to Harlow-Nakayama model	2 ✓	free shear flows (133)
Jones and Launder	1970 (69)	e-equation similar to Prandtl's; equation for dissipation rate:	2	boundary layer laminarisation (69)
		$\frac{D\delta}{Dt} + A_1 \overline{u_1 u_2} \frac{\partial}{\partial x_2} \frac{\partial U_1}{\partial x_2} + A_2 \frac{\partial^2}{\partial e^2}$ $- \frac{\partial}{\partial x_2} (A_3 \frac{\rho e^2}{\delta} \frac{\partial \delta}{\partial x_2}) = 0;$ $v_t \equiv \rho e^2 / \delta$		

Ng, Rodi and Spalding 1970, (104,  
1971 119)

e-equation similar to Prandtl's;  
equation for energy-length product:

2

wall boundary  
layers and  
free shear flow

$$\frac{De}{Dt} - A_1 v_t \left( \frac{\partial U_1}{\partial x_2} \right)^2 + A_2 e$$

(76, 101, 102, 103,  
104, 119)

$$- \frac{\partial}{\partial x_2} (A_3 v_t \lambda \frac{\partial e}{\partial x_2} + A_4 v_t e \frac{\partial \lambda}{\partial x_2}) = 0;$$

$$v_t = e^{\frac{1}{2}\lambda}$$

Saffman 1970 (125) e-equation:

2

wall boundary  
layers,  
jets

$$\frac{De}{Dt} - A_1 e \left| \frac{\partial U_1}{\partial x_2} \right| + A_2 e (\bar{w}^2)^{\frac{1}{2}} - \frac{\partial}{\partial x_2} (A_3 v_t \frac{\partial e}{\partial x_2}) = 0;$$

(125)

$\bar{w}^2$ - equation :

$$\frac{D\bar{w}^2}{Dt} - A_4 \bar{w}^2 \frac{\partial U_1}{\partial x_2} + A_5 (\bar{w}^2)^{\frac{3}{2}} - \frac{\partial}{\partial x_2} (A_6 v_t \frac{\partial \bar{w}^2}{\partial x_2}) = 0;$$

$$v_t = A_7 e / (\bar{w}^2)^{\frac{1}{2}}$$

Wolfshtein 1970 (151) e-equation similar to Prandtl's;  
equation for energy-length product:

2



channel flow

(151)

$$\frac{DeL}{Dt} - A_1 v_t \left( \frac{\partial U_1}{\partial x_2} \right)^2 + A_2 e^{3/2} + A_3 \frac{L}{e^2} \left( \frac{\partial e}{\partial x_2} \right)^2$$

$$- \frac{\partial}{\partial x_2} (A_4 v_t \frac{\partial e L}{\partial x_2}) = 0 ;$$

$$v_t \equiv A_5 e^{1/2} L$$

Spalding 1971 (135) e-equation similar to Prandtl's;  
equation for "vorticity-fluctuation-squared".

2

concentration of  
turbulent free jets,  
wall boundary layers

(47, 135)

$$\frac{D\bar{w}^2}{Dt} - A_1 \frac{e}{v_t} \left( \frac{\partial U_1}{\partial x_2} \right)^2 + A_2 (\bar{w}^2)^{3/2}$$

$$- A_3 v_t \left( \frac{\partial^2 U_1}{\partial x_2^2} \right)^2 - A_4 \frac{\partial}{\partial x_2} (v_t \frac{\partial \bar{w}^2}{\partial x_2}) = 0 ;$$

$$v_t \equiv e / (\bar{w}^2)^{1/2}$$

Rotta 1969 (122) e-equation:

3

channel flow

(122)

$$\frac{De}{Dt} + \overline{u_1 u_2} \frac{\partial U_1}{\partial x_2} + A_1 e^{\frac{3}{2}} - \frac{\partial}{\partial x_2} (A_2 e^{\frac{1}{2}} L \frac{\partial e}{\partial x_2})$$

$$+ A_3 e \frac{\partial L}{\partial x_2} = 0 ;$$

shear-stress equation:

$$\frac{D \overline{u_1 u_2}}{Dt} + A_4 e \frac{\partial U_1}{\partial x_2} + A_5 \frac{\overline{u_1 u_2} e}{L}$$

$$+ A_6 e L^2 \frac{\partial^3 U}{\partial x_2^3} - \frac{\partial}{\partial x_2} (A_7 e^{\frac{1}{2}} L \frac{\partial \overline{u_1 u_2}}{\partial x_2})$$

$$+ A_8 e^{\frac{1}{2}} \overline{u_1 u_2} \frac{\partial L}{\partial x_2} = 0 ;$$

eL-equation:

$$\frac{DeL}{Dt} + A_9 \overline{u_1 u_2} L \frac{\partial U}{\partial x_2} + A_{10} e^{\frac{3}{2}} + A_{11} \overline{u_1 u_2} L^3 \frac{\partial^3 U}{\partial x_2^3}$$

$$- \frac{\partial}{\partial x_2} (A_{12} e^{\frac{1}{2}} L^2 \frac{\partial e}{\partial x_2} + A_{13} e^{\frac{1}{2}} L \frac{\partial L}{\partial x_2}) = 0 .$$

---

Hanjalic	1970	(55)	e-equation similar to Prandtl's; dissipation equation similar to Jones-Launder model; shear-stress equation:	3	asymmetric channels; wall jets, boundary layers, free shear flows
			$\frac{Du_1 u_2}{Dt} - A_1 e \frac{\partial U_1}{\partial x_2} + A_2 \frac{\overline{u_1 u_2}}{\rho e}$ $- A_3 \frac{\partial}{\partial x_2} \left( \frac{\rho e^2}{D} \frac{\partial \overline{u_1 u_2}}{\partial x_2} \right) = 0$	(55)	
Donaldson	1969	(38)	Turbulence intensity equation for three components; prescribed length scale.	4	boundary layer transition
Kolovandin	1970	(74)	Similar to Donaldson's model	4	natural convection

Rotta

1951 (120)

Turbulence-intensity equation for the  
3 components:

$$\frac{D \bar{u}_i^2}{Dt} + A_1 \bar{u}_i \bar{u}_2 \frac{\partial \bar{u}_1}{\partial x_2} + A_2 (\bar{u}_i^2)^{\frac{3}{2}} / L$$

$$- \frac{\partial}{\partial x_2} (A_3 (\bar{u}_2^2)^{\frac{1}{2}} L \frac{\partial \bar{u}_i^2}{\partial x_2}) = 0 ;$$

5

channel flow  
(120, 123)

shear-stress equation:

$$\frac{D \bar{u}_1 \bar{u}_2}{Dt} + \bar{u}_2^2 \frac{\partial \bar{u}_1}{\partial x_2} + A_4 \frac{\bar{u}_1 \bar{u}_2 e}{L}$$

$$- \frac{\partial}{\partial x_2} (A_5 (\bar{u}_2^2)^{\frac{1}{2}} L \frac{\partial \bar{u}_1 \bar{u}_2}{\partial x_2}) = 0 ;$$

eL-equation:

$$\frac{D e L}{Dt} + A_6 \bar{u}_1 \bar{u}_2 L \frac{\partial \bar{u}_1}{\partial x_2} + A_7 e^{\frac{3}{2}}$$

$$+ \frac{\partial}{\partial x_2} (A_8 (\bar{u}_2^2)^{\frac{1}{2}} L^2 \frac{\partial e}{\partial x_2} - A_9 (\bar{u}_2^2)^{\frac{1}{2}} e L \frac{\partial L}{\partial x_2}) = 0$$

Daly and  
Harlow

1970 (33)

Differential equations for the turbulent intensities and shear stress; dissipation rate equation:

5

✓ channel flows,  
free flows

(33, 58, 118)

$$\frac{D\theta}{Dt} + A_1 \overline{u_1 u_2} \frac{\partial}{e} \frac{\partial U_1}{\partial x_2} - \frac{\partial}{e} \frac{\partial}{\partial x_2} \left( \frac{\rho e}{\overline{u_1 u_2}} \frac{\partial e}{\partial x_2} \right)$$

$$+ A_2 \frac{\partial^2 \theta}{\partial x_2^2} - \frac{\partial}{\partial x_2} \left( A_3 \overline{u_1 u_2} e \frac{\partial \theta}{\partial x_2} \right) = 0.$$

143

Chou

1945 (25)

Differential equations for the turbulence intensities and shear stress; equations for third-order correlations; equation for "vorticity decay"

9

channel flow and flat-plate boundary layer.

(26, 27)

$$\frac{D\overline{w^2}}{Dt} + A_1 \frac{\overline{w^2 u_1 u_2}}{e} \frac{\partial U_1}{\partial x_2} + A_2 \frac{(\overline{w^2})^3}{2}$$

$$+ A_3 \frac{\overline{w^2}}{e} = 0$$

---

Davydov	1961	(34, 35)	Differential equations for turbulence intensities, shear stress, third-order correlations, dissipation, dissipation flux.	10	none
Kolovandin and Vatutin	1969	(75)	Differential equations for turbulence intensities, shear stress, third-order correlations, turbulence scales, pressure-velocity correlations.	16	none

---

Appendix 2Spectral balance in non-homogeneous turbulence

Rotta, in 1951, has shown that the quantity  $R_i^i$ , defined as the sum of the three cross-diagonal components of the joint correlation at two points,  $\sigma$  and  $\sigma'$ , obeys the following equation:

$$\begin{aligned}
 & \frac{U_n + U_n'}{2} \frac{\partial R_i^i}{\partial x_n} - (U_n - U_n') \frac{\partial R_i^i}{\partial r_n} \\
 & + R_n^i \frac{\partial U_i}{\partial x_n} + R_i^n \frac{\partial U_n'}{\partial x_n} \\
 & + \frac{\partial}{\partial x_n} \left( \frac{R_{in}^i + R_{in}^{in}}{2} + \frac{\overline{p' u_n} + \overline{p u_n'}}{\rho} \right) \\
 & - \frac{\partial}{\partial r_n} (R_{in}^i - R_{in}^{in}) - \frac{\nu \frac{\partial^2 R_i^i}{\partial x_n^2}}{2} \\
 & - 2\nu \frac{\frac{\partial^2 R_i^i}{\partial r_n^2}}{\partial r_n^2} = 0, \tag{A.2-1}
 \end{aligned}$$

where  $R_i^n \equiv \overline{u_i u_n'}$ ,

$$R_{in}^i \equiv \sum_{i=1}^3 \overline{u_i u_i' u_n'},$$

$$R_{in}^{in} \equiv \sum_{i=1}^3 \overline{u_i u_n' u_i},$$

and  $2\vec{r}$  is the vector between  $\sigma$  and  $\sigma'$ .

Multiplication of Equation (A.2-1) by

$\frac{k^2}{2\pi^2} \frac{\sin kr}{kr}$  and integrate over the whole  $\vec{r}$  space leads to the equation for the energy spectrum  $E(k)$ ,

$$U_n \frac{\partial E}{\partial x_n} + G_{in} \frac{\partial U_i}{\partial x_n} + \frac{\partial F_n}{\partial x_n} + T_1$$

I            II            III            IV

$$+ T_2 + \frac{\nu}{2} \frac{\partial^2 E}{\partial x_n^2} + 2\nu k^2 E = 0$$

V            VI            VII

(A2-2)

In this equation  $E$ ,  $G$ ,  $F$ ,  $T_1$  and  $T_2$  are defined as:

$$E(k) = \frac{k^2}{2\pi^2} \int_{Vol} \frac{1}{2} R_i^i(\vec{r}) \frac{\sin kr}{kr} dVol , \quad (A.2-3)$$

$$F_n(k) = \frac{k^2}{2\pi} \int_{Vol} \left( \frac{1}{2} R_{in}^i + \frac{\overline{p u_n}}{\rho} \right) \frac{\sin kr}{kr} dVol , \quad (A.2-4)$$

$$G_{in}(k) = \frac{k^2}{2\pi^2} \int_{Vol} R_i^n(\vec{r}) \frac{\sin kr}{kr} dVol , \quad (A.2-5)$$

$$T_1 = - \frac{k^2}{4\pi^2} \int_{Vol} \sum_{n=1}^3 \frac{\partial}{\partial r_n} (R_{in}^i - R_i^{in}) \frac{\sin kr}{kr} dVol , \quad (A.2-6)$$

$$\begin{aligned}
 T_2 = & \frac{k^2}{4\pi^2} \int_{Vol} \sum_{n=1}^3 \left\{ \left[ \frac{U_n(\frac{\vec{r}}{2}) + U_n(-\frac{\vec{r}}{2})}{2} - U_n(0) \right] \frac{\partial R_i^n}{\partial x_n} \right. \\
 & + \left[ U_n(\frac{\vec{r}}{2}) - U_n(-\frac{\vec{r}}{2}) \right] \frac{\partial R_i^n}{\partial r_n} \\
 & + \left. \left[ \frac{\partial U_i(\frac{\vec{r}}{2})}{\partial x_n} - \frac{\partial U_i(0)}{\partial x_n} \right] R_i^n \right\} \sin \frac{kr}{kr} dVol \quad (A.2-7)
 \end{aligned}$$

In equation (A.2-2), Term I represents the convection of E at the wave number k. Term II is the generation of E due to the working of the mean motion, while Term III is the turbulent diffusion of E. Terms IV and V deserve more comments. They represent the transfer of energy from lower wave numbers to higher ones; IV represents the transfer that is produced by the self-stretching of the turbulence and is called inertial transfer; V represents the transfer resulting from the interaction of the mean motion with the turbulence (Lumley and Panofsky 1964). Since both IV and V represent the transfer of the energy from one wave number to the other, and no net contribution of energy is resulted, the integrals of IV and V with respect to k from 0 to  $\infty$  must vanish. Finally the last two terms in Equation (A.2-2) represent respectively the rate of energy dissipation and viscous diffusion of E.

Appendix 3The assumed starting profiles

(a) If the starting mean-velocity profile is not given, we assume that it obeys the  $\frac{1}{7}$ -power law,

$$\frac{U}{U_G} = \eta^{1/7}, \quad (\text{A.3-1})$$

where  $\eta \equiv y/y_G$

(b) For the starting profile of  $e$ , we assume:

$$e = a + b\eta + c\eta^2 + d\eta^3 \quad (\text{A.3-2})$$

In this equation, the quantities  $a$ ,  $b$ ,  $c$  and  $d$  are evaluated from the following conditions for  $e$ :

(i) at  $\eta = (\eta)_B$ ,

$$e = C_1^{-\frac{1}{2}} \left(\frac{\tau}{\rho}\right)_B$$

and  $de/d\eta = \epsilon + |\epsilon|$ ,

$$\text{where } \epsilon \equiv \frac{y_G}{2\rho C_1^{\frac{1}{2}}} \frac{dp}{dx};$$

(ii) at  $\eta = 1$ ,

$$e = 0,$$

and  $de/d\eta = 0$ .

(c) For  $\ell$ , we assume:

$$= C_1^{\frac{1}{4}} \ell_m \quad (\text{A.3-3})$$

In this equation,  $\ell_m$  is the mixing length; thus,

$$\ell_m = \kappa y \text{ for } \lambda/\kappa > \eta > 0$$

$$\text{and } \ell_m = \lambda \cdot y_G \text{ for } 1 > \eta > \lambda/\kappa,$$

where  $\lambda \equiv 0.09$ , a constant.

(d) For enthalpy, we assume:

$$\frac{H}{H_G} = \frac{T_S}{T_G} + (T_{S,a} - T_S)U/(T_G U_G)$$

$$- \sigma_H (\gamma - 1) M^2 U^2 / (2 U_G^2) , \quad (A.3-4)$$

the Crocco temperature profile.

In the above equation,  $T_{S,a}$  is given by

$$T_{S,a} = T_G + \frac{\sigma_H U_G^2}{2 C_p}$$

For subsonic flows, the last term of Equation (A.3-4) can be neglected.

Appendix 4Method of evaluating turbulence levels from hot wires.

Because the hot wire responds to the magnitude of the cooling velocity only, but gives no indication as to its direction, there will be more unknowns than equations available for the deduction of the various turbulence correlations. Many previous investigators have proposed different ways of obtaining a closed set of equations for the hot-wire signals. Two main approaches can be identified.

The first approach reduces the higher-order correlations present in the equations into lower-order ones by assuming a certain wave-form of the fluctuating velocities. For example, Escudier (1967) reduced all even-order correlations into second-order terms and all odd order terms to zero by assuming that the fluctuations correspond to a square wave form. On the other hand, Zaric (1969) calculated the second-order correlations from the mean and rms signals by assuming that the probability density of the velocity fluctuation is Gaussian. However Durst and Whitelaw (1969) have found that Zaric's method is only applicable over a limited part of a boundary layer.

The second approach is to neglect the higher-order correlations so that the equations become determinate

(e.g. Champagne and Sleicher 1967, Guitton 1968). But the influence on the result due to the neglect of the higher-order terms is dependent on the level of the turbulence. We choose to follow this approach in the present investigation.

The hot-wire response equations.

The response of a constant-temperature hot wire, placed at an angle  $\beta$  to the effective cooling velocity  $U_{\text{eff}}$  is given by (Hinze 1959, Champagne et al 1967):

$$\Gamma = A + BU_{\text{eff}}^n (\cos^2 \beta + c^2 \sin^2 \beta)^{n/2}, \quad (\text{A.4-1})$$

where  $\Gamma$  is the hot-wire bridge voltage.

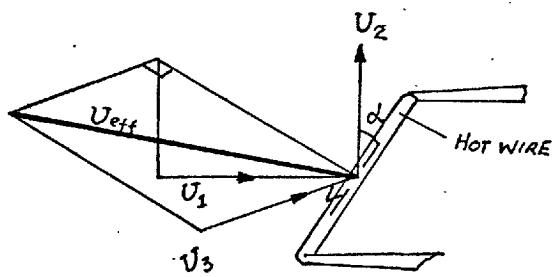
In the present investigation,  $A$ ,  $B$ ,  $n$  and  $c$  in Equation (A.4-1) are assumed constants.

The linearised form of Equation (A.4-1) reads:

$$\Gamma = K U_{\text{eff}} (\cos^2 \beta + c^2 \sin^2 \beta)^{1/2}, \quad (\text{A.4-2})$$

where  $K$  is a constant.

For a hot wire in a turbulent field as shown below, whose response obeys Equation (A.4-2), Champagne and Sleicher have derived an equation for the hot-wire bridge voltage in terms of the mean and fluctuating velocity components and the angle of inclination  $\alpha$ .



The equation, re-written in the present notation entails:

$$\begin{aligned}
 \left(\frac{\Gamma}{K}\right)^2 = & \cos^2 \alpha \left\{ U_1^2 - U_2^2 + \sec^2 \alpha (U_2^2 + U_3^2) \right. \\
 & - 2 \tan \alpha U_1 U_2 \\
 & + c^2 [2U_2^2 + U_3^2 - \sec^2 \alpha (U_2^2 + U_3^2)] \\
 & \left. + 2 \tan \alpha U_1 U_2 \right. \\
 & \left. + \tan^2 \alpha (U_1^2 + U_2^2 + U_3^2) \right\} . \quad (A.4-3)
 \end{aligned}$$

In the above equation  $U_1$ ,  $U_2$  and  $U_3$  are taken to represent the instantaneous velocities, e.g.  $U_1 = U_1 + u_1$ , etc. Taking the time mean and root-mean-square of Equation (A.4-3) result the following equations respectively:

$$\begin{aligned}
 \overline{\frac{\Gamma^2}{K^2}} = & U_1^2 \cos^2 \alpha \left\{ 1 + \frac{\overline{u_1^2}}{U_1^2} - \frac{\overline{u_2^2}}{U_1^2} - \frac{\overline{U_2^2}}{U_1^2} \right. \\
 & + \sec^2 \alpha \left( \frac{\overline{U_3^2}}{U_1^2} + \frac{\overline{U_2^2}}{U_1^2} + \frac{\overline{u_3^2}}{U_1^2} + \frac{\overline{u_2^2}}{U_1^2} \right)
 \end{aligned}$$

$$\begin{aligned}
 & - 2 \tan \alpha \left( \frac{\overline{U_2^2}}{U_1^2} + \frac{\overline{U_1 U_2}}{U_1^2} \right) \\
 & + c^2 \left[ \tan^2 \alpha + \frac{\overline{U_1^2}}{U_1^2} + \frac{\overline{U_2^2}}{U_1^2} + \frac{\overline{U_2^2}}{U_1^2} \right. \\
 & \left. + 2 \tan \alpha \left( \frac{\overline{U_2^2}}{U_1^2} + \frac{\overline{U_1 U_2}}{U_1^2} \right) \right] \} \quad (A.4-4)
 \end{aligned}$$

$$\begin{aligned}
 \frac{\overline{\Gamma^2}}{K^2} = U_1^2 \cos^2 \alpha & \left\{ \left( 1 - \tan \alpha \frac{\overline{U_2^2}}{U_1^2} \right) \right. \\
 & + \sec^2 \alpha \left( \frac{\overline{U_3^2}}{U_1^2} + \frac{\overline{U_3^2}}{U_1^2} \right) \\
 & + c^2 \left[ 2 \tan \alpha \frac{\overline{U_2^2}}{U_1^2} + \tan^2 \alpha \left( 1 + \frac{\overline{U_2^2}}{U_1^2} \right) \right. \\
 & \left. \left. + \sec^4 \alpha \frac{\overline{U_2^2}}{U_1^2} \right] \right\} \quad (A.4-5)
 \end{aligned}$$

In deriving Equation (A.4-5), the third- and higher-order correlation terms and terms containing  $c^4$  have to be neglected.

Subtraction of Equation (A.4-5) from Equation (A.4-4) yields an equation for the rms value of the a.c. component of the bridge voltage,

$$\frac{\overline{Y^2}}{K^2} = U_1^2 \cos^2 \alpha \left\{ \frac{\overline{U_1^2}}{U_1^2} + \tan^2 \alpha \frac{\overline{U_2^2}}{U_1^2} - 2 \tan \alpha \frac{\overline{U_1 U_2}}{U_1^2} \right\}$$

$$\begin{aligned}
 & + c^2 \tan \alpha \left[ \tan \alpha \frac{\overline{u_1}^2}{U_1^2} \right. \\
 & + \tan \alpha (2 + \tan^2 \alpha) \frac{\overline{u}^2}{U_1^2} \\
 & \left. + 2 \frac{\overline{u_1 u_2}}{U_1^2} \right] \} \quad (\text{A.4-6})
 \end{aligned}$$

For two-dimensional flows, further simplification to Equations (A.4-4 to 6) results. For such a flow,

$$U_3 = \overline{u_2 u_3} = \overline{u_1 u_3} = 0 .$$

Furthermore, in the present experiments,  $\frac{U_2}{U_1}$  is small as can be seen from Fig. 7.13(a). Therefore it can be neglected also in Equations (A.4-4 to 6). Thus, the signals generated by the hot wire at four different inclinations, are as follows,

$$\left[ \frac{\bar{\Gamma}^2}{K^2} \right]_1 = U_1^2 \left\{ 1 + \frac{\overline{u_2}^2}{U_1^2} + c^2 \frac{\overline{u_3}^2}{U_1^2} \right\} , \quad (\text{A.4-7})$$

$$\left[ \frac{\bar{\Gamma}^2}{K^2} \right]_1 = U_1^2 \left\{ \frac{\overline{u_1}^2}{U_1^2} \right\} , \quad (\text{A.4-8})$$

$$\left[ \frac{Y^2}{K^2} \right]_2 = \frac{U_1^2}{2} \left\{ (1 + c^2) \frac{\overline{u_1^2}}{U_1^2} + (1 - 3c^2) \frac{\overline{u_2^2}}{U_1^2} - 2(1 - c^2) \frac{\overline{u_1 u_2}}{U_1^2} \right\},$$

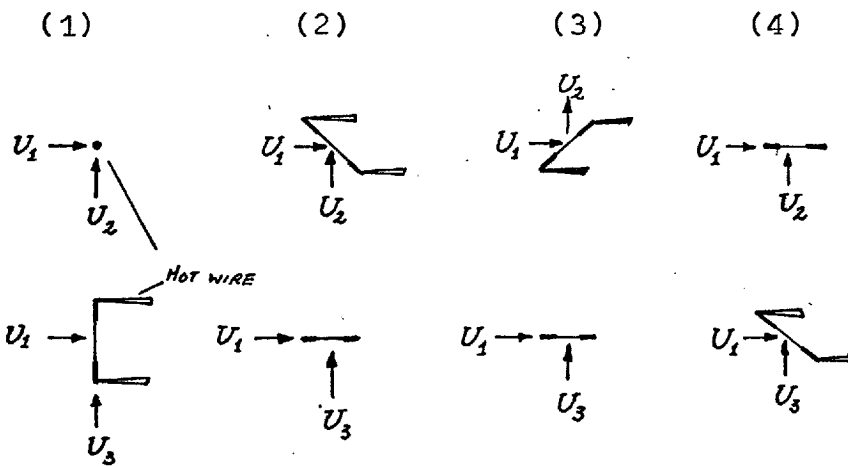
(A.4-9)

$$\left[ \frac{Y^2}{K^2} \right]_3 = \frac{U_1^2}{2} \left\{ (1 + c^2) \frac{\overline{u_1^2}}{U_1^2} + (1 - 3c^2) \frac{\overline{u_2^2}}{U_1^2} + 2(1 - c^2) \frac{\overline{u_1 u_2}}{U_1^2} \right\},$$

(A.4-10)

$$\left[ \frac{Y^2}{K^2} \right]_4 = \frac{U_1^2}{2} \left\{ (1 + c^2) \frac{\overline{u_1^2}}{U_1^2} + (1 - 3c^2) \frac{\overline{u_2^2}}{U_1^2} \right\}$$

(A.4-11)



#### Determination of the quantities n and c of the hot wire

The value of n was found by plotting the calibration curve of a DISA 55F04 gold-plated probe with different values of n. The best fitted value was found

to be 0.45, which accords with the value for  $n$  found by Collis and Williams (1959) and more recently by Gebhart et al (1970). This value was used to set the lineariser throughout the experiment. A typical sample of the linearised calibration curve is displayed in Fig.7.9.

Champagne et al (1967) suggested that the tangential cooling coefficient,  $c$ , may not only depend on the length to the diameter ratio of the hot wire but also the shape and size of the supporting prongs. Measurements were carried out to determine its value for the gold-plated probes. A linearised DISA55FO2 gold-plated probe was placed at three angles ( $\alpha = -45^\circ, 0^\circ, 45^\circ$ ) to the main stream, the flow rate of which could be varied from 10 m/s to 30m/s. From the slope of the three calibration plots, two values of  $c$  were determined according to Equation (A.4-2). The mean value of  $c$  was found to be 0.29. This value is about 30% greater than the value of  $c$  proposed by Champagne et al (1967) for the same length-to-diameter ratio.

#### Method of measuring the hot-wire signals

Although calculation of the turbulence intensities from digitised sample data like those by Frenkiel and Klebanoff (1967) and Van Atta and Chen (1968) offers many other advantages, it nevertheless requires large computer

storage and computing time. The mean signals of the hot wire in the present investigation were measured from true-integration and rms meter.

Single wires placed at four different inclinations were used to obtain the required signals. The use of single wires instead of X-wires eliminates the error induced by the various mutual interferences of the X-wires (see Wyngaard 1968, Jerome et al 1971).

Appendix 5Tabulated results of experimentsof radial wall jets

(Case (a) in Tables (i) to (iv);  
Case (b) in Tables (v) to (viii)).

$r = 15.30$  CM

$Y_{1/2} = .848$  CM

$U_{max} = 56.61$  M/S

$Y/Y_{1/2}$	$U/U_{max}$	$\sqrt{U}/U_{max}$	$\sqrt{V}/U_{max}$	$\sqrt{W}/U_{max}$	$\sqrt{e}/U_{max}$	$\overline{UV}/U_{max}^2$
.214	.838	.128	-	.011	-	-
.229	.857	.126	-	.036	-	-
.259	.934	.124	.026	.050	.097	.00104
.304	1.000	.119	.091	.046	.122	.00272
.349	.961	.123	.099	.102	.133	.00312
.409	.946	.132	.107	.106	.142	.00432
.469	.898	.145	.095	.098	.141	.00469
.544	.855	.157	.084	.099	.144	.00541
.619	.751	.171	.044	.084	.138	.00589
.709	.767	.176	.013	.077	.136	.00626
.799	.651	.182	-	.039	-	.00590
.888	.579	.184	-	-	-	-
.978	.514	.178	-	-	-	-
1.068	.456	.171	-	-	-	-
1.158	.354	.160	-	-	-	-
1.233	.300	.149	-	-	-	-

Table (i)

$$\begin{aligned}
 r &= 22.92 \text{ CM} \\
 Y_{1/2} &= 1.007 \text{ CM} \\
 U_{max} &= 38.97 \text{ M/S}
 \end{aligned}$$

$Y/Y_{1/2}$	$U/U_{max}$	$\sqrt{U}/U_{max}$	$\sqrt{V}/U_{max}$	$\sqrt{W}/U_{max}$	$\sqrt{e}/U_{max}$	$\bar{U}\bar{V}/U_{max}^2$
.061	.952	.211	—	—	—	—
.073	.893	.211	—	—	—	—
.086	.928	.210	—	—	—	—
.111	.951	.209	—	—	—	—
.149	.970	.209	—	.099	—	—
.199	.982	.209	.064	.100	.170	-.00286
.262	1.000	.209	.086	.104	.176	-.00094
.325	.895	.215	.082	.092	.175	.00052
.401	.925	.217	.092	.109	.184	.00186
.527	.814	.224	.100	.119	.193	.00431
.653	.748	.224	.117	.141	.204	.00621
.779	.657	.223	.125	.143	.207	.00788
.906	.583	.218	.136	.146	.209	.00815
1.032	.472	.211	.146	.144	.208	.00856
1.158	.421	.201	.149	.138	.202	.00819
1.284	.308	.186	.157	.137	.197	.00721
1.410	.212	.168	.170	.137	.195	.00611
1.536	.221	.148	.170	.139	.188	.00423
1.662	.081	.129	.165	.135	.176	.00336
1.789	.093	.109	.159	.129	.164	.00204

Table (ii)

$$r = 30.53 \text{ CM}$$

$$Y_{1/2} = 1.414 \text{ CM}$$

$$U_{max} = 28.41 \text{ M/S}$$

$Y/Y_{1/2}$	$U/U_{max}$	$\sqrt{U}/U_{max}$	$\sqrt{V}/U_{max}$	$\sqrt{W}/U_{max}$	$\sqrt{E}/U_{max}$	$\bar{U}\bar{V}/U_{max}^2$
.013	.724	.235	—	—	—	—
.019	.835	.241	—	—	—	—
.027	.867	.246	—	—	—	—
.045	.918	.251	—	—	—	—
.072	.836	.251	—	—	—	—
.099	.941	.248	—	.207	—	—
.135	.943	.247	—	.197	—	—
.180	.992	.246	—	.177	—	—
.233	.897	.244	—	.165	—	.01850
.287	1.000	.245	—	.157	—	.02241
.341	.934	.245	—	.157	—	.02544
.431	.859	.249	—	.147	—	.02458
.521	.806	.251	.183	.149	.244	.01209
.611	.772	.252	.199	.145	.249	.01175
.736	.715	.253	.199	.149	.251	.01369
.880	.632	.249	.201	.155	.252	.01356
1.059	.435	.240	.203	.150	.246	.01158
1.239	.398	.221	.218	.162	.247	.00625
1.419	.285	.201	.204	.157	.233	.00648
1.598	.227	.183	.192	.141	.212	.00452
1.778	.149	.152	.181	.146	.197	.00404

Table (iii)

$r = 45.80 \text{ CM}$   
 $Y_{1/2} = 2.703 \text{ CM}$   
 $U_{\max} = 17.17 \text{ M/S}$

$Y/Y_{1/2}$	$U/U_{\max}$	$\sqrt{\bar{u}}/U_{\max}$	$\sqrt{\bar{v}}/U_{\max}$	$\sqrt{\bar{w}}/U_{\max}$	$\sqrt{e}/U_{\max}$	$\bar{uv}/U_{\max}^2$
.011	.117	.147	-	-	-	-
.012	.725	.247	-	-	-	-
.015	.641	.253	-	-	-	-
.018	.743	.258	-	-	-	-
.021	.781	.260	-	-	-	-
.026	.719	.263	-	-	-	-
.035	.771	.267	-	-	-	-
.049	.852	.271	-	-	-	-
.063	.932	.276	-	.277	-	-
.082	.946	.274	-	.268	-	-
.101	.978	.271	.062	.268	.273	-.00029
.129	.924	.268	.093	.269	.277	.00181
.176	.941	.266	.125	.255	.275	.00370
.223	1.000	.265	.148	.248	.278	.00664
.270	.928	.265	.157	.257	.284	.00833
.317	.873	.265	.165	.257	.286	.01016
.364	.931	.265	.174	.256	.288	.01211
.411	.850	.268	.172	.252	.287	.01362
.458	.919	.270	.171	.249	.286	.01473
.524	.779	.272	.172	.249	.288	.01606
.599	.778	.275	.164	.243	.286	.01722
.693	.684	.271	.172	.241	.284	.01833
.787	.631	.267	.172	.241	.292	.01911
.891	.538	.263	.166	.231	.274	.01894
.975	.536	.265	.166	.228	.269	.01884
1.068	.404	.242	.164	.231	.265	.01776
1.162	.415	.236	.168	.218	.254	.01641
1.303	.192	.211	.161	.210	.239	.01362
1.444	.333	.158	.155	.200	.223	.01044
1.585	.132	.171	.138	.173	.194	.00811
1.773	.119	.138	.130	.163	.179	.00682
1.961	.176	.111	.124	.119	.160	.00371

Table (iv)

$$\begin{aligned}
 r &= 9.09 \text{ CM} \\
 Y_{1/2} &= .695 \text{ CM} \\
 U_{max} &= 14.87 \text{ M/S}
 \end{aligned}$$

$Y/Y_{1/2}$	$U/U_{max}$	$\sqrt{\bar{U}}/U_{max}$	$\sqrt{\bar{V}}/U_{max}$	$\sqrt{\bar{W}}/U_{max}$	$\sqrt{\bar{e}}/U_{max}$	$\bar{uv}/U_{max}^2$
.066	.884	.243	-	-	-	-
.124	.968	.292	-	-	-	-
.161	.989	.290	-	-	-	-
.216	1.000	.286	-	.164	-	-
.271	.984	.284	.151	.175	.259	.01708
.344	.961	.284	.170	.171	.263	.02078
.417	.921	.286	.191	.167	.270	.02525
.490	.877	.286	.202	.165	.274	.02736
.563	.827	.289	.203	.157	.273	.02865
.636	.772	.290	.199	.160	.273	.02958
.709	.714	.286	.203	.157	.271	.02962
.782	.662	.284	.194	.154	.267	.02854
.855	.601	.278	.197	.141	.261	.02746
.965	.523	.265	.198	.139	.254	.02478
1.075	.450	.253	.179	.130	.238	.02159
1.184	.378	.229	.176	.148	.230	.01752
1.294	.319	.210	.165	.146	.215	.01378
1.477	.239	.181	.151	.136	.192	.00957
1.660	.170	.144	.145	.137	.174	.00614
1.842	.143	.118	.118	.119	.145	.00314
2.062	.122	.093	.094	.099	.117	.00146
2.281	.116	.075	.070	.078	.091	.00087
2.537	.109	.058	.053	.073	.076	.00069

Table (v)

$r = 16.69 \text{ CM}$   
 $Y_{1/2} = 1.369 \text{ CM}$   
 $U_{\max} = 9.51 \text{ M/S}$

$Y/Y_{1/2}$	$U/U_{\max}$	$\sqrt{u}/U_{\max}$	$\sqrt{v}/U_{\max}$	$\sqrt{w}/U_{\max}$	$\sqrt{e}/U_{\max}$	$\bar{u}\bar{v}/U_{\max}^2$
.029	.736	.284	-	-	-	-
.042	.832	.322	-	-	-	-
.097	.958	.332	.133	.083	.259	.00257
.227	1.000	.322	.209	.278	.335	.01400
.376	.948	.322	.256	.268	.347	.02372
.561	.829	.328	.263	.255	.348	.03524
.784	.664	.316	.245	.232	.327	.03663
1.062	.453	.274	.225	.216	.293	.02715
1.340	.260	.246	.204	.191	.250	.01697
1.618	.159	.153	.174	.176	.208	.00825

Table (vi)

$$r = 26.79 \text{ CM}$$

$$Y_{1/2} = 2.223 \text{ CM}$$

$$U_{max} = 5.33 \text{ M/S}$$

$Y/Y_{1/2}$	$U/U_{max}$	$\sqrt{\bar{U}^2}/U_{max}$	$\sqrt{\bar{V}^2}/U_{max}$	$\sqrt{\bar{W}^2}/U_{max}$	$\sqrt{\bar{e}}/U_{max}$	$\bar{U}\bar{V}/U_{max}^2$
.016	.520	.254	-	-	-	-
.024	.673	.294	-	-	-	-
.039	.819	.327	-	-	-	-
.073	.916	.338	.185	.325	.356	.00600
.130	.988	.333	.204	.311	.362	.00689
.210	1.000	.333	.239	.314	.365	.01316
.302	.995	.327	.276	.312	.375	.02061
.416	.941	.333	.282	.300	.375	.02772
.587	.821	.333	.294	.299	.378	.03400
.759	.684	.321	.286	.290	.367	.03366
.930	.554	.307	.254	.258	.336	.02920
1.102	.422	.276	.253	.249	.312	.02581
1.330	.273	.228	.246	.222	.284	.01825
1.559	.172	.180	.205	.197	.238	.01030
1.787	.137	.145	.151	.172	.192	.00459

Table (vii)

$r = 42.09 \text{ CM}$

$Y_{1/2} = 3.575 \text{ CM}$

$U_{\max} = 3.24 \text{ K/S}$

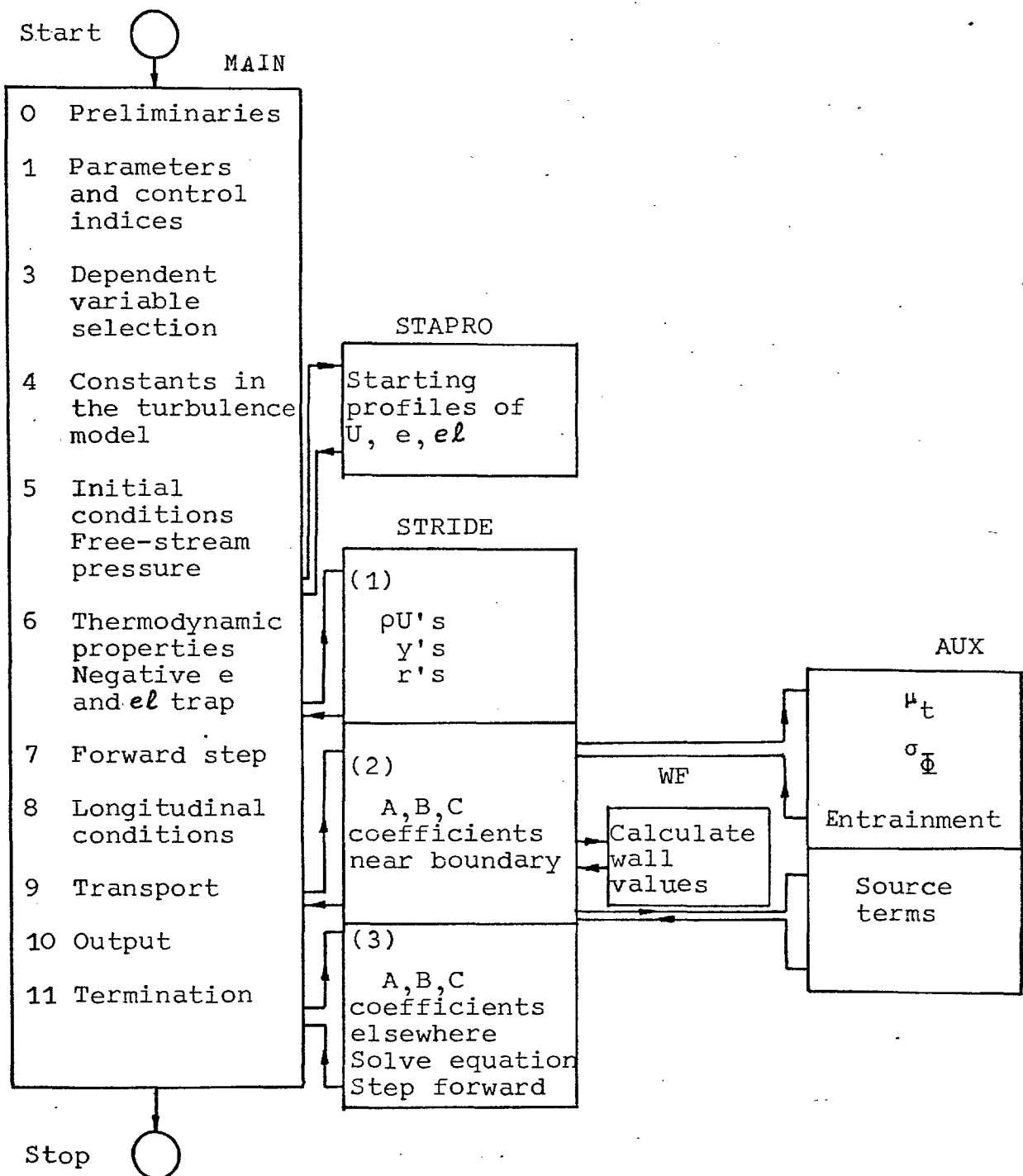
$Y/Y_{1/2}$	$U/U_{\max}$	$\sqrt{U}/U_{\max}$	$\sqrt{V}/U_{\max}$	$\sqrt{W}/U_{\max}$	$\sqrt{e}/U_{\max}$	$\bar{uv}/U^2_{\max}$
.011	.380	.206	-	-	-	-
.015	.524	.266	-	-	-	-
.023	.671	.313	-	-	-	-
.041	.835	.332	.138	.320	.341	-.00442
.066	.905	.337	.179	.314	.349	-.00290
.115	.976	.342	.195	.321	.359	.00104
.186	1.000	.332	.256	.324	.375	.01001
.293	.975	.332	.277	.320	.381	.01871
.400	.926	.332	.303	.327	.393	.02552
.542	.842	.337	.295	.313	.386	.03049
.684	.729	.332	.293	.318	.385	.03299
.826	.618	.318	.282	.290	.364	.03281
.968	.526	.304	.248	.243	.326	.02721
1.110	.410	.269	.239	.236	-.304	.02213
1.252	.321	.242	.220	.196	.270	.01734
1.430	.205	.201	.211	.182	.243	.01241
1.607	.175	.177	.165	.166	-.208	.00730
1.820	.138	.144	.124	.128	.162	.00367

Table (viii)

Appendix 6Sample listing of the computer program

The program listed below is suitable for the calculation of constant-property boundary layers using the two-equation model. Most of the symbols in the program are identical to those used by Patankar and Spalding (1970) in their GENMIX4 program. Additional symbols are explained by way of comment statements in the listing.

A 30-point cross-stream grid has been used for all the calculations reported.



Function of individual parts in  
the program









```

TEST=1005.
WRITE(6,100) TEST,RMI,RME,DX
1005 CONTINUE
CHAPTER 10B ----- TESTS FOR PRINTOUT
IPRINT=0
IF(ISTEP.EQ.0) GO TO 102
IF(ITEST.EQ.1) GO TO 102
IF(IFIN.EQ.1) GO TO 102
IF(FLOAT(ISTEP/NSTA).EQ.FLOAT(ISTEP)/ANSTA) GO TO 102
IPRINT=0
GO TO 105
CHAPTER 10C ----- STATION VARIABLES
102 IPRINT=1
103 IPRINT=IPRINT+1
UBAR=.0
DO 108 I=2,NP1
108 UBAR=UBAR+(U(I)+U(I+1))*(OM(I+1)-OM(I))
UBAR=.5*UBAR
CHAPTER 10D ----- PROFILE VARIABLES
C ----- TEST 6
IF(ITEST.EQ.0) GO TO 1006
TEST=1006.
WRITE (6,100) TEST
1006 CONTINUE
IF(IPRINT.LT.2) GO TO 105
T=PEI/(RHO(NP3)*U(NP3)*R(NP3))
DEL1=Y(NP3)-T
DEL2=T*(1.-UBAR/U(NP3))
H12=DEL1/DEL2
R2=DEL2*U(NP3)/ANU
SS=TAUI/(RHO(NP3)*U(NP3)**2)
GF=(1.-1./H12)/SQRT(SS)
WRITE(6,906) XU,DX,H12,R2 ,SS,PEI,RME,GF,ISTEP
906 FORMAT(1H06X,2HXU,8X,2HDX,7X,3HH12.9X,2HR2,9X,2HSS,9X,
1 3HPEI 7X,3HRME 7X,2HGF 6X,5HISTEP/(1H 1P8E11.3*I4))
UFAC=U(NP3)
TKFAC=UFAC**2
TFAC=RU(NP3)*U(NP3)
YFAC=1.
ALFAC=Y(NP3)
VFAC=U(NP3)*DEL1
C CALCULATE AND WRITE PROFILE VARIABLES
904 J=0
IPR=1
DO 905 IPRO=1,13
OP(1)=0.
OP(2)=0.
OP(NP2)=0.
OP(NP3)=0.
GO TO (910,920,930,940,942,960,970,975,962,962,962,
1 962), IPRO
910 DO 911 I=1,NP2
911 OP(I)=Y(I)/YFAC
OP(NP3)=Y(NP3)
GO TO 980
920 DO 921 I=1,NP3
921 OP(I)=U(I)/UFAC
OP(NP3)=U(NP3)

```



```

SUBROUTINE AUX(K)
C***** FOR BOUNDARY LAYERS
DIMENSION YEDGE(6)
COMMON/GENRAL/ AJE(5),AJI(5),CSALFA,DPDX(43),DX,EMU(43),F(5,43),
1 FS(5,43),H,IFIN,INDE(5),INDI(5),ISTEP,ITEST,IUTRAP,KEX,KIN,KRAD,
2 N,NEQ,NPH,NP1,NP2,NP3,OM(43),PEI,PR(5),PREF(5,43),PSIE,PSII,
3 R(43),RHO(43),RME,RMI,RU(43),SD(5,43),SU(5,43),TAUE,TAUI,U(43),
4 XD,XU,Y(43),YE,YI
COMMON/GM4/AK,ALMG,EWALL,IPRINT,BPI
COMMON/CONST/AQ,C1,C2,C3,C4,SRC1,CL
GOTO(100,200),K
100 CONTINUE
IF(ISTEP.GT.0) GOTO 21
DO 22 J=1,5
DO 22 I=1,NP3
FS(J,I)=.0
SU(J,I)=.0
22 SD(J,I)=.0
21 CONTINUE
EMU(2)=(RHO(2)+RHO(3))*(F(2,2)+F(2,3))
1 /SQRT(8.*(F(1,2)+F(1,3)))
EMU(NP1)=(RHO(NP1)+RHO(NP2))*(F(2,NP1)+F(2,NP2))
1 /SQRT(8.*(F(1,NP1)+F(1,NP2)))
90 DO 92 I=3,N
92 EMU(I)=(RHO(I)+RHO(I+1))*(F(2,I)+F(2,I+1))/ SQRT(8.*(F(1,I)
1 +F(1,I+1)))
20 CONTINUE
C ----- TEST 10
IF(ITEST.EQ.0) GO TO 1010
TEST=1010.
WRITE(6,101) TEST
WRITE(6,101) (EMU(I),I=1,NP3)
WRITE(6,101) (SD(1,I),I=1,NP3)
1010 CONTINUE
C----- MODIFICATION OF EMU ARRAY -----
DO 24 I=2,NP1
24 EM U(I)=EMU(I)/(Y(I+1)-Y(I))
IF(KRAD.EQ.0) GO TO 25
DO 26 I=2,NP1
26 EM U(I)=EM U(I)*.5*(R(I)+R(I+1))
25 CONTINUE
C----- PREF'S -----
IF(ISTEP.GT.0) GO TO 28
DO 27 J=1,NPH
DO 27 I=1,NP3
101 FORMAT(1H ,3X,1P11E11.3)
27 PREF(J,I)=PREF(J,1)
28 CONTINUE
C 2 2 2 2 2 2 ENTRAINMENT
IF(KIN.EQ.2) RMI=2.*EMU(2)
IF(KEX.EQ.2) RME=-2.*EMU(NP1)
RETURN
C 3 3 3 3 3 3 SOURCES
C USE OF FS ARRAY
200 CONTINUE
BK=(TAUI+YI*DPDX(1))/(SRC1*.5*(RHO(2)+RHO(3)))
GENKP=C1*BK**1.5*(Y(3)-YI)**.5*(R(2)+R(3))/(CL*YI)
GENKLP=GENKP*CL*YI

```

```

DO 11 I=3,NP1
T=R(I)*RHO(I)*F(1,I)**1.5
AL=F(2,I)/F(1,I)
YPM=.5*(Y(I+1)-Y(I-1))
IF(I.EQ.3) YPM=.5*(Y(4)+Y(3))-YI
IF(I.EQ.NP1) YPM=Y(NP3)-YE-.5*(Y(NP1)+Y(N))
ALI=(F(2,I+1)+F(2,I))/(F(1,I+1)+F(1,I))
GENKM=GENKP
GENKP=.5*EM U(I)*(U(I+1)-U(I))**2
GENKLM=GENKLP
GENKLP=GENKP*ALI
IF(I.EQ.NP1) GENKP=GENKP*2.*((Y(NP3)-YE-Y(NP1))/(Y(NP2)-Y(NP1)))
FS(1,I)=(GENKP+GENKM)/YPM
FS(2,I)=C1*T/AL
FS(3,I)=C2*(GENKLP+GENKLM)/YPM
FS(4,I)=C3*T
FS(5,I)=(C4*AL/Y(I))**AQ*FS(3,I)/C2
SU(1,I)=(FS(1,I)-FS(2,I))*YPM
SU(2,I)=(FS(3,I)-FS(4,I)-FS(5,I))*YPM
11 CONTINUE
ALI=(F(2,NP1)+F(2,NP2))/(F(1,NP1)+F(1,NP2))
GENKLP=GENKP*ALI
T=.25*(RHO(NP1)+RHO(NP2))*(R(NP1)+R(NP2))*.
1 (.5*(F(1,NP1)+F(1,NP2)))**1.5
FS(1,NP2)=GENKP/(Y(NP3)-YE-Y(NP1))
FS(2,NP2)=C1*T/ALI
FS(3,NP2)=C2*FS(1,NP2)*ALI
FS(4,NP2)=C3*T
FS(5,NP2)=(C4*ALI/(Y(NP3)-YE))**AQ*FS(3,NP2)/C2
IF(KEX.NE.3) GOTO 12
AL=F(2,NP3)/F(1,NP3)
T=RHO(NP3)*R(NP3)*F(1,NP3)**1.5
FS(2,NP3)=C1*T/AL
FS(4,NP3)=C3*T
12 SU(1,NP2)=.5*(FS(1,NP2)+FS(1,NP3)-FS(2,NP2)-FS(2,NP3))*YE
SU(2,NP2)=.5*(FS(3,NP2)+FS(3,NP3)-FS(4,NP2)-FS(4,NP3))
1 -FS(5,NP2)-FS(5,NP3))*YE
C-----TEST 11
IF(ITEST.EQ.0) GOTO 1011
WRITE(6,101) TEST
WRITE(6,101) ((FS(J,I),I=1,NP3),J=1,5)
WRITE(6,101) ((SU(J,I),I=1,NP3),J=1,2)
1011 CONTINUE
RETURN
END

```

1010 END STATE

```

SUBROUTINE STRIDE(ISW)
C***** STRIDE ROUTINE BASED ON THE GENMIX4 VERSION OF THE
C***** PATANKAR-SPALDING PROGRAM
      DIMENSION A(5,43),AU(43),B(5,43),BU(43),C(5,43),CU(43),FDIFE(5),
      1 FDIFI(5),GE(5),GI(5),TTPF(5)
      COMMON/GENRAL/ AJE(5),AJI(5),CSALFA,DPDX(43),DX,EMU(43),F(5,43),
      1 FS(5,43),H,IFIN,INDE(5),INDI(5),ISTEP,ITEST,IUTRAP,KEX,KIN,KRAD,
      2 N,NEQ,NPH,NP1,NP2,NP3,OM(43)*PEI,PR(5)*PREF(5,43),PSIE,PSII,
      3 R(43),RHO(43),RME,RMI,RU(43),SD(5,43),SU(5,43),TAUE,TAUI,U(43),
      4 XD,XU,Y(43),YE,YI
      COMMON/GM4/AK,ALMG,EWALL,IPRINT,BPI
      COMMON/CONST/AQ,C1,C2,C3,C4,SRC1,CL
C
      GO TO (1000,2000,3000), ISW
C
C***** ***** S T R I D E 1 *****
1000 IF(ISTEP.GT.0) GO TO 1100
      OM(1)=0.
      OM(2)=0.
      OM(NP2)=1.
      OM(NP3)=1.
      OMI=.5*OM(3)
      OME=.5*(1.-OM(NP1))
      IF(KEX.EQ.2) BPE=1.
      IF(KIN.EQ.2) BPI=1.
      Y(1)=0.
      IF(KRAD.EQ.1) GO TO 1100
      DO 1001 I=1,NP3
1001 R(I)=1.
      R25=1.
      RN15=1.
      IF(ITEST.EQ.0) GO TO 9018
      WRITE(6,9010) (R(I),I=1,NP3),R25,RN15
9010 FORMAT(1H ,1P11E11.3)
9018 CONTINUE
C----- CALCULATION OF RHO*U 'S -----
1100 DO 1101 I=1,NP3
      IF(RHO(I).GT.0.) GO TO 1101
      WRITE(6,1108) RHO(I),I,RHO(I)
1108 FORMAT(25H NEGATIVE OR ZERO RHO(I)=,1PE11.3,6H AT I=,I3,6X,
      121HSET TO ABS OF RHO(I)=,E11.3)
      RHO(I)=ABS(RHO(I))
1101 RU(I)=RHO(I)*U(I)
      RU3=RU(3)
      RUN1=RU(NP1)
      DO 1102 I=2,NP1
      RU(I)=.5*(RU(I)+RU(I+1))
1102 CONTINUE
      IF(ITEST.EQ.0) GO TO 9019
      WRITE(6,9010) (RU(I),I=1,NP3),RUN1,RU3,PEI
9019 CONTINUE
C----- CALCULATION OF Y 'S AND R 'S -----
C ----- Y'S FOR PLANE GEOMETRY
      YI=PEI*OMI/(RPI*RU(2))
      Y(3)=YI+PEI*OM(3)/(RU(2)+RU3)
      Y(2)=2.*YI-Y(3)
      DO 1103 I=4,NP1
1103 Y(I)=Y(I-1)+PEI*(OM(I)-OM(I-1))/RU(I-1)

```

```

YN15=Y(NP1)+PEI*(1.-OM(NP1))/(RU(NP1)+RUN1)
YE=PEI*OME/(BPE*RU(NP1))
Y(NP3)=YN15+YE
Y(NP2)=2.*YN15-Y(NP1)
IF(KRAD.EQ.0) RETURN
C ----- Y'S AND R'S FOR AXISYMMETRICAL GEOMETRY
IF(CSALFA.EQ.0.) GO TO 1110
C ----- CSALFA NE ZERO
COSD2=.5*CSALFA
IF(R(1).NE.0.) GO TO 1105
C----- R(1)=0.
DO 1106 I=2,NP3
Y(I)=SQRT(ABS(Y(I)/COSD2))
1106 R(I)=Y(I)*CSALFA
YI=SQRT(ABS(YI/COSD2))
YN15=SQRT(ABS(YN15/COSD2))
GO TO 1107
C ----- R(1) NE 0.
1105 R1D2=.5*R(1)
R1D2SQ=R1D2*R1D2
DO 1104 I=2,NP3
Y(I)=Y(I)/(R1D2+SQRT(ABS(R1D2SQ+COSD2*Y(I))))
1104 R(I)=R(1)+Y(I)*CSALFA
YI=YI/(R1D2+SQRT(ABS(R1D2SQ+COSD2*YI)))
YN15=YN15/(R1D2+SQRT(ABS(R1D2SQ+COSD2*YN15)))
1107 R25=R(1)+YI*CSALFA
RN15=R(1)+YN15*CSALFA
YE=Y(NP3)-YN15
RETURN
C ----- CSALFA EQ ZERO
1110 DO 1111 I=2,NP3
Y(I)=Y(I)/R(1)
1111 R(I)=R(1)
YI=YI/R(1)
YN15=YN15/R(1)
R25=R(1)
RN15=R(1)
YE=Y(NP3)-YN15
RETURN
C***** S T R I D E 2 *****
C ----- PRELIMINARIES FOR COEFFICIENTS
2000 CALL AUX(1)
PX=PEI/DX
G=RMI-RME
PD8=.125*PX
PD4=.25*PX
PG=PX+G
PGD8=.125*PG
PGD4=PGD8+PGD8
RMID2=.5*RMI
GD4=.25*G
BOMP=OM(3)-OM(2)
PGOMP=PGD4*BOMP
P40MP=PD4*BOMP
C ----- GRID POINT 2
C ----- TAUI, BPI, TI
IF(KIN.NE.1) GO TO 2001
CALL WF(0,1,2,3,BPI,T1,TAUI)

```

GO TO 2002

2001 T1=0.

IF (KRAD.EQ.0) BPI=.33333+.66667\*RU(1)/RU(2)

IF (KRAD.EQ.1) BPI=(R(1)\*(5.\*RU(1)+RU(2))+3.\*R25\*  
1 (RU(1)+RU(2)))/6./(R(1)+R25)/RU(2)

C ----- BOUNDARY COEFFICIENTS FOR VELOCITY

2002 HLP=RMID2-GD4\*(OM(2)+OM(3))

AHLP=ABS(HLP)

THLP=HLP+HLP

TP=EM U(2)

TTP=TP+AHLP+ABS(TP-AHLP)

AD=TTP-THLP-T1-PGOMP

BD=2.\*(T1+RMI)

CD=P40MP\*(3.\*U(2)+U(3))-DPDX(2)\*(R(1)+R25)\*YI

DU=AD+BD+PX\*ROMP

AU(2)=AD/DU

BU(2)=BD/DU

CU(2)=CD/DU

C ----- BOUNDARY COEFFICIENTS FOR F'S

IF (NEQ.EQ.1) GO TO 2304

DO 2300 J=1,NPH

TPF2=TP/PREF(J,2)

TTPF(J)=TPF2+AHLP+ABS(TPF2-AHLP)

IF (KIN.NE.1) GO TO 2301

CALL WF(J,1,2,3,FDIFI(J),T1F,GI(J))

IF (INDI(J).EQ.2) GO TO 2303

AJI(J)=GI(J)\*(F(J,1)-.5\*(F(J,2)+F(J,3))-FDIFI(J))

GO TO 2302

2301 T1F=0.

FDIFI(J)=0.

C ----- COEFFICIENTS

2302 ADF=TTPF(J)-THLP-T1F-PGOMP+.5\*SD(J,2)

BDF=2.\*(T1F+RMI)

DF=ADF+BDF+PX\*ROMP-2.\*SD(J,2)

T=-T1F\*FDIFI(J)

GO TO 2305

2303 ADF=TTPF(J)-THLP-PGOMP+.5\*SD(J,2)

BDF=0.

DF=ADF+PX\*ROMP-2.\*SD(J,2)+RMI\*2.

T=RMI\*F(J,1)+AJI(J)\*R(1)

2305 TT=3.\*F(J,2)+F(J,3)

CDF=P40MP\*TT+2.\*(T+SU(J,2))

A(J,2)=ADF/DF

B(J,2)=BDF/DF

2300 C(J,2)=CDF/DF

C

C MATCH OF THE COUETTE FLOW SOLUTION FOR K AND KL

C

IF (J.GT.2) GOTO 2306

A(J,2)=-1.

B(J,2)=.0

C(J,2)=2.\*(TAUI+DPDX(1)\*YI)/(SRC1\*(RHO(2)+RHO(3)))

IF (J.EQ.2) C(J,2)=C(J,2)\*CL\*YI

2306 CONTINUE

C

C

C ----- GRID POINT NP2

C----- TAUE, BPE, TNP3

```

2304 IF(KEX.NE.1) GO TO 2003
  CALL WF(0,NP3,NP2,NP1,BPE,TNP3,TAUE)
  GO TO 2310
2003 TNP3=0.
  IF(KRAD.EQ.0) BPE=.33333+.66667*RU(NP3)/RU(NP1)
  IF(KRAD.EQ.1) BPE=(R(NP3)*(5.*RU(NP3)+RU(NP1))+3.*RN15*
    1      (RU(NP3)+RU(NP1)))/6./(R(NP3)+RN15)/RU(NP1)
C ----- BOUNDARY COEFFICIENTS FOR VELOCITY
2310 B0MM=OM(NP2)-OM(NP1)
  HLM=RMID2-GD4*(OM(NP1)+OM(NP2))
  AHLM=ABS(HLM)
  THLM=HLM+HLM
  TM=EM U(NP1)
  TTM=TM+AHLM+ABS(TM-AHLM)
  PG0MM=PGD4*B0MM
  P40MM=PD4*B0MM
  AD=2.* (TNP3-RME)
  BD=TTM+THLM-TNP3-PG0MM
  CD=P40MM*(3.*U(NP2)+U(NP1))-DPDX(NP2)*(RN15+R(NP3))*YE
  DU=AD+BD+PX*B0MM
  AU(NP2)=AD/DU
  BU(NP2)=BD/DU
  CU(NP2)=CD/DU
  IF(NEQ.EQ.1) RETURN
C ----- BOUNDARY COEFFICIENTS FOR F'S
  CALL AUX(2)
  DO 2320 J=1,NPH
    TMF=TM/PPEF(J,NP1)
    TTMF=TMF+AHLM+ABS(TMF-AHLM)
    IF(KEX.NE.1) GO TO 2311
    CALL WF(J,NP3,NP2,NP1,FDIFE(J),TNP3F,GE(J))
    IF(INDE(J).EQ.2) GO TO 2313
    AJE(J)=GE(J)*(.5*(F(J,NP2)+F(J,NP1))+FDIFE(J)-F(J,NP3))
    GO TO 2312
2311 TNP3F=0.
  FDIFE(J)=0.
C ----- COEFFICIENTS
2312 ADF=2.* (TNP3F-RME)
  BDF=TTMF+THLM-TNP3F-PG0MM+.5*SD(J,NP2)
  DF=ADF+BDF+PX*B0MM-2.*SD(J,NP2)
  T=-TNP3F*FDIFE(J)
  GO TO 2315
2313 ADF=0.
  BDF=TTMF+THLM-PG0MM+.5*SD(J,NP2)
  DF=BDF+PX*B0MM-2.*SD(J,NP2)-RME*2.
  T=-RME*F(J,NP3)-AJE(J)*R(NP3)
2315 TT=3.*F(J,NP2)+F(J,NP1)
  CDF=P40MM*TT+2.*(T+SU(J,NP2))
  A(J,NP2)=ADF/DF
  B(J,NP2)=BDF/DF
2320 C(J,NP2)=CDF/DF
  RETURN
C***** S T R I D E 3 *****
3000 DO 3005 I=3,NP1
  B0MP=B0MP
  B0MP=OM(I+1)-OM(I)
  B0M=B0MM+B0MP
  B0MT3=B0M*3.

```

```

PGOMM=PGOMP
PGOMP=PGD4*BOMP
PBOM=PX*BOM
THLM=THLP
    HLP=RMID2-GD4*(OM(I+1)+OM(I))
THLP=HLP+HLP
    AHLP=ABS(HLP)
TTM=TTP
    TP=EM U(I)
TTP=TP+AHLP+ABS(TP-AHLP)
AD=TTP-THLP-PGOMP
BD=TTM+THLM-PGOMM
CD=PD4*(BOMT3*U(I)+BOMP* U(I+1)+BOMM*U(I-1))-  

1      DPDX(I)*R(I)*(Y(I+1)-Y(I-1))
        DU=AD+BD+PBOM
        AU(I)=AD/DU
        BU(I)=BD/DU
        CU(I)=CD/DU

```

C ----- START OF J LOOP

```

IF(NEQ.EQ.1) GO TO 3005
DO 3004 J=1,NPH

```

```

3002 TTMF=TTPF(J)
3003 TPF=EM U(I)/PREF(J,I)
    TTPF(J)=TPF+AHLP+ABS(TPF-AHLP)
    AD=TTPF(J)-THLP-PGOMP
    BD=TTMF+THLM-PGOMM
    CD=PD4*(ROMT3*F(J,I)+BOMP*F(J,I+1)+BOMM*F(J,I-1))
    CD=CD+2.*SU(J,I)
    DF=AD+BD+PROM-2.*SD(J,I)
        A(J,I)=AD/DF
        B(J,I)=BD/DF
3004 C(J,I)=CD/DF

```

```

3005 CONTINUE
IF(IEST.EQ.0) GO TO 9013
WRITE(6,9001) (AU(I),I=2,NP2)
WRITE(6,9002) (BU(I),I=2,NP2)
WRITE(6,9003) (CU(I),I=2,NP2)

```

```

9001 FORMAT(7H AU(I) ,1P11E11.3)
9002 FORMAT(7H BU(I) ,1P11E11.3)
9003 FORMAT(7H CU(I) ,1P11E11.3)
IF(NEQ.EQ.1) GO TO 9013
DO 9000 J=1,NPH
    WRITE(6,9004) (A(J,I),I=2,NP2)
    WRITE(6,9005) (B(J,I),I=2,NP2)
9000 WRITE(6,9006) (C(J,I),I=2,NP2)
9004 FORMAT(8H A(J,I) ,1P11E11.3)
9005 FORMAT(8H B(J,I) ,1P11E11.3)
9006 FORMAT(8H C(J,I) ,1P11E11.3)
9013 CONTINUE

```

C-----

```

IF(KIN.EQ.2.AND.RU(1).NE.0.) U(1)=U(1)-DPDX(1)*DX/RU(1)
IF(KEX.EQ.2.AND.RU(NP3).NE.0.) U(NP3)=U(NP3)-DPDX(NP3)*DX/RL(NP3)
C----- SOLVE FOR DOWNSTREAM U 'S -----

```

```

3047 BU(2)=RU(2)*U(1)+CU(2)
DO 3048 I=3,NP2
    T=1.-BU(I)*AU(I-1)
    AU(I)=AU(I)/T
3048 BU(I)=(BU(I)*BU(I-1)+CU(I))/T

```

```

DO 3050 IDASH=2,NP2
I=N+4-IDASH
U(I)=AU(I)*U(I+1)+BU(I)
C TEST FOR NEGATIVE VELOCITY
C IUTRAP=0 NO ACTION, =1 SET U'S TO ZERO, =2 PRINT AND STOP
IF(IUTRAP.EQ.0) GO TO 3050
IF(I.EQ.2.OR.I.EQ.NP2.OR.U(I).GE.0.) GO TO 3050
IF(IUTRAP.EQ.1) GO TO 3051
IFIN=1
ITEST=1
WRITE(6,3120)
3120 FORMAT(10X,33HAT LEAST ONE VELOCITY IS NEGATIVE)
RETURN
3051 U(I)=1.E-30
3050 CONTINUE
IF(KIN.EQ.3)U(I)=.5*(U(2)+U(3))
IF(KEX.EQ.3)U(NP3)=.5*(U(NP1)+U(NP2))
72 IF(NEQ.EQ.1) GO TO 3060
DO 3320 J=1,NPH
C----- SOLVE FOR DOWNSTREAM F IS -----
B(J,2)=B(J,2)*F(J,1)+C(J,2)
DO 3148 I=3,NP2
T=1.-B(J,I)*A(J,I-1)
A(J,I)=A(J,I)/T
3148 B(J,I)=(B(J,I)*B(J,I-1)+C(J,I))/T
DO 3150 IDASH=2,NP2
I=N+4-IDASH
3150 F(J,I)=A(J,I)*F(J,I+1)+B(J,I)
C----- ADJUST F(J,1) AND F(J,NP3) -----
GO TO (3210,3220,3230),KIN
3210 IF(INDI(J).EQ.2) F(J,1)=FDIFI(J)+.5*(F(J,2)+F(J,3))+AJI(J)/GI(J)
GO TO 3220
3230 F(J,1)=.5*(F(J,2)+F(J,3))
3220 GO TO (3310,3320,3330),KEX
3310 IF(INDE(J).EQ.2) F(J,NP3)=FDIFE(J)+.5*(F(J,NP2)+  

1 F(J,NP1))-AJE(J)/GE(J)
GO TO 3320
3330 F(J,NP3)=.5*(F(J,NP1)+F(J,NP2))
3320 CONTINUE
3060 XU=XD
PSII=PSII-RMI*DX
PSIE=PSIE-RME*DX
PEI=PSIE-PSII
ISTEP=ISTEP+1
RETURN
END

```

```

SUBROUTINE WF(J,I1,I2,I3,OUT1,OUT2,OUT3)
COMMON/GENRAL/ AJE(5),AJI(5),CSALFA,DPDX(43),DX,EMU(43),F(5,43),
1 FS(5,43),H,IFIN,INDE(5),INDI(5),ISTEP,ITEST,IUTRAP,KEX,KIN,KRAD,
2 N,NEQ,NPH,NP1,NP2,NP3,OM(43),PEI,PR(5),PREF(5,43),PSIE,PSII,
3 R(43),RHO(43),RME,RMI,RU(43),SD(5,43),SU(5,43),TAUE,TAUI,L(43),
4 XD,XU,Y(43),YE,YI
COMMON/GM4/AK,ALMG,EWALL,IPRINT,BPI
COMMON/CONST/A0,C1,C2,C3,C4,SRC1,CL
C EFFECTS OF PRESSURE GRADIENT, MASS TRANSFER AND
C RADIUS VARIATION ARE NEGLECTED
C FOR VELOCITY,      OUT1=BP,      OUT2=T,      OUT3=TAU
C FOR F'S,           OUT1=FIDIF,   OUT2=T,      OUT3=G
C
I25=I3-1/I1
JDASH=J+1
GO TO (100,200,200,200), JDASH
C LOG-LAW
100 UREF=.5*(U(I2)+U(I3))
RHOREF=.5*RHO(I1)+.25*(RHO(I2)+RHO(I3))
RREF=.5*(R(I2)+R(I3))
VREF=EMU(I1)
YREF=YE-YI*(YE-YI)*OM(I1)
RE=UREF*RHOREF*YREF/VREF
RRUREF=RREF*RU(I25)
C ----- LOG LAW
ER=RE*EWALL
NIT=0
SHALF=SQRT(TAUI/(RHOREF*UREF**2))
101 SHALF1=SHALF
SHALF=AK ALOG(ER*SHALF)
IF(ABS(SHALF -SHALF1).LT..0001.OR.NIT.GT.10) GO TO 102
NIT=NIT+1
GO TO 101
102 S=SHALF**2
OUT1=AK/(AK+SHALF)
EM U(I25)=.25*RHOREF*RREF*ABS(U(I3)-U(I2))*(AK/OUT1)**2
103 OUT2=S*RRUREF
OUT3=OUT2*UREF/R(I1)
RETURN
200 CONTINUE
OUT1=.0
OUT2=.0
OUT3=.0
RETURN
END

```

FILE SPACE

```

SUBROUTINE STAPRO
C CALCULATION OF THE STARTING PROFILES
DIMENSION DOM(50),DY(50),DU(50),DRHO(50)
COMMON/GENRAL/ AJE(5),AJI(5),CSALFA,DPDX(43),DX,EMU(43),F(5,43),
1 FS(5,43),H,IFIN,INDE(5),INDI(5),ISTEP,ITEST,IUTRAP,KEX,KIN,KRAD,
2 N,NEQ,NPH,NP1,NP2,NP3,OM(43),PEI,PR(5),PREF(5,43),PSIE,PSII,
3 R(43),RHO(43),RME,RMI,RU(43),SD(5,43),SU(5,43),TAUE,TAUI,U(43),
4 XD,XU,Y(43),YE,YI
COMMON/GM4/AK,ALMG,EWALL,IPRINT,BPI
COMMON/CONST/AQ,C1,C2,C3,C4,SRC1,CL
READ(5,41) L,UG,(DY(I),DU(I),I=1,L)
WRITE(6,42) L,UG,(DY(I),DU(I),I=1,L)
42 FORMAT(1H I2,F10.4/(6F10.4))
41 FORMAT(I2,F10.4/(6F10.4))
DOM(1)=.0
DRU=RHO(1)*DU(1)*UG
DO 39 I=2,L
DU(I)=DU(I)*UG
DRUM=DRU
DRU=RHO(I)*DU(I)
39 DOM(I)=DOM(I-1)+(DRU+DRUM)*(DY(I)-DY(I-1))*5
PEI=DOM(L)
DO 38 I=1,L
38 DOM(I)=DOM(I)/PEI
DO 40 I=1,NP3
Y(I)=UINTER(OM(I),DOM,DY,L)
U(I)=UINTER(OM(I),DOM,DU,L)
40 CONTINUE
C CALCULATE INITIAL VALUE OF U(2) AND BPI
UT=SQRT(TAUI*2./(RHO(2)+RHO(3)))
SHALF=UT/U(3)
DO 43 IT=1,2
BPI=AK/(AK+SHALF)
43 SHALF=AK/(ALOG(EWALL*.5*OM(3)*PEI*SHALF*BPI/EML(1)))
U(2)=2.*UT/SHALF-U(3)
C
C INITIAL E PROFILE
ATK=TAUI/(RHO(1)*SRC1)
BTK=-Y(NP3)*DPDX(1)/(RHO(1)*SRC1)
BTK=.5*(BTK+ABS(BTK))
DTK=2*ATK+BTK
CTK=ATK-2.*DTK
DO 603 I=3,NP1
ETA=Y(I)/Y(NP3)
603 F(1,I)=ATK+BTK*ETA+CTK*ETA**2+DTK*ETA**3
C
C INITIAL EL PROFILE
ALEMG=.09
ALEMG=ALEMG*SQRT(SRC1)
DO 604 I=3,NP1
F(2,I)=ALEMG*Y(NP3)
DUMMY=CL*Y(I)
IF(F(2,I).GT.DUMMY) F(2,I)=DUMMY
F(2,I)=F(1,I)*F(2,I)
604 CONTINUE
F(1,1)=.0
F(2,1)=.0
F(1,2)=F(1,3)

```

F(2,2)=.0  
F(1,np3)=.0  
F(2,np3)=.0  
F(1,np2)=.5\*(F(1,np1)+F(1,np3))  
F(2,np2)=.5\*(F(2,np1)+F(2,np3))  
RETURN  
END

```
FUNCTION UINTER(A,B,C,I)
C LINEAR INTERPOLATION ROUTINE
DIMENSION B(I),C(I)
IF(A.LT.B(1))GO TO 23
J=2
69 IF(A-B(J))212,211,210
210 J=J+1
IF(J.LE.I)GO TO 69
WRITE(6,21)
21 FORMAT(1X,5HSTOP2)
STOP
211 UINTER=C(J)
RETURN
212 UINTER=C(J-1)+(C(J)-C(J-1))*(A-B(J-1))/(B(J)-B(J-1))
200 RETURN
23 WRITE(6,20)
20 FORMAT(1X,5HSTOP1)
STOP
END
```

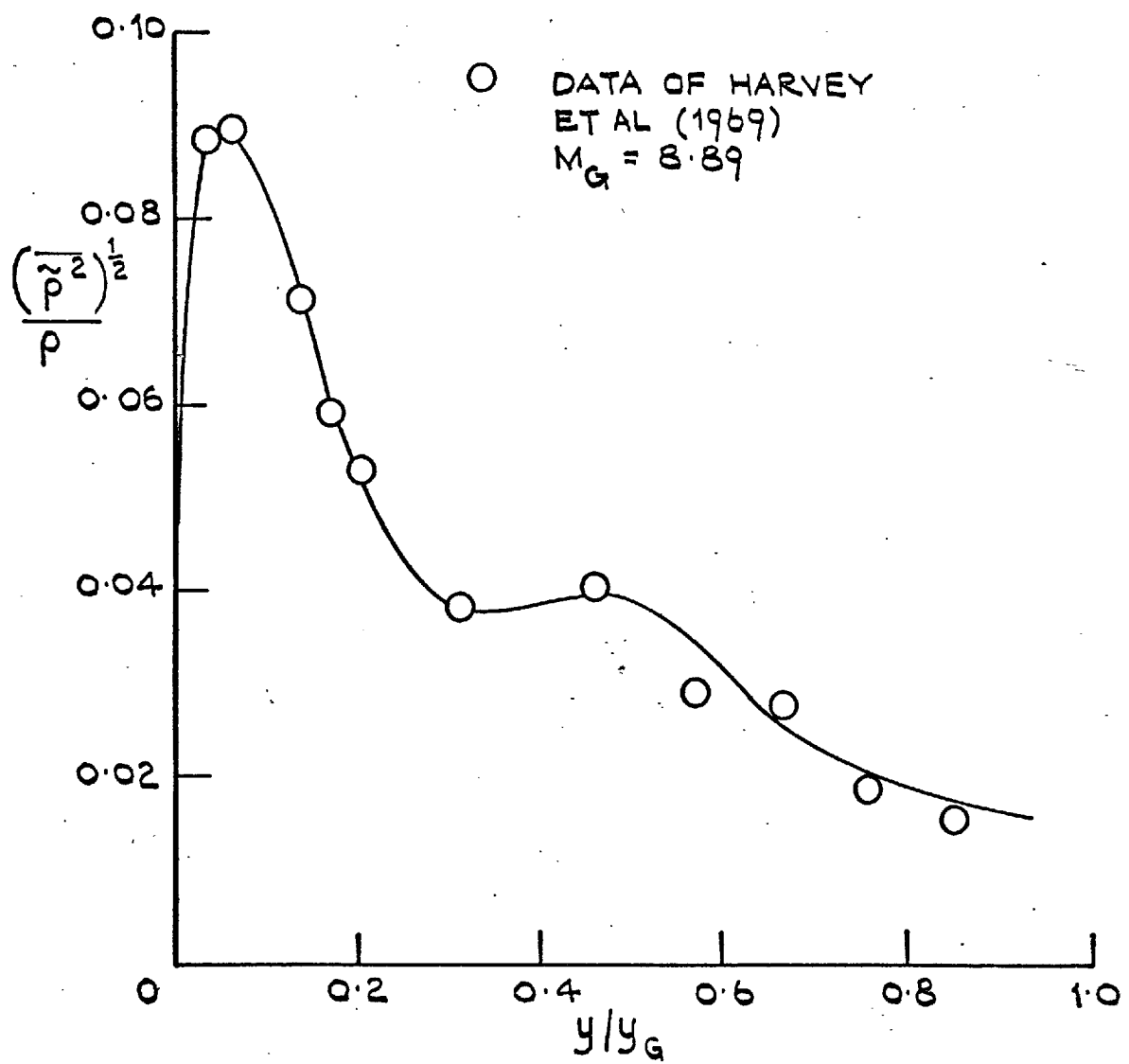


FIG. 2.1: DISTRIBUTION OF DENSITY FLUCTUATIONS  
IN A ADIABATIC SUPERSONIC FLAT  
PLATE BOUNDARY

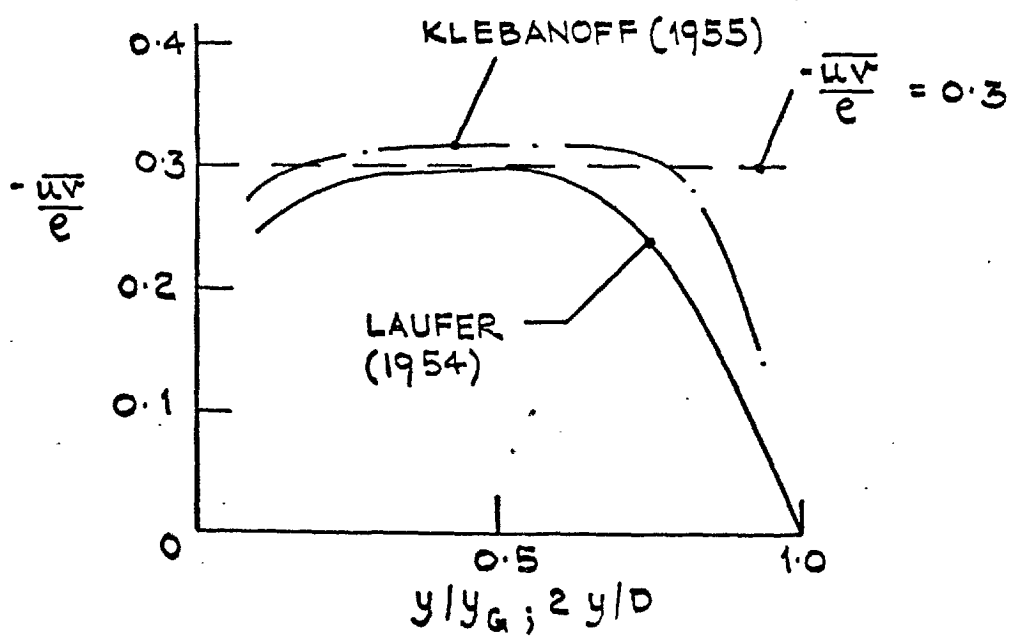
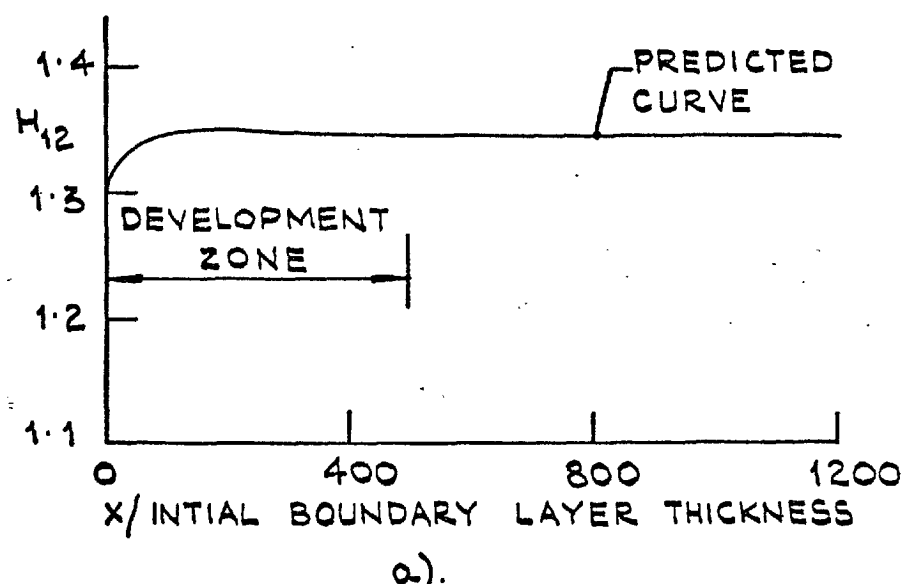
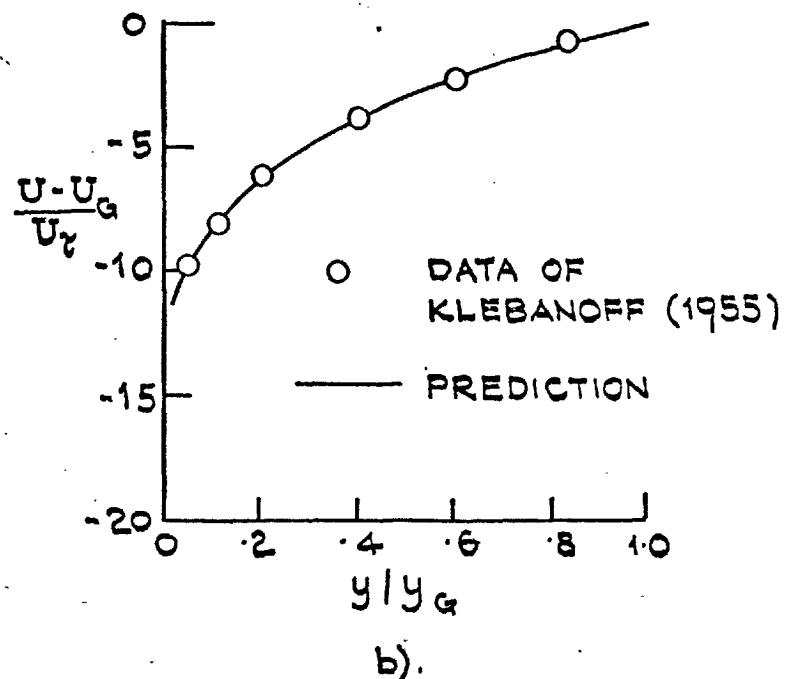


FIG. 4.1: VARIATION OF  $\bar{u}v/e$  ACROSS  
FLAT-PLATE BOUNDARY LAYER  
AND A CIRCULAR PIPE.

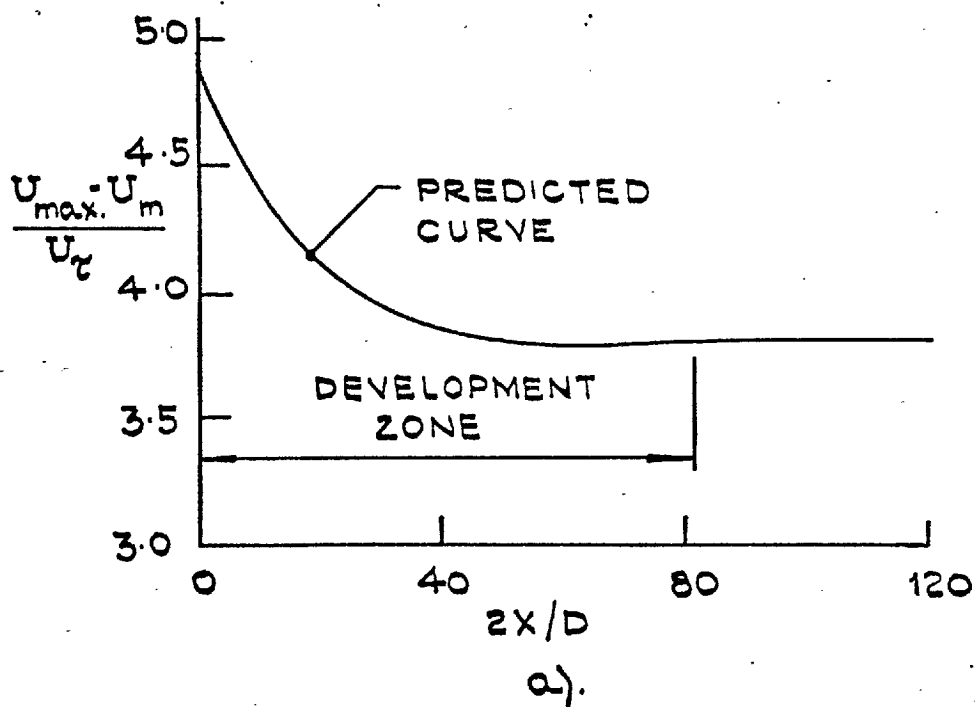


a).

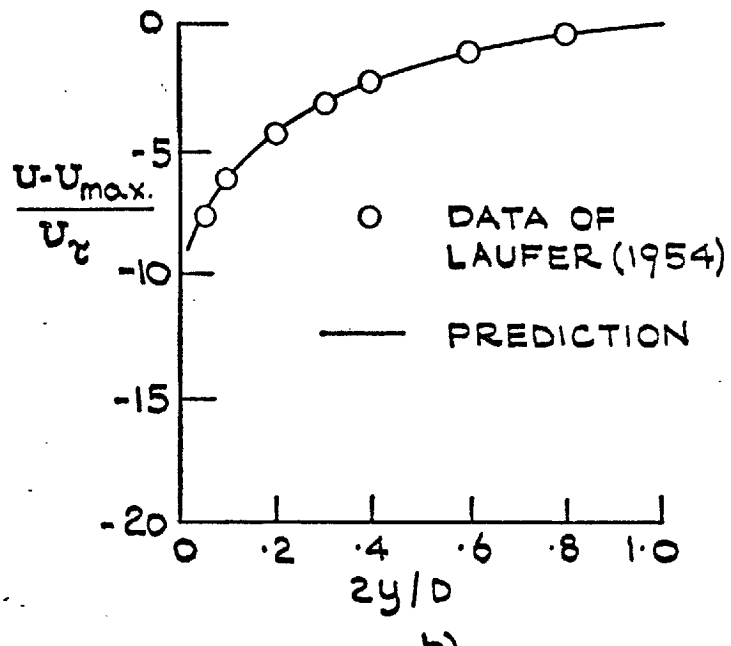


b).

FIG.4.2: PREDICTION OF A CONSTANT  
WALL-SHEAR FLAT-PLATE  
FLOW.



a).



b).

FIG. 4.3: PREDICTIONS OF A DEVELOPED PIPE FLOW.

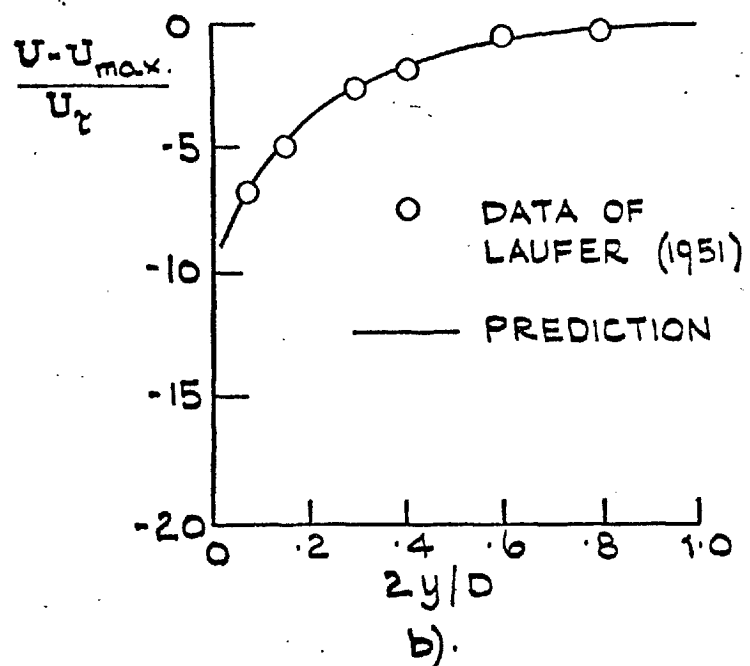
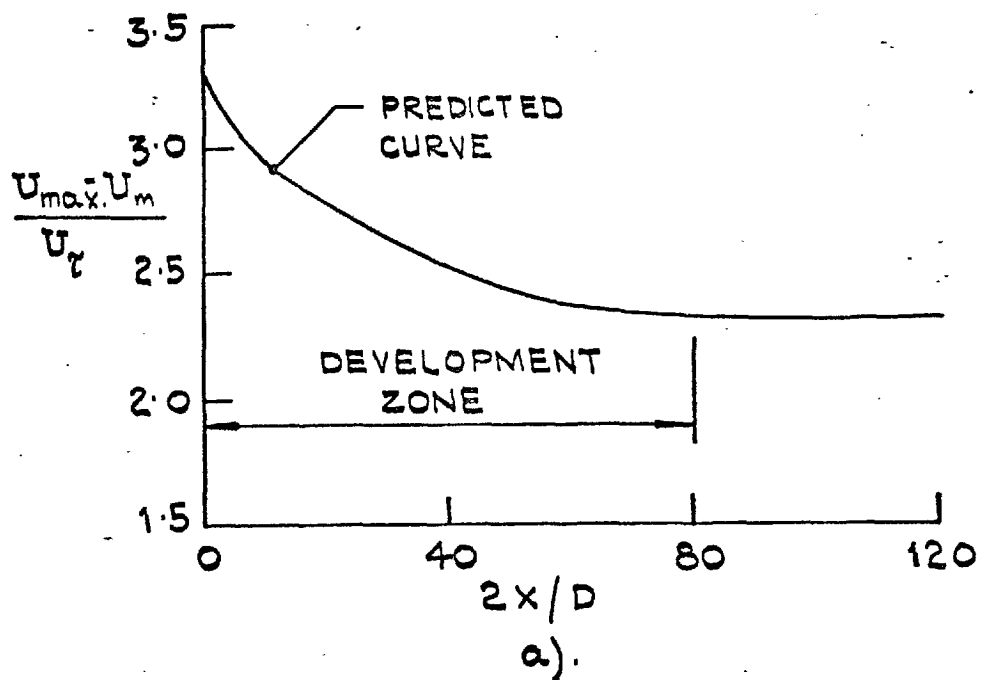


FIG. 4.4: PREDICTIONS OF A DEVELOPED CHANNEL FLOW.

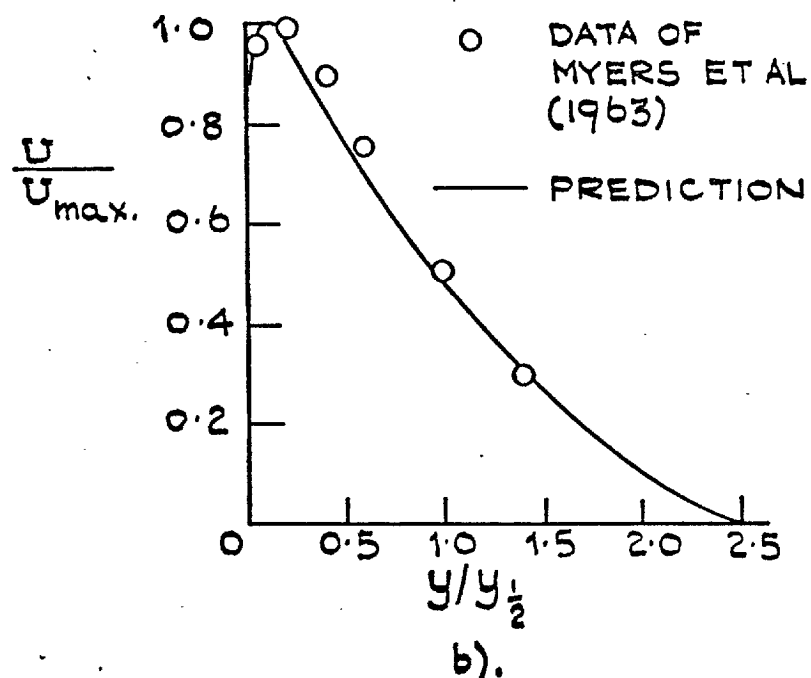
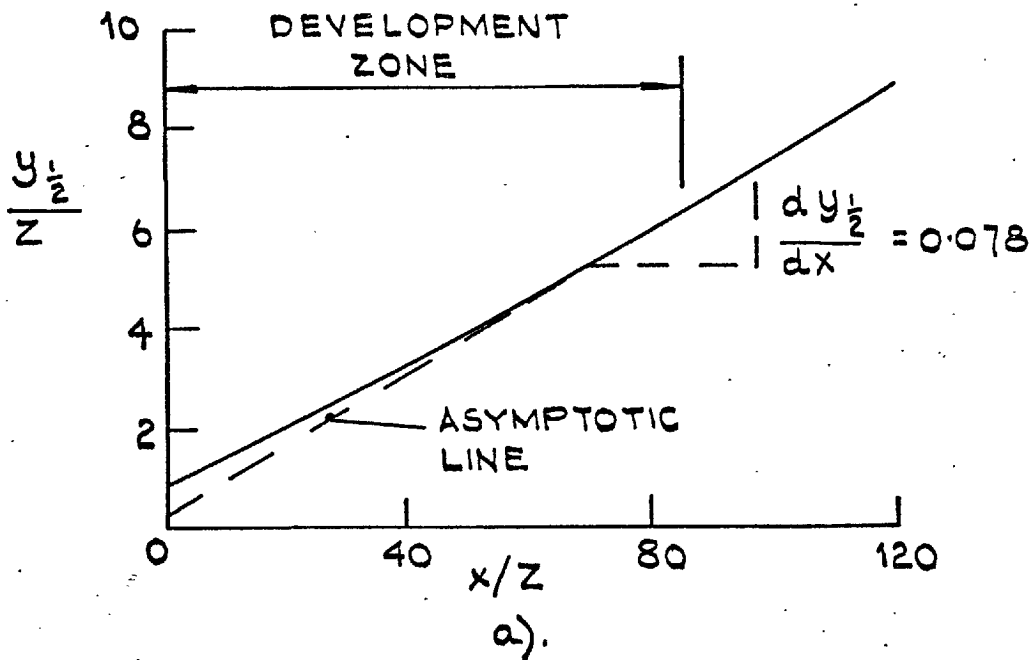


FIG. 4.5: PREDICTIONS OF A PLANE WALL JET WITH CONSTANT  $\tau_s / (\rho U_{max.}^2)$

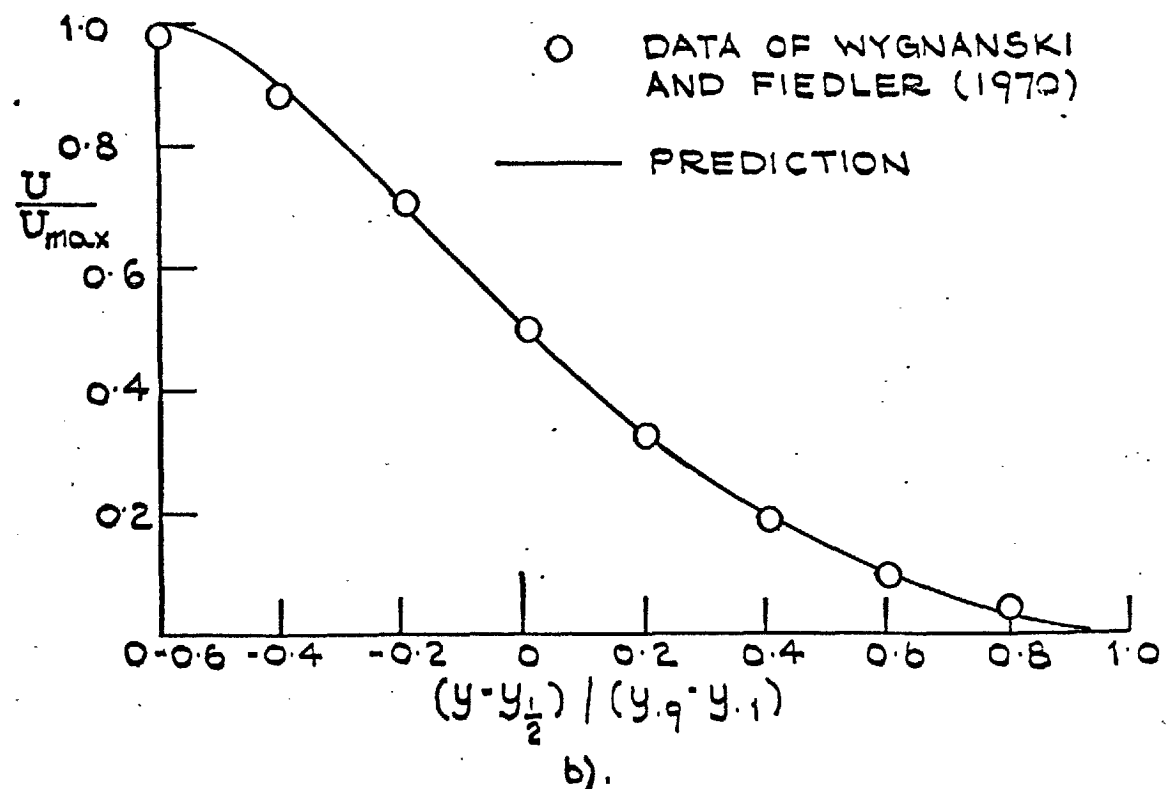
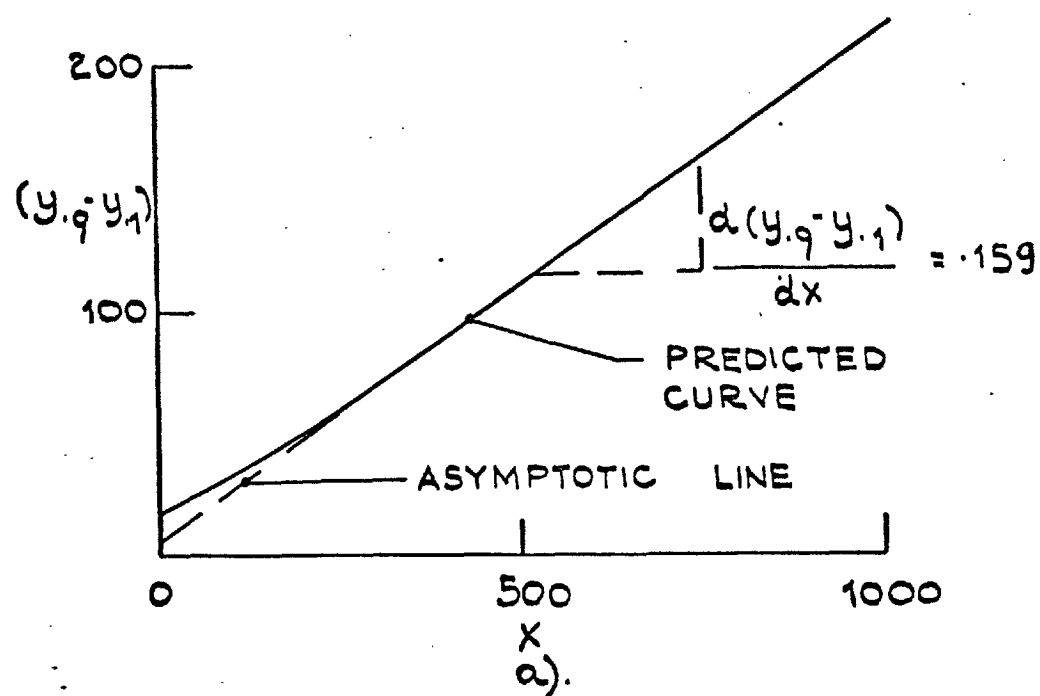
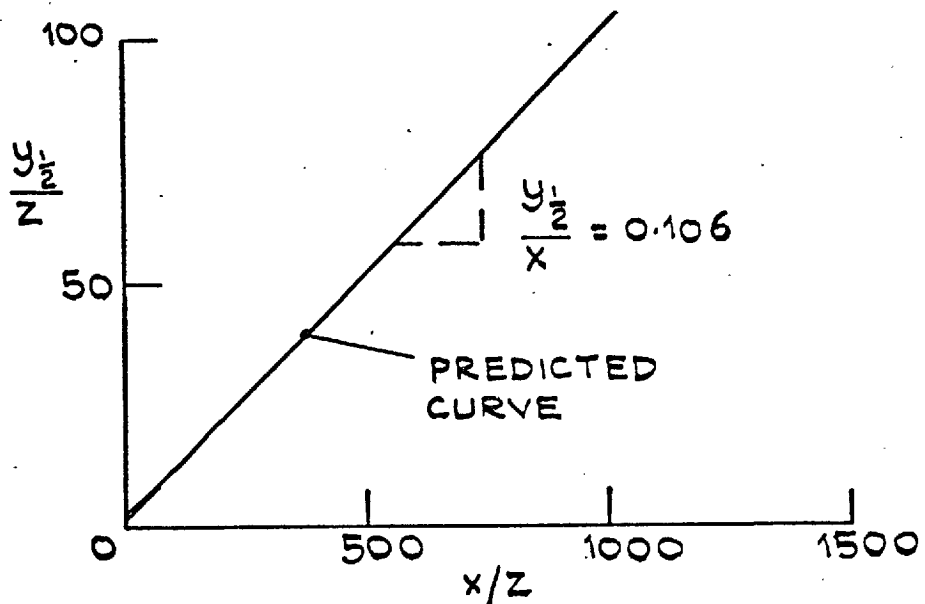
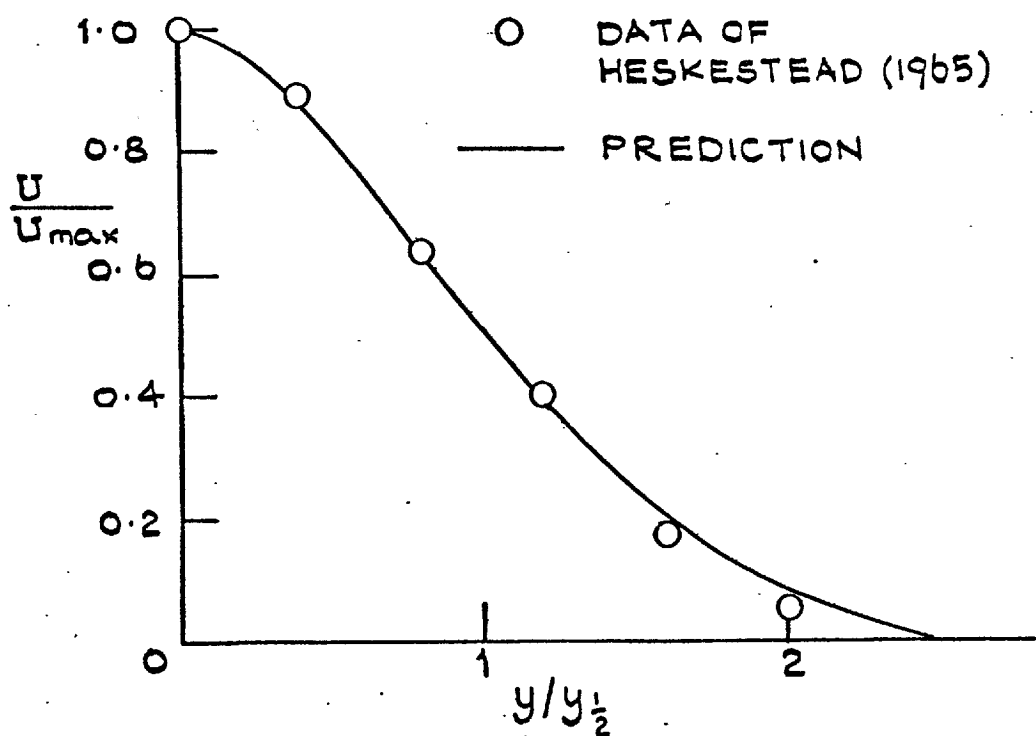


FIG. 4.6: PREDICTION OF A PLANE MIXING LAYER.



a).



b).

FIG. 4.7: PREDICTION OF A PLANE JET

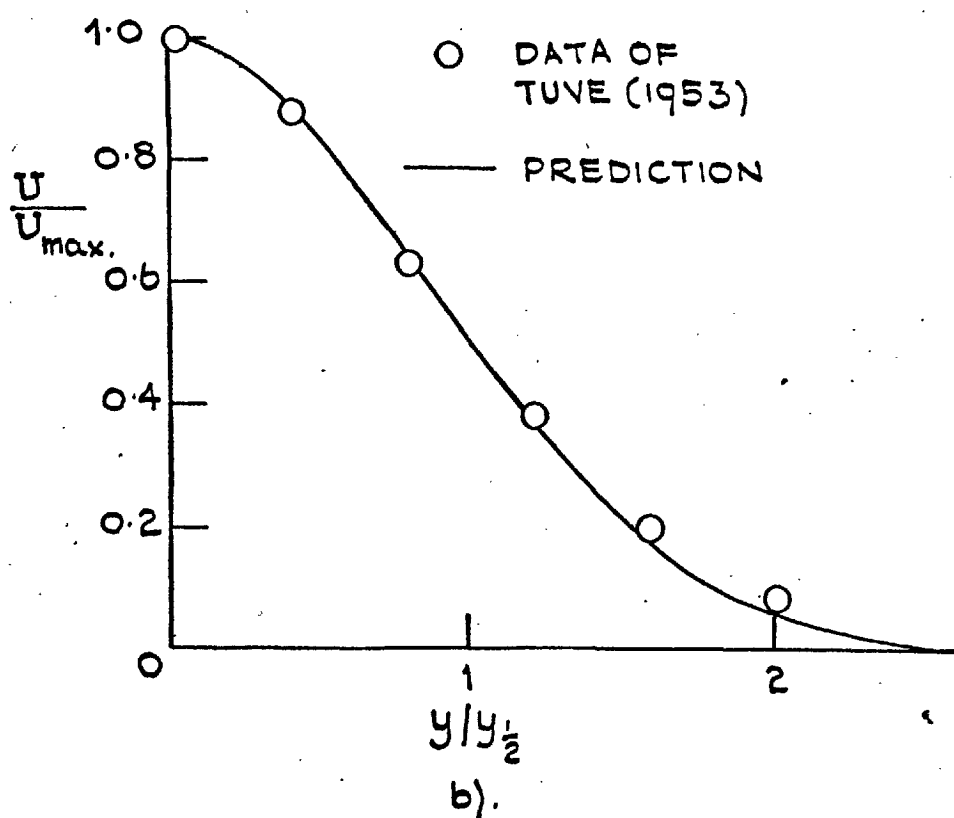
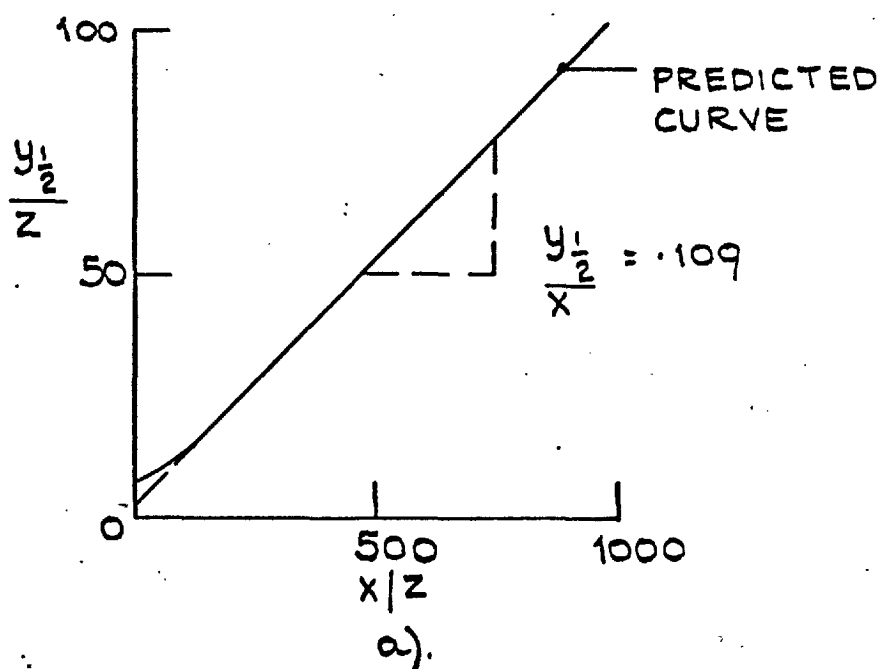


FIG. 4.8 : PREDICTION OF A RADIAL JET

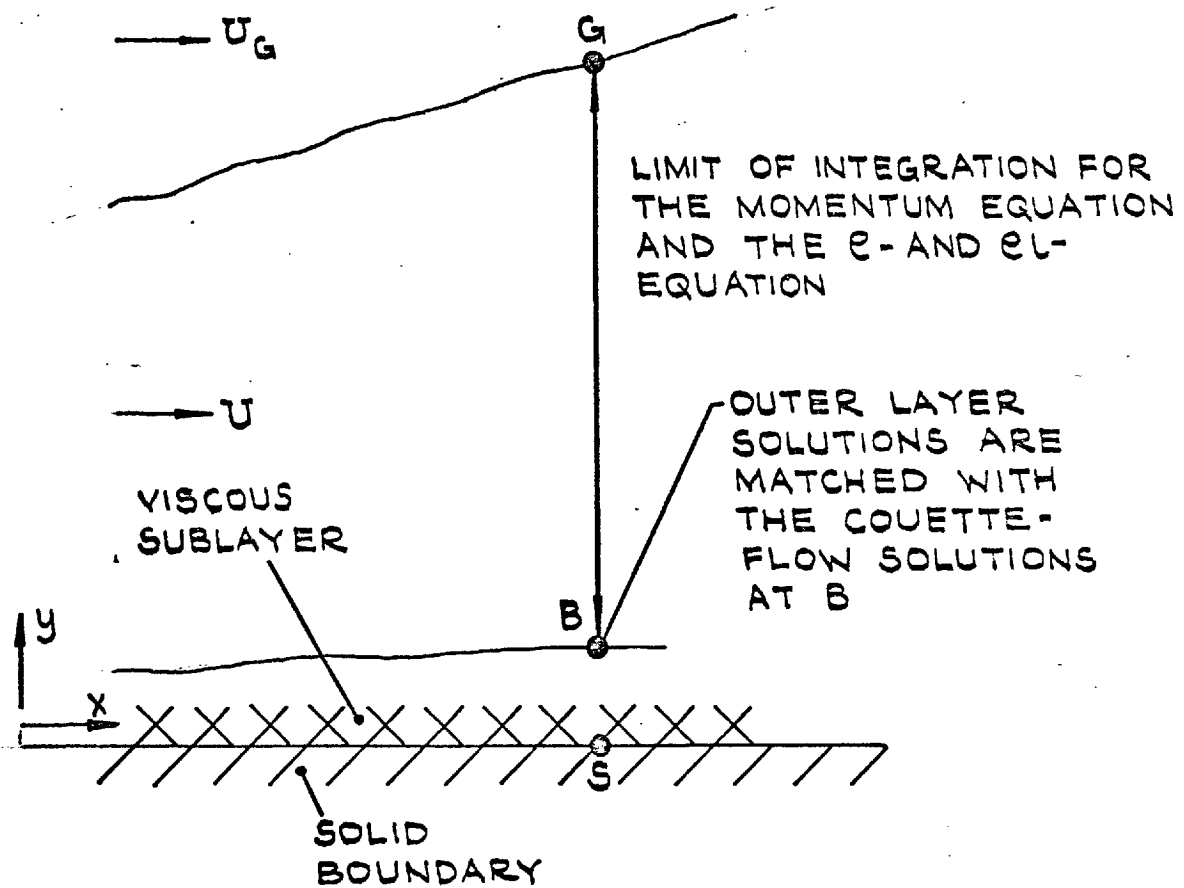


FIG. 5.1: TREATMENT OF THE DIFFERENTIAL EQUATIONS NEAR THE WALL.

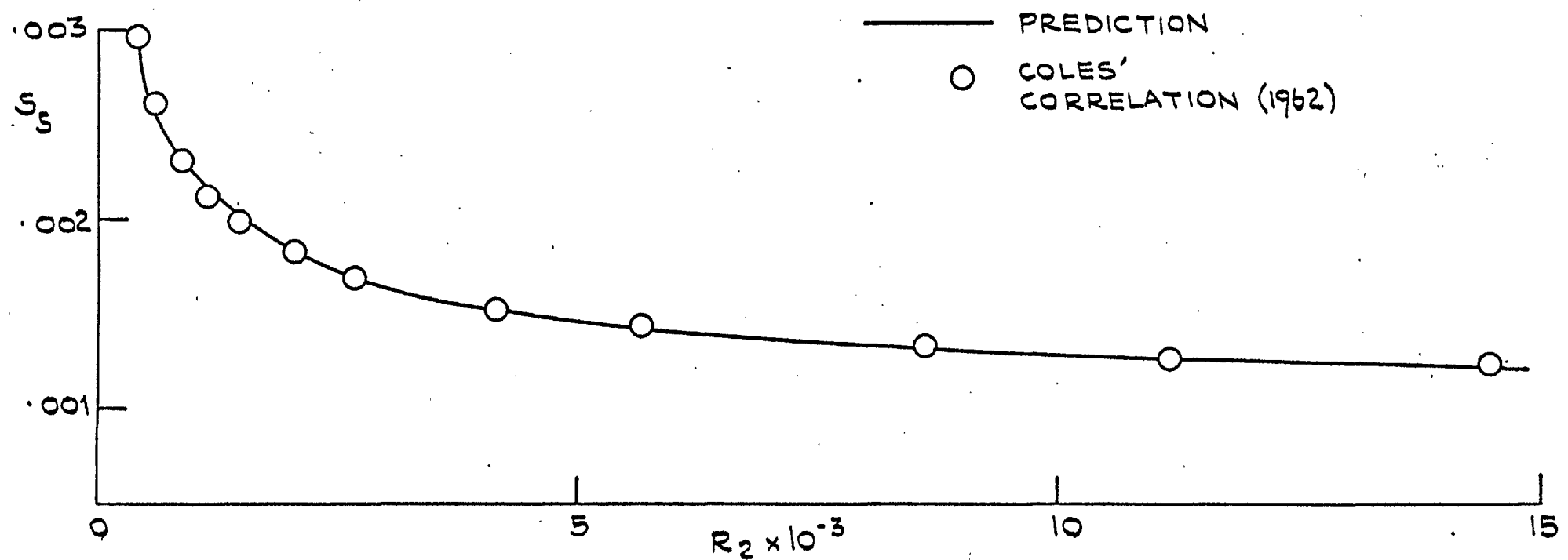
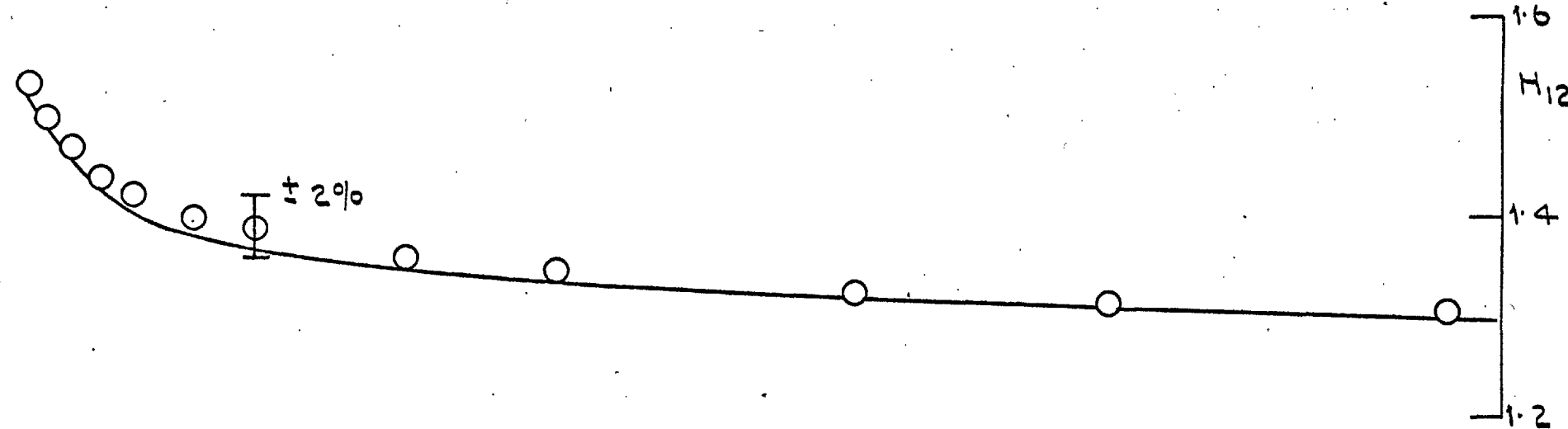


FIG. 6.1: COMPARISON OF THE CALCULATION OF THE SHAPE FACTOR AND FRICTION COEFFICIENT OF A FLAT PLATE WITH COLES' CORRELATION.

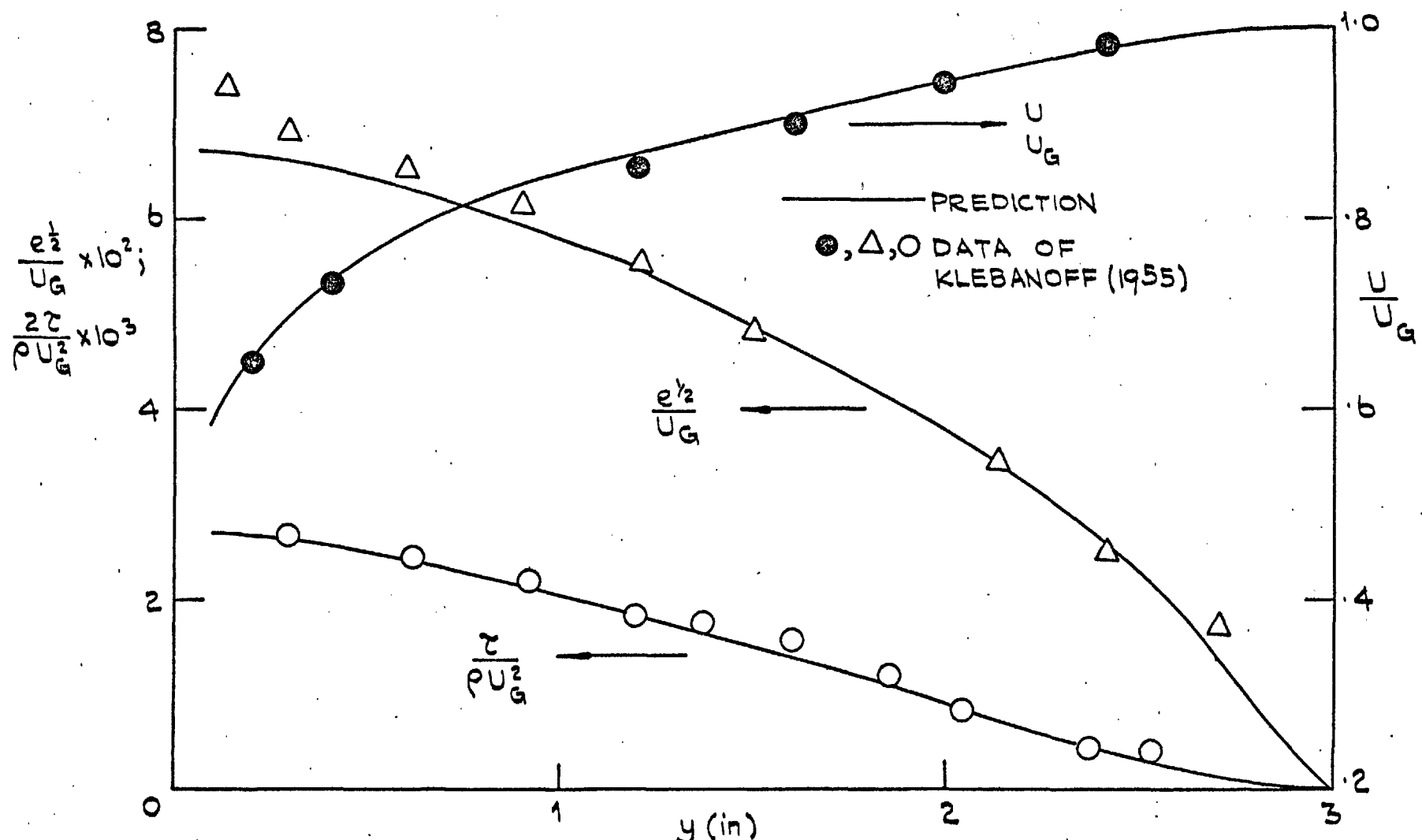
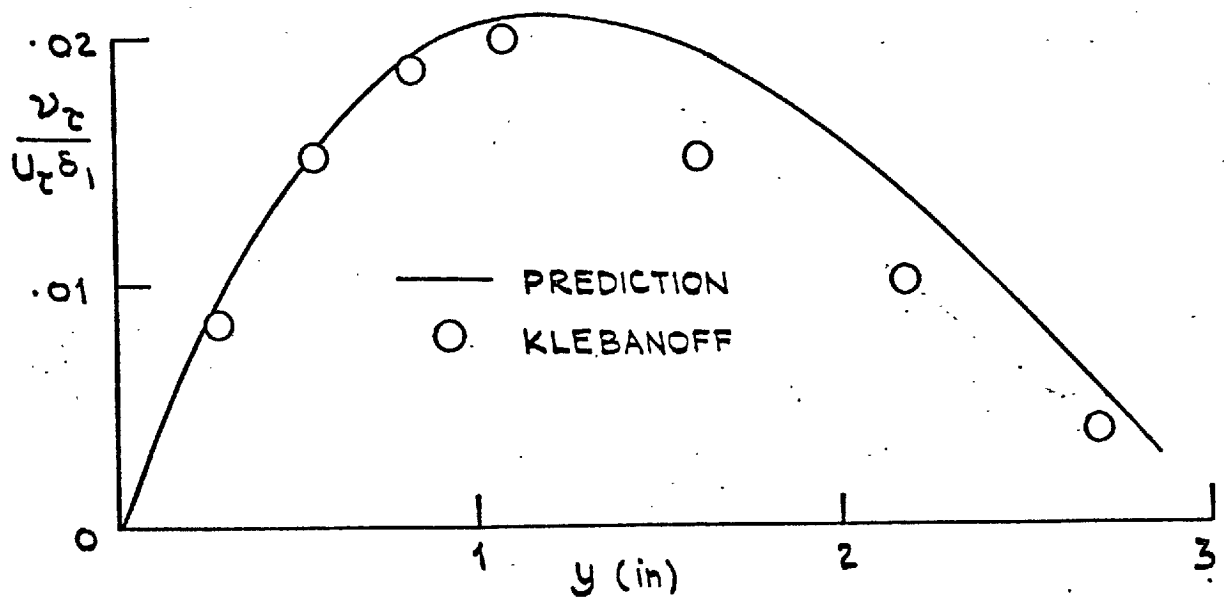
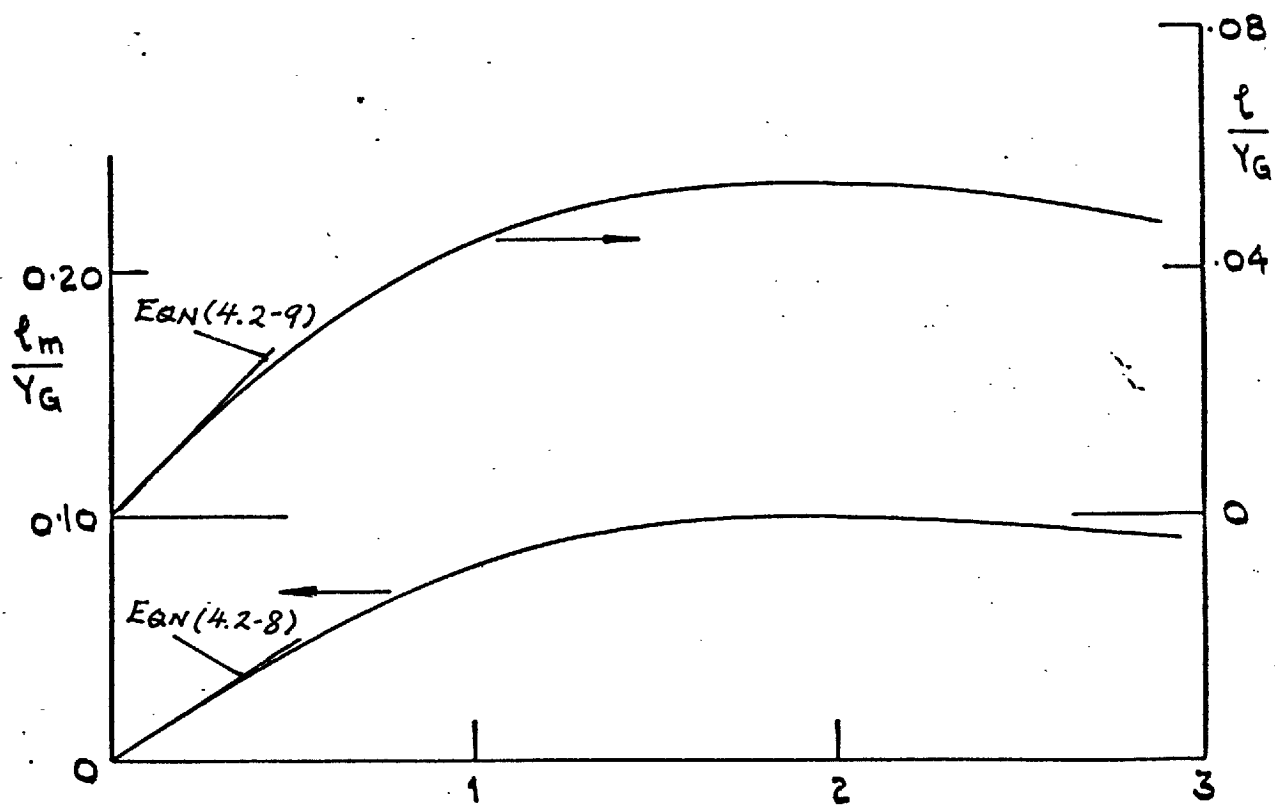


FIG. 6.2 (CONTINUED)



b). COMPARISON OF TURBULENT VISCOSITY PROFILE



c). PREDICTED LENGTH SCALES

FIG. b. 2: COMPARISON OF PREDICTIONS WITH DATA  
FOR A FLAT-PLATE BOUNDARY LAYER

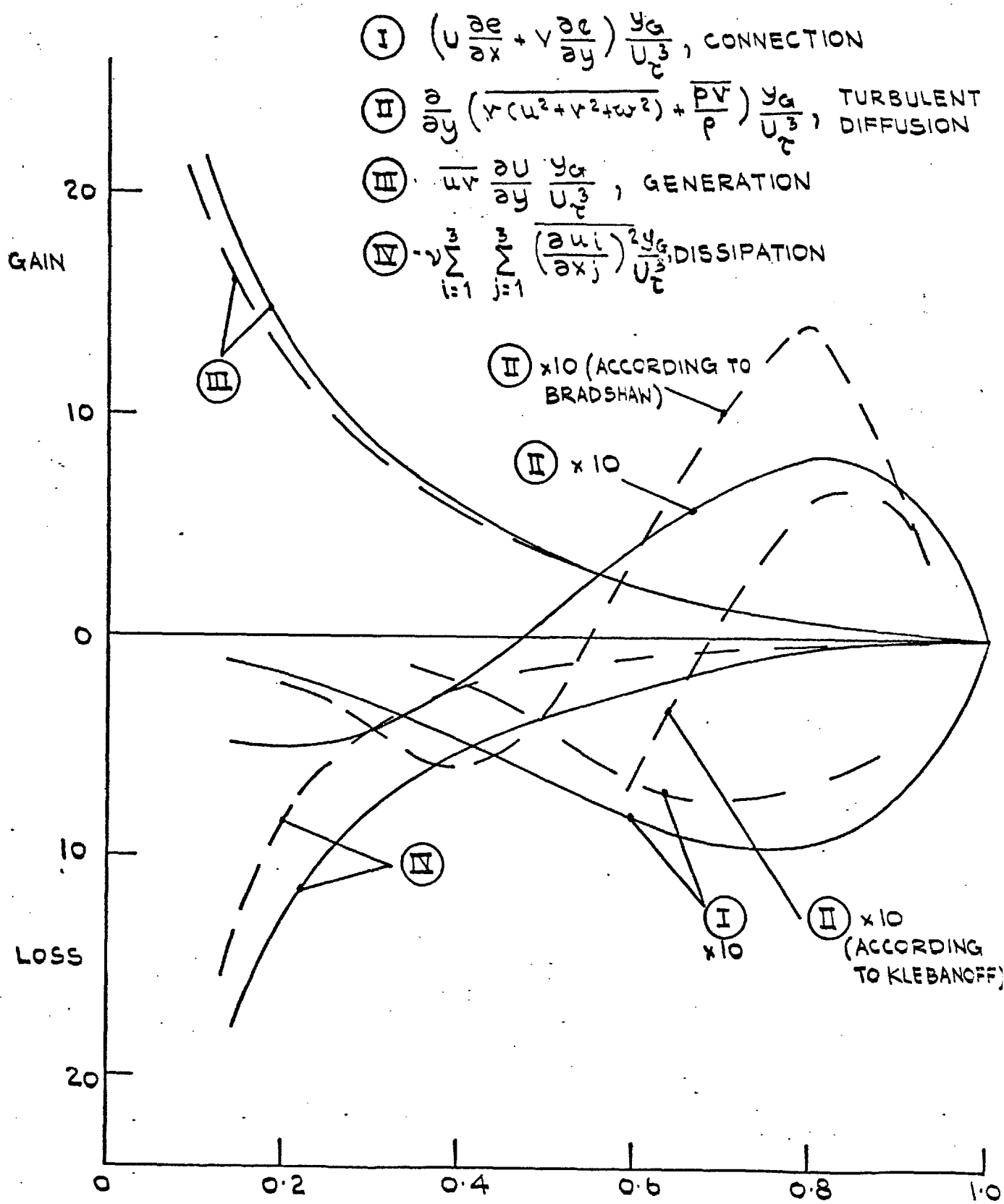


FIG. 6.3: TURBULENT KINETIC ENERGY BALANCE  
OF A FLAT-PLATE FLOW; — PREDICTIONS;  
— — — MEASUREMENTS OF KLESANOFF (1955)

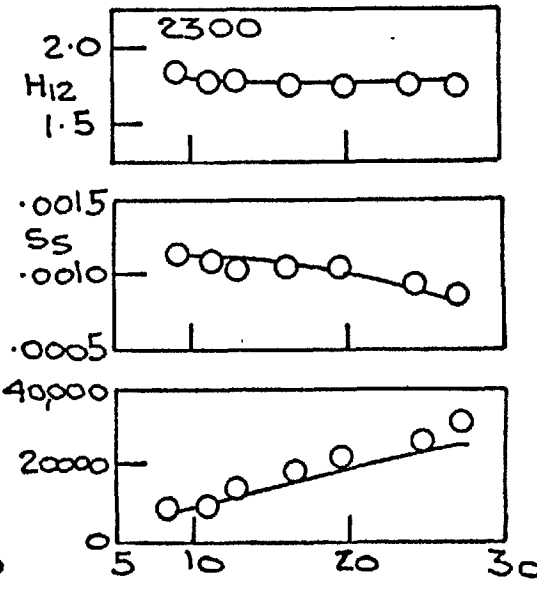
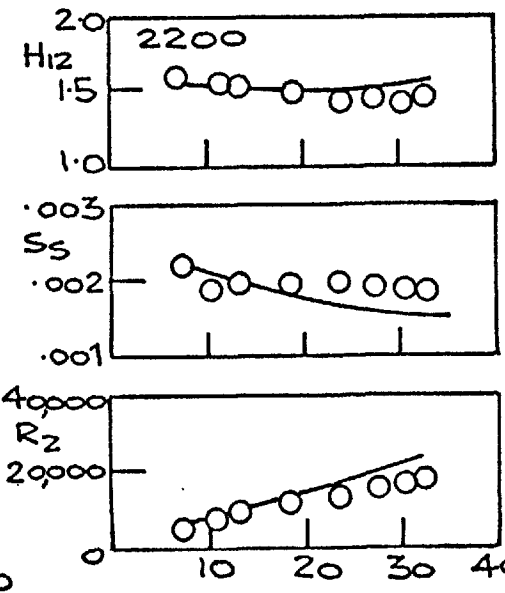
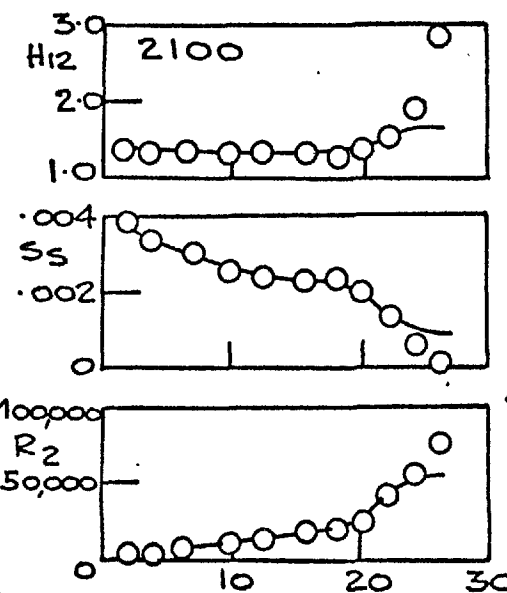
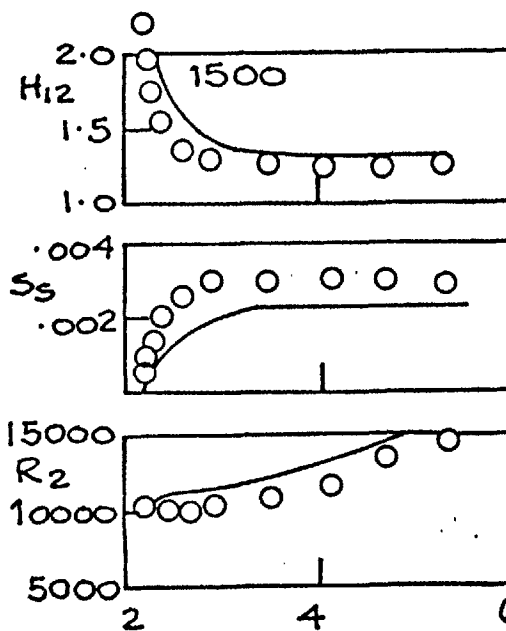
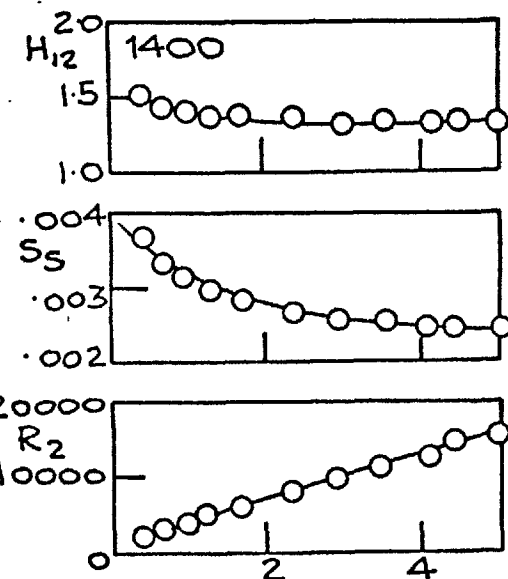
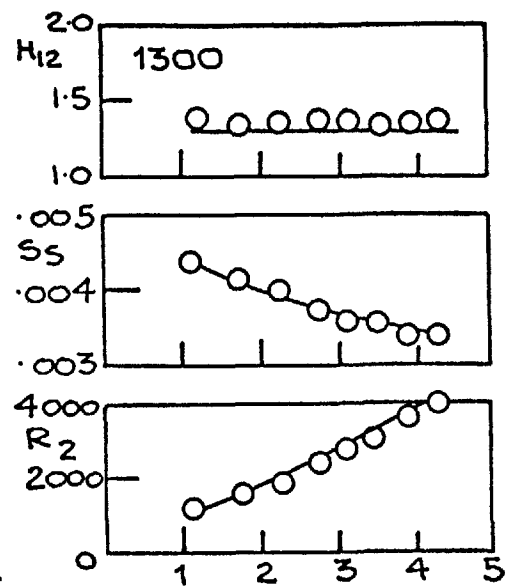
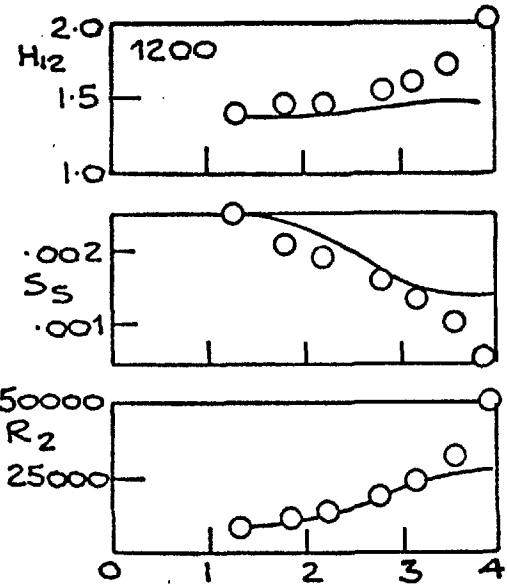
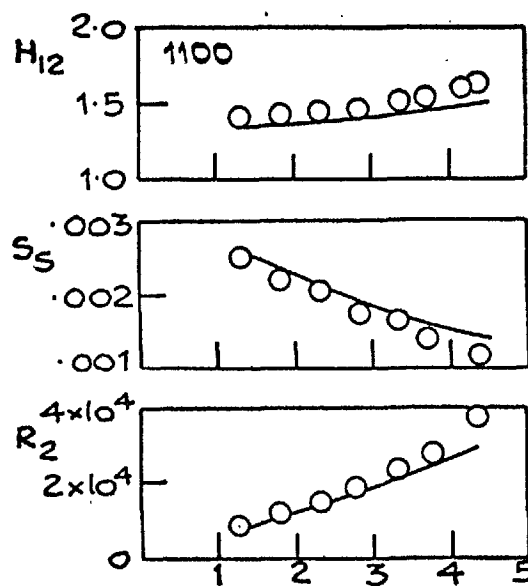


FIG. 6.4 (CONTINUED)

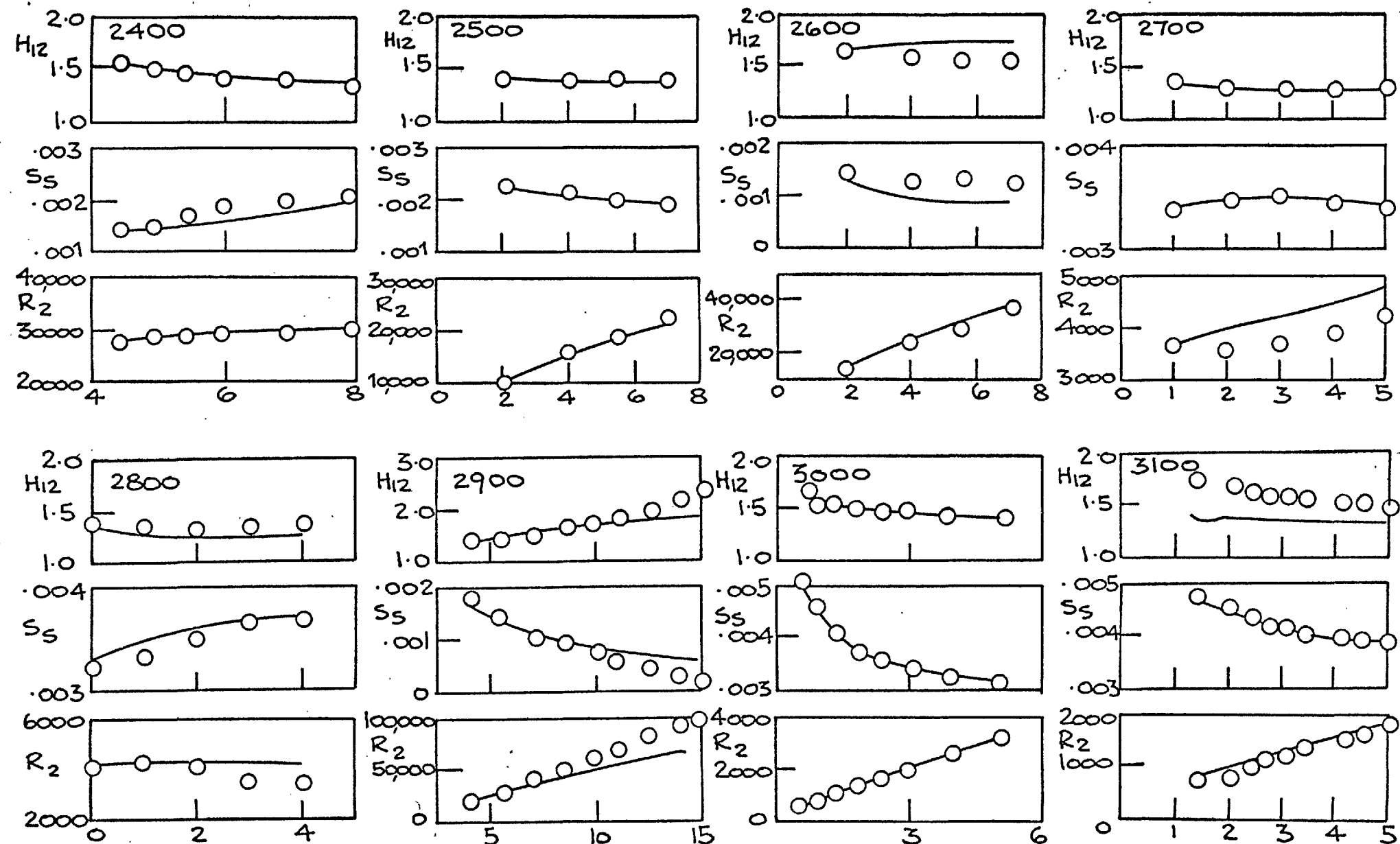


FIG. 6.4 (CONTINUED)

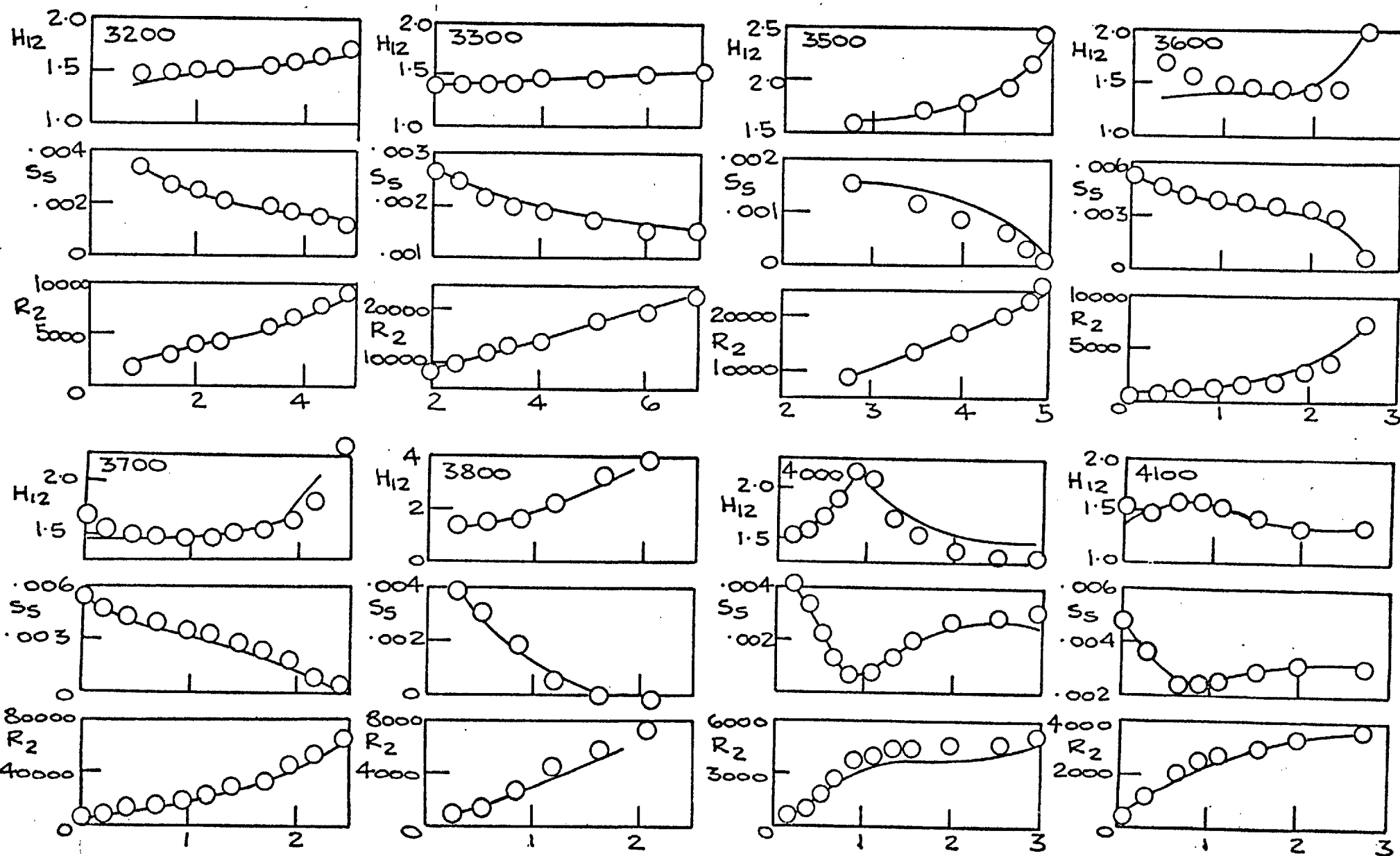


FIG. 6.4 (CONTINUED)

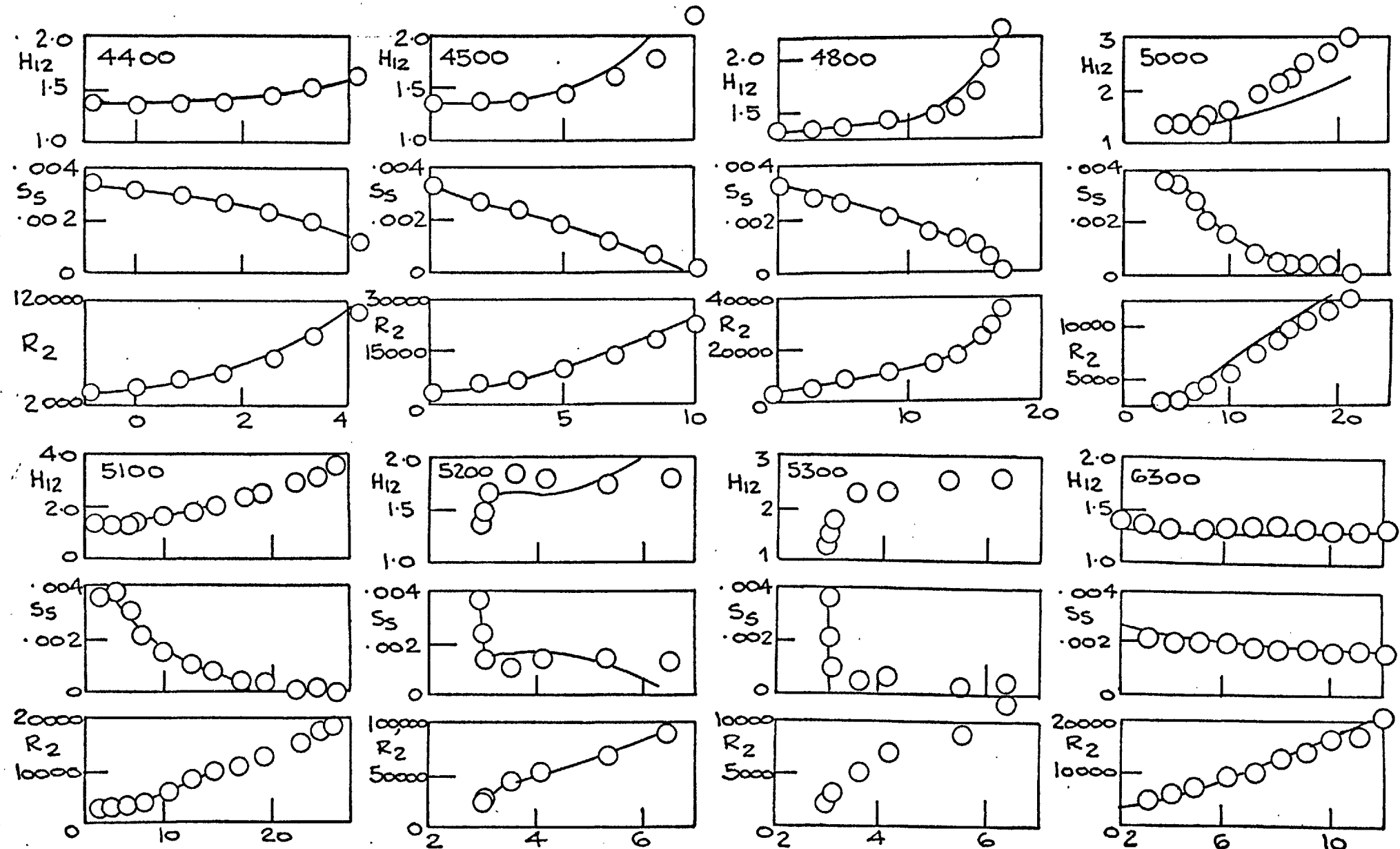


FIG. 6.4: COMPARISON OF PREDICTIONS WITH EXPERIMENTAL  
 DATA COLLECTED BY COLES AND HIRST (1968);  
 — PREDICTIONS; ○ DATA.

IDENT	Investigator/s	Nature of experiment	Year
1100	Ludwieg and Tillmann	Mild adverse pressure gradient	1949
1200	Ludwieg and Tillmann	Strong adverse pressure gradient	1949
1300	Ludwieg and Tillmann	Accelerating flow	1949
1400	Wieghardt and Tillmann	Flat plate flow	1944
1500	Tillmann	Ledge flow	1945
2100	Schubauer and Klebanoff		1950
2200	Clauser	Flow No. 1	1954
2300	Clauser	Flow No. 2	1954
2400	Bradshaw and Ferriss	Relaxing flow	1965
2500	Bradshaw	$\alpha = -.15$	1966
2600	Bradshaw and Ferriss	$\alpha = -.255$	1965
2700	Herring and Norbury	$\beta = -.35$	1967
2800	Herring and Norbury	$\beta = -.53$	1967
2900	Perry		1966
3000	Bell	Constant pressure	1966
3100	Bell	Series D	1966
3200	Bell	Series E	1966
3300	Bradshaw	$\alpha = 0 \rightarrow -.255, C$	1967
3500	Newman	Airfoil, Series 2	1951
3600	Moses	Case 1	1964
3700	Moses	Case 2	1964
3800	Moses	Case 3	1964
4000	Moses	Case 5	1964
4100	Moses	Case 6	1964

Table 6.4-I continued.

IDENT	Investigator/s	Nature of experiment	Year
4400	Schubauer and Spangenberg	Flow A	1960
4500	Schubauer and Spangenberg	Flow B	1960
4800	Schubauer and Spangenberg	Flow E	1960
5000	Fraser	Flow A	1956
5100	Fraser	Flow B	1956
5200	Stratford	Experiment 5	1959
5300	Stratford	Experiment 6	1959
6300	Bauer	Spillway, 60°	1951

Table 6.4-I Name of investigator/s and nature of the experiment for flows shown in Fig.6.4.

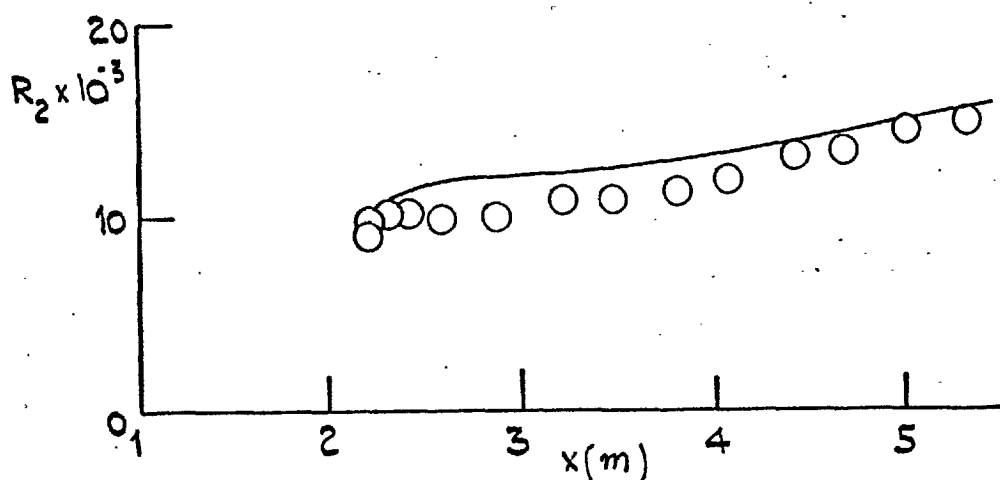
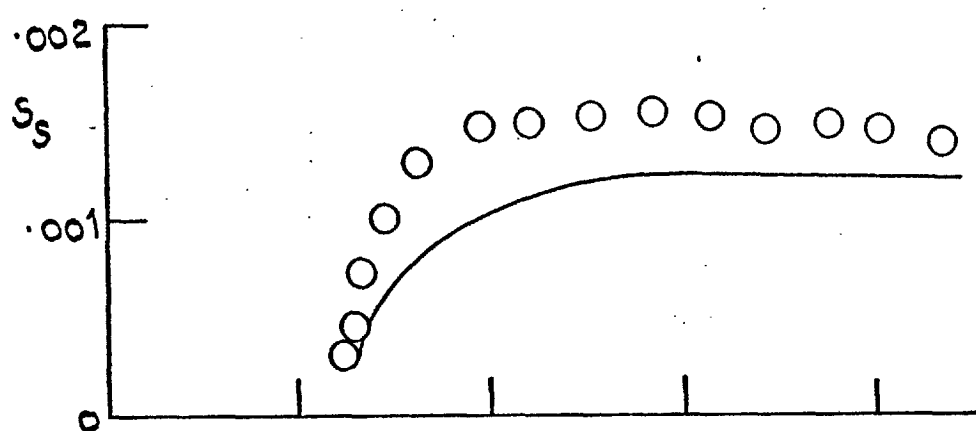
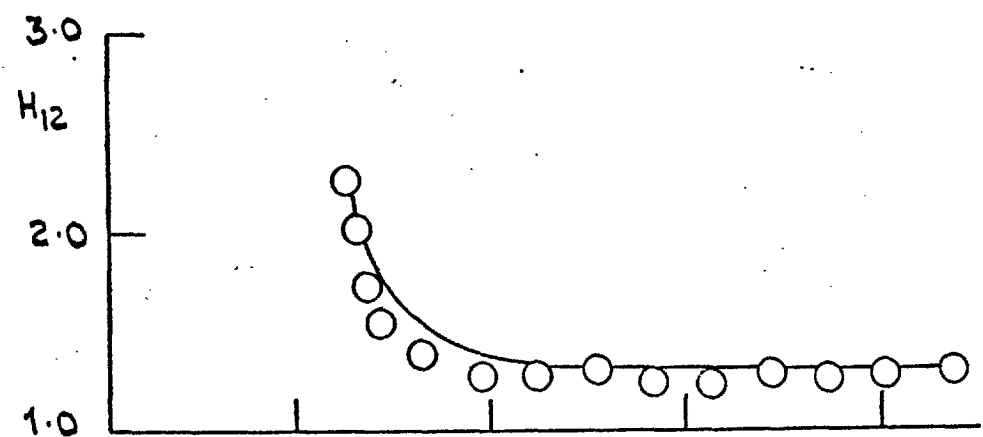


FIG. 6.5: COMPARISON OF PREDICTION OF  $H_{12}$ ,  $S_s$  AND  $R_2$  WITH EXPERIMENT OF TILLMAVN (1945) N  
 LEDGE FLOW; — PREDICTION WITH  $e$ -STARTING-  
 PROFILE FROM EQUATION (A3.2) AND  $\varphi$  FROM  
 EQUATION (A3.3); ○ DATA.

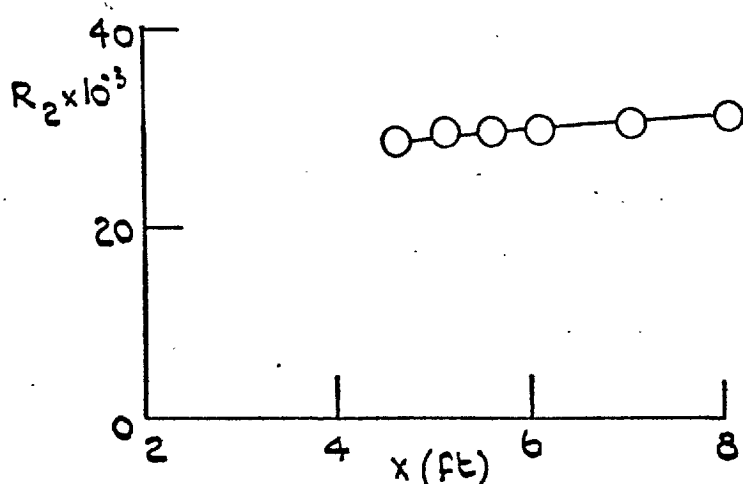
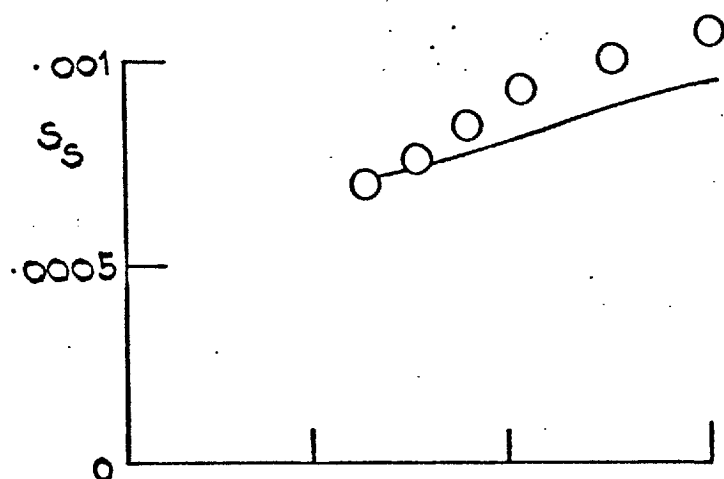
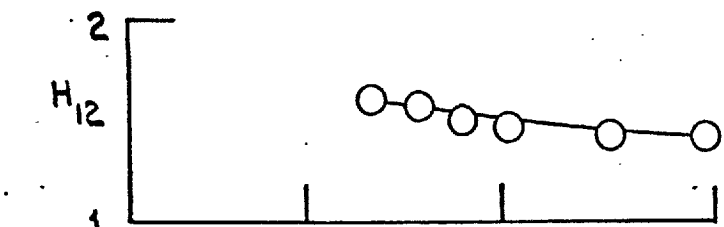


FIG. b'b: COMPARISON OF PREDICTION OF  $H_{12}$ ,  
 $S_s$  AND  $R_2$  WITH THE EXPERIMENT OF  
 BRADSHAW AND FERRISS (1965) (IDENT: 2400)  
PREDICTION USING THE REPORTED  
 INITIAL PROFILES, OR PREDICTION USING  
 INITIAL  $\epsilon$  AND  $\tau$  PROFILES RECOMMENDED  
 IN APPENDIX 3; O DATA.

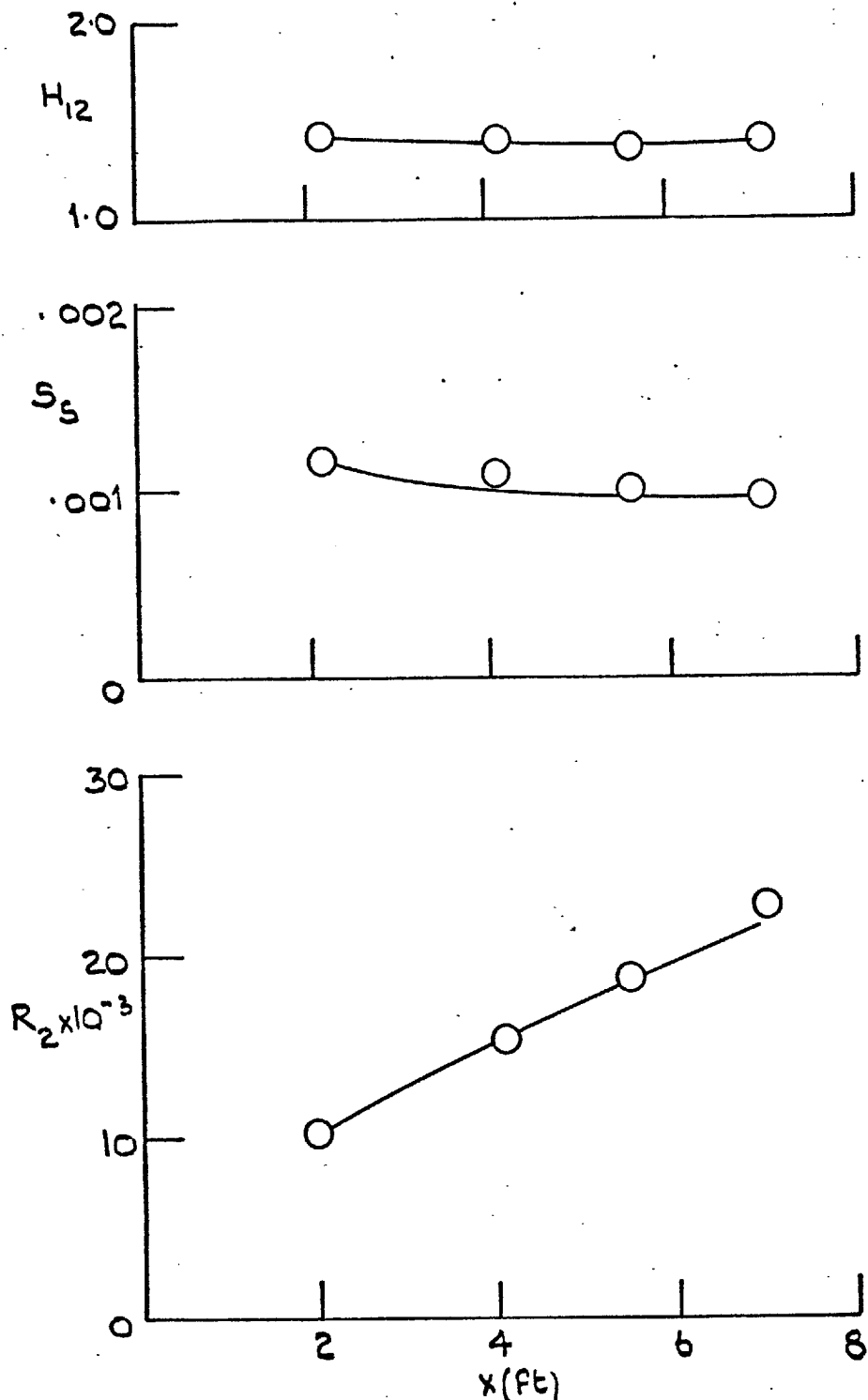


FIG. 6.7: COMPARISON OF PREDICTION OF  $H_{12}$  -  
 $S_s$  AND  $R_2$  WITH THE EXPERIMENT OF  
BRADSHAW (1965) "α = -0.15" (DENT = 2500)  
— PREDICTION USING THE REPORTED  
INITIAL PROFILES, OR PREDICTION USING THE  
INITIAL  $e$  AND  $\epsilon$  PROFILES RECOMMENDED IN  
APPENDIX 3; ○ DATA.

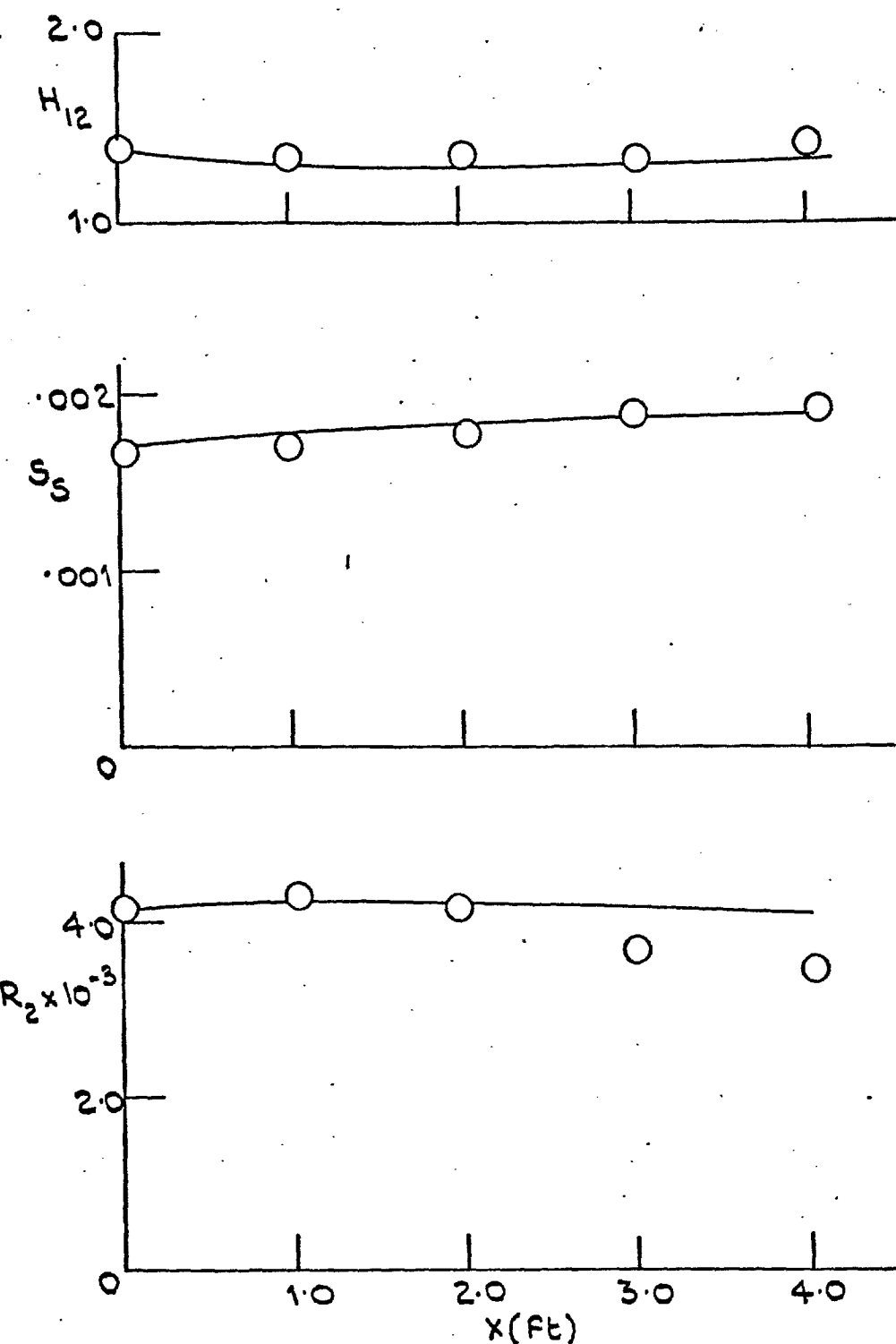


FIG. 6.8: COMPARISON OF PREDICTION OF  $H_{12}$ ,  
 $S_s$  AND  $R_2$  WITH THE EXPERIMENT  
 OF HERRING AND NORBURY (1967)  
" $\beta = -0.53$ " ( $\text{IDENT} = 2800$ );  
— PREDICTION, O DATA.

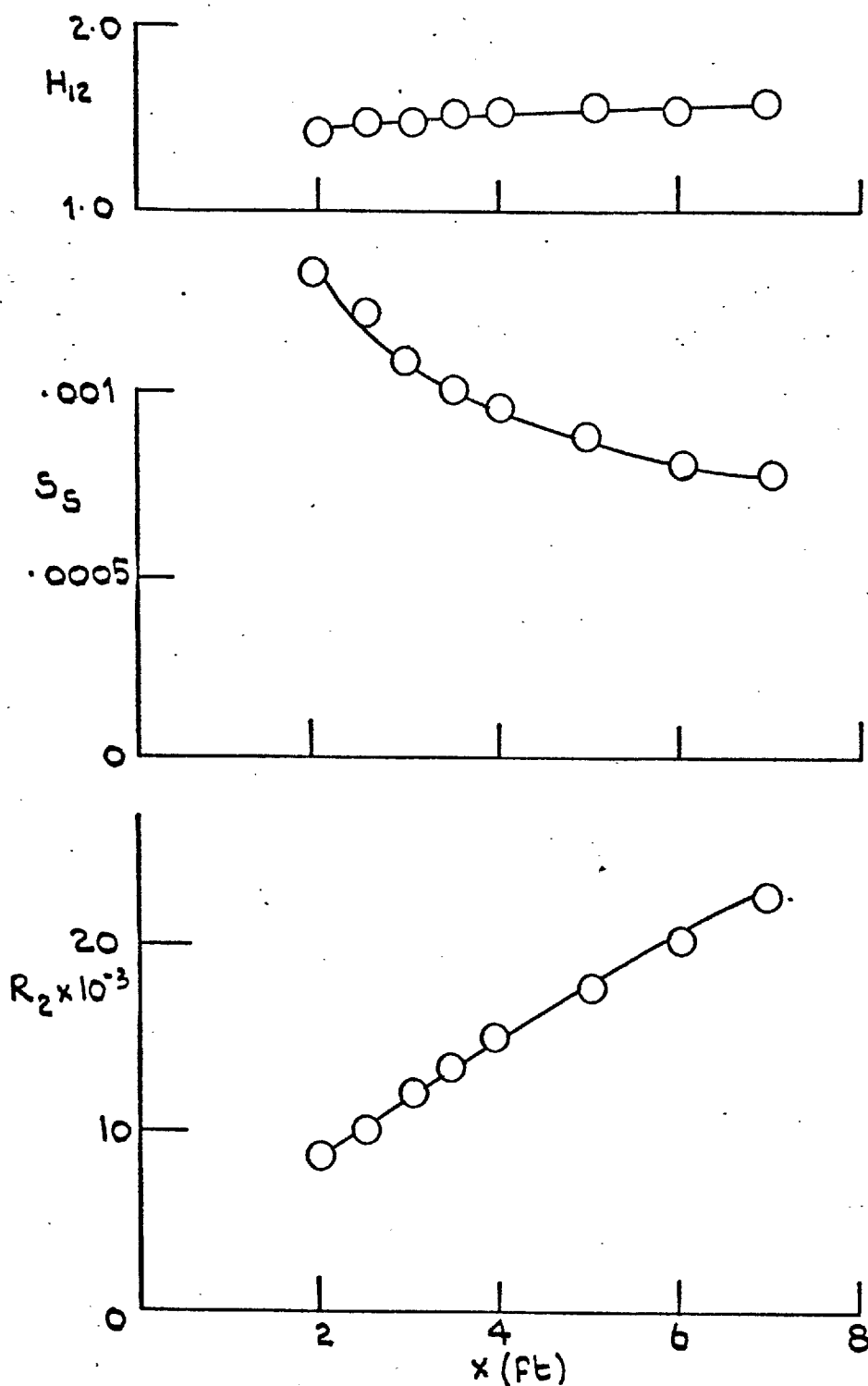


FIG. 6.9: COMPARISON OF PREDICTED OF  $H_{12}$ ,  $S_s$  AND  $R_2$  WITH THE EXPERIMENT OF BRADSHAW (1967)

" $\alpha = 0 \rightarrow -0.255$ , FLOW C" (IDENT = 3300);

PREDICTION USING THE REPORTED INITIAL PROFILES, OR PREDICTION USING THE INITIAL  $\epsilon$  AND  $\delta$  PROFILES RECOMMENDED IN APPENDIX 3;

O DATA.

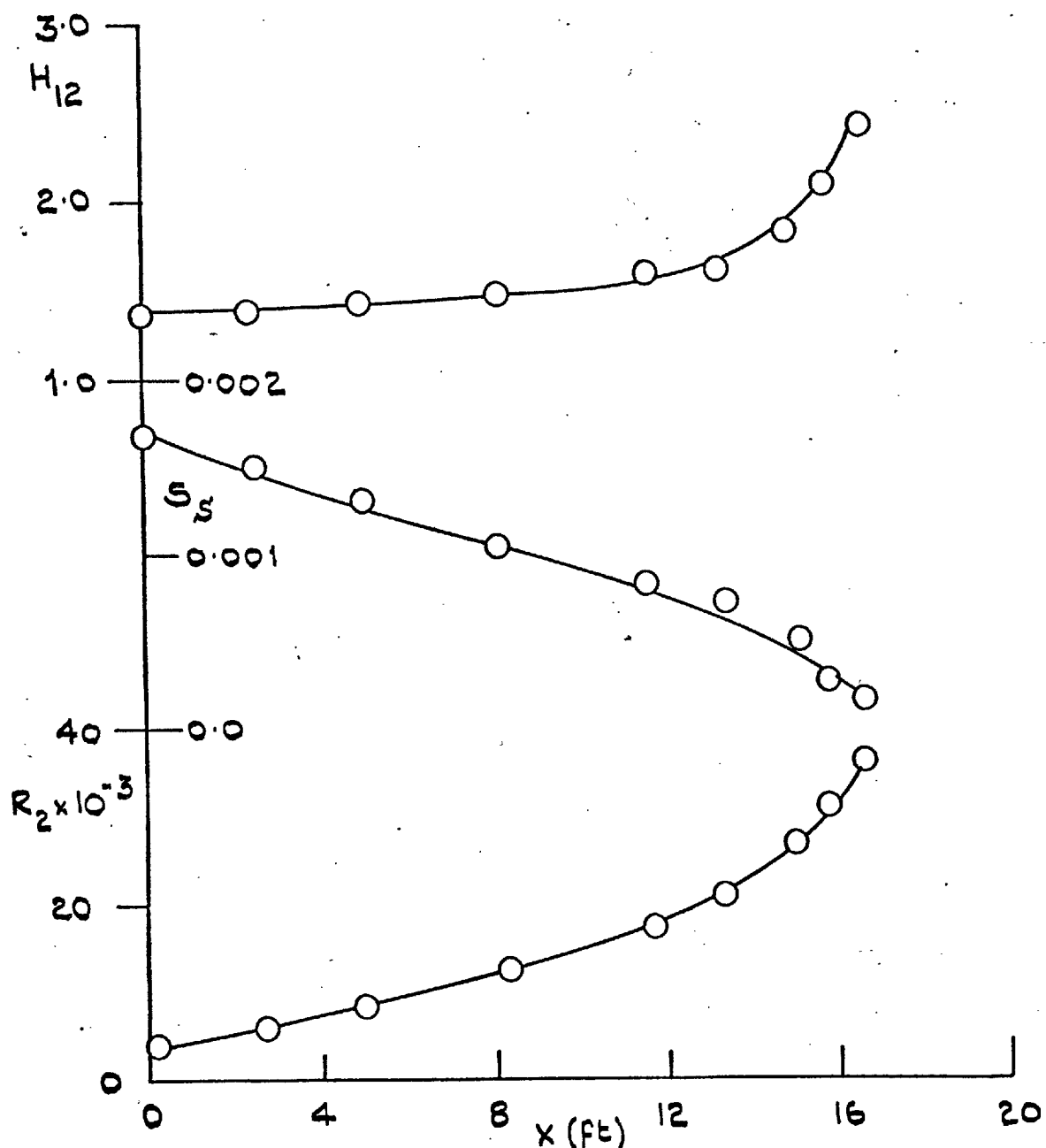


FIG. 6.10: COMPARISON OF PREDICTION OF  $H_{12}$ ,  
 $S_s$  AND  $R_2$  WITH THE EXPERIMENT OF  
 SCHUBAUER AND SPANGENBERG (1950)  
 "FLOW E" (IDENT = 4800);  
 — PREDICTION; O DATA.

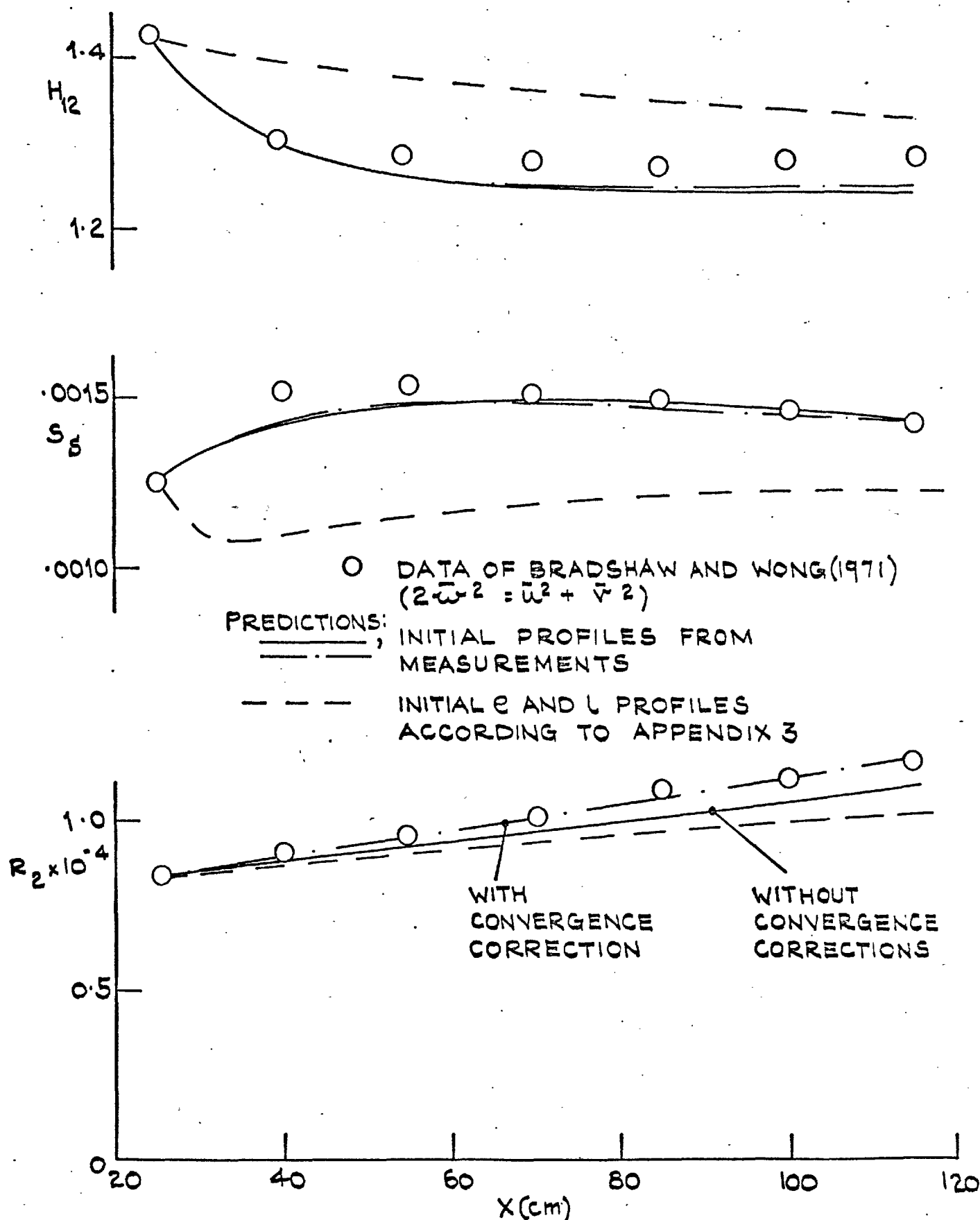
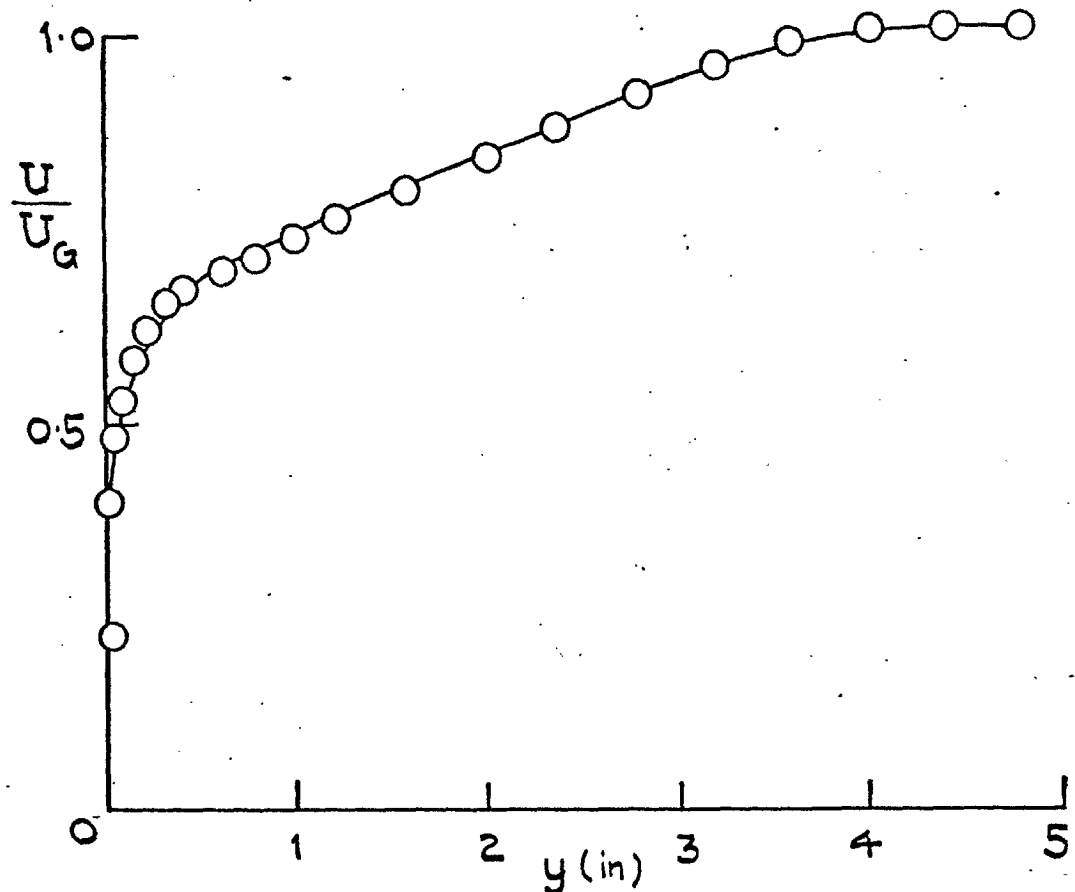
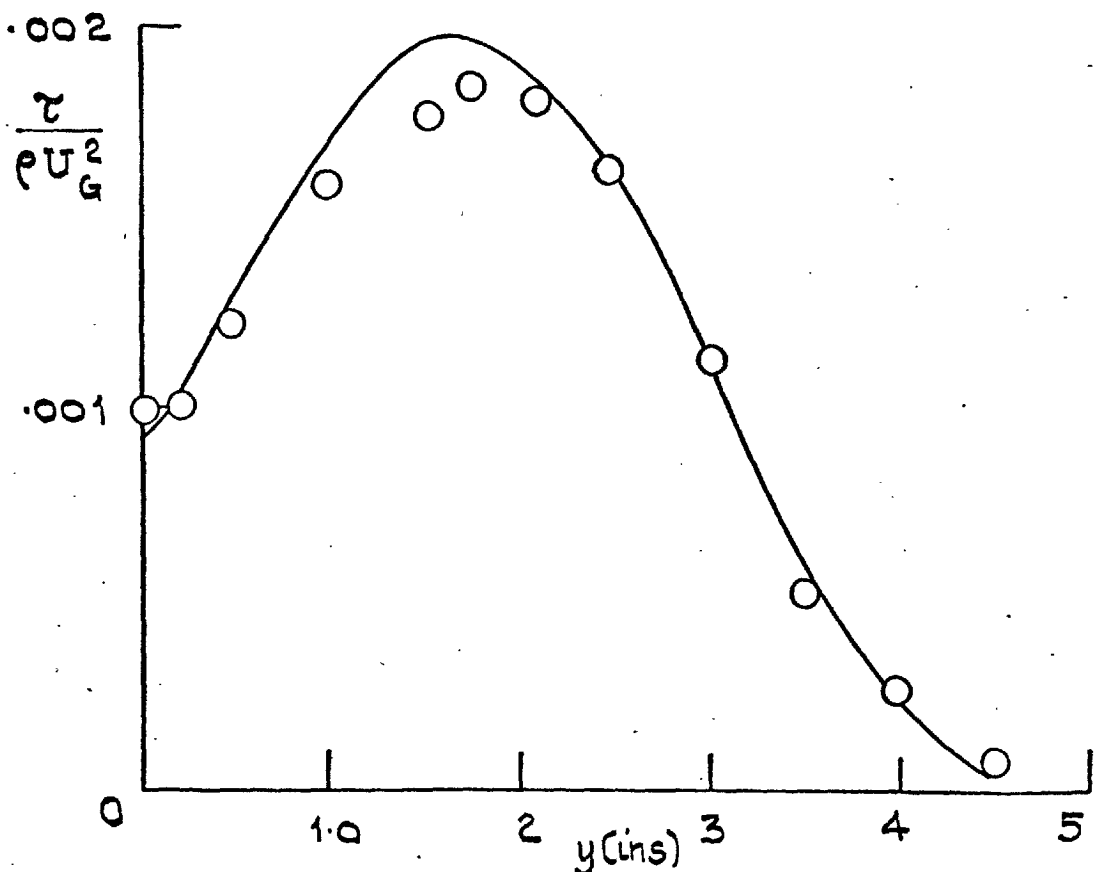


FIG. 6.11: COMPARISON OF PREDICTIONS OF  $H_{12}$ ,  $S_S$ ,  $R_2$  WITH EXPERIMENT OF BRADSHAW AND WONG (1971)

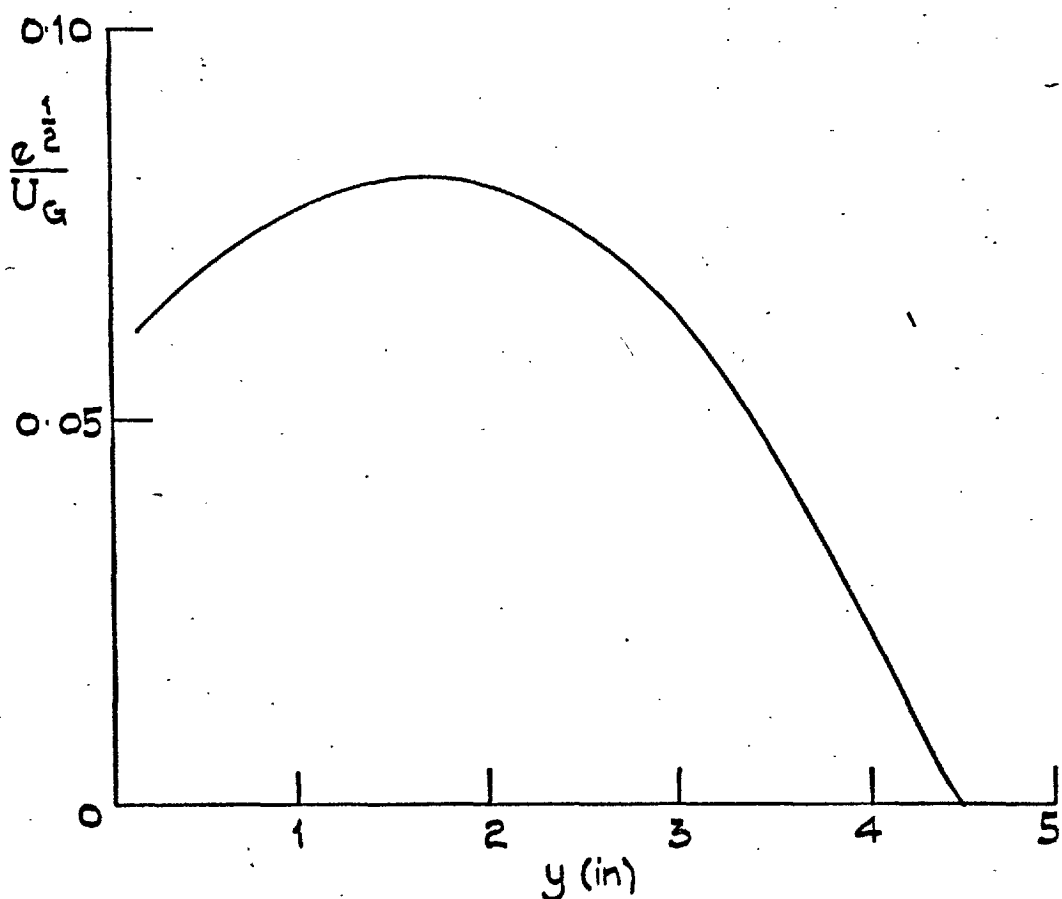


a). COMPARISON OF MEAN VELOCITY PROFILES



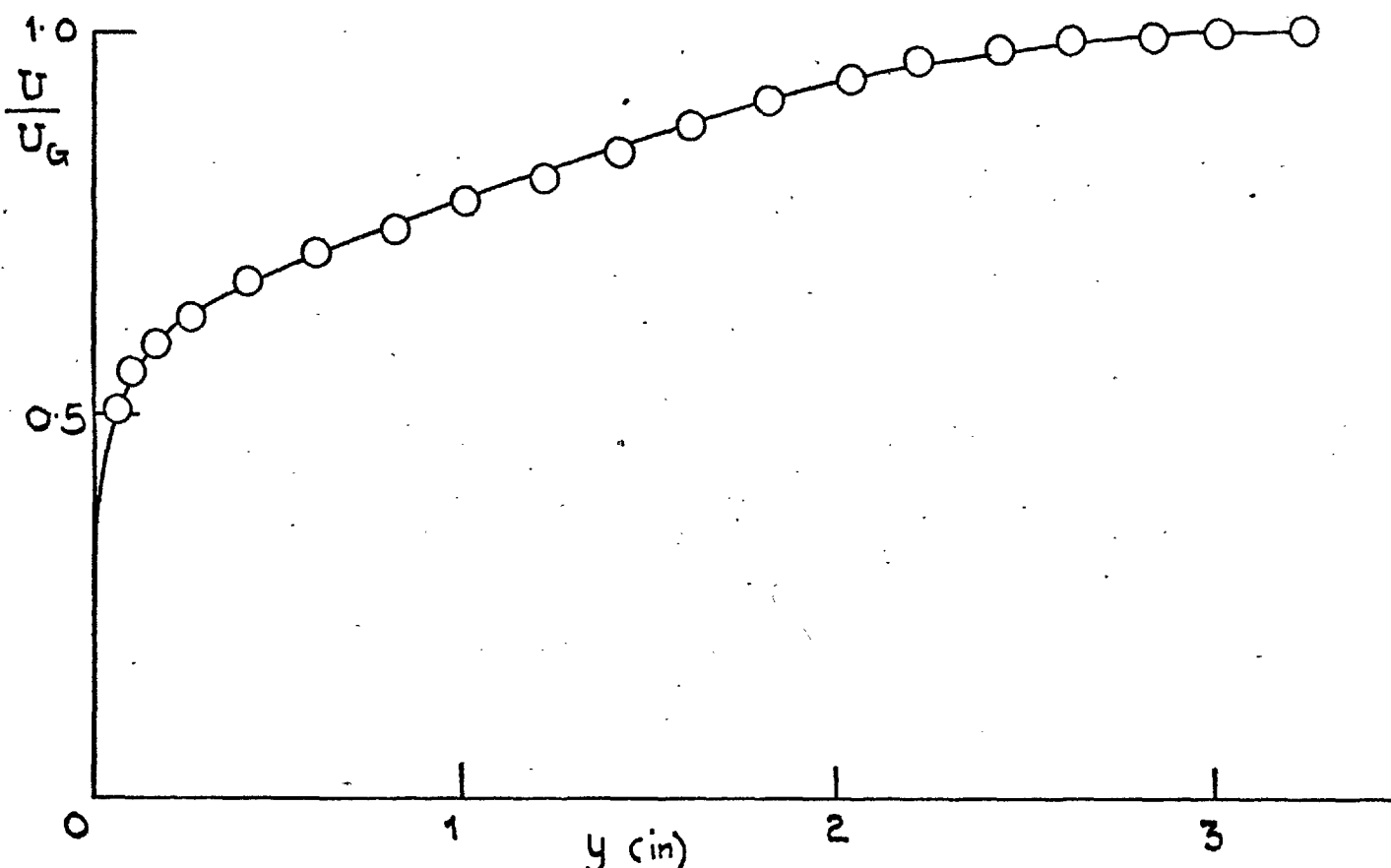
b) COMPARISON OF SHEAR STRESS PROFILES

FIG. 6.12 (CONTINUED)

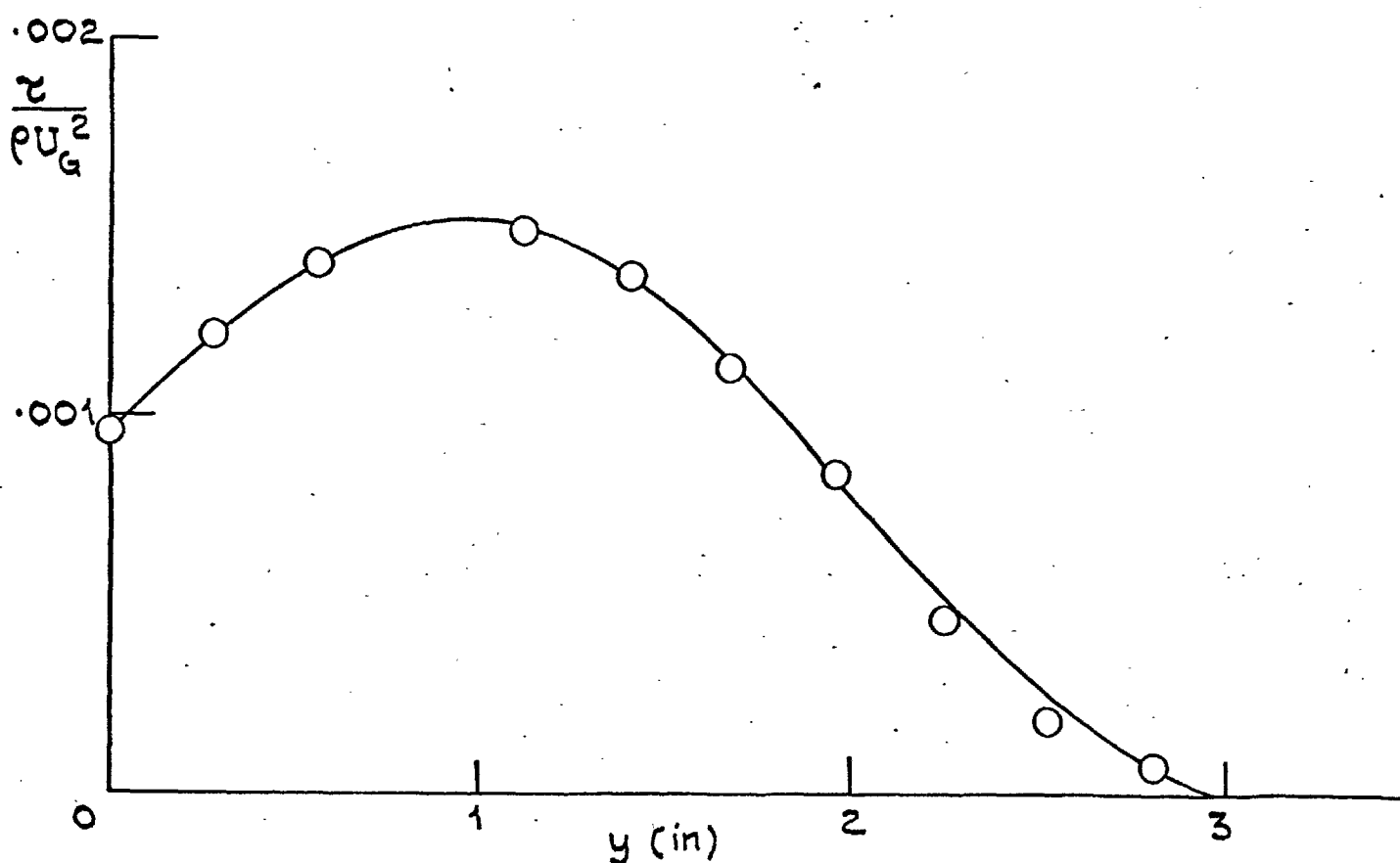


c). PREDICTED TURBULENT KENETIC ENERGY PROFILE.

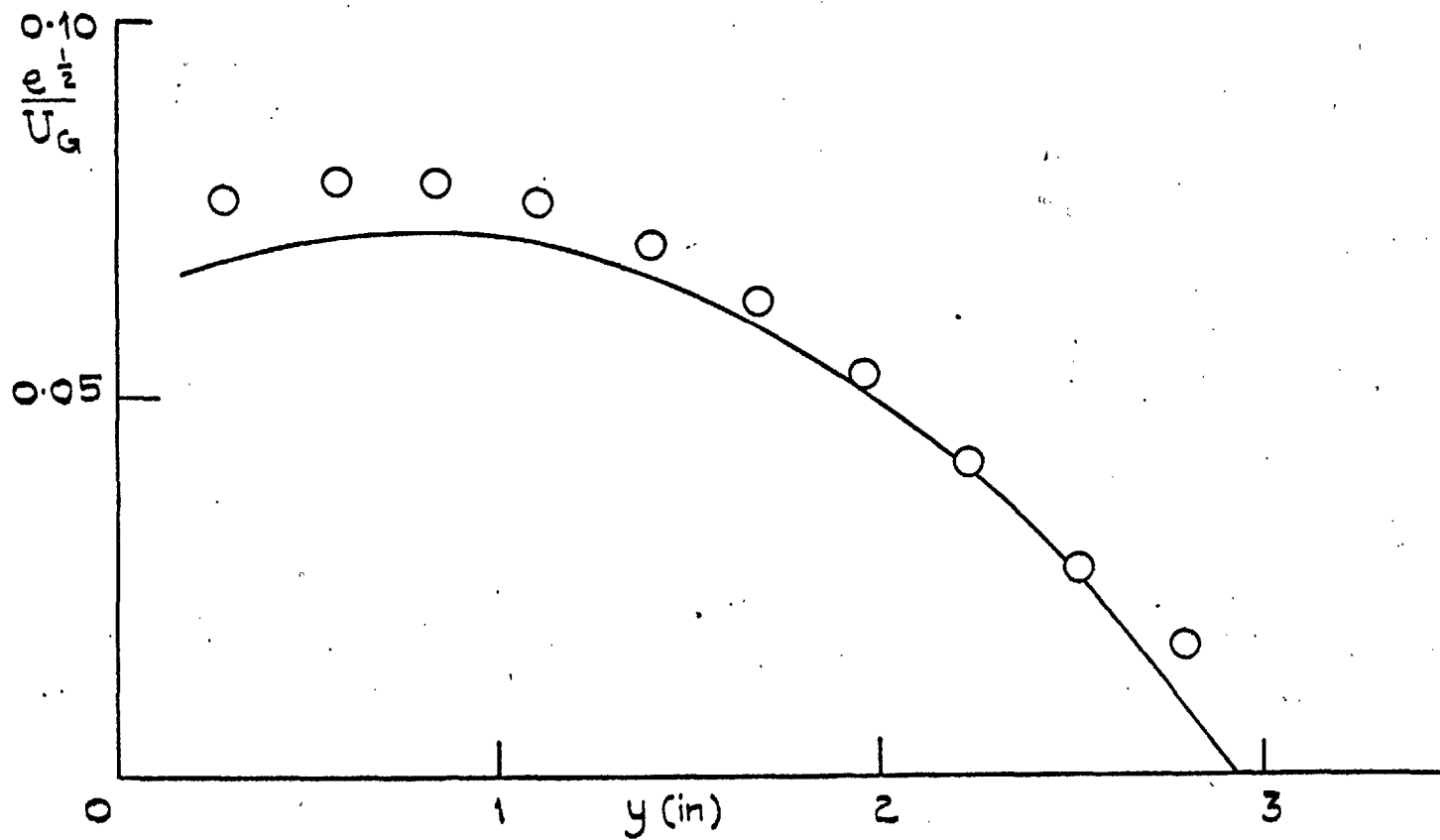
FIG. 6.12: COMPARISON OF PREDICTED  $U, \tau$  AND  $e$  PROFILES WITH THE EXPERIMENT OF BRADSHAW AND FERRISS AT  $x = 7.9$  ft.  
— PREDICTION    O DATA.



a). COMPARISON OF MEAN-VELOCITY PROFILES

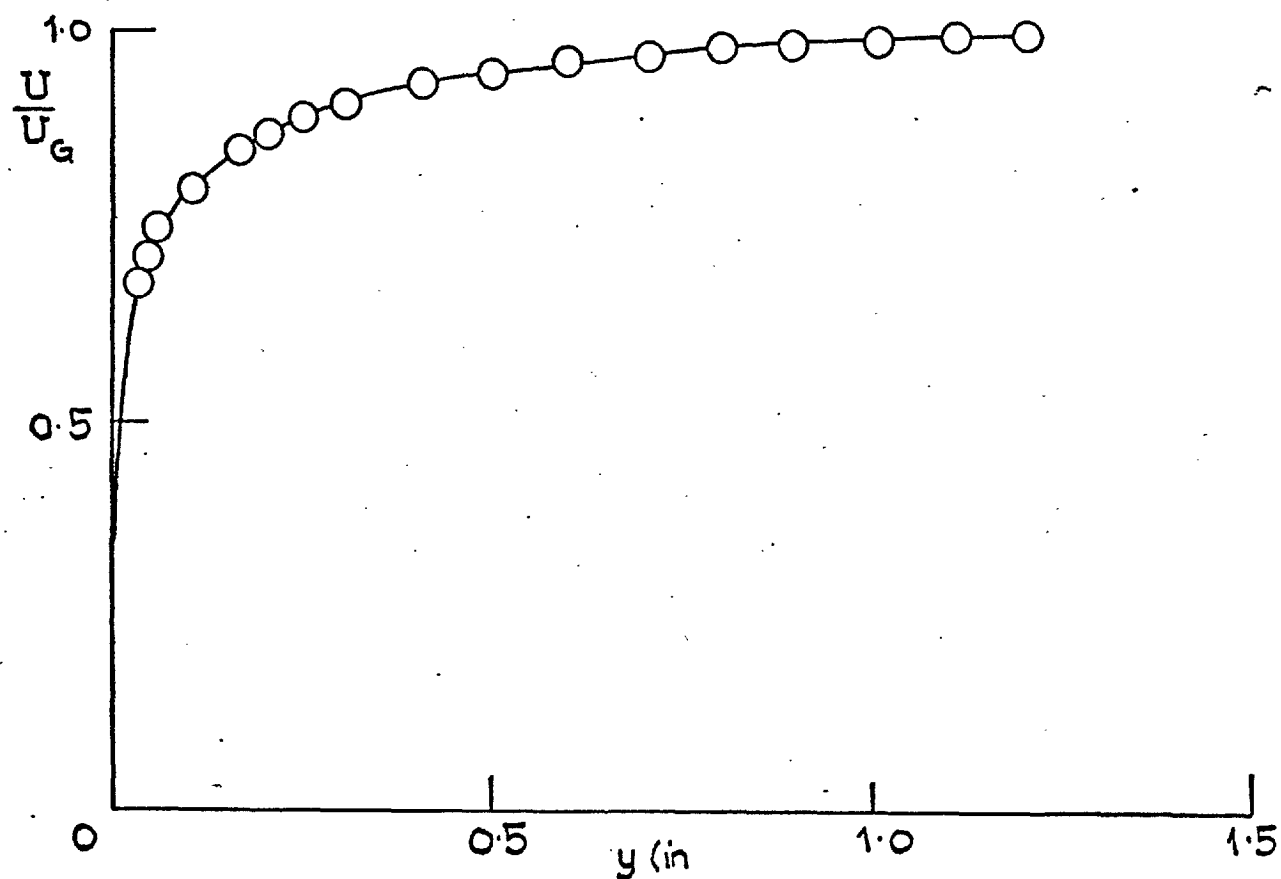


b). COMPARISON OF SHEAR-STRESS PROFILES

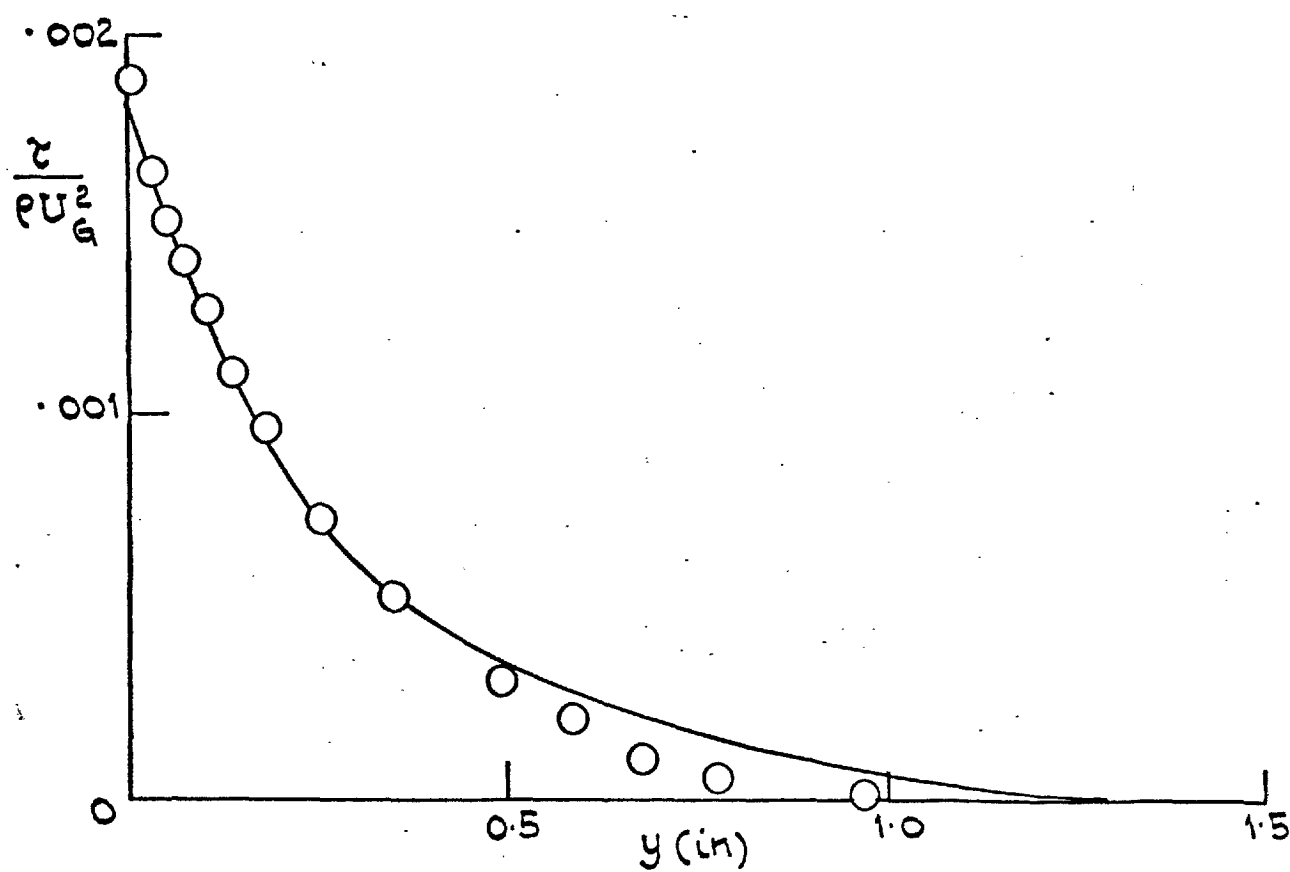


c). COMPARISON OF TURBULENT KINETIC ENERGY PROFILE

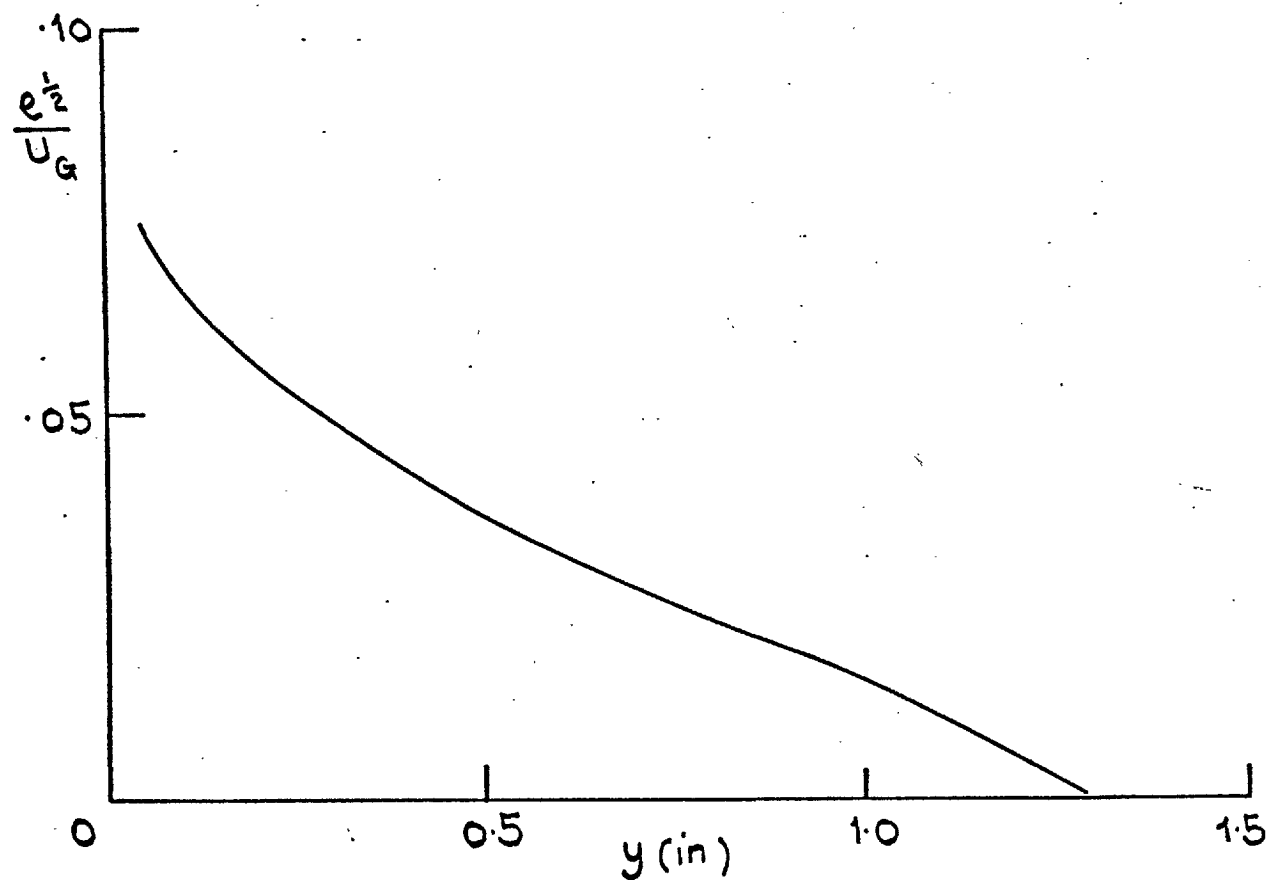
FIG. 6.13: COMPARISON OF PREDICTED  $U$ ,  $\tau$  AND  $e$  PROFILES WITH  
THE EXPERIMENT OF BRADSHAW " $\alpha = 0.15$  AT  $x = 7$  ft;  
— PREDICTION; ○ DATA



a). COMPARISON OF MEAN VELOCITY PROFILES

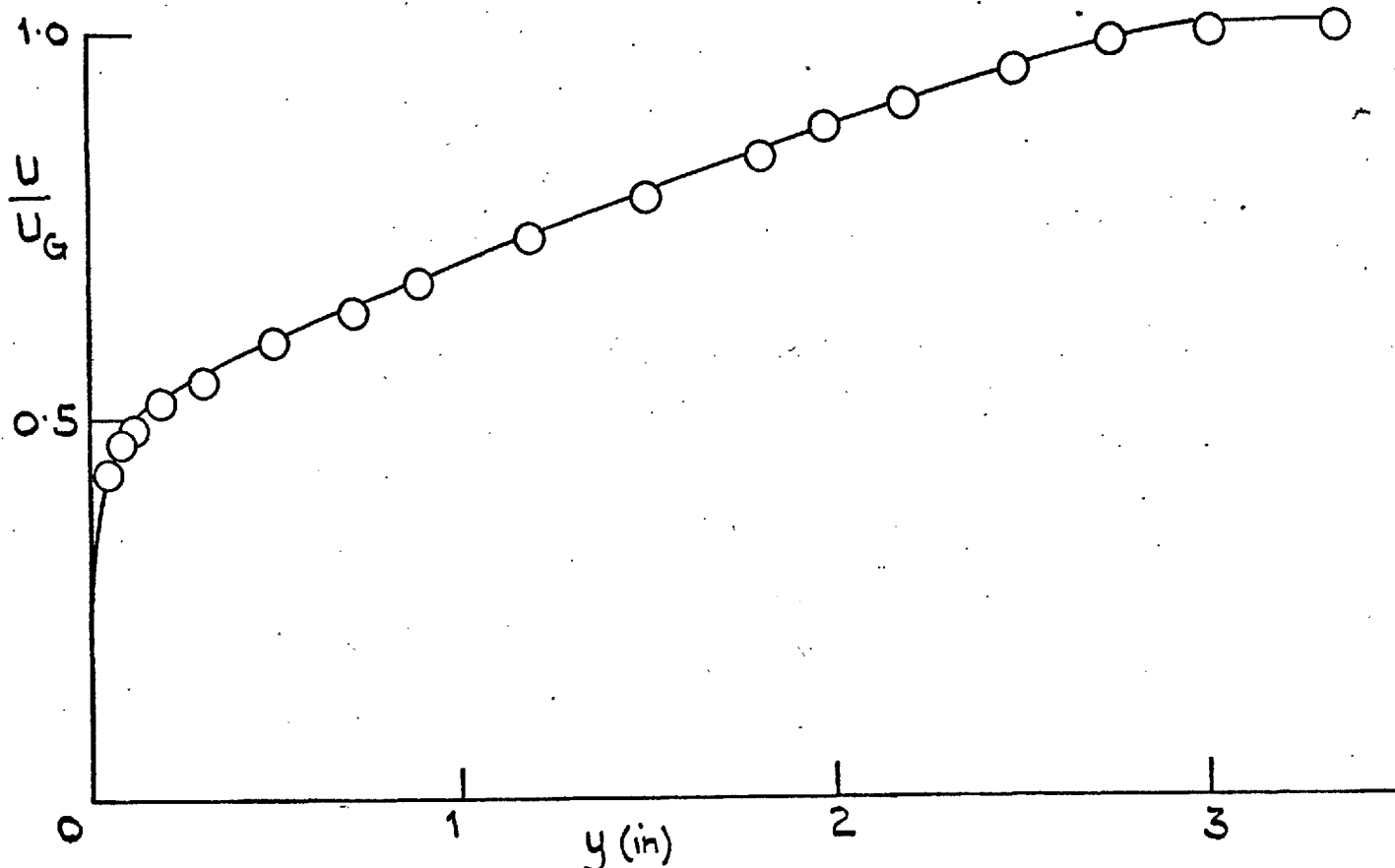


b). COMPARISON OF SHEAR-STRESS PROFILES

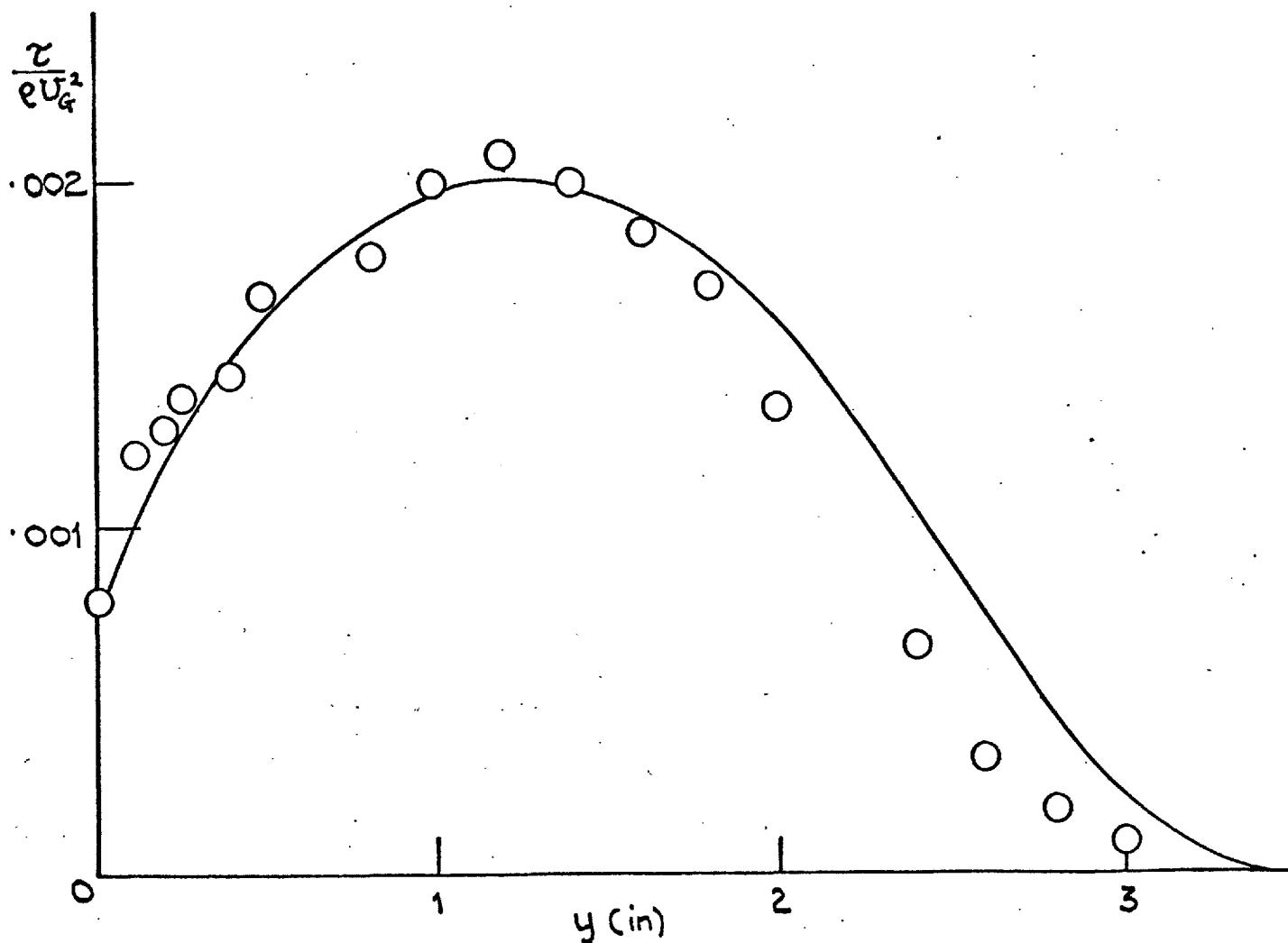


c). PREDICTED TURBULENT KINETIC ENERGY PROFILE

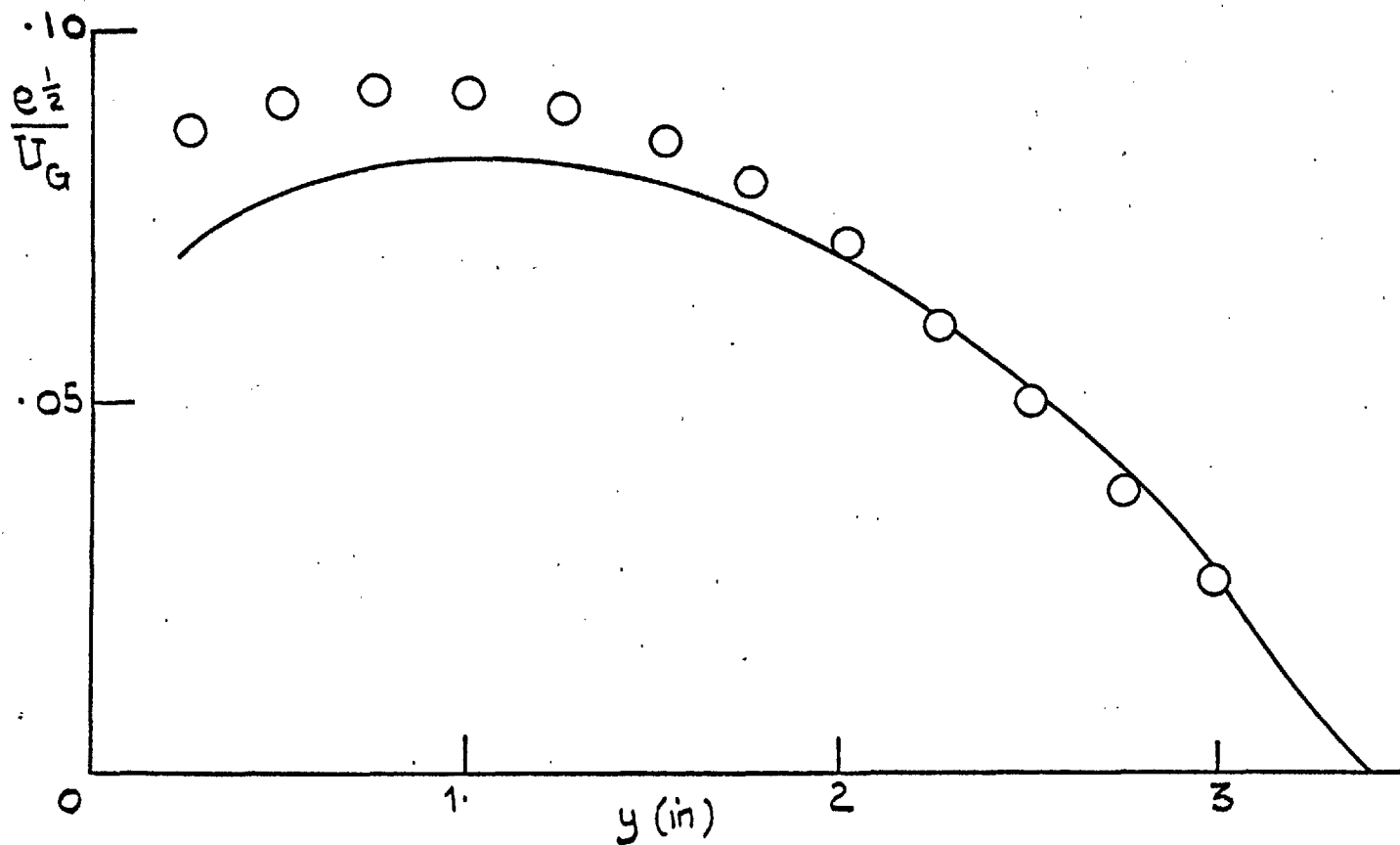
FIG. b.14: COMPARISON OF PREDICTED  $U$ ,  $\tau$  AND  $e$   
 PROFILES WITH THE EXPERIMENT OF  
 HERRING AND NORBURY " $\beta = -0.53$ " AT  $x = 4\text{ft}$ ;  
 — PREDICTION; O DATA



a). COMPARISON OF MEAN-VELOCITY PROFILES



b). COMPARISON OF SHEAR-STRESS PROFILES



c). COMPARISON OF TURBULENT - KINETIC ENERGY PROFILES.

FIG. 6.15: COMPARISON OF PREDICTED PROFILES OF  $U$ ,  $\tau$  AND  $e$   
 WITH THE EXPERIMENT OF BRADSHAW " $\alpha = 0 \rightarrow -0.255$ ,  
 FLOW C" AT  $X = 7$  ft; — PREDICTION      ○ DATA.

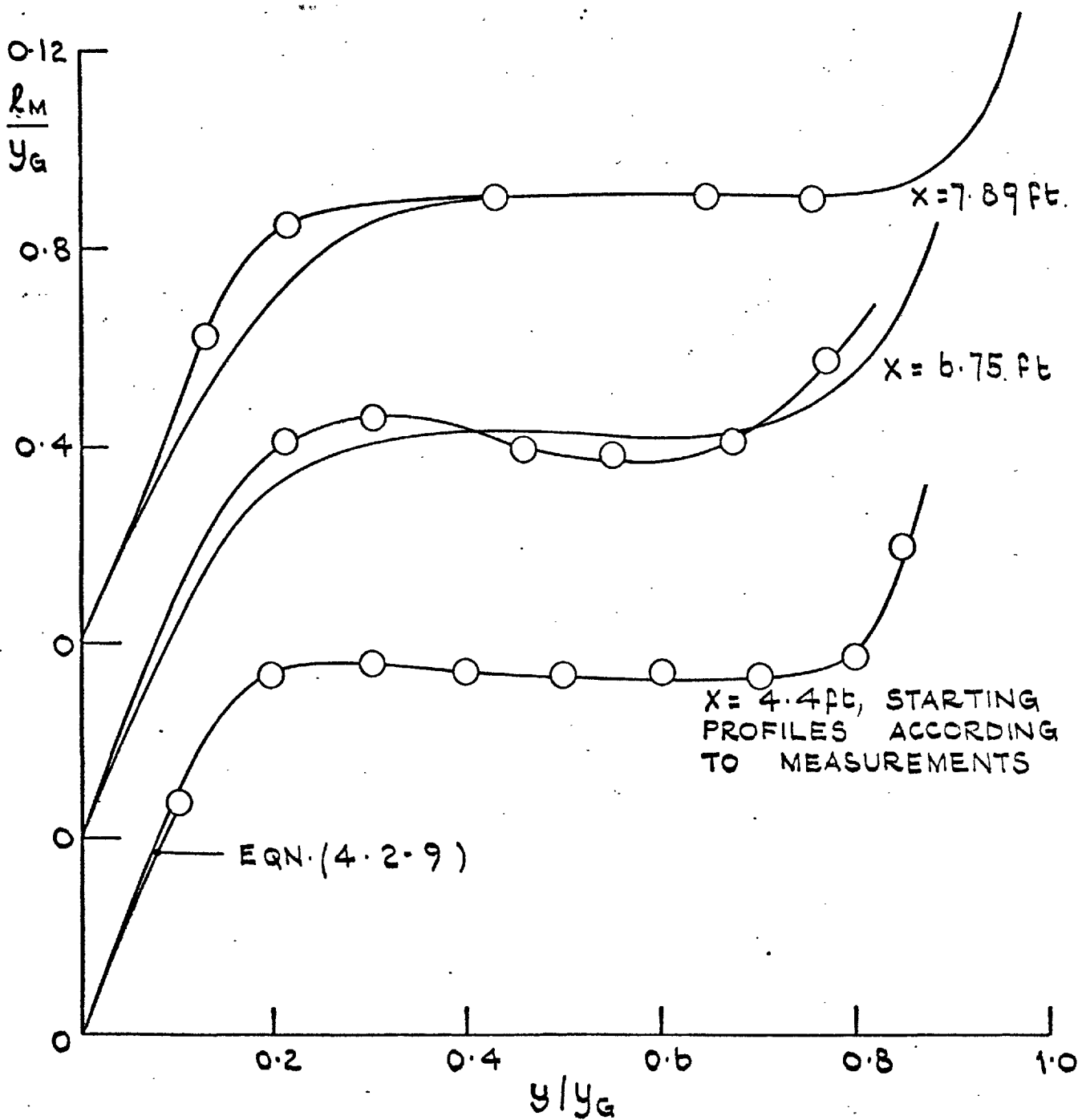


FIG. b.16: COMPARISON OF THE PREDICTED MIXING LENGTH DISTRIBUTIONS WITH EXPERIMENTS;  
PREDICTIONS —○— DATA OF BRADSHAW AND FERRIS (RELAXING FLOW IDENT = 2400)

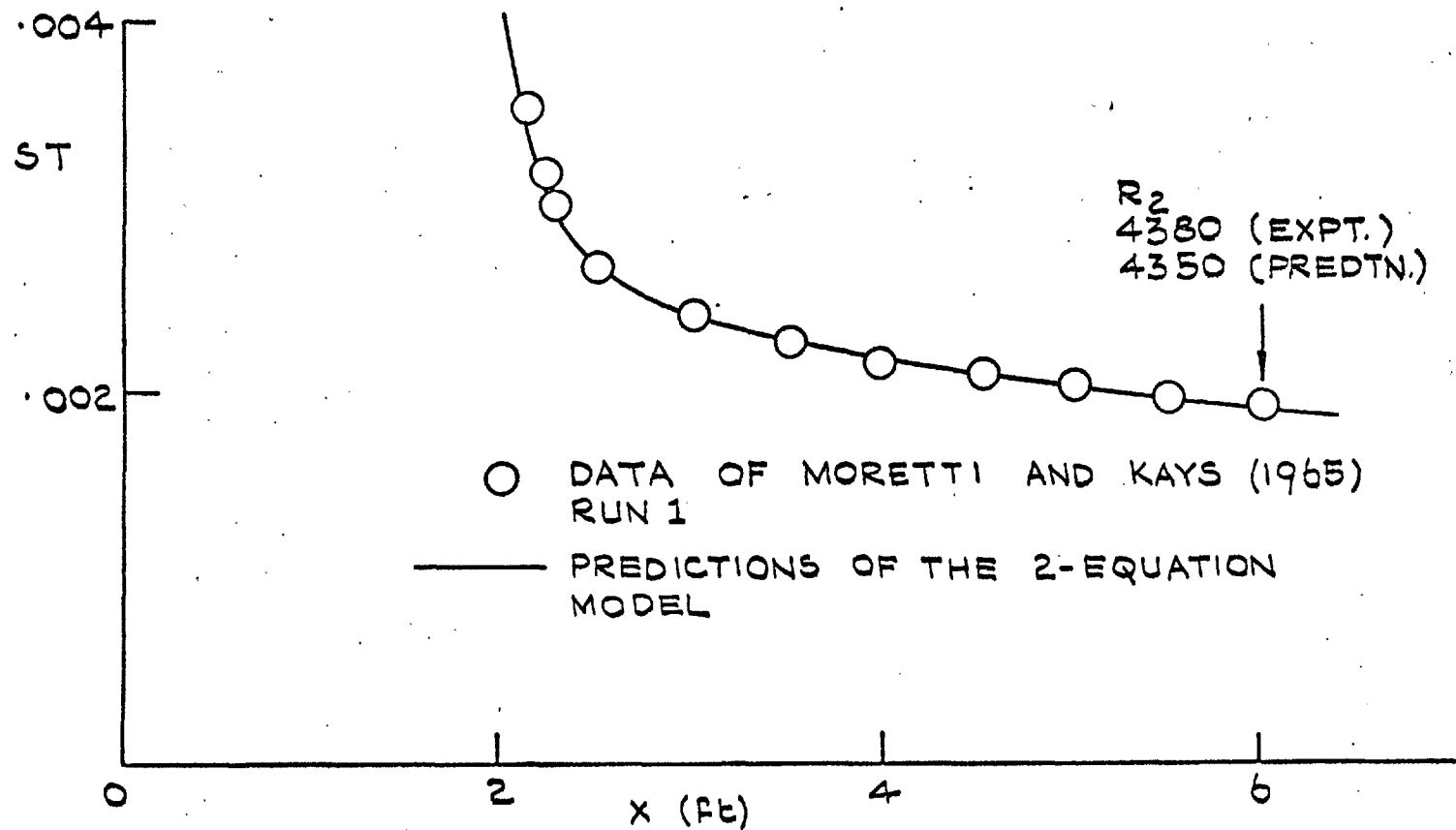


FIG. 6.17: COMPARISON OF PREDICTED STANTON NUMBER  
DISTRIBUTION WITH EXPERIMENT FOR A  
FLAT-PLATE FLOW

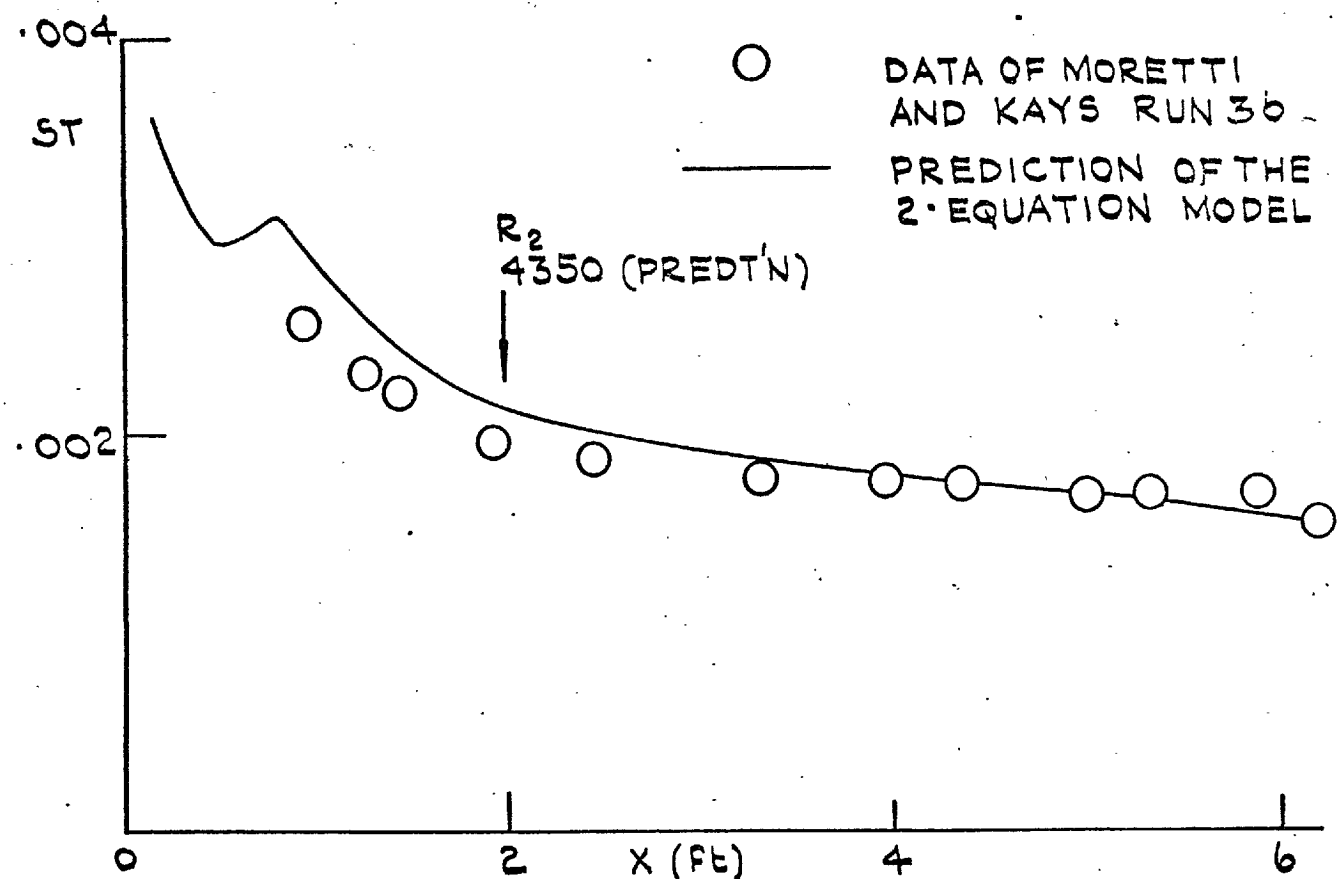


FIG. 6.18: COMPARISON OF PREDICTED ST WITH EXPERIMENT FOR A DECLERATED FLOW

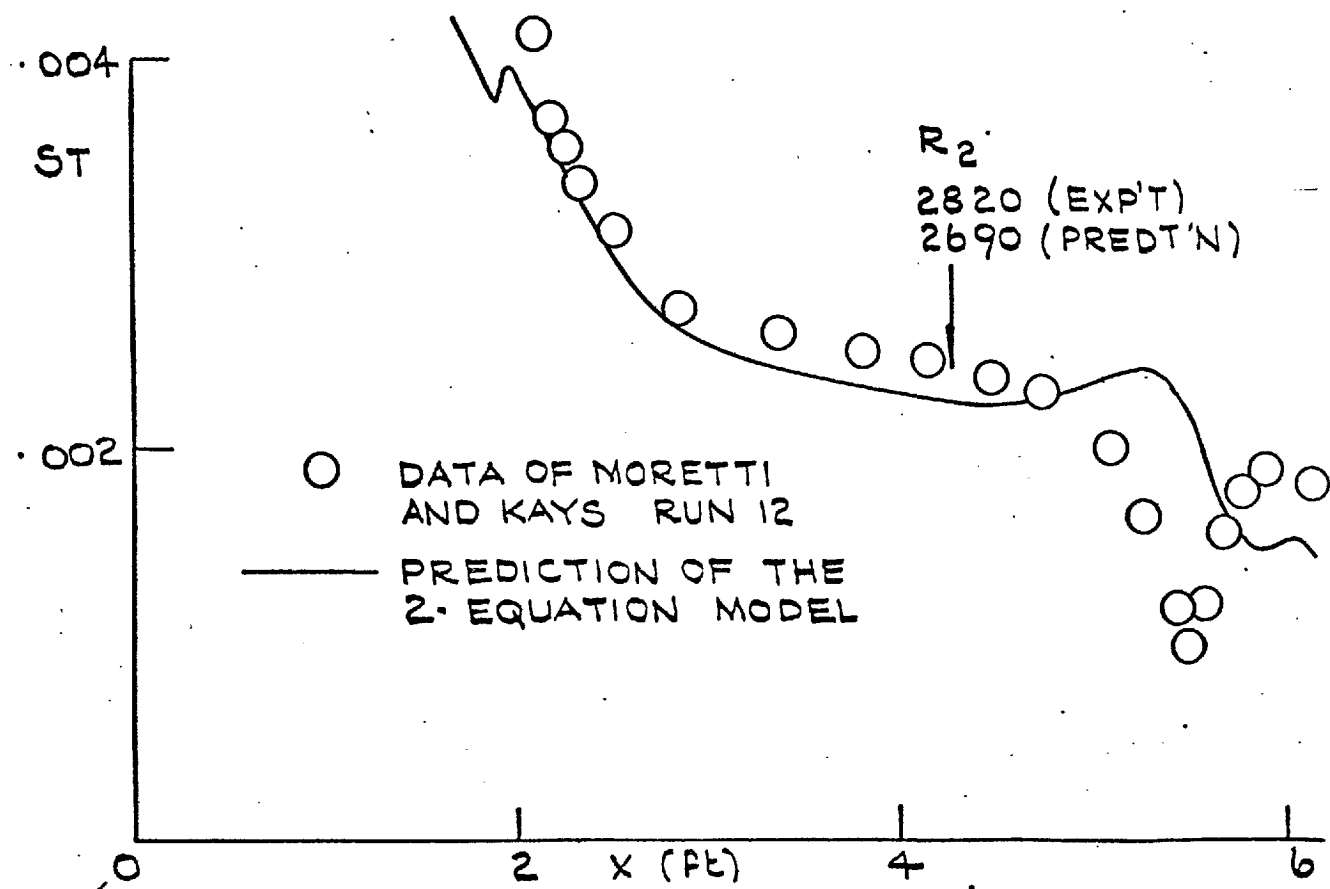


FIG. 6.19: COMPARISON OF PREDICTED ST WITH EXPERIMENT FOR SUDDENLY ACCELERATED FLOWS

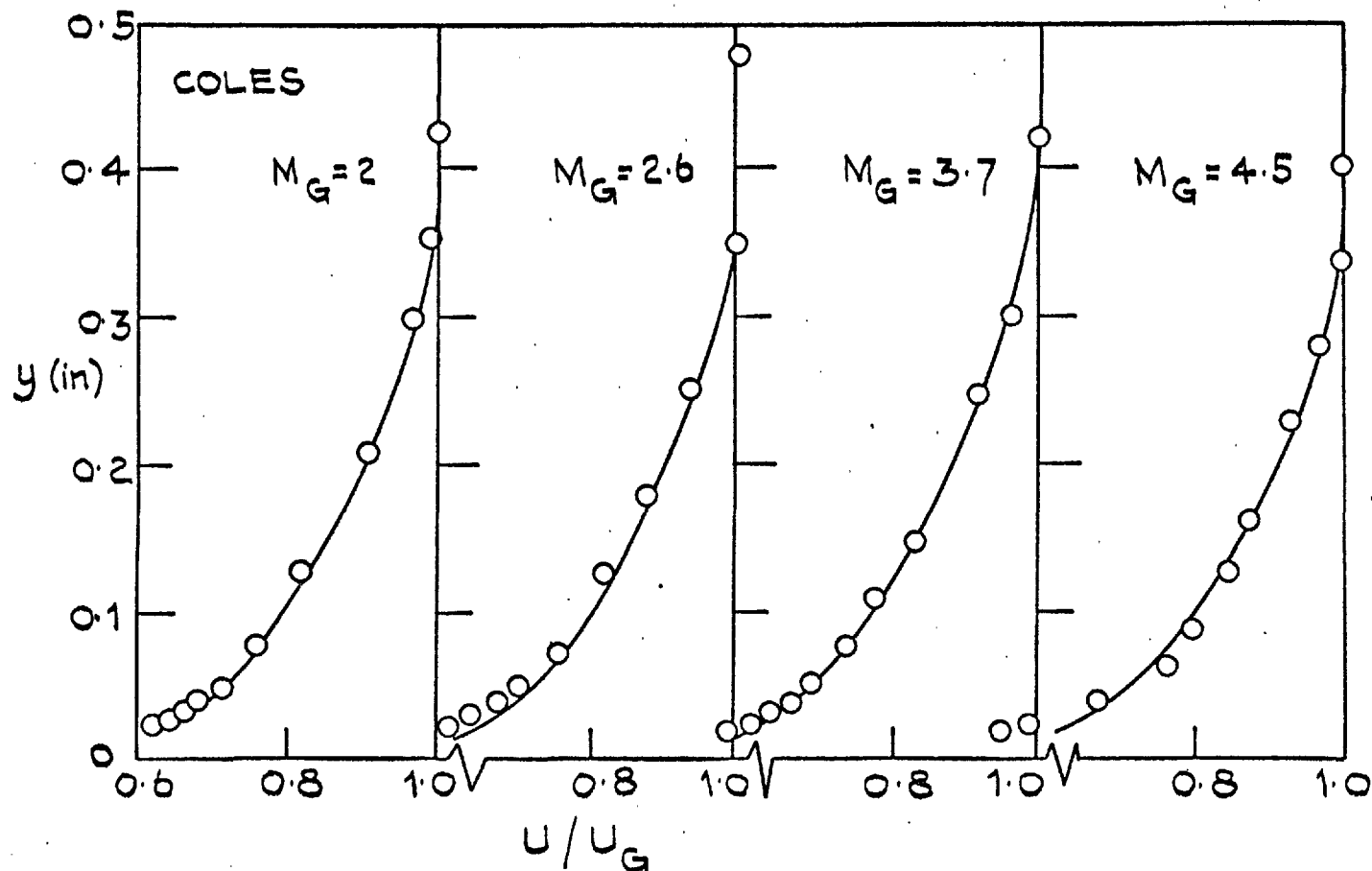
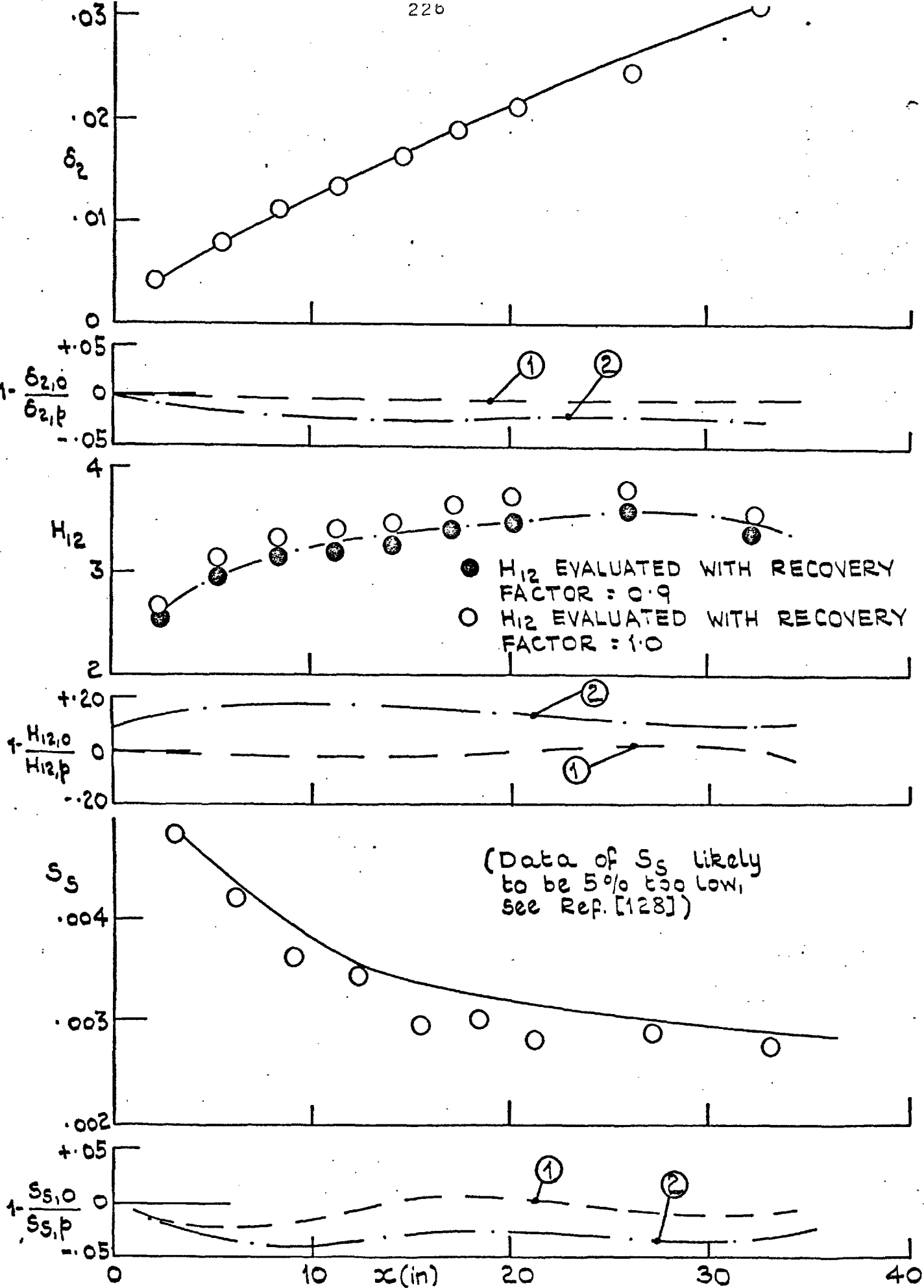
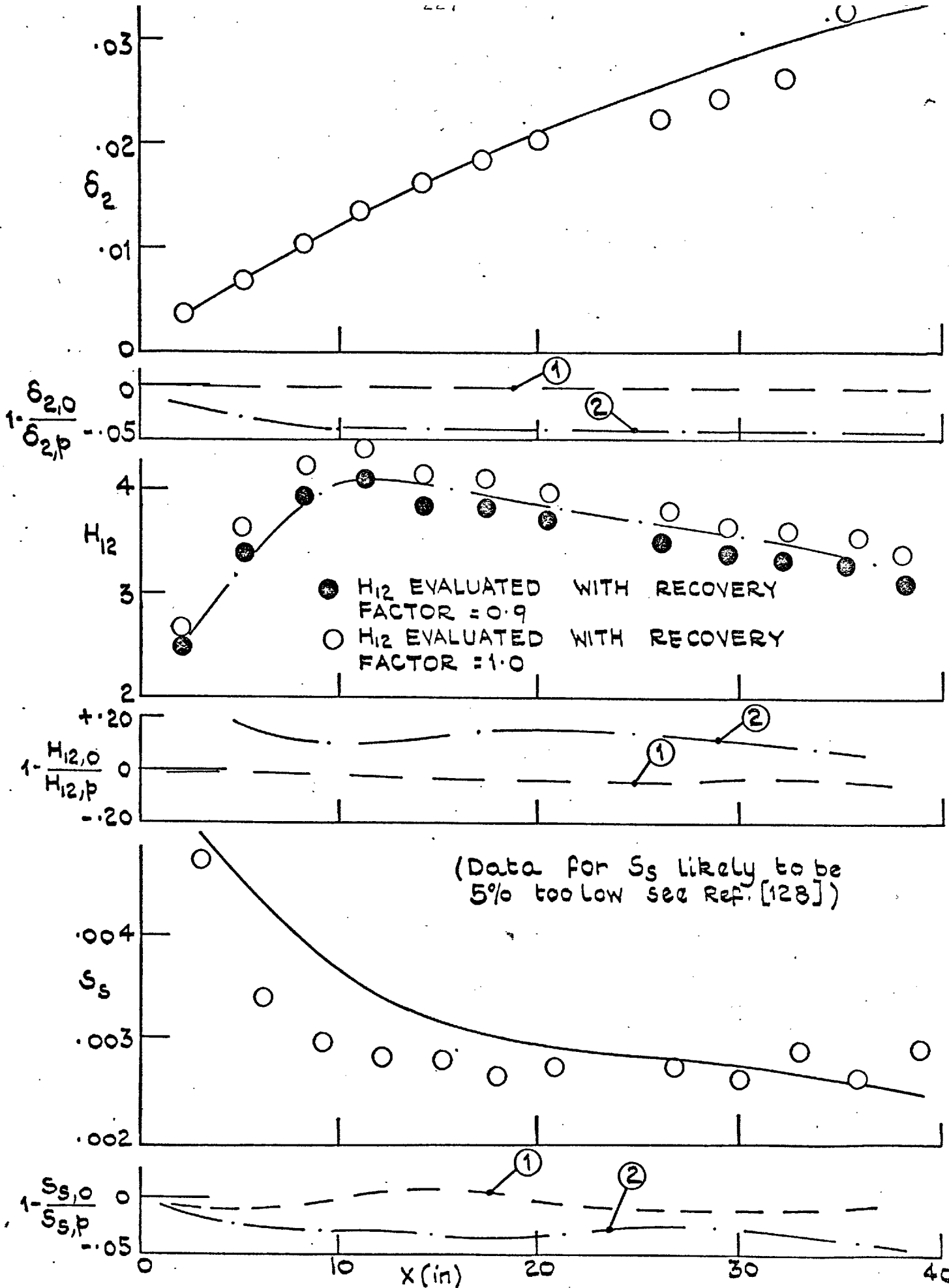


FIG. 6.20: COMPARISON OF THE PREDICTED MEAN  
VELOCITY PROFILES WITH EXPERIMENT ON  
A FLAT PLATE; O DATA  
— PRESENT PREDICTION



**FIG. 6.21: COMPARISON OF PRESENT PREDICTION WITH EXPERIMENT AND PREDICTIONS FROM OTHER MODELS OF TURBULENCE; O DATA OF SIVASEGRAM MG 2.2 to 2.35; — PRESENT PREDICTION; (1) PATANKAR-SPALDING; (2) BRADSHAW**



**FIG. 6.22: COMPARISON OF THE PRESENT PREDICTION WITH EXPERIMENT AND PREDICTIONS FROM OTHER MODELS OF TURBULENCE; ○ DATA OF SIVASEGERAM MG 2.6 to 2.15; — PRESENT PREDICTION;**

**(1) • PATANKAR - SPALDING ; (2) BRADSHAW.**

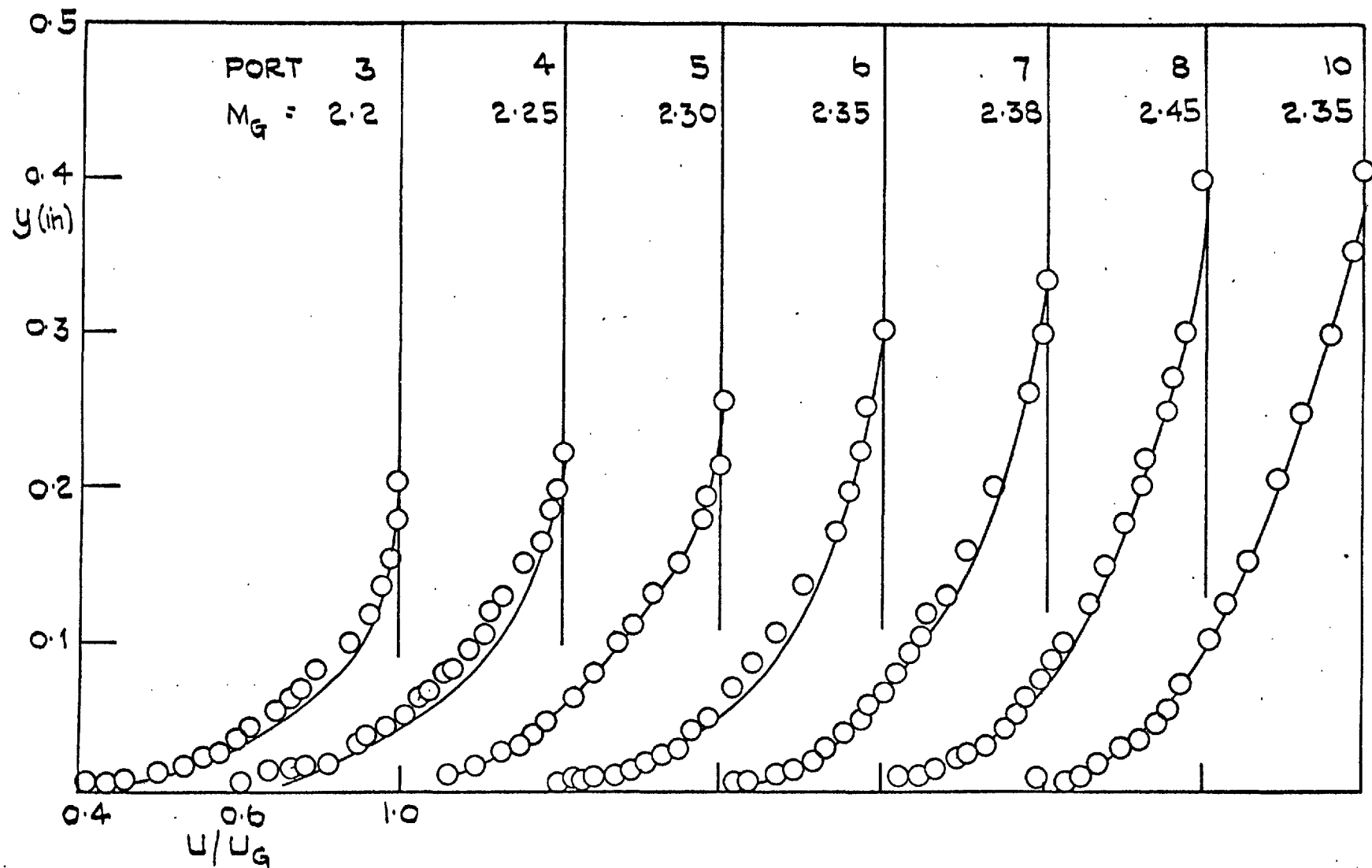


FIG. 6.23: COMPARISON OF THE PREDICTION OF THE TWO-EQUATION MODEL  
 WITH EXPERIMENT FOR AN ACCELERATING BOUNDARY LAYER;  
 O DATA OF SIVASEGARAM (1969); — PREDICTION

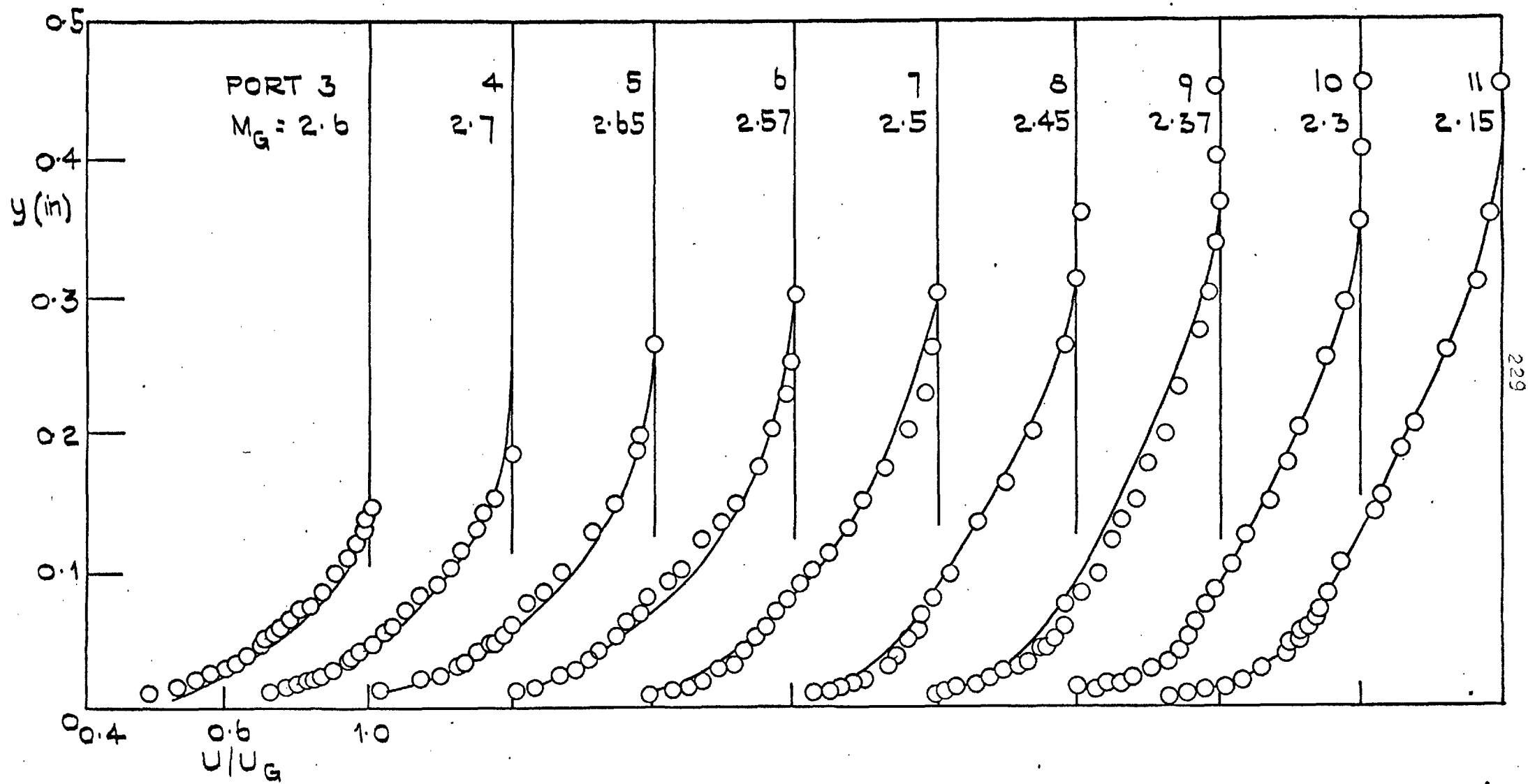


FIG. b.24: COMPARISON OF THE PREDICTION OF THE TWO-EQUATION  
MODEL WITH DATA OF A DECELERATING FLOW;  
O DATA OF SIVASEGARAM (1969); — PREDICTION

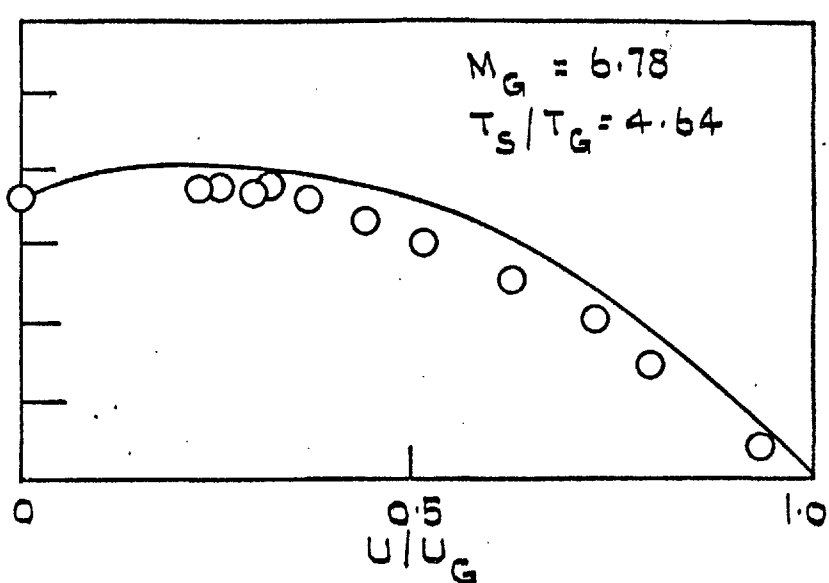
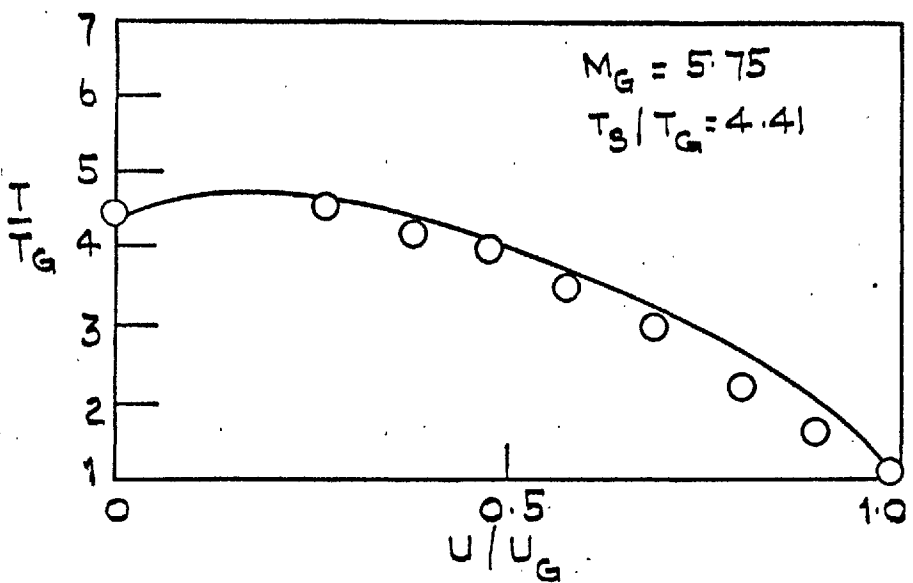
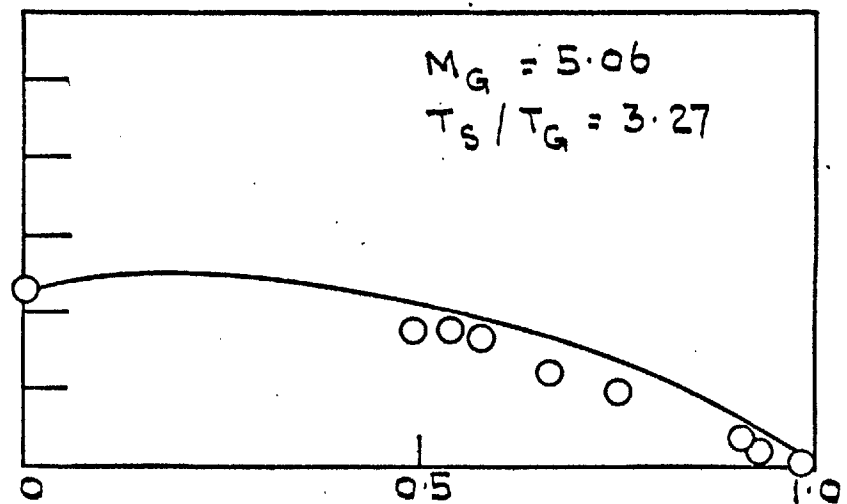
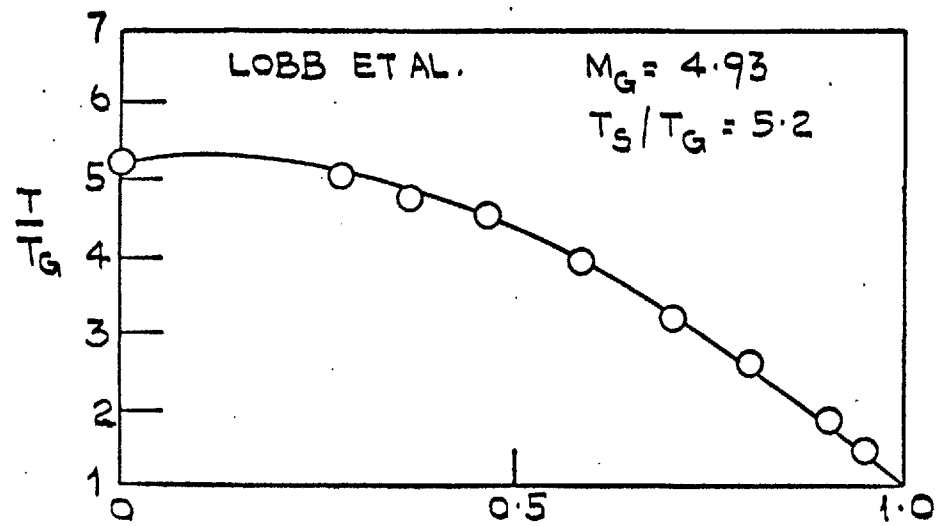


FIG. 6.25: COMPARISON OF THE PREDICTIONS OF THE STATIC TEMPERATURE PROFILE FROM THE PRESENT MODEL WITH EXPERIMENT; — PREDICTION;  
○ DATA OF LOBB ET AL. (1955), ZERO PRESSURE-GRADIENT FLOW

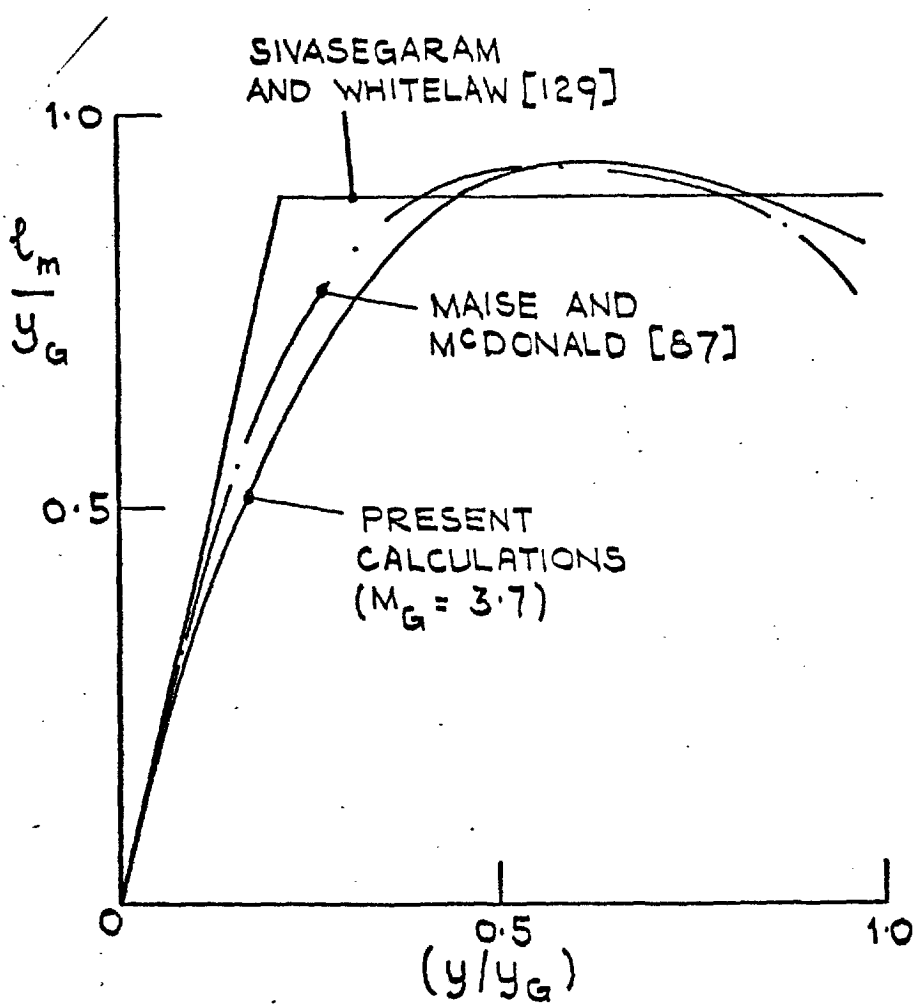
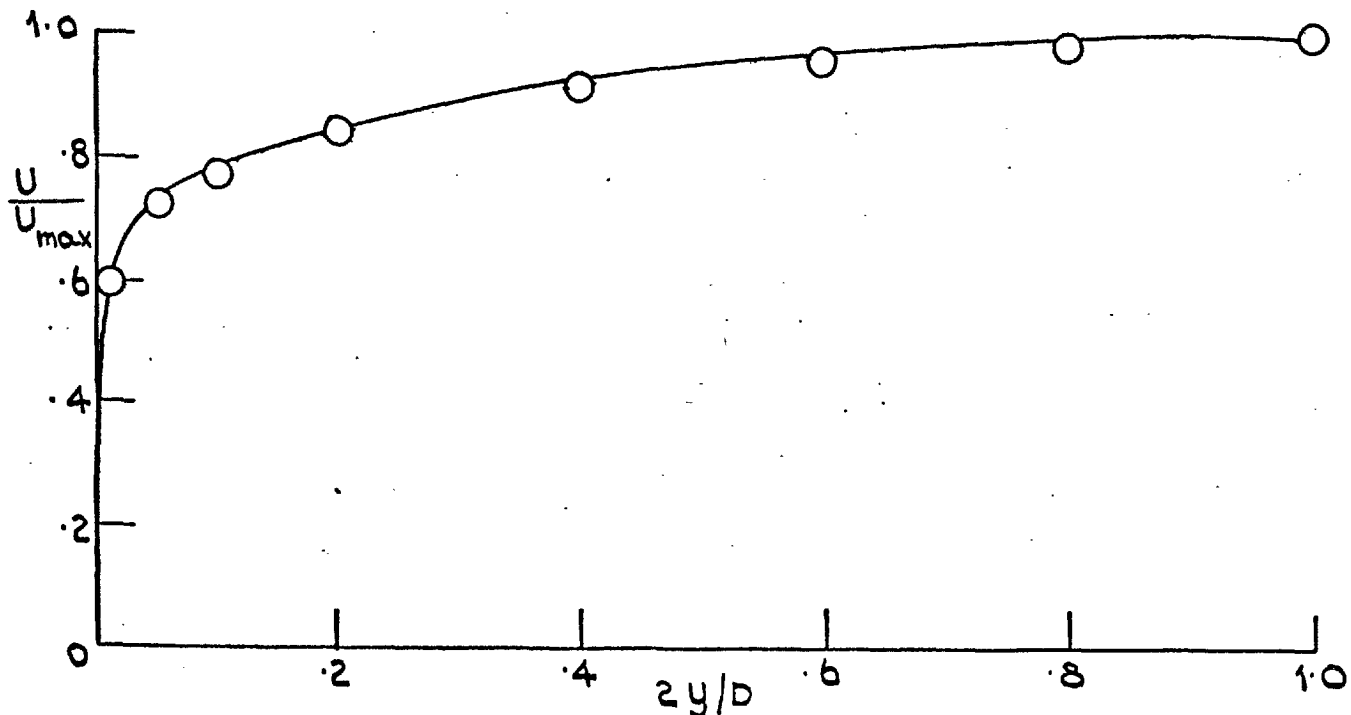
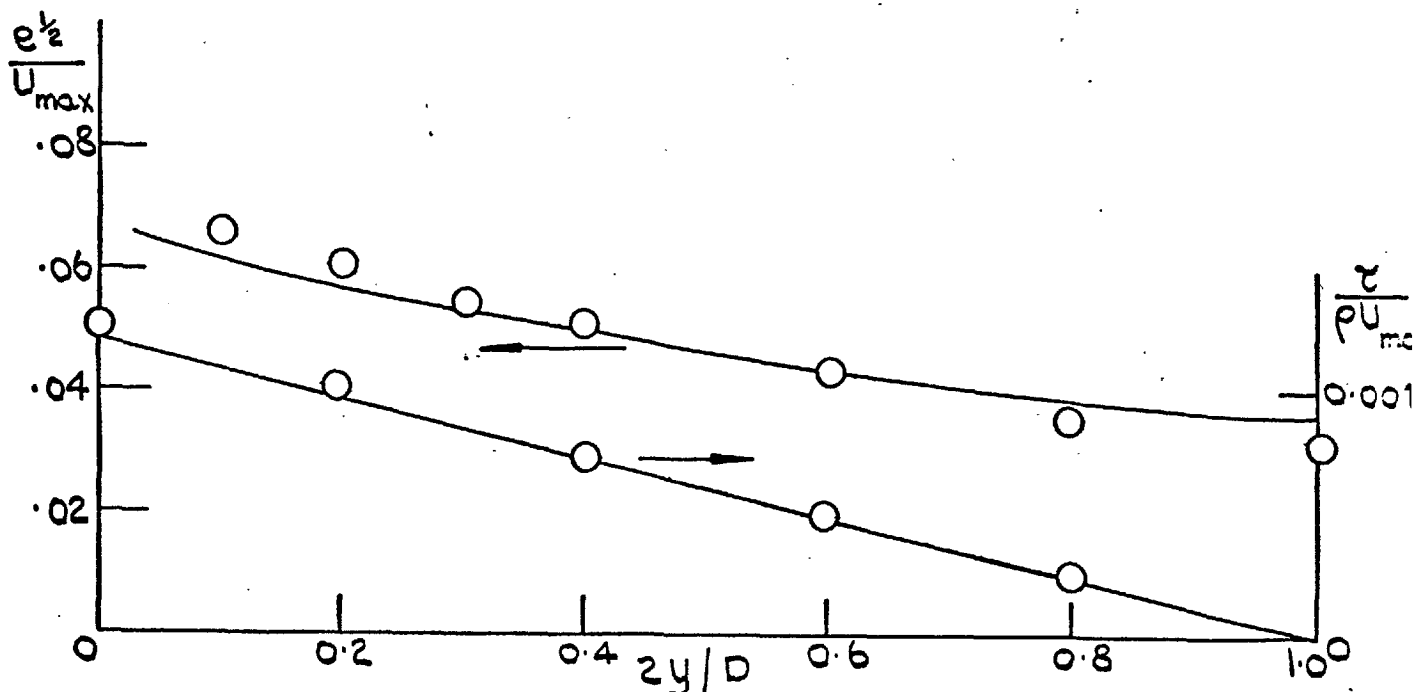
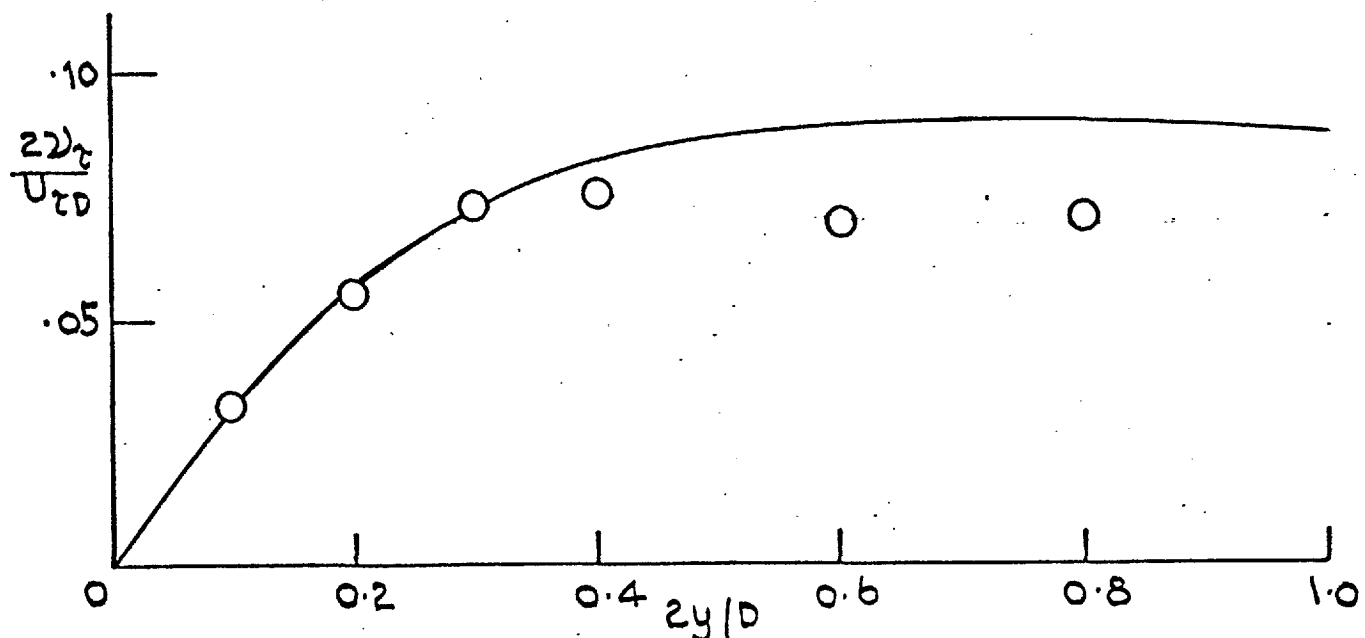


FIG. 6.26: COMPARISON OF THE PREDICTED  
MIXING-LENGTH DISTRIBUTION ACROSS  
A FLAT-PLATE BOUNDARY LAYER  
WITH THE DISTRIBUTIONS PROPOSED  
IN REFS. [129] AND [87].

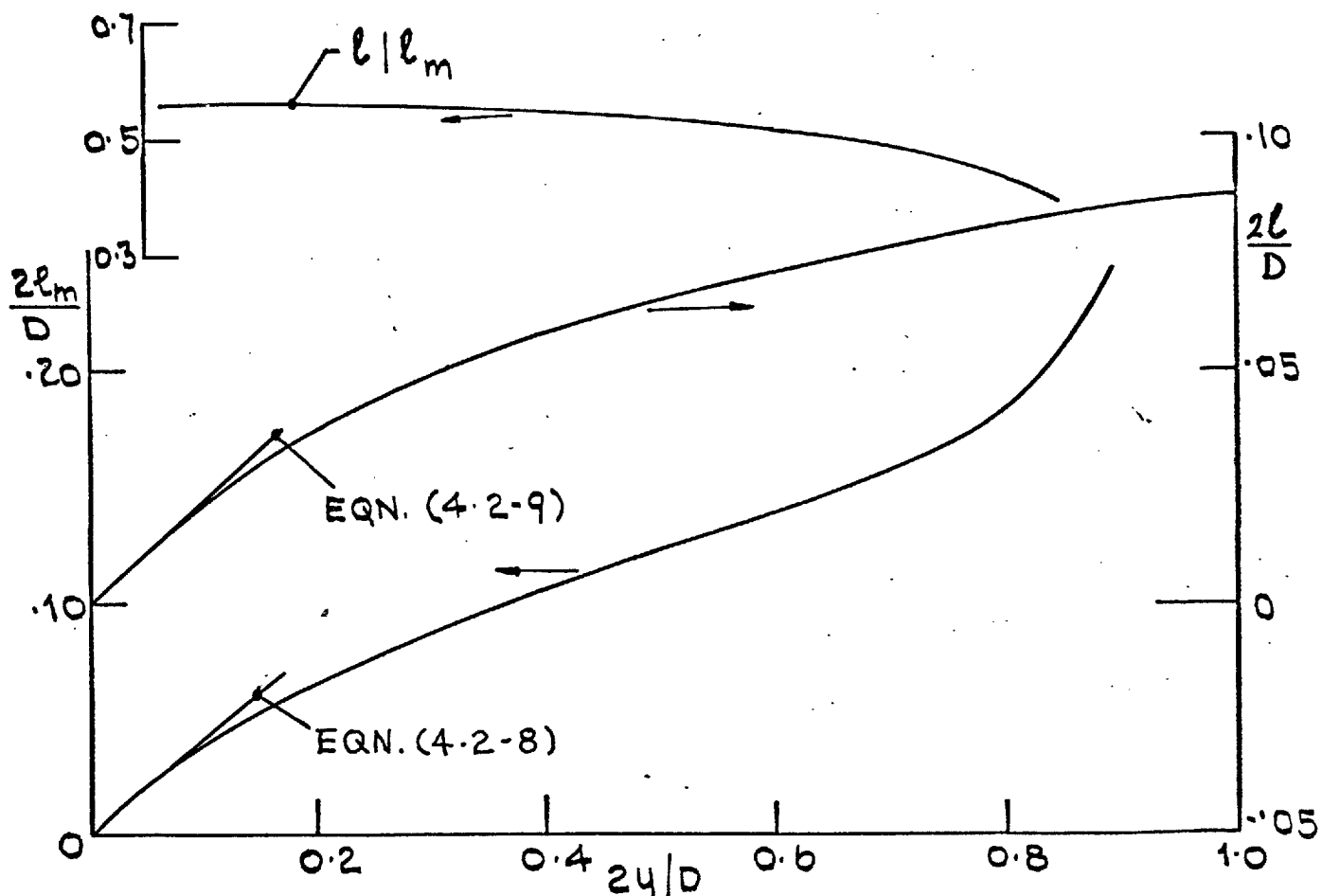


a). COMPARISON OF MEAN - VELOCITY PROFILES

b). COMPARISON OF  $\tau$  AND  $\epsilon$  - PROFILESFIG. 6.27 (CONTINUED)



c). COMPARISON OF TURBULENT-VISCOSITY PROFILES



d). PREDICTED LENGTH SCALES

FIG. b-27: COMPARISON OF PREDICTIONS WITH PIPE FLOW  
 DATA (LAUFER 1954); ○ DATA  $R_D = 500,000$ ;  
 — PRESENT PREDICTIONS  $R_D = 508,000$

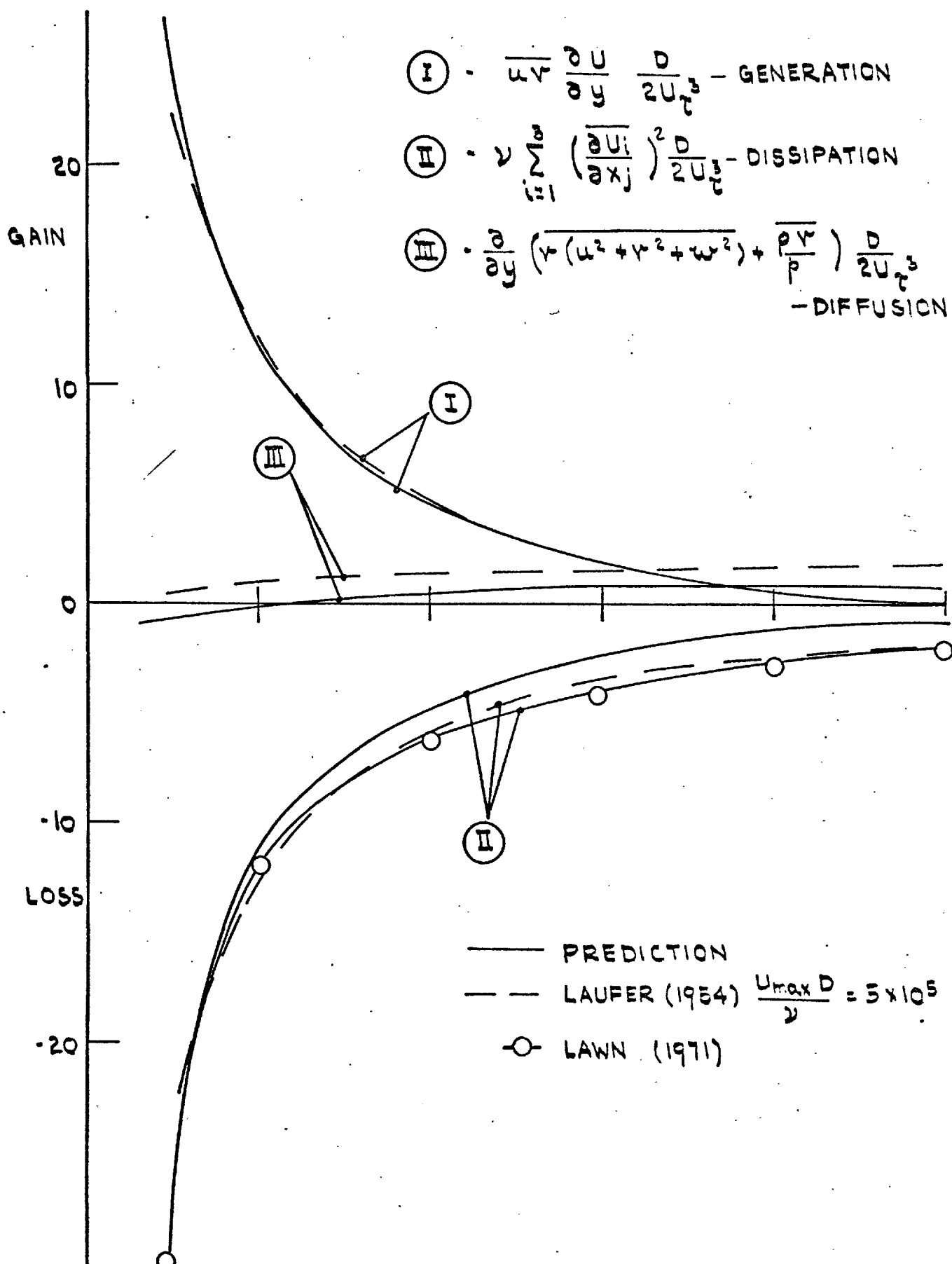
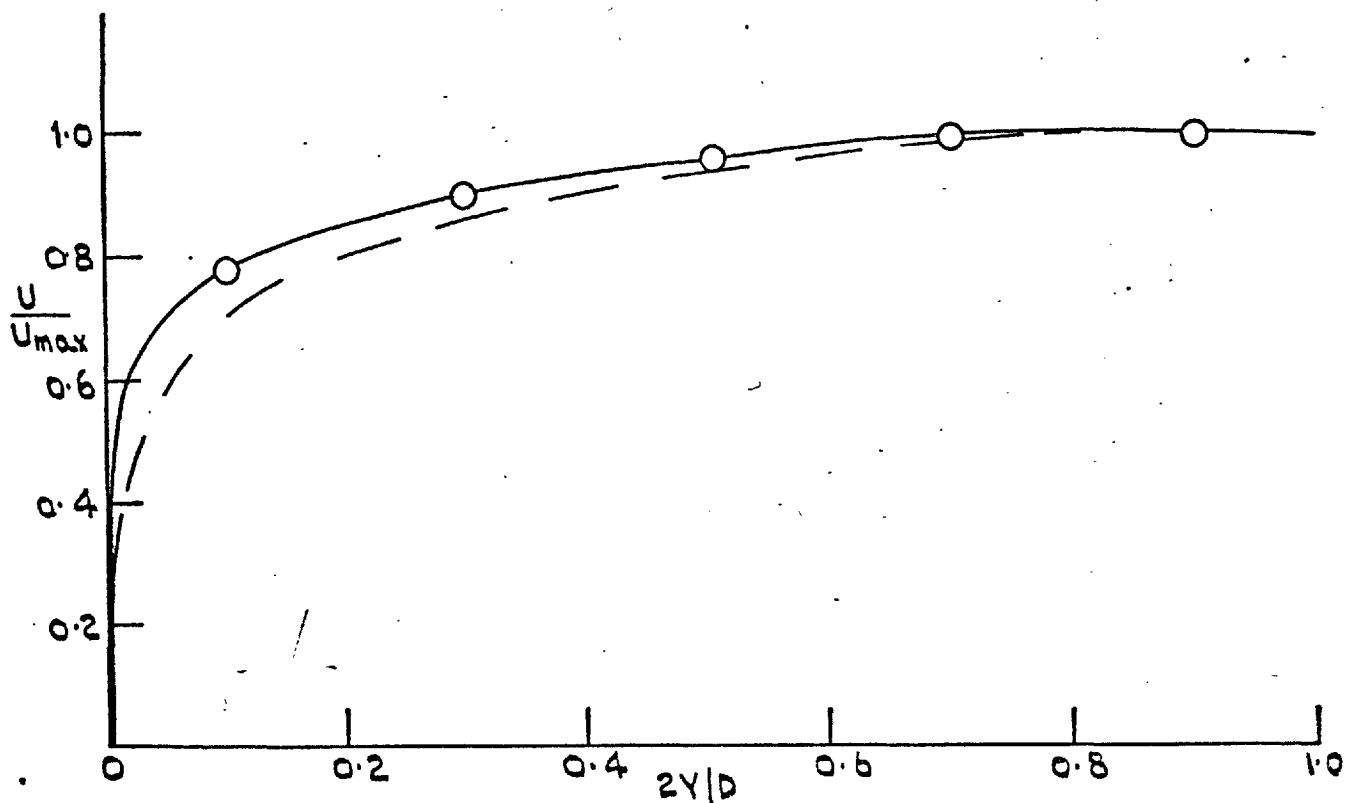


**FIG. 6.28:** COMPARISON OF THE PREDICTED TURBULENT KINETIC ENERGY BALANCE WITH EXPERIMENT FOR A DEVELOPED PIPE FLOW



a). COMPARISON OF MEAN-VELOCITY PROFILES

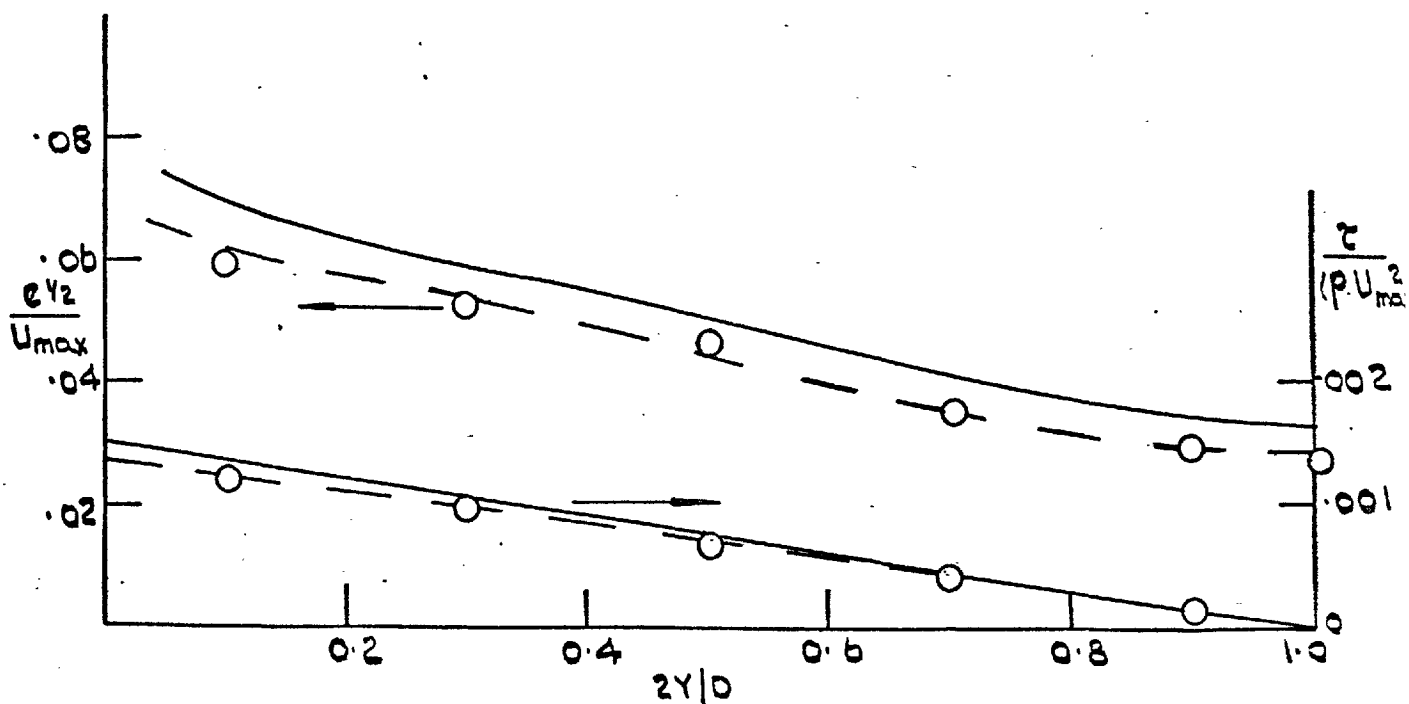
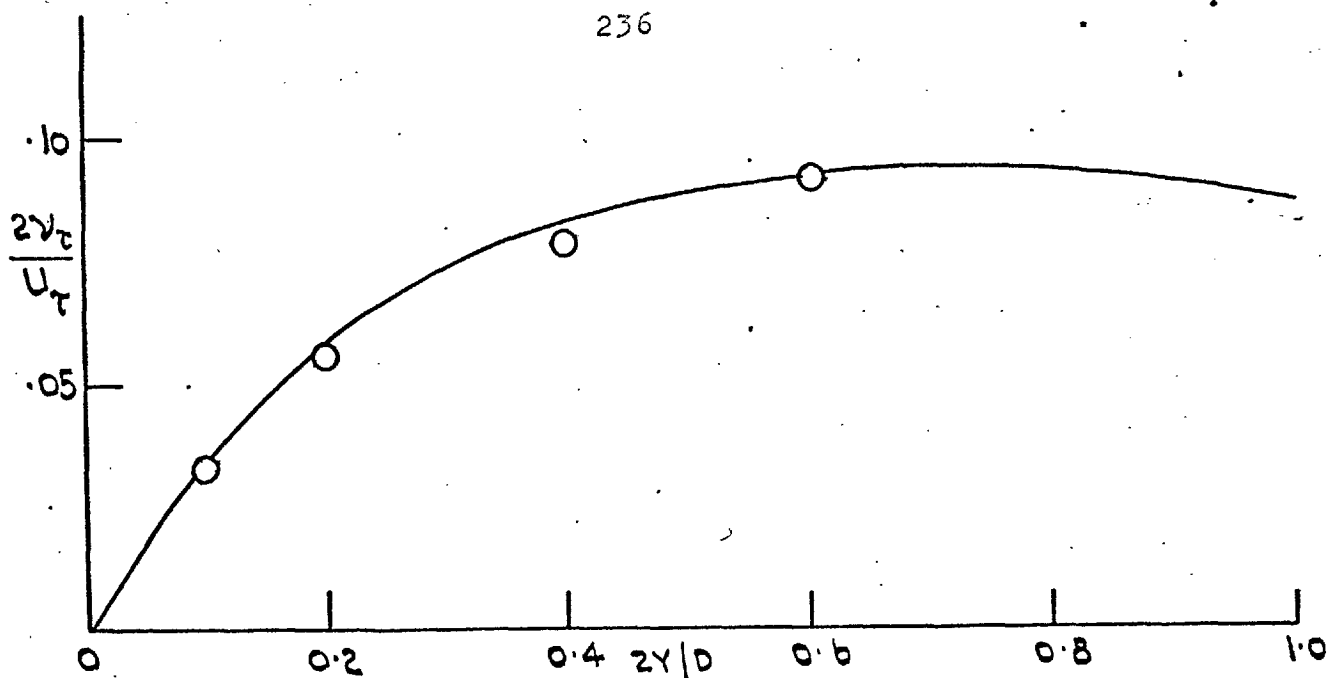
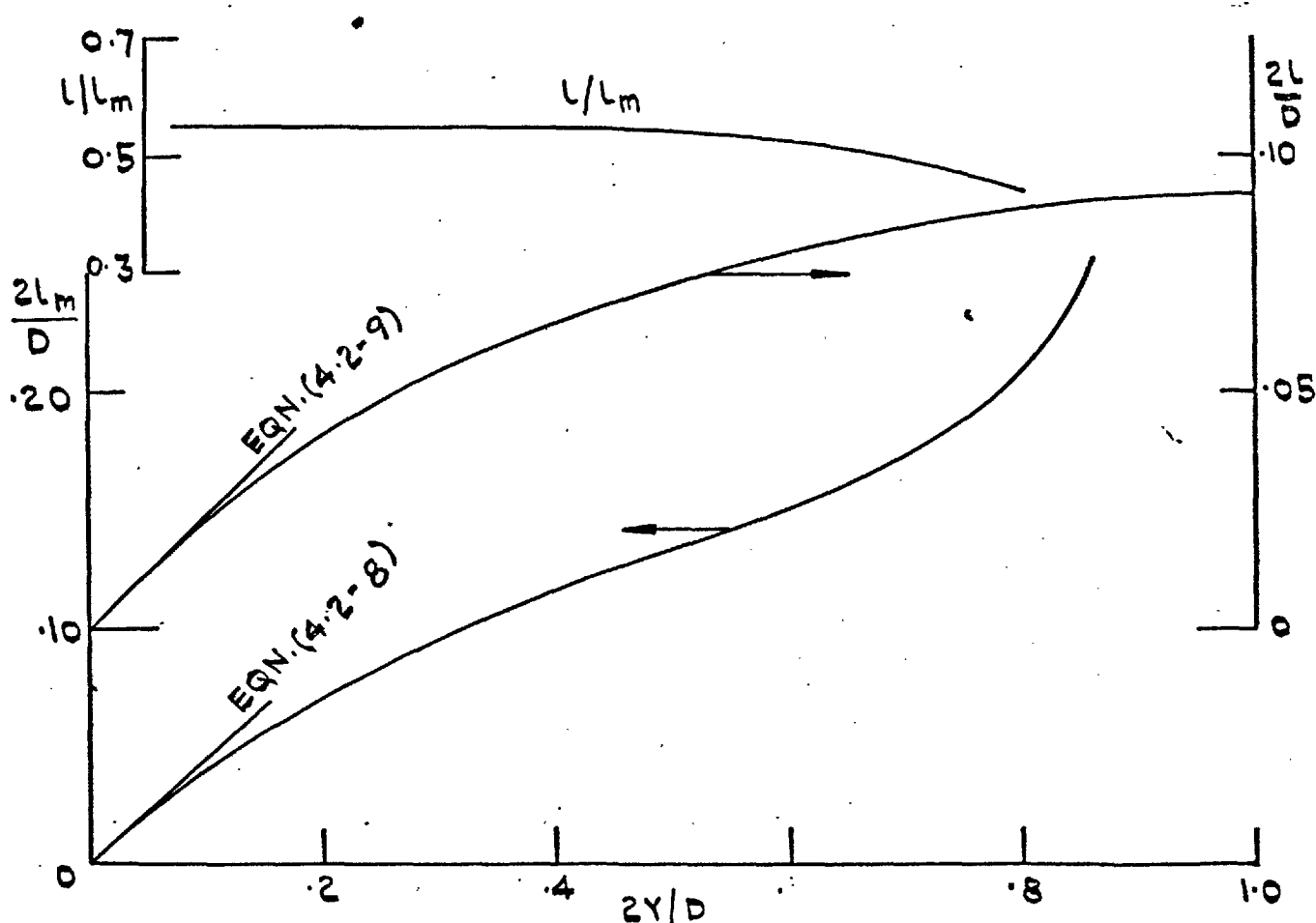
b). COMPARISON OF  $\epsilon$  AND  $\tau$  PROFILES

FIG. 6.29 (CONTINUED)

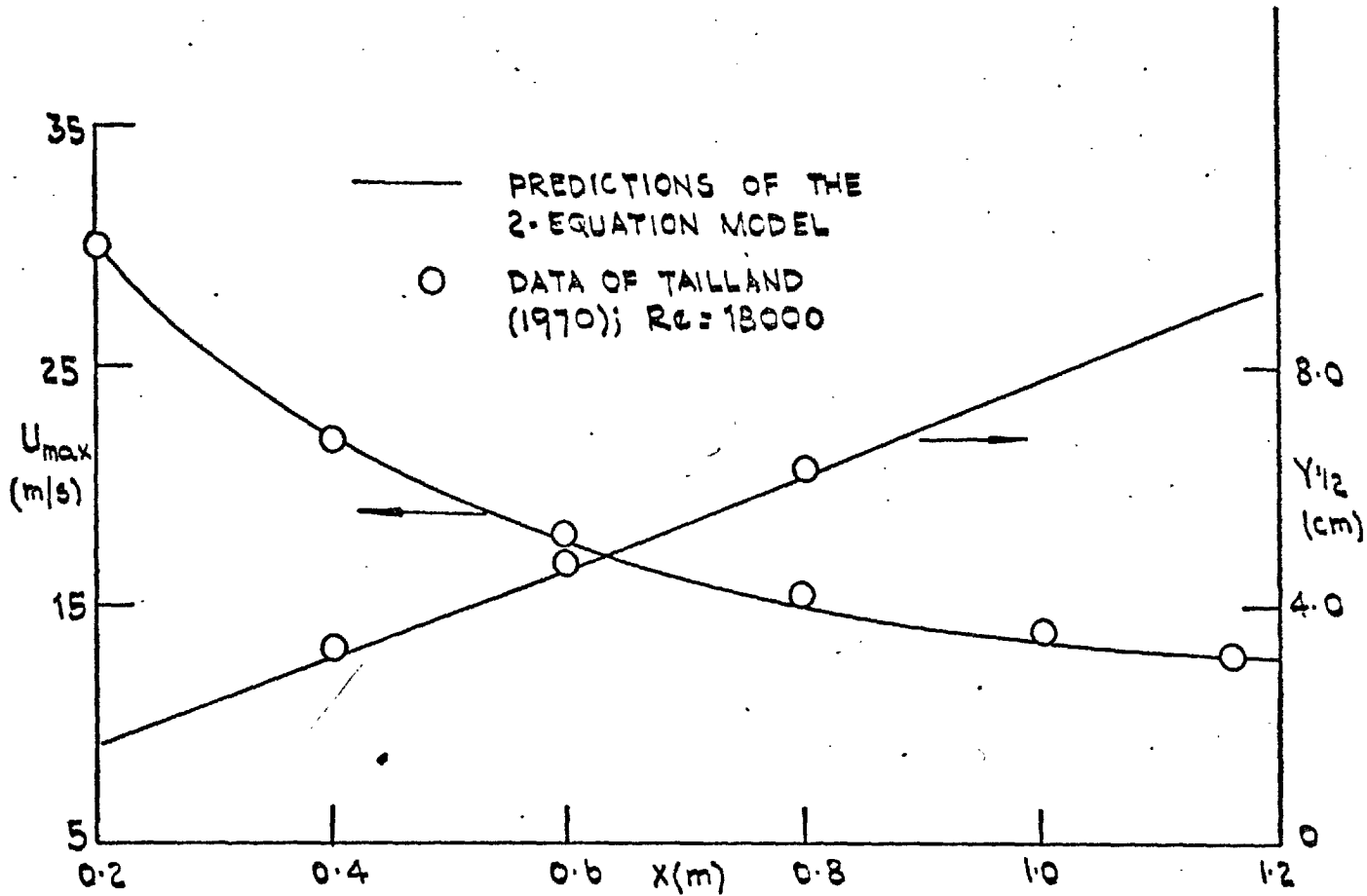


c). COMPARISON OF TURBULENT VISCOSITY PROFILES

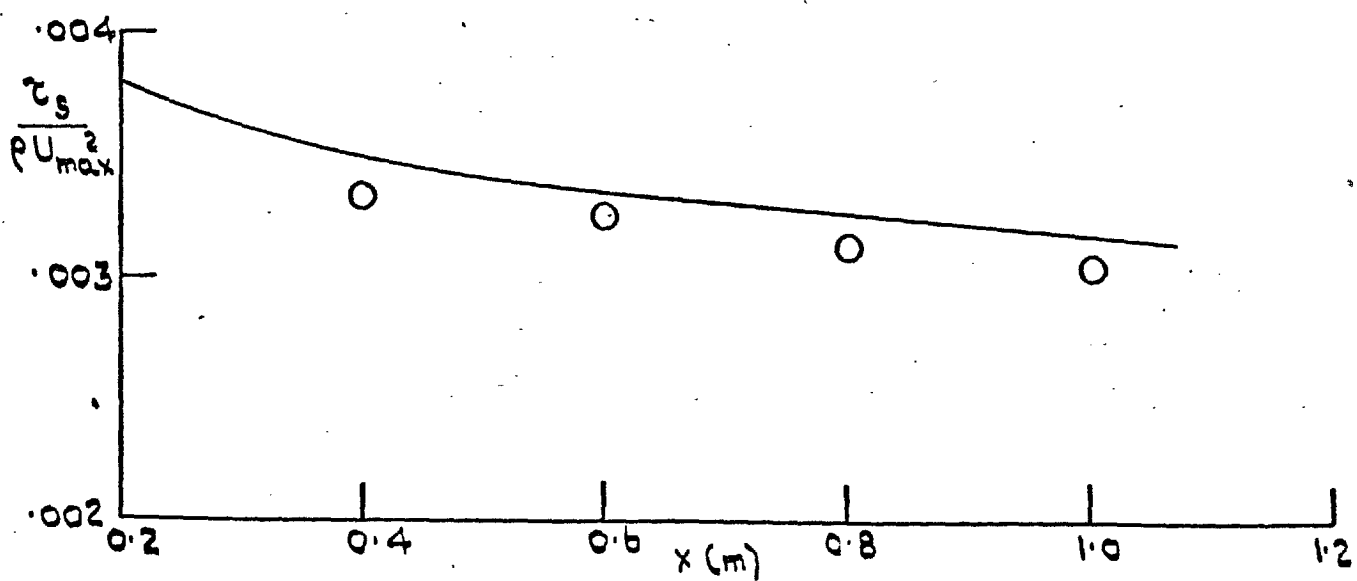


d). PREDICTED LENGTH SCALES.

FIG. b. 29: COMPARISON OF PREDICTIONS WITH CHANNEL FLOW DATA (LAUFER 1950); O DATA; — PREDICTIONS OF THE TWO-EQUATION MODEL; - - PREDICTIONS OF DALY AND HARLOW (1970)

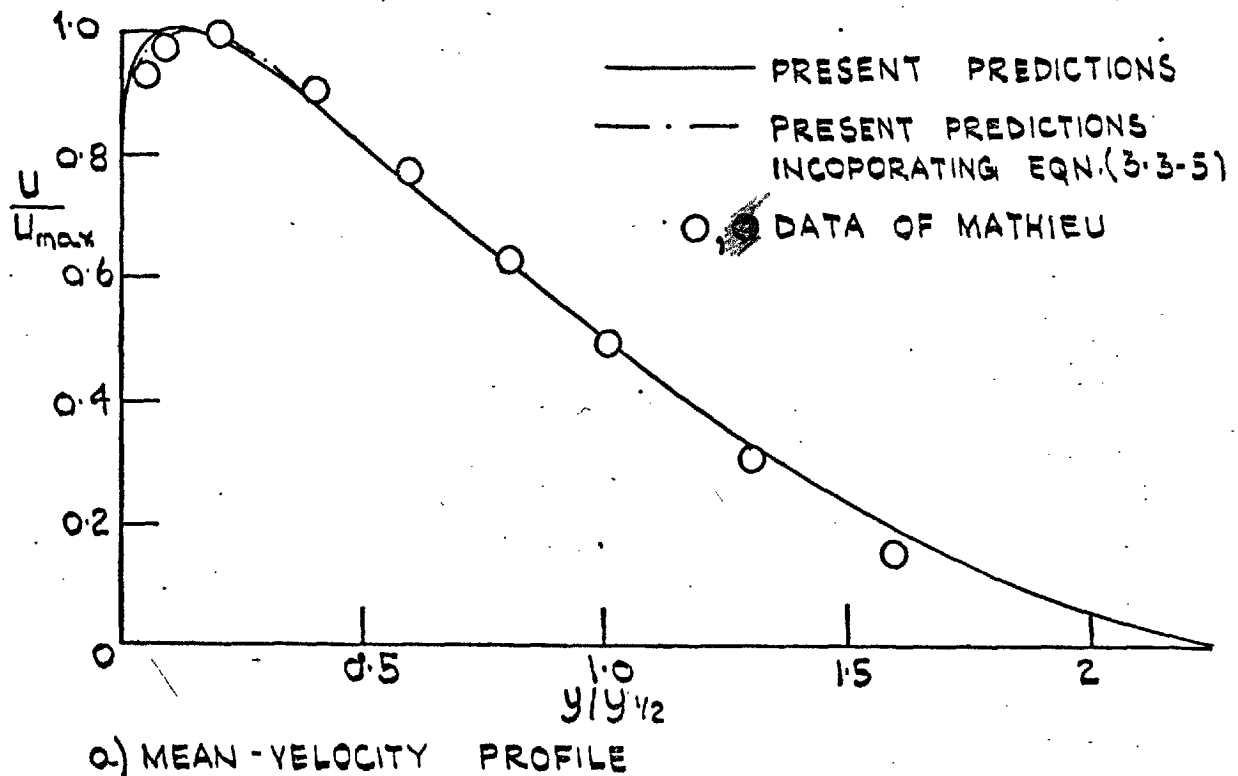


a). COMPARISON OF GROWTH RATE AND VELOCITY DECAY

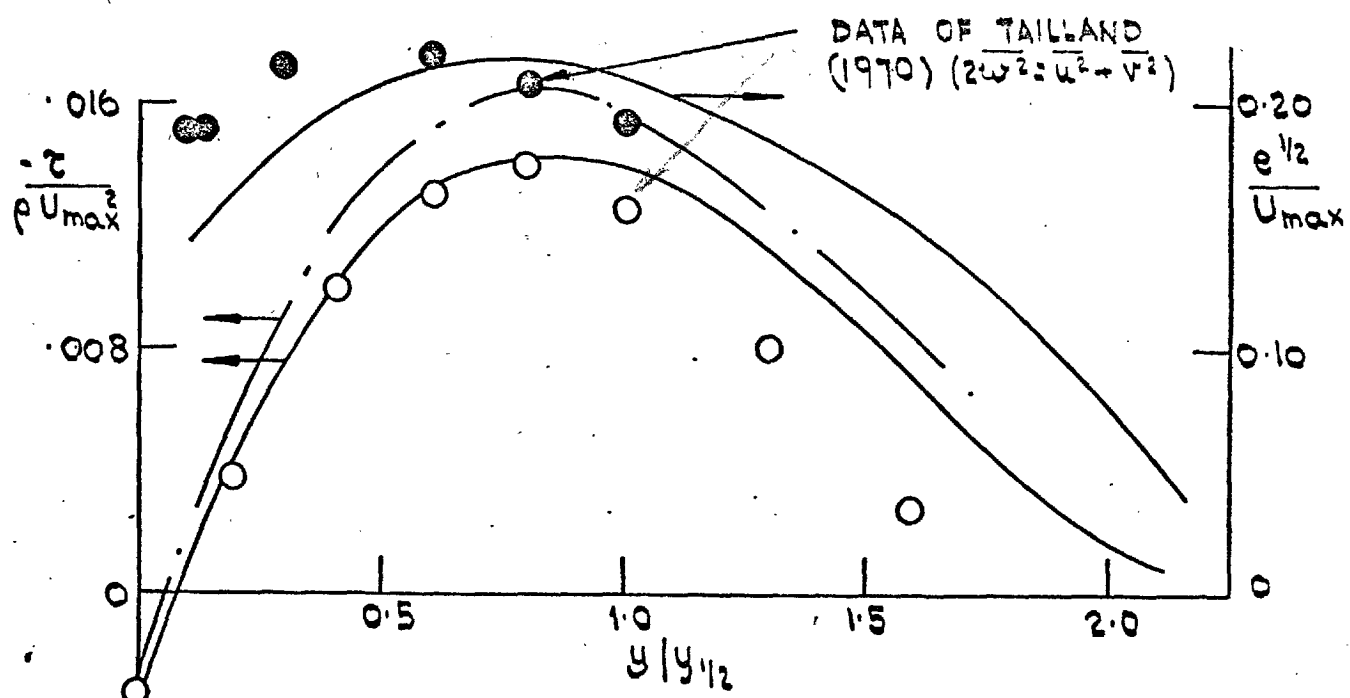


b). COMPARISON OF FRICTION COEFFICIENT

FIG. 6.30: COMPARISON OF PREDICTIONS WITH MEASUREMENTS  
FOR A PLANE WALL JET IN STAGNATION SURROUNDINGS



a) MEAN - VELOCITY PROFILE



b). e- AND z PROFILES

FIG. b.31: COMPARISON OF PREDICTION WITH DATA OF A PLANE WALL JET;  $\circ, \bullet$  DATA OF TAILLAND (1970)  
AT  $x = 800$  cm.

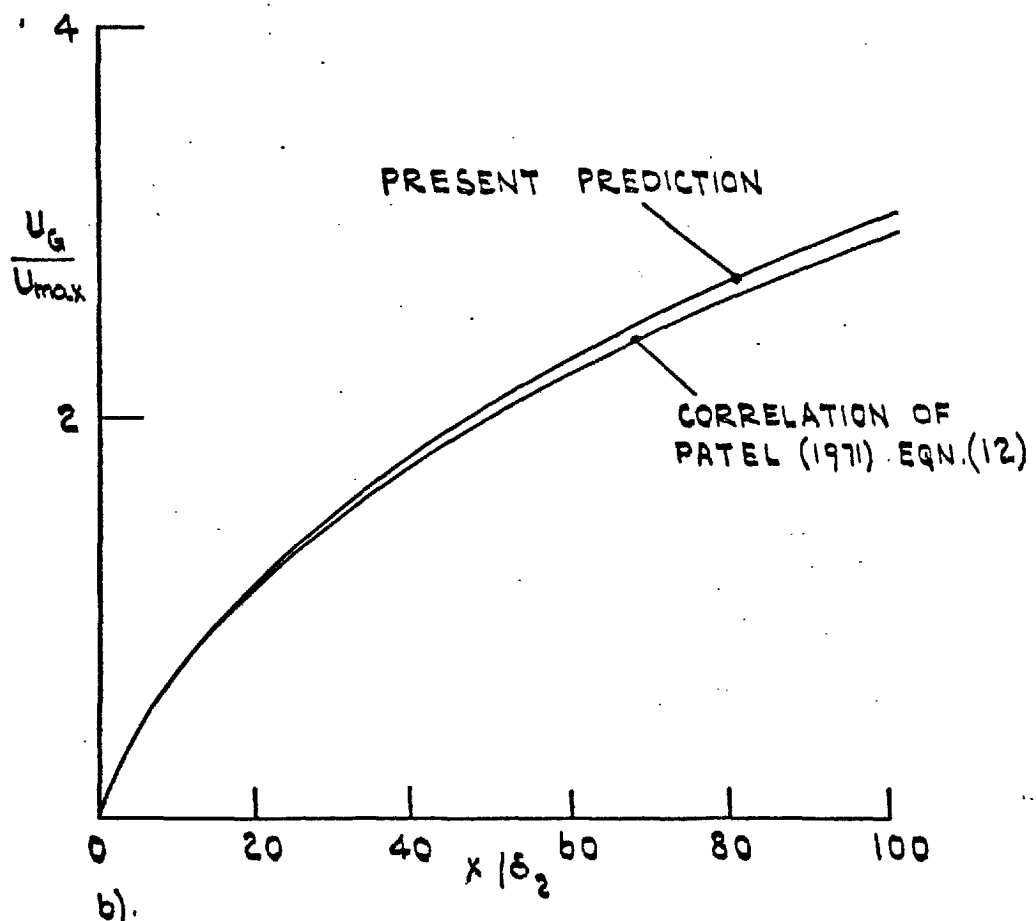
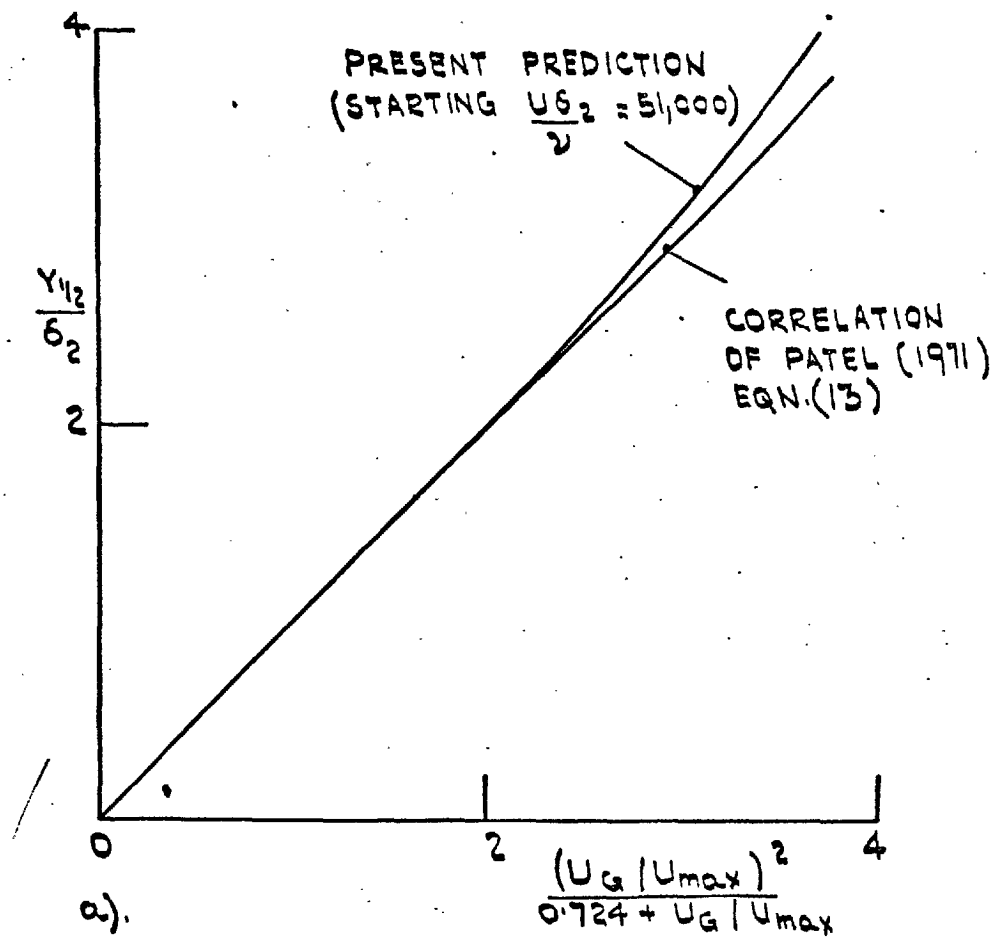
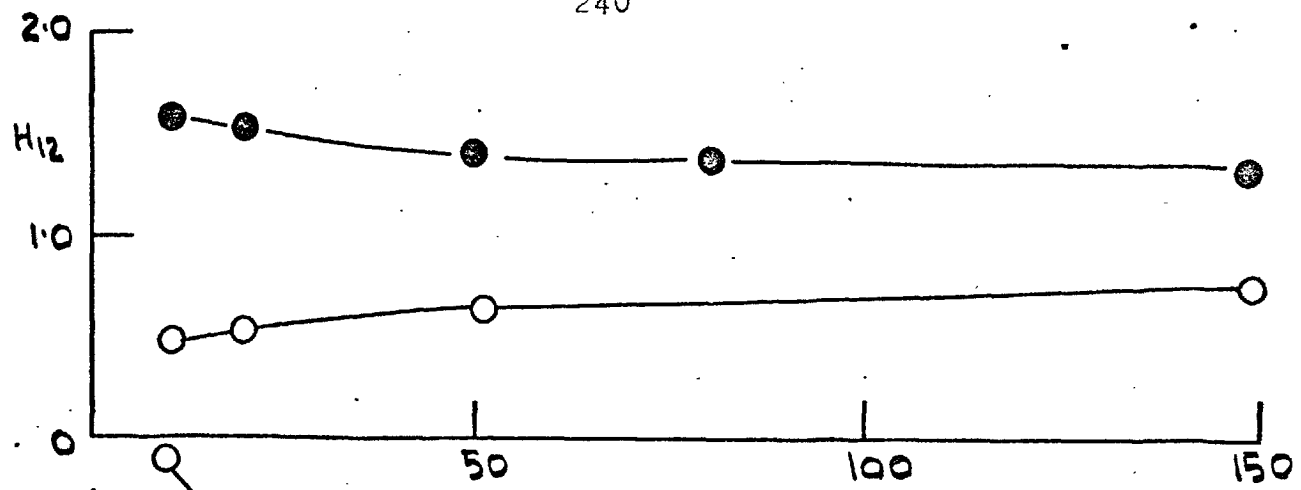
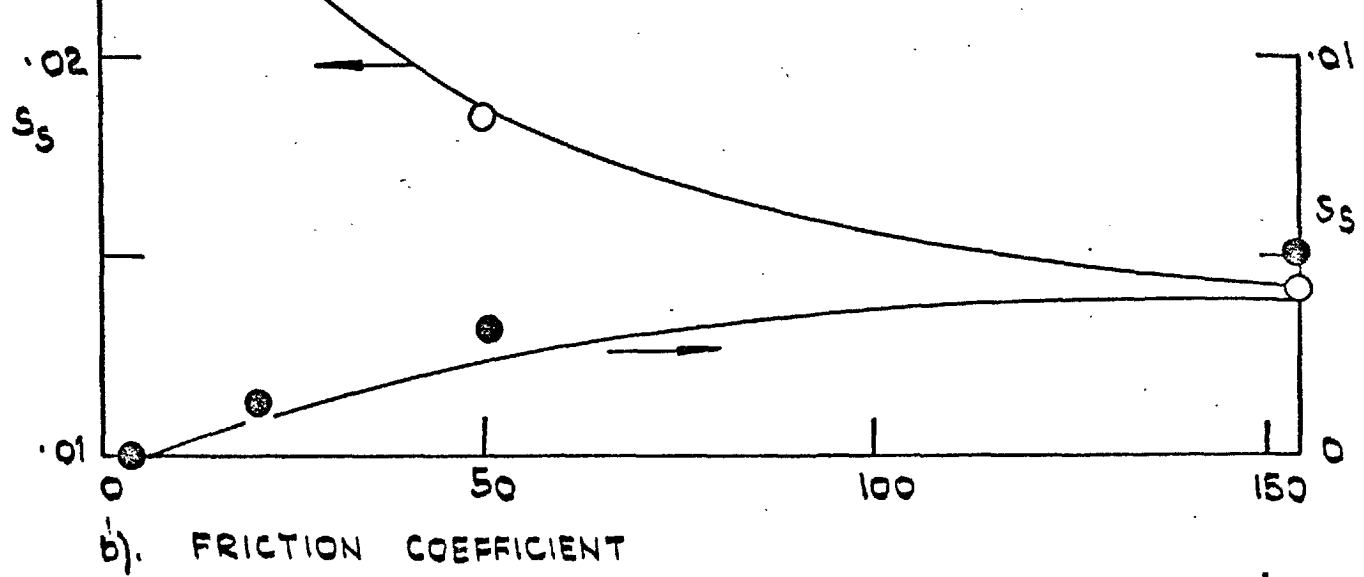


FIG. b.32: COMPARISON OF THE TWO-EQUATION MODEL PREDICTION WITH THE CORRELATION OF PATEL FOR PLANE WALL JET IN A UNIFORM MAIN STREAM



a) SHAPE FACTOR



b). FRICTION COEFFICIENT

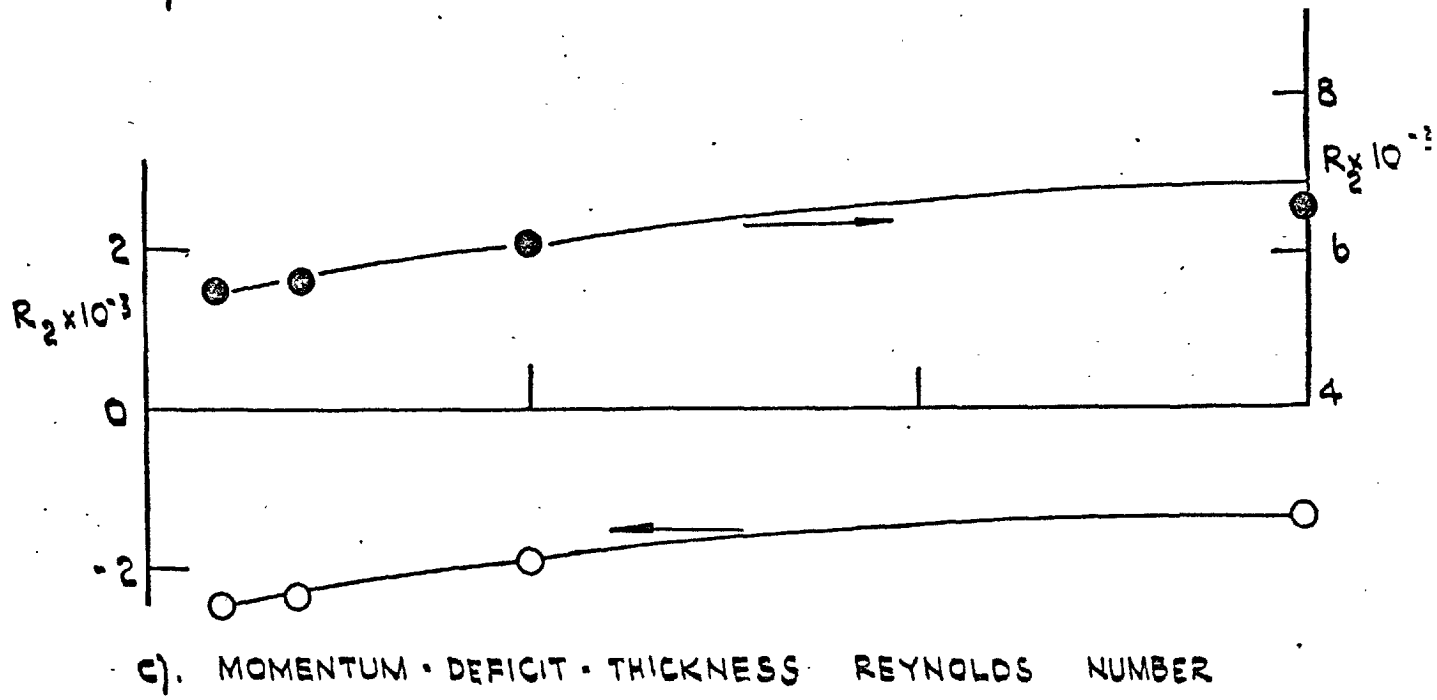
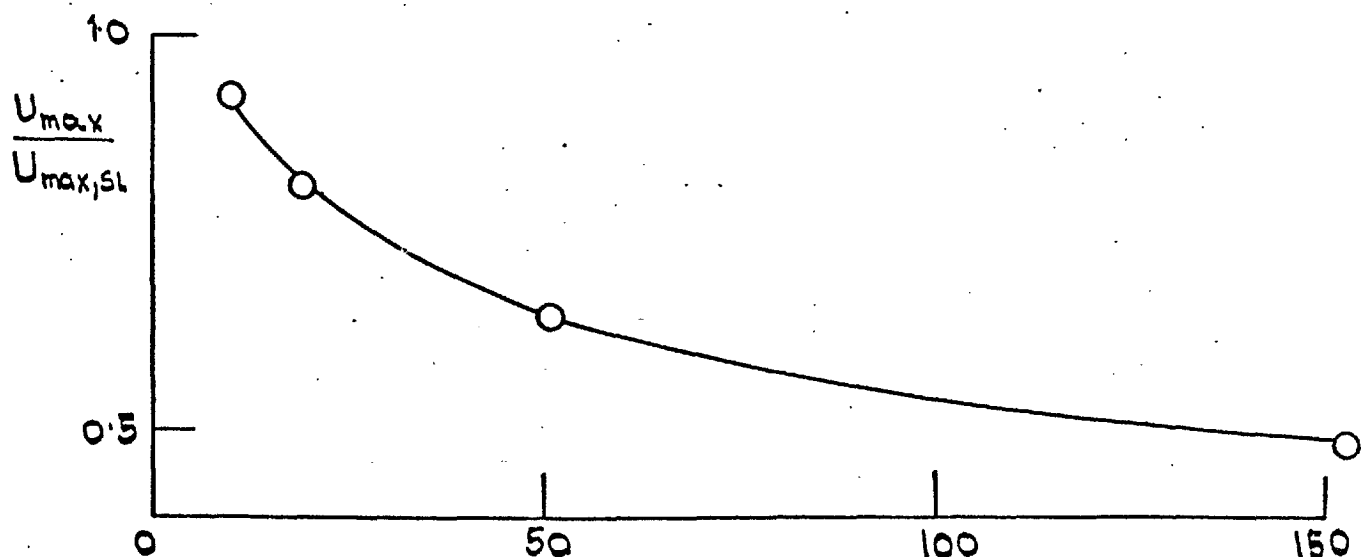
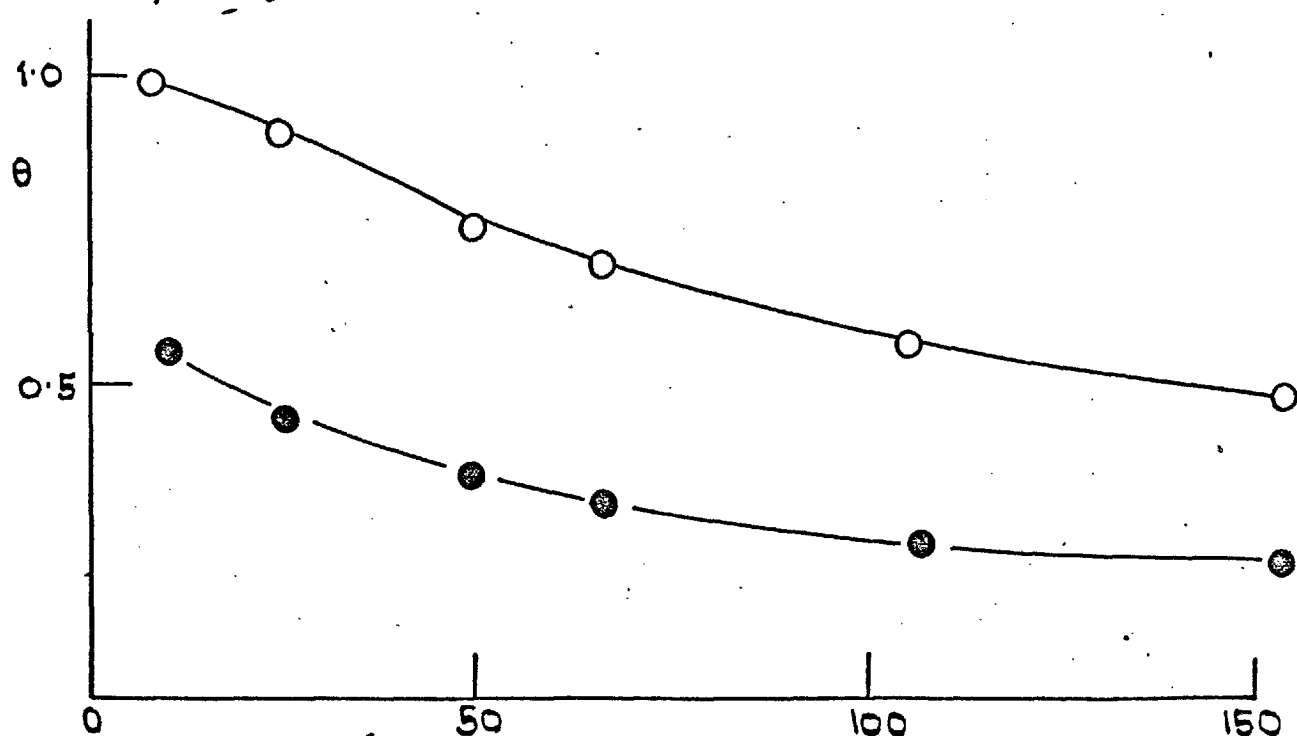


FIG. b.33 (CONTINUED)



d). VELOCITY DECAY



e). FILM-COOLING EFFECTIVENESS

FIG. b.33: COMPARISON OF PREDICTIONS WITH DATA

OF KACKER AND WHITELAW (1971);

○  $U_{max,SL} | U_G = 2.3, d/Z = 0.126 ;$

●  $U_{max,SL} | U_G = 0.75, d/Z = 1.14 ;$

— PREDICTIONS.

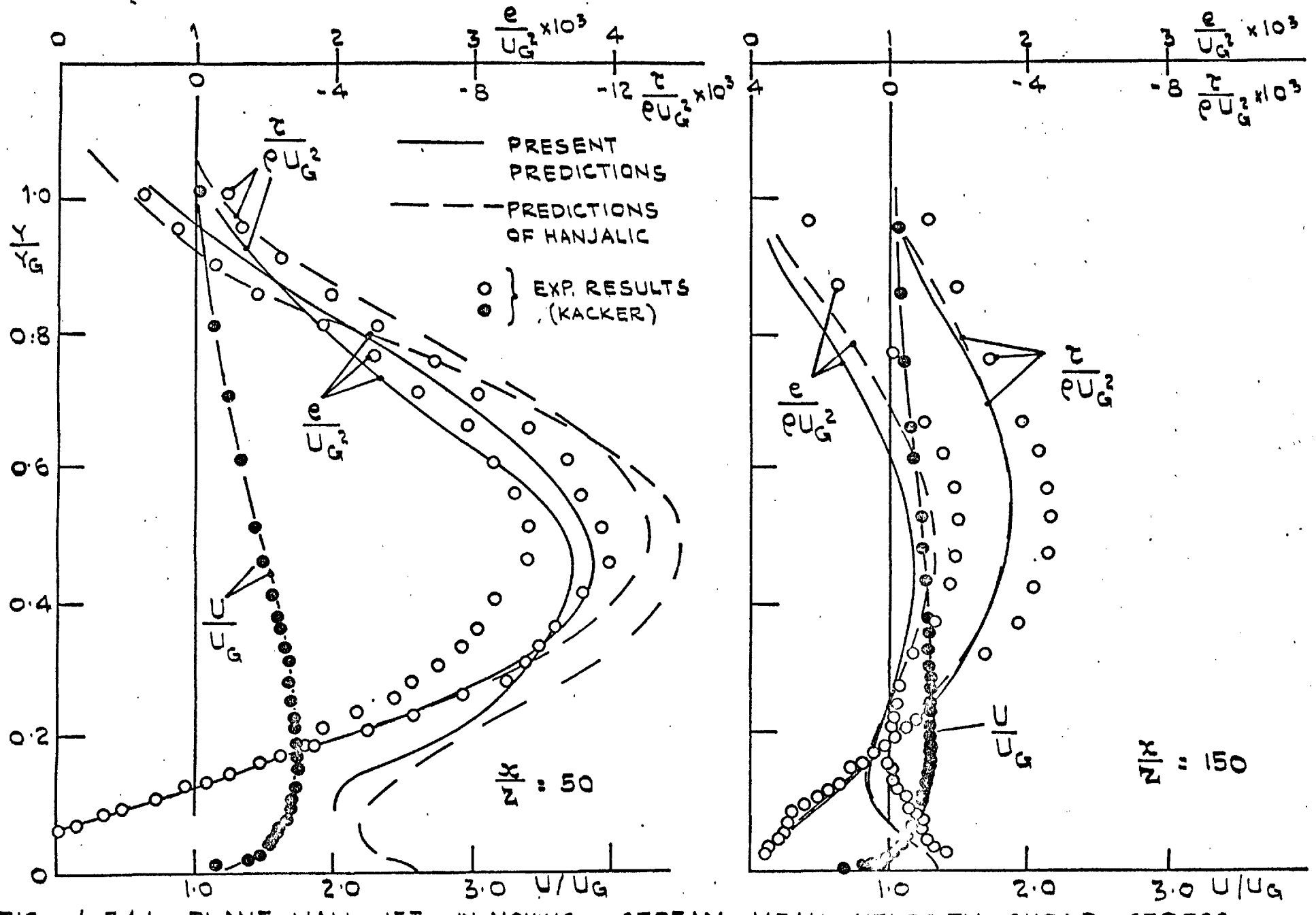
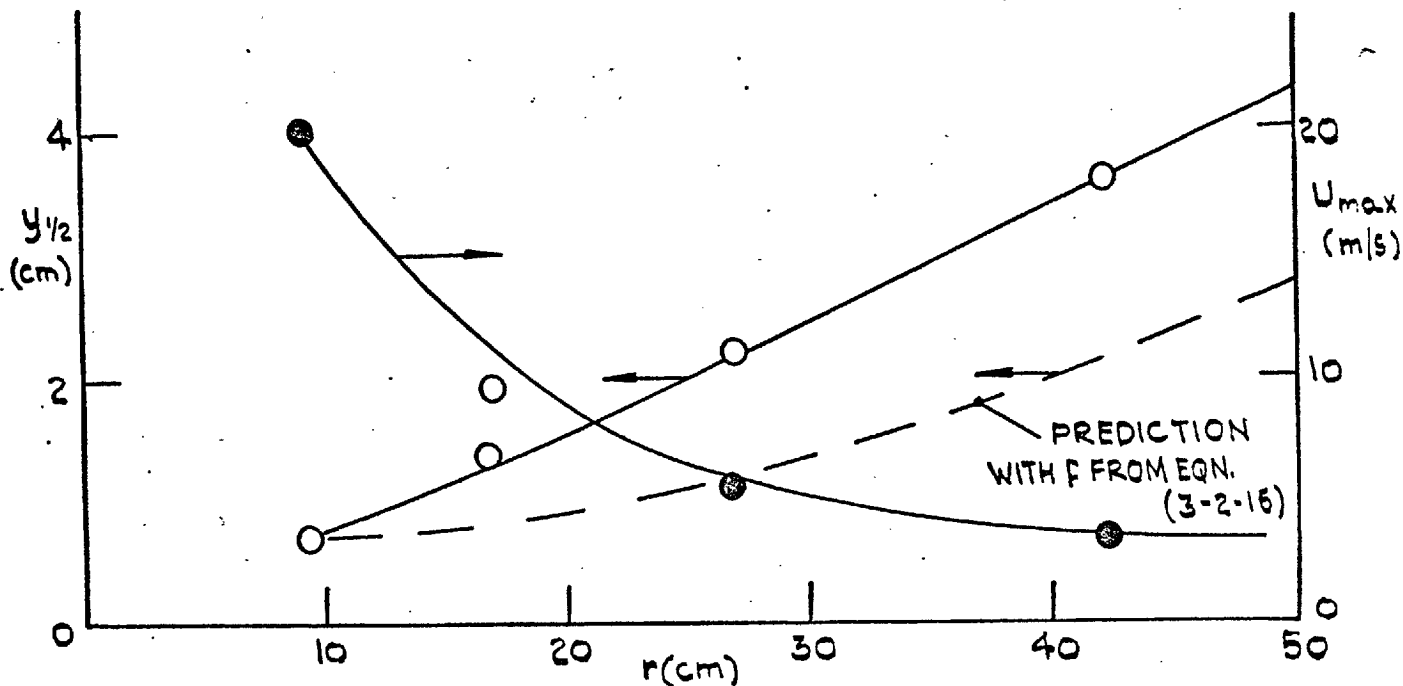
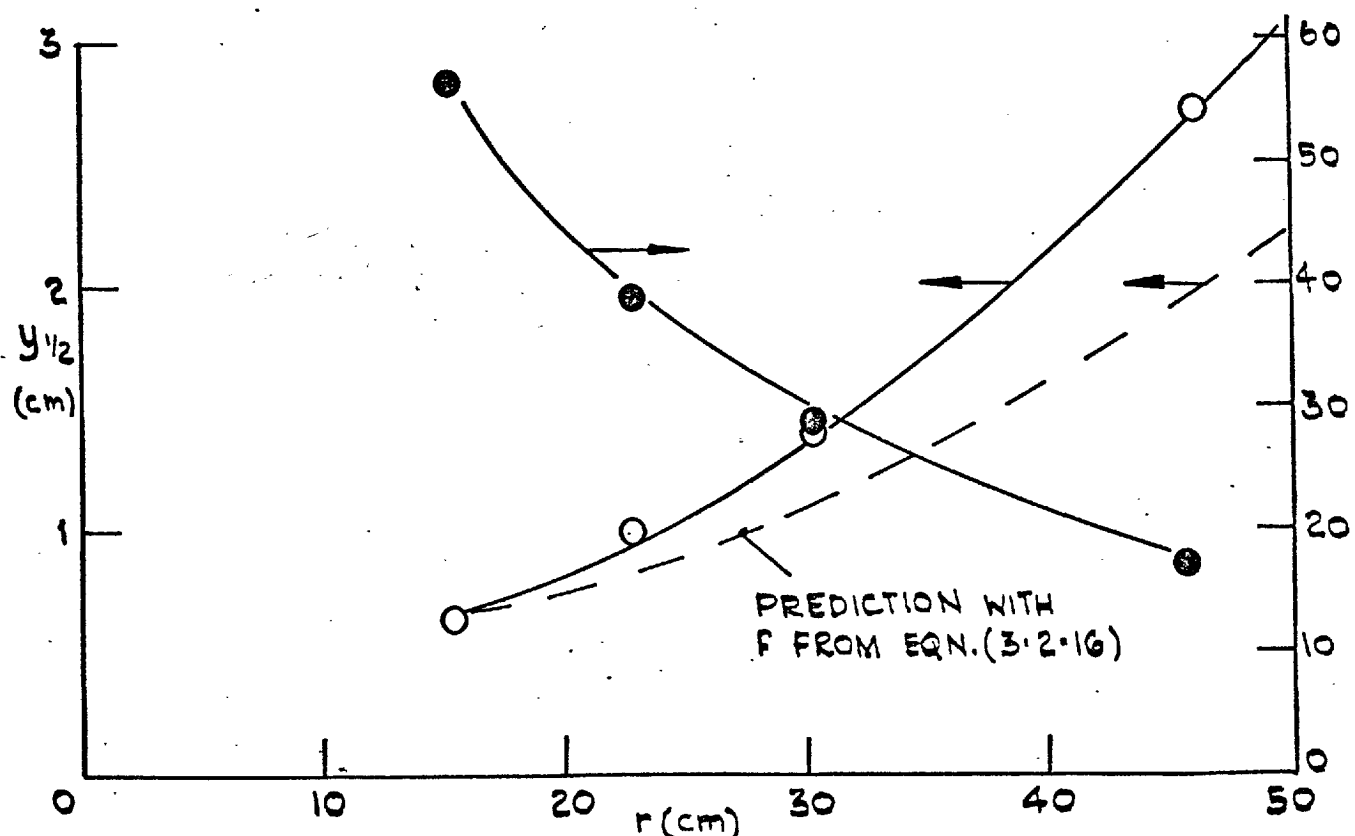


FIG. 6.34: PLANE WALL JET IN MOVING STREAM - MEAN VELOCITY, SHEAR STRESS  
AND TURBULENCE ENERGY ( $U_{max,sl}/U_G = 2.3$ )



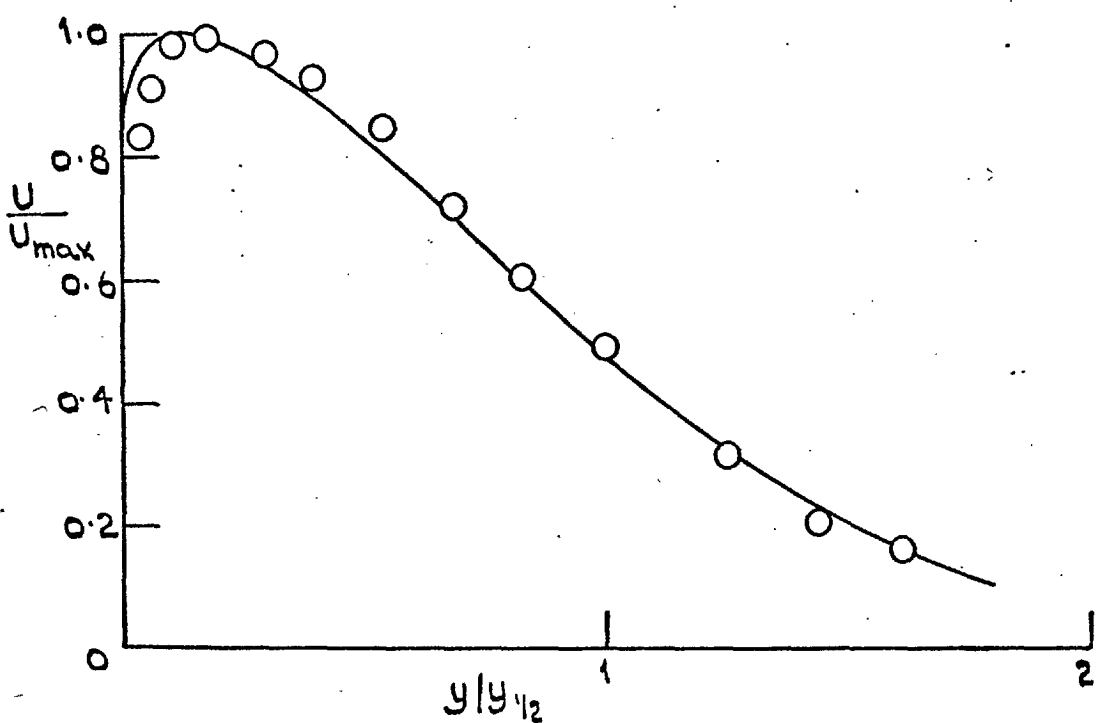
a). COMPARISON OF PREDICTED GROWTH RATE AND DECAY  
OF RADIAL WALL-JET (CASE b)



b). COMPARISON OF PREDICTED GROWTH RATE AND DECAY  
OF RADIAL WALL JET (CASE (a))

FIG. 6.35: COMPARISON OF PREDICTIONS WITH EXPERIMENTS  
OF RADIAL WALL JET.

O DATA, — PREDICTION BY TWO-EQUATION MODEL



a). MEAN VELOCITY PROFILES

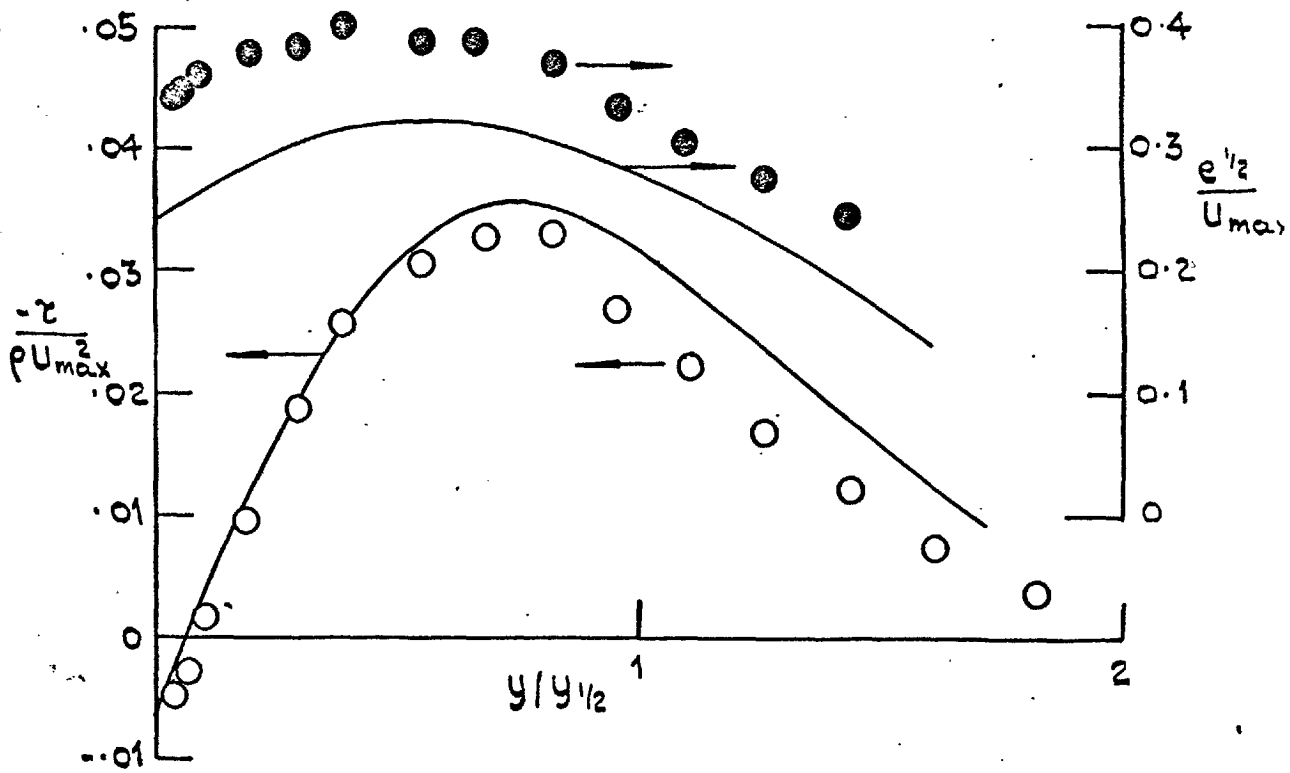
b).  $e$  AND  $\tau$  PROFILES.

FIG. 6.3b: COMPARISON OF PREDICTION WITH DATA  
FOR A RADIAL WALL JET (CASE b  $r = 45$  cm)

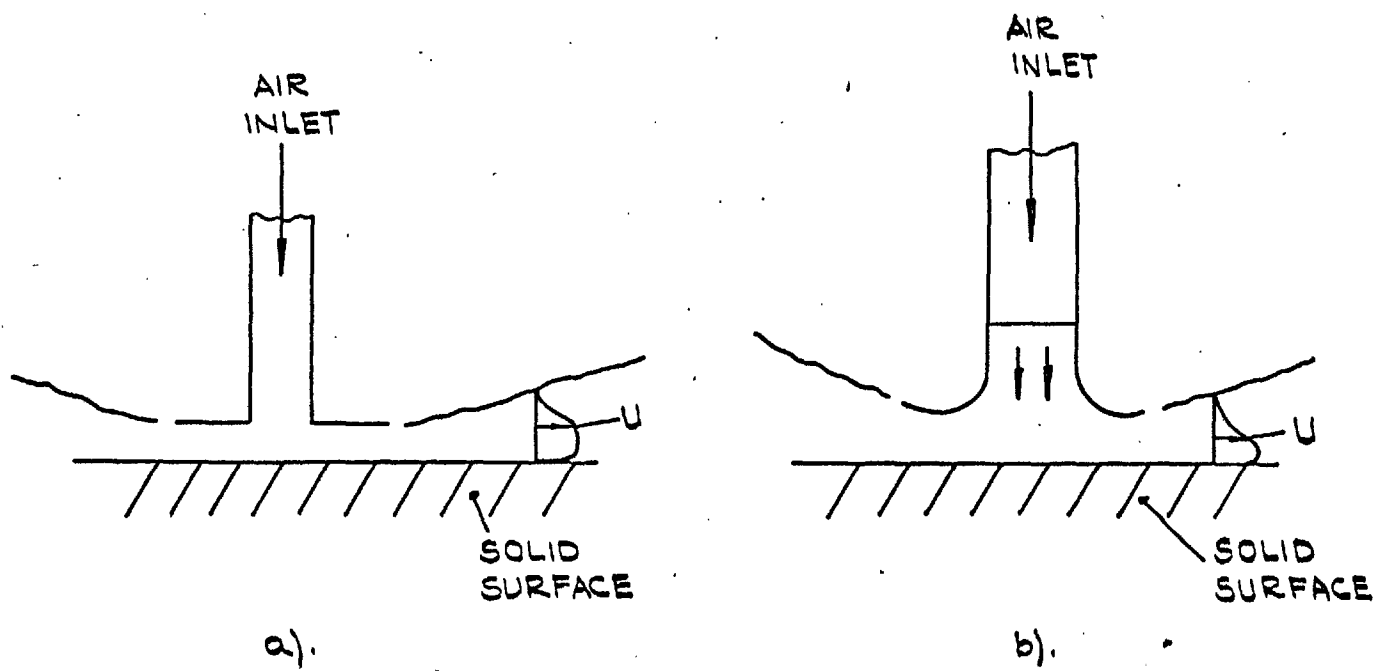


FIG. 7.1: TWO POSSIBLE CASES OF  
RADIAL WALL-JET FLOW

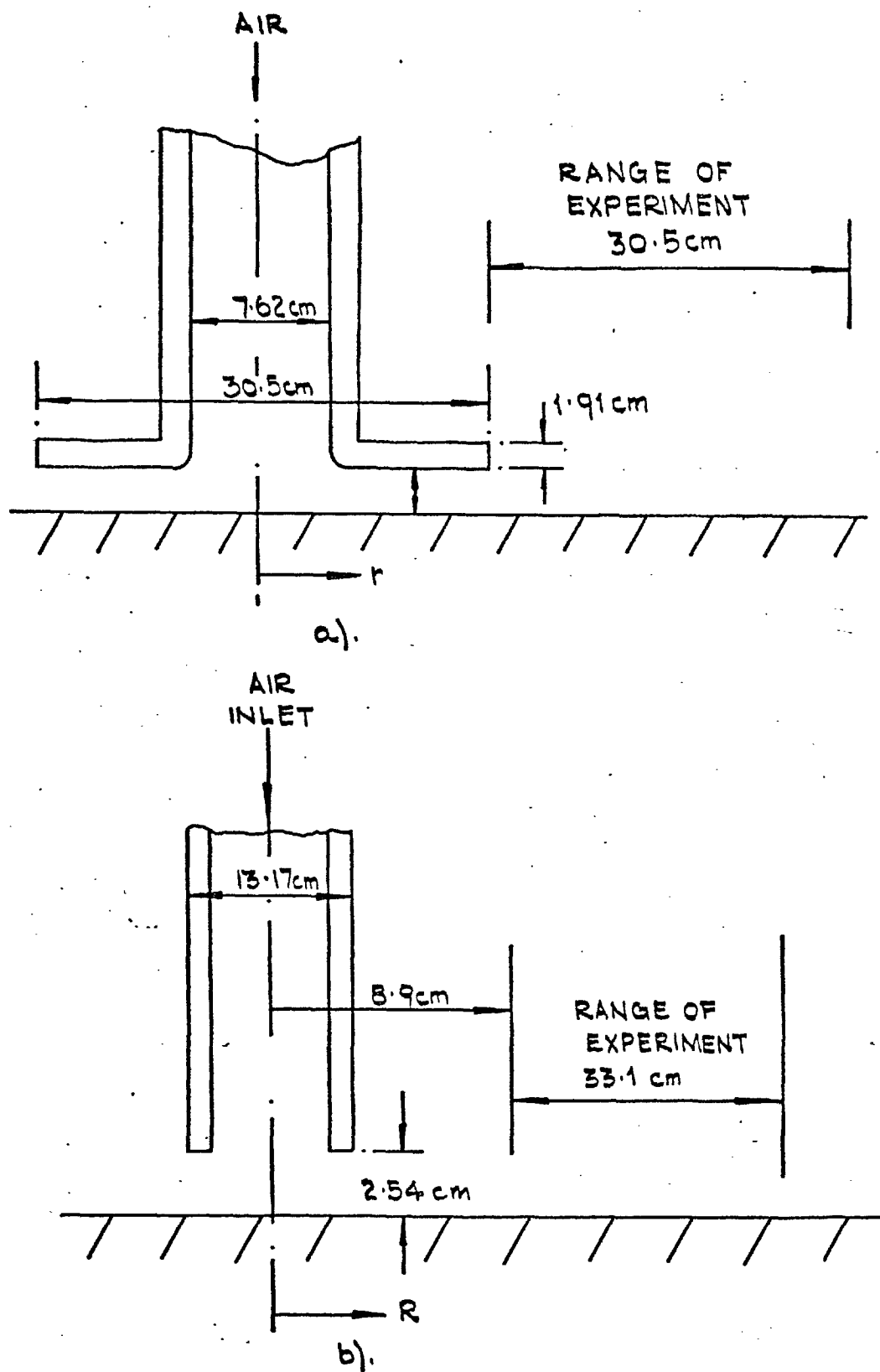


FIG. 7.2: GEOMETRY OF THE WALL-JET  
EXITS IN THE EXPERIMENT

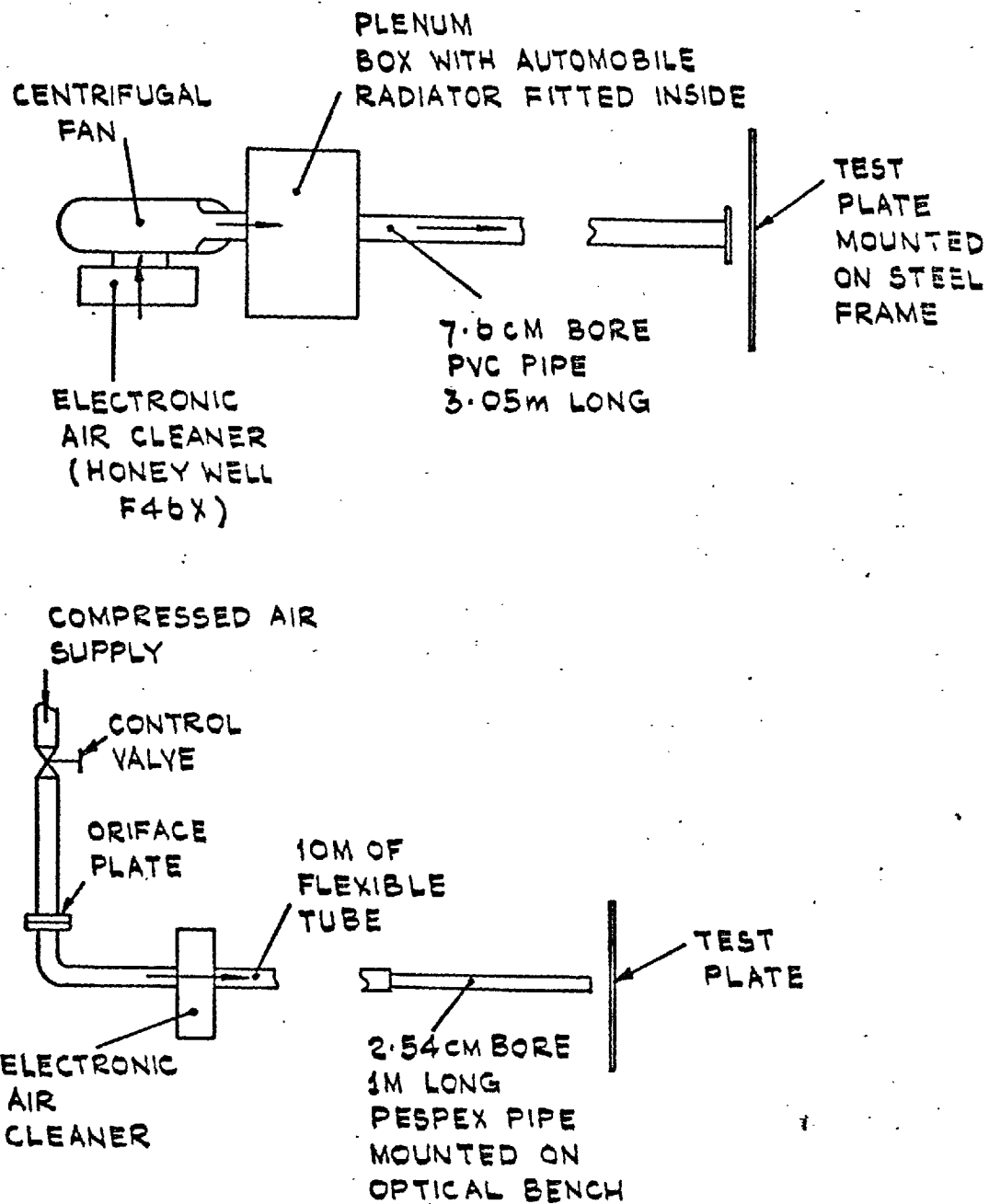


FIG. 7.3: LAY OUT OF THE TEST RIGS

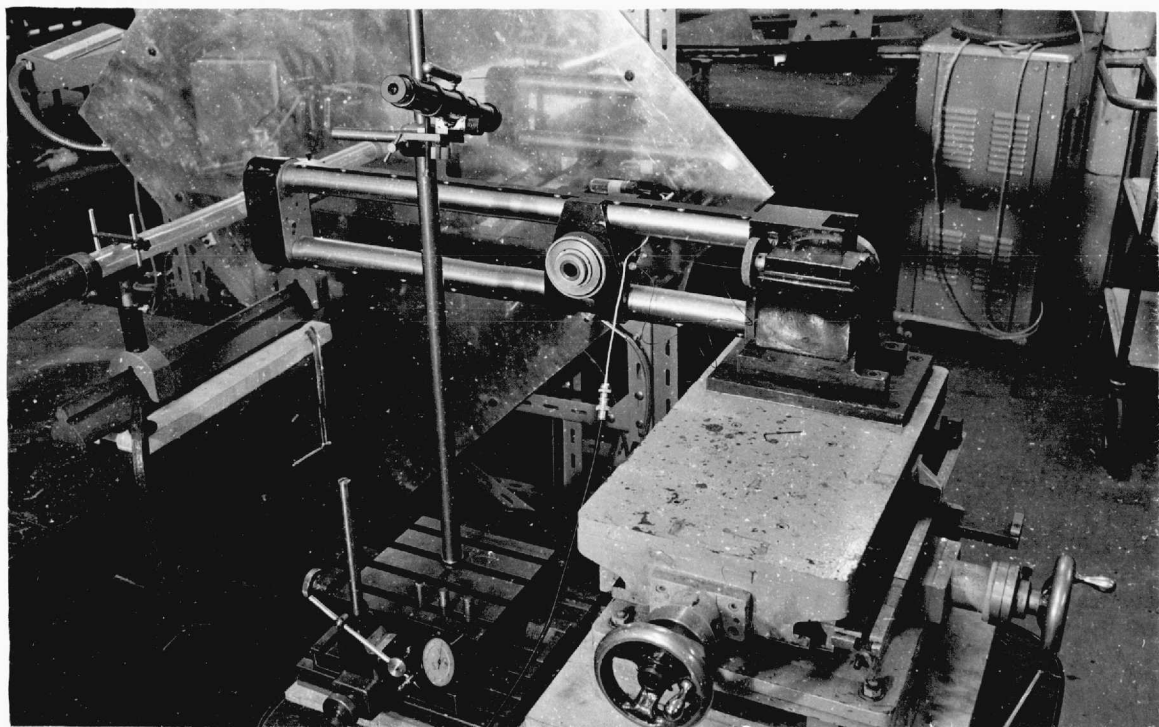


Figure 7.4 Traversing mechanism and test plate for case (b)

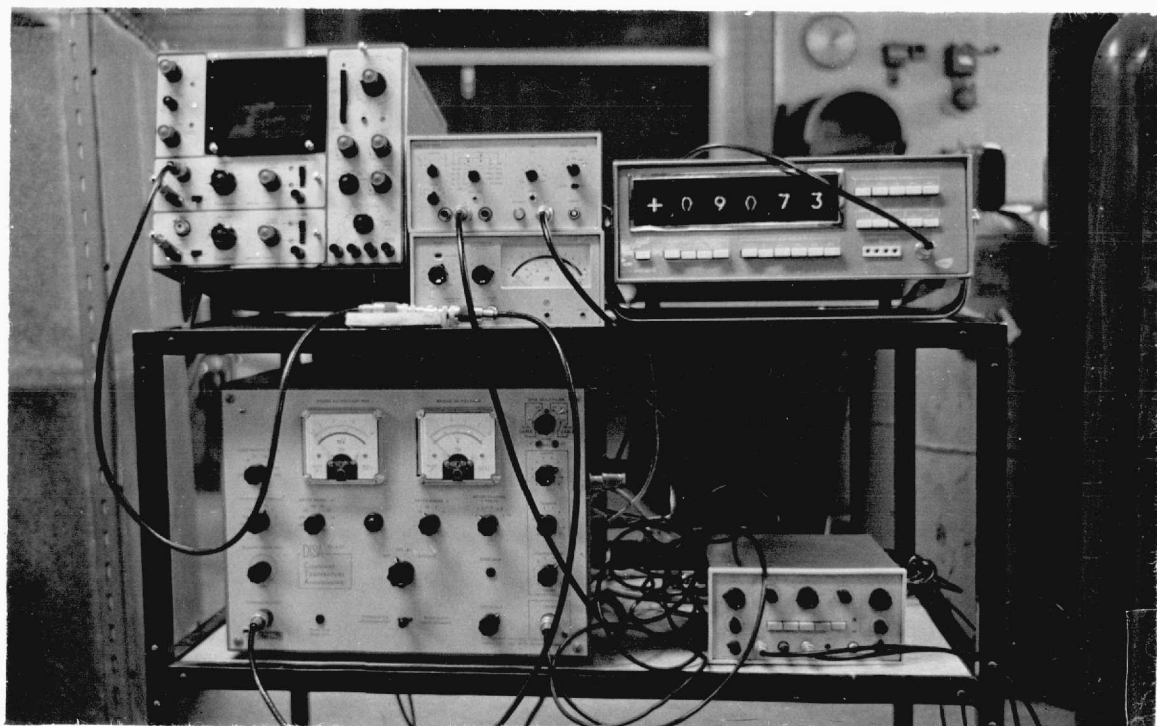


Figure 7.5 Hot-wire instrumentation

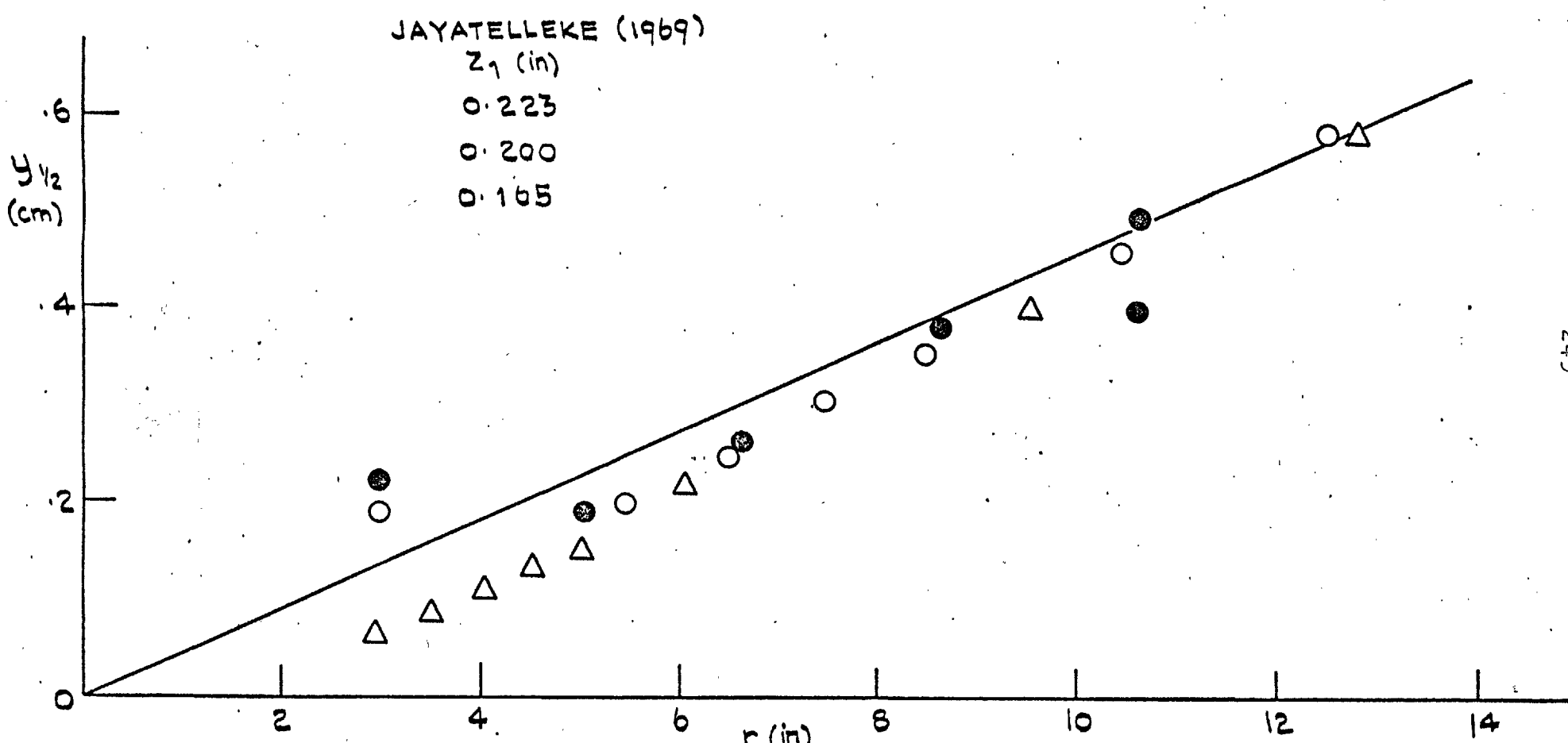


FIG. 7.6: GROWTH OF RADIAL-WALL JETS MEASURED  
BY JAYATELLEKE (1969)

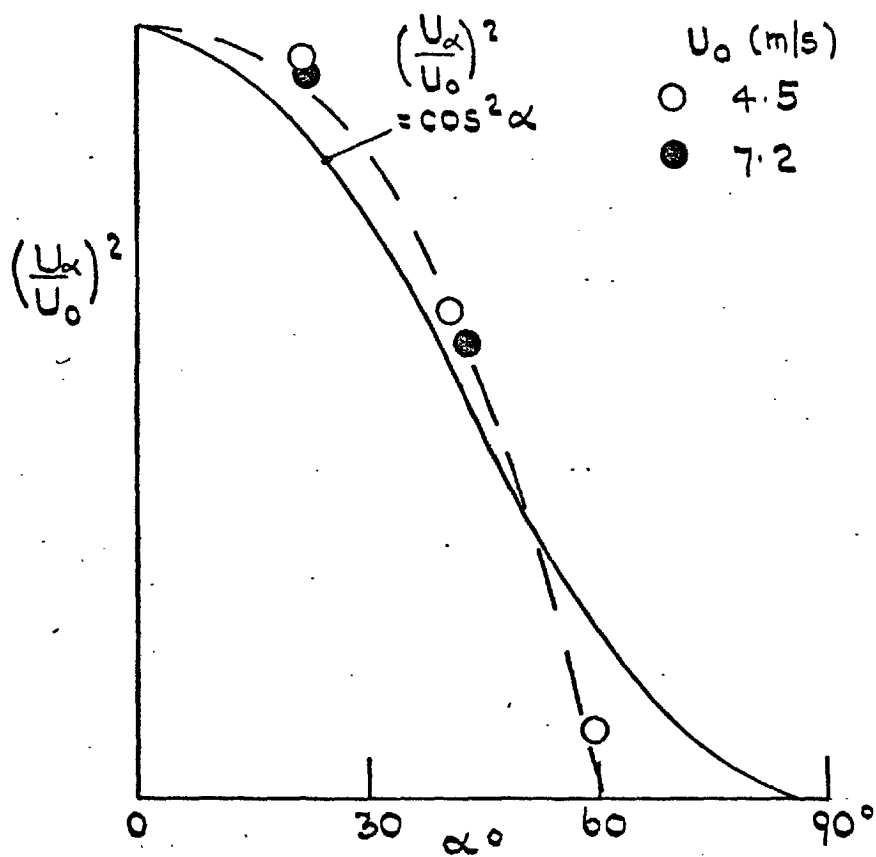


FIG. 7.7: YAW CHARACTERISTICS OF THE  
0.082 mm DIA. PITOT TUBE WITH  
WITH 0.020 mm WALL THICKNESS

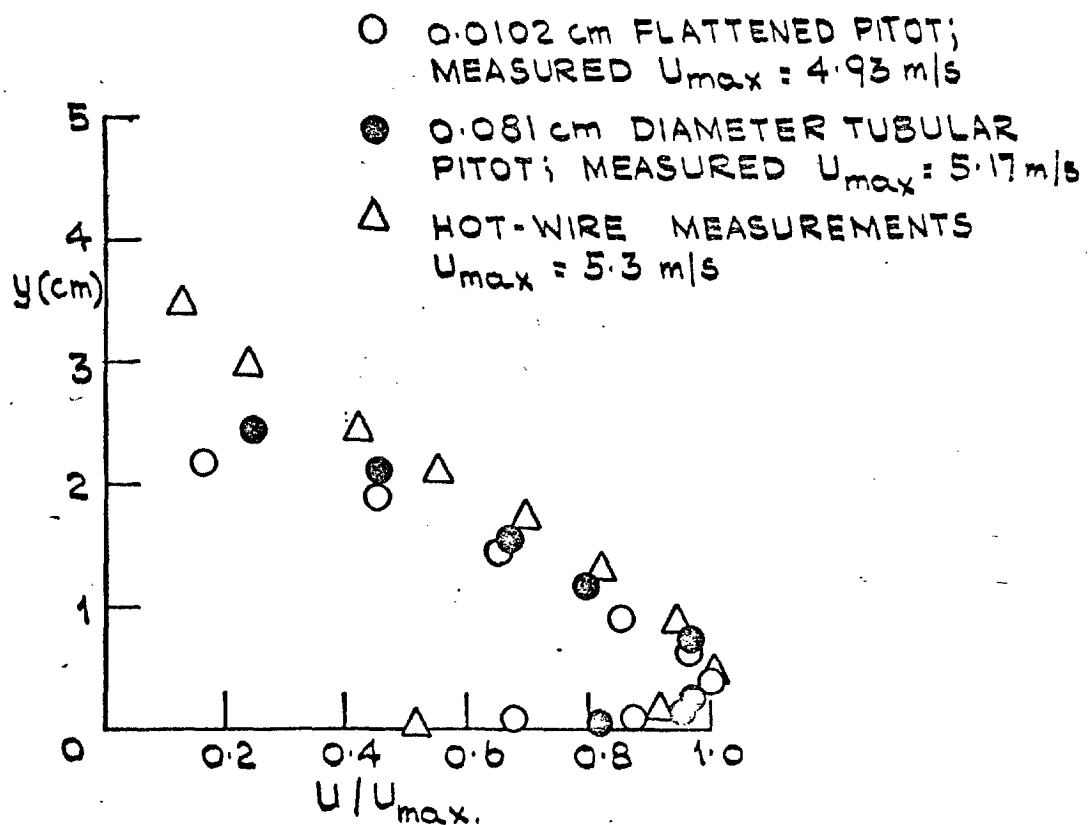


FIG. 7.8: COMPARISON OF VELOCITY  
PROFILES MEASURED BY  
HOT-WIRE AND PITOTS  
AT  $r = 26.8 \text{ cm.}$

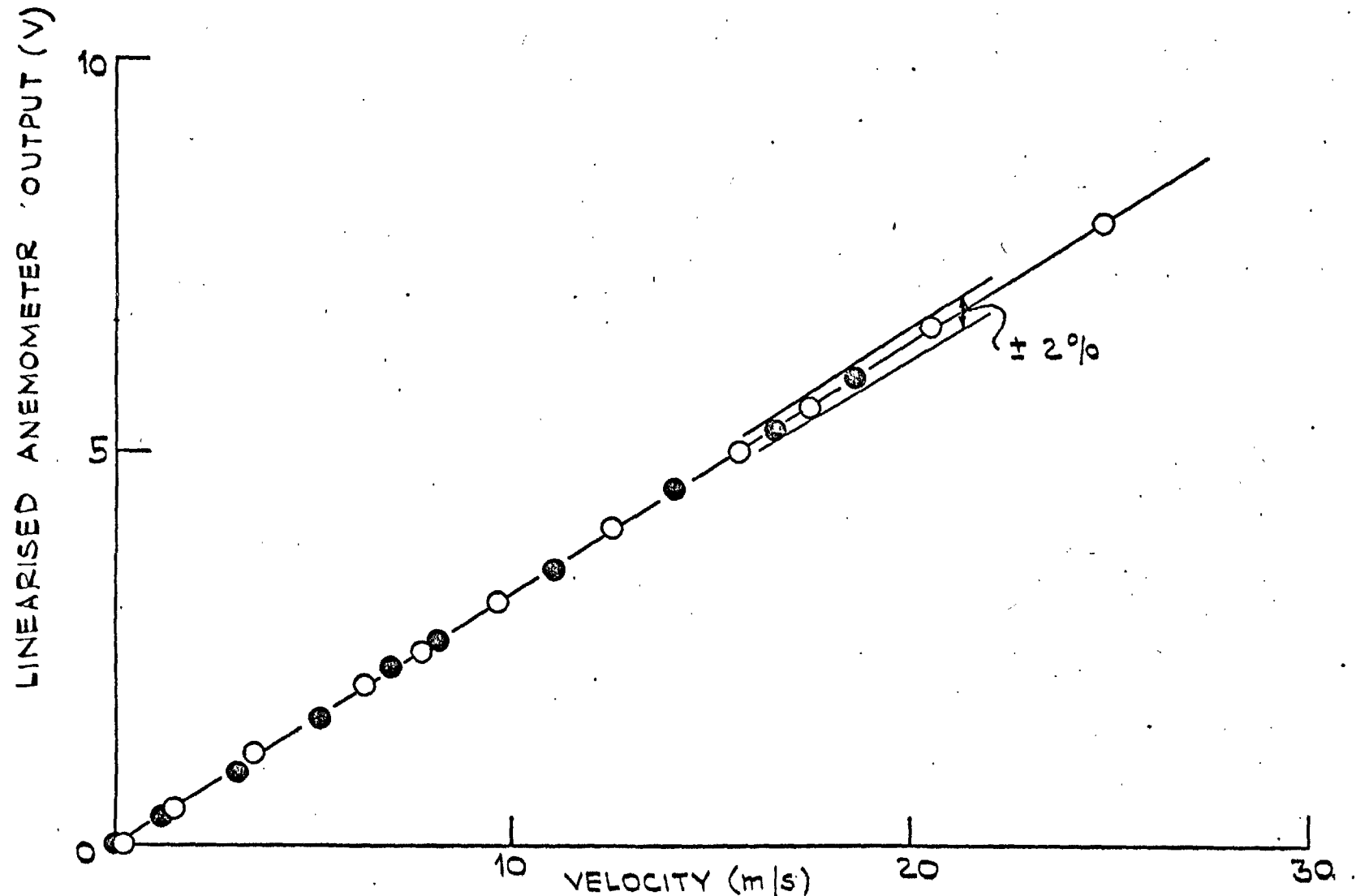


FIG. 7.9: A LINEARISED CALIBRATION CURVE OF THE CONSTANT  
TEMPERATURE HOT-WIRE; ○ FIRST CALIBRATION;  
○ RE-CALIBRATION AFTER 5 OPERATIONAL HOURS.

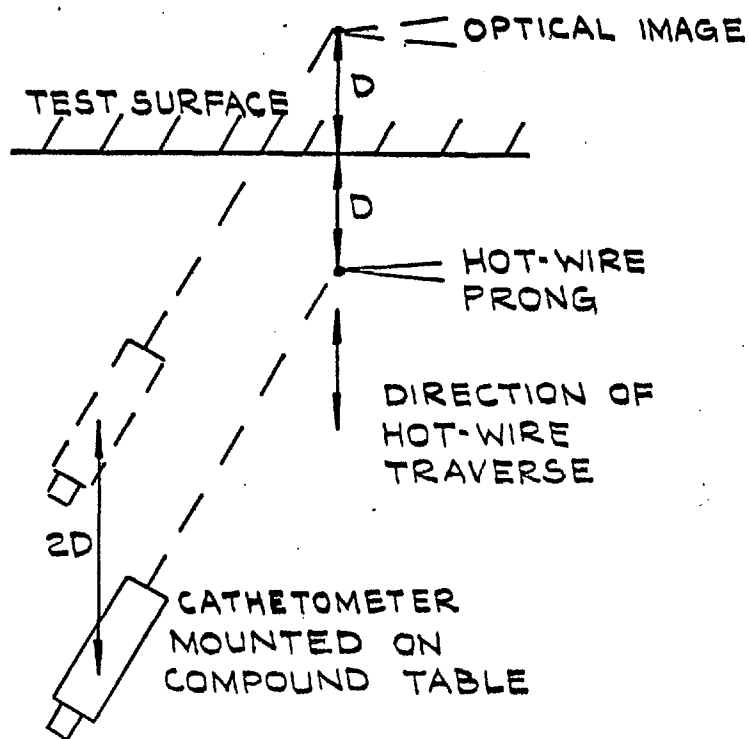


FIG 7.10 : MEASUREMENT OF THE DISTANCE  
OF HOT-WIRE FROM THE WALL

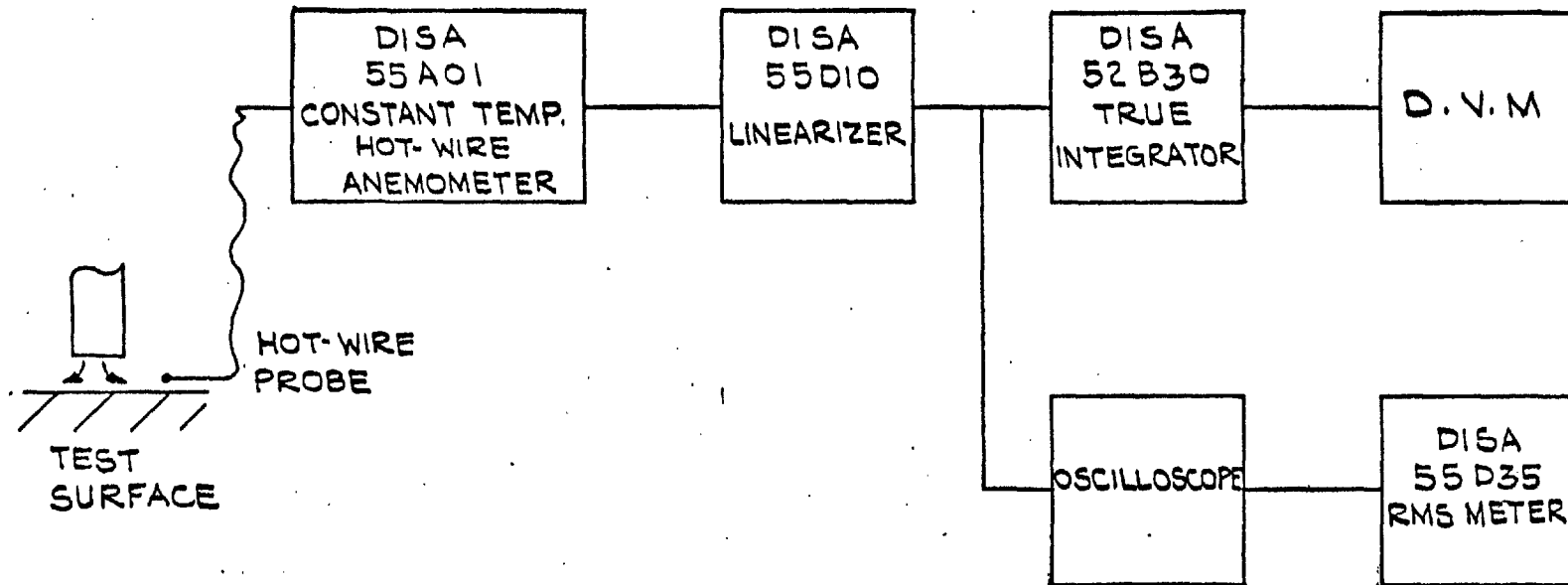
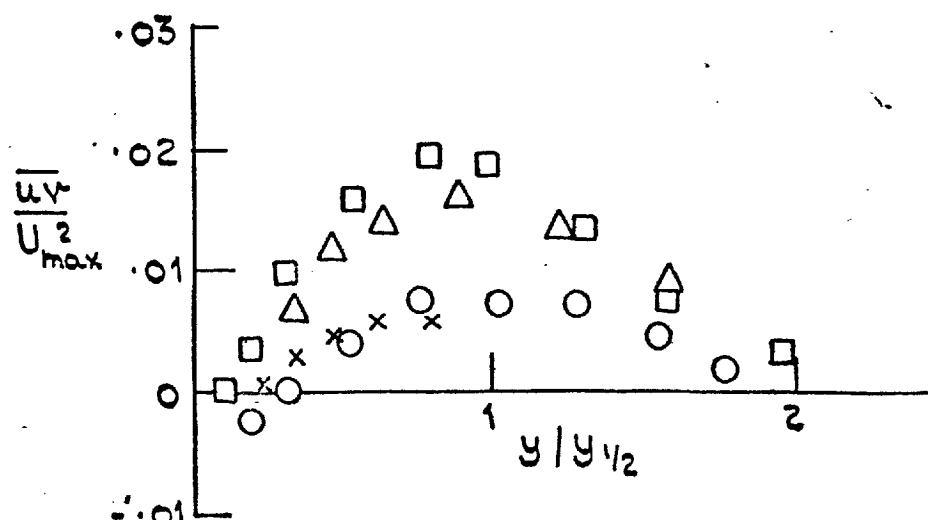
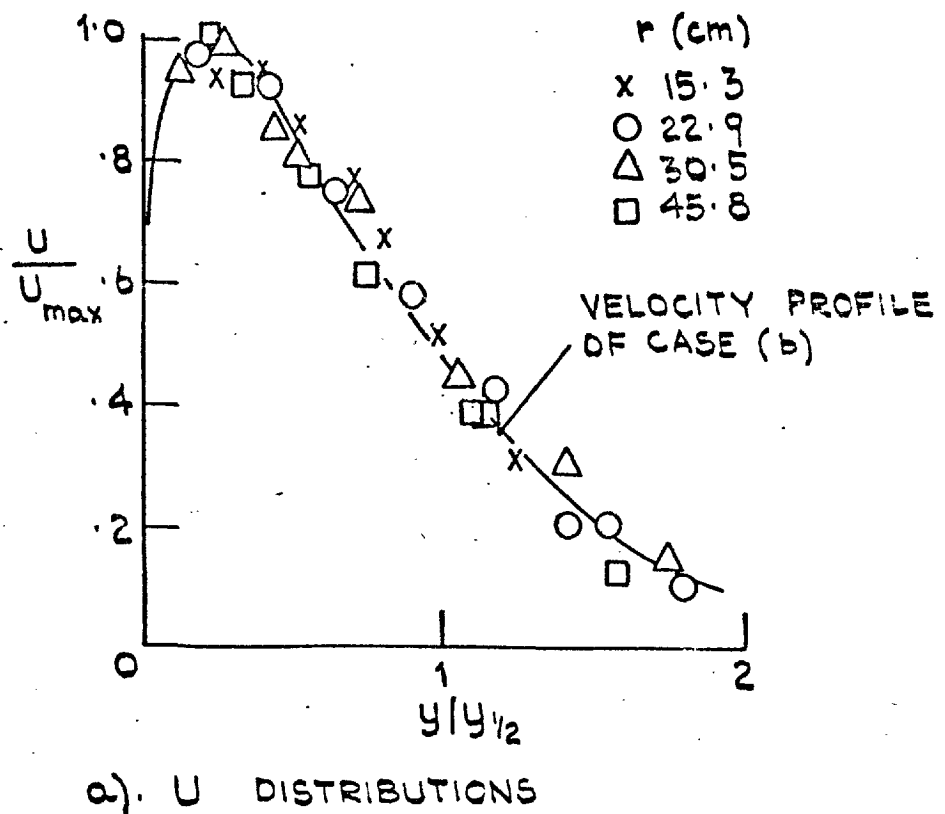
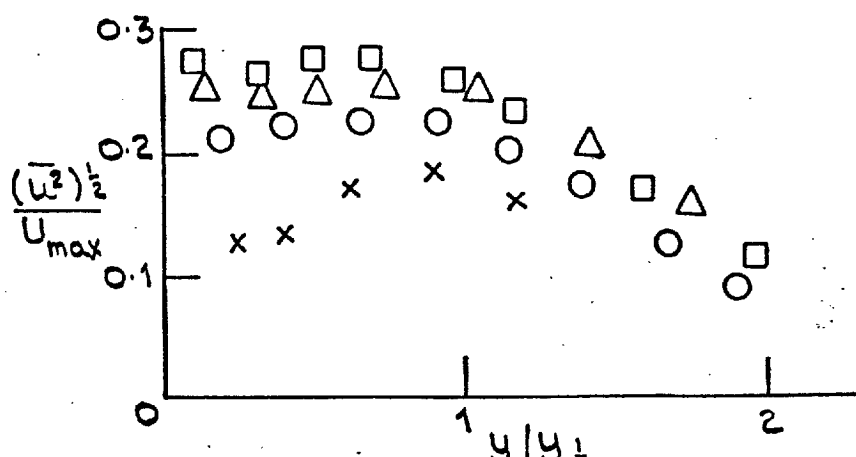
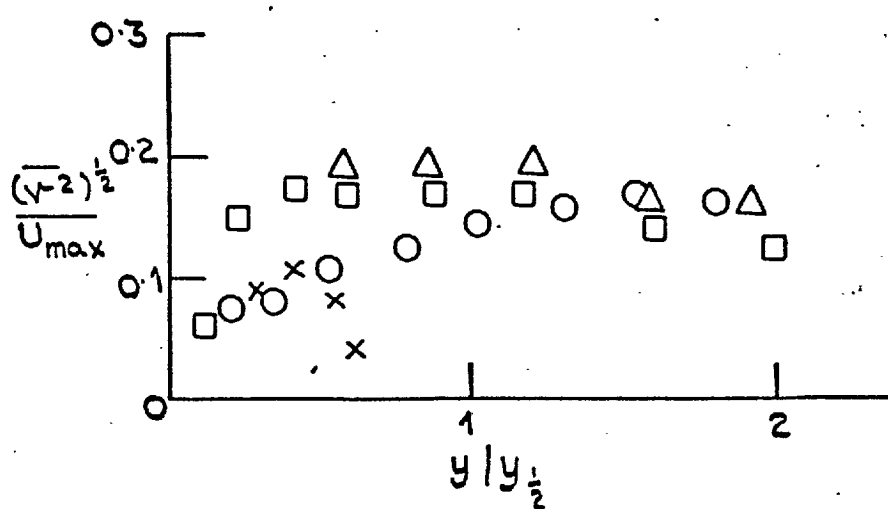
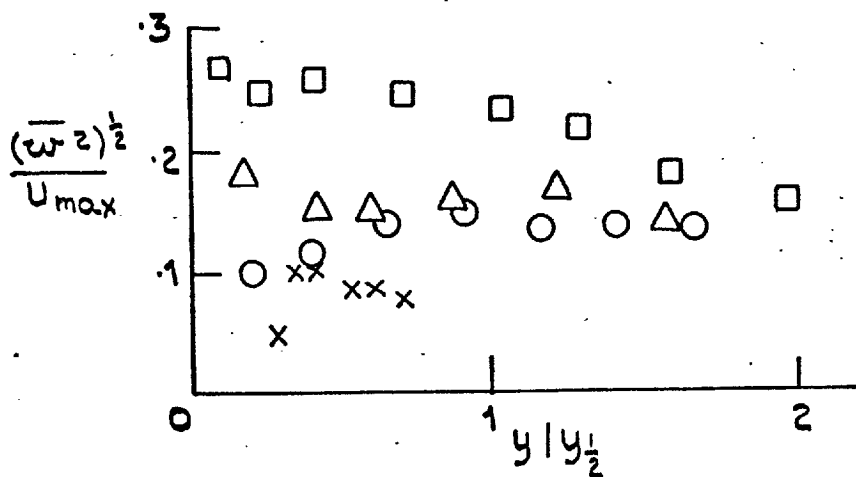
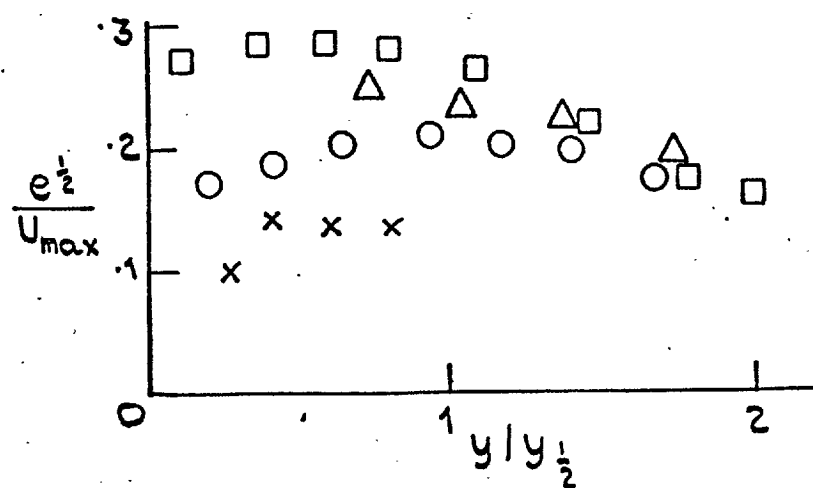


FIG. 7.11: BLOCK DIAGRAM OF THE  
HOT-WIRE CIRCUITRY

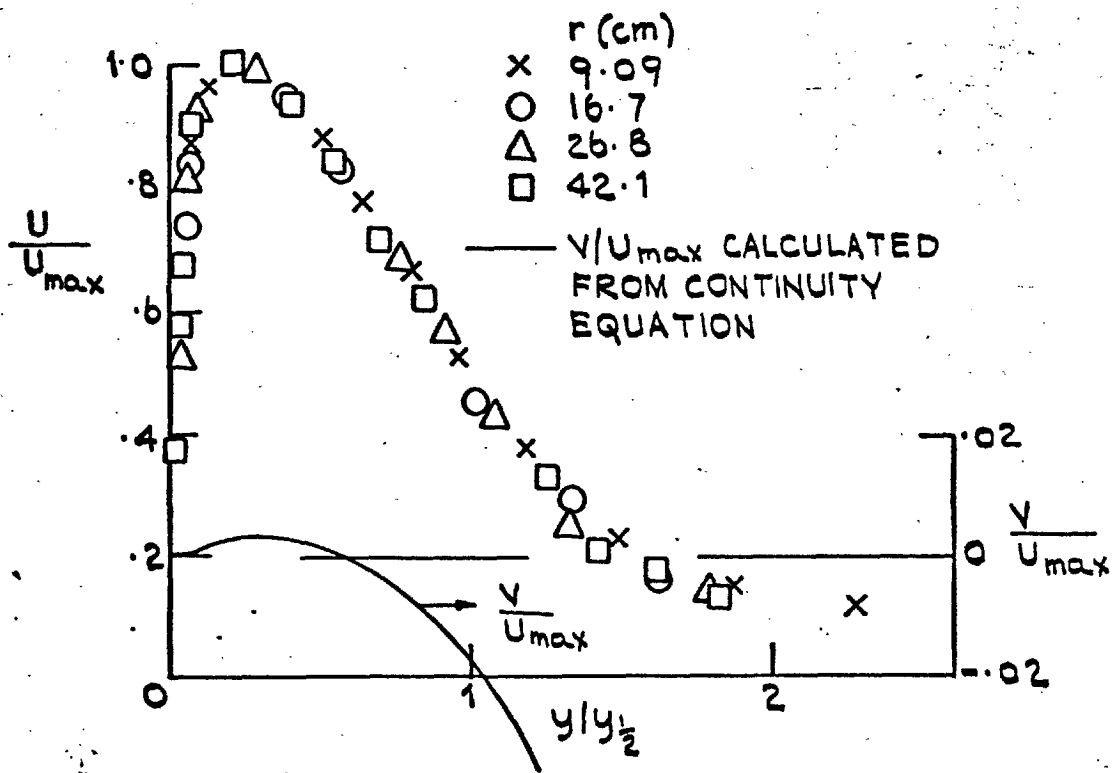
b).  $\bar{u}v$  DISTRIBUTIONSFIG. 7.12 (CONTINUED)

c).  $\bar{u}^2$  DISTRIBUTIONSd).  $\bar{v}^2$  DISTRIBUTIONS

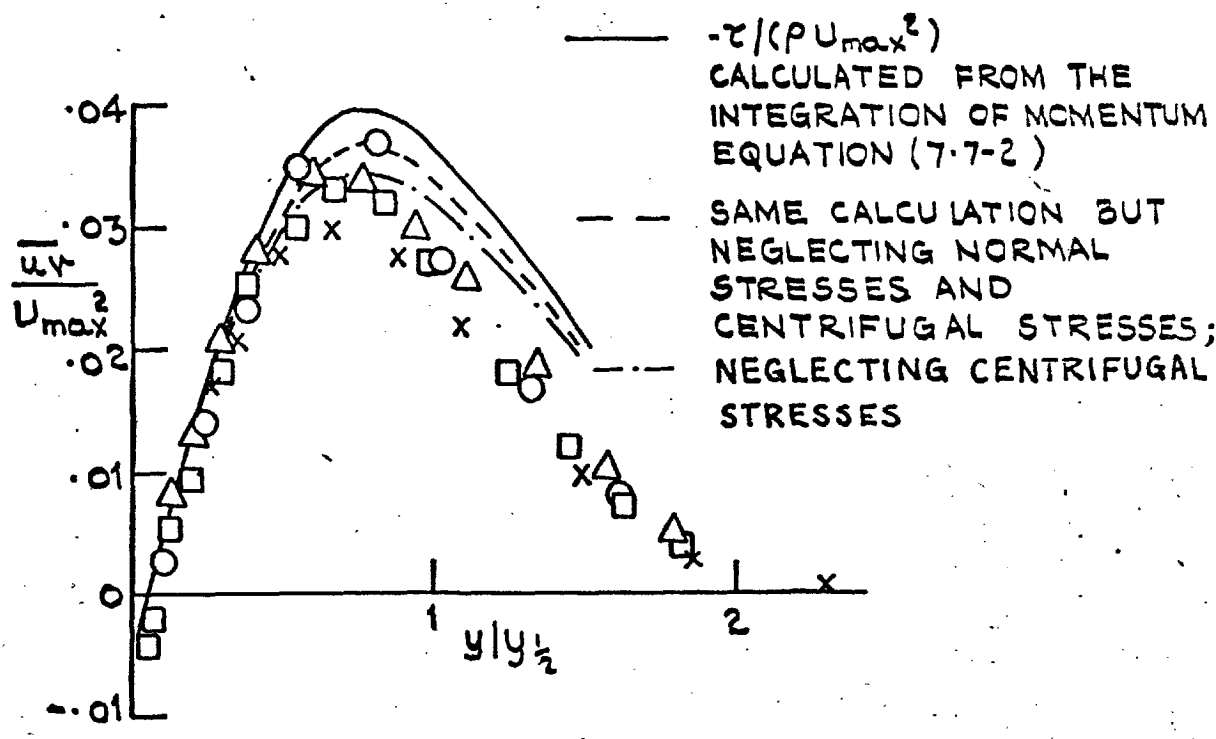
e).  $\bar{w}^2$  DISTRIBUTIONS

f). e DISTRIBUTIONS

FIG. 7.12: MEASURED MEAN-VELOCITY  
AND TURBULENCE PROFILES  
OF CASE (a)



a). U AND V DISTRIBUTIONS.

b).  $\bar{u}\bar{v}$  DISTRIBUTIONFIG. 7.13 (CONTINUED)

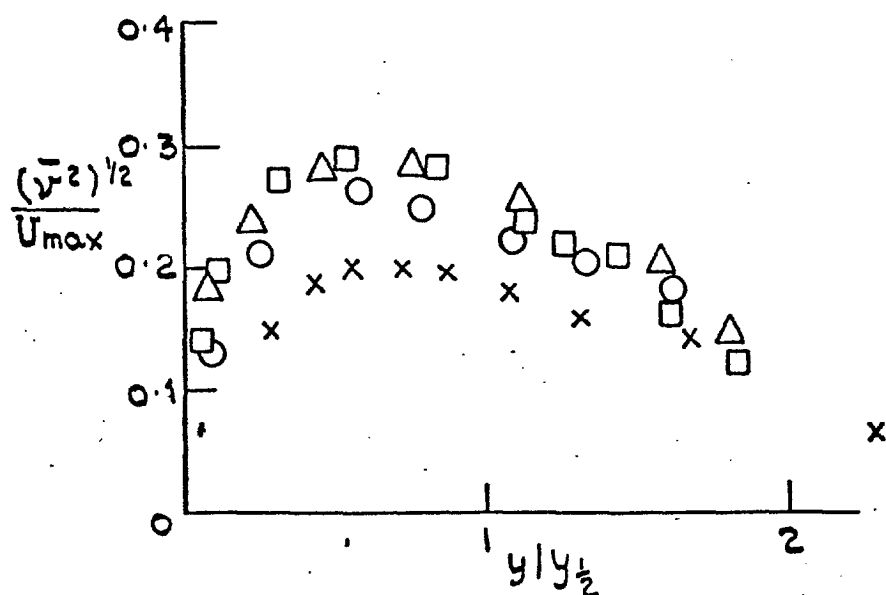
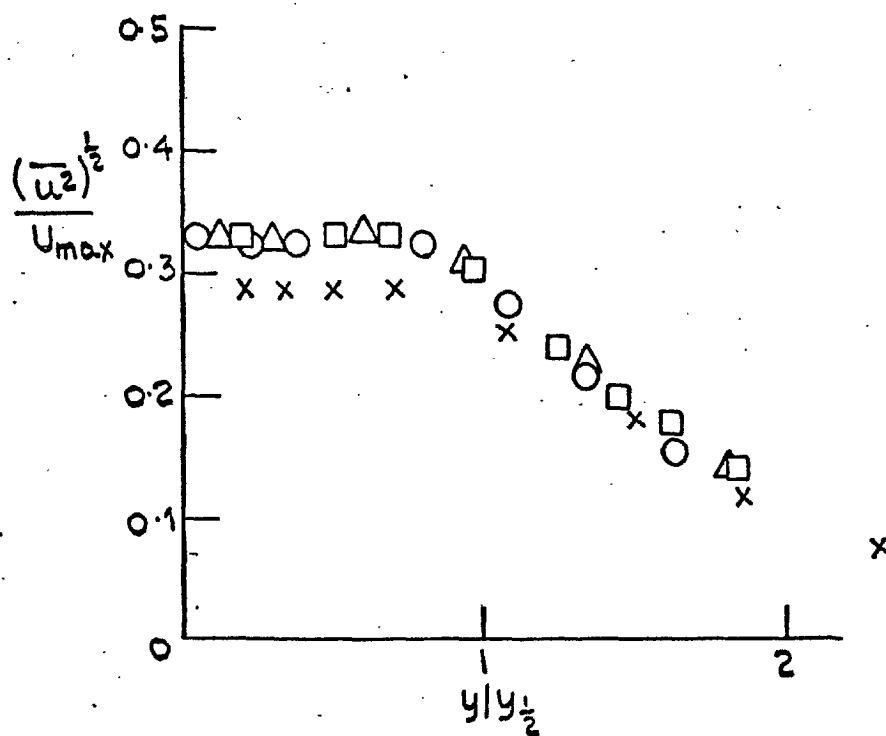
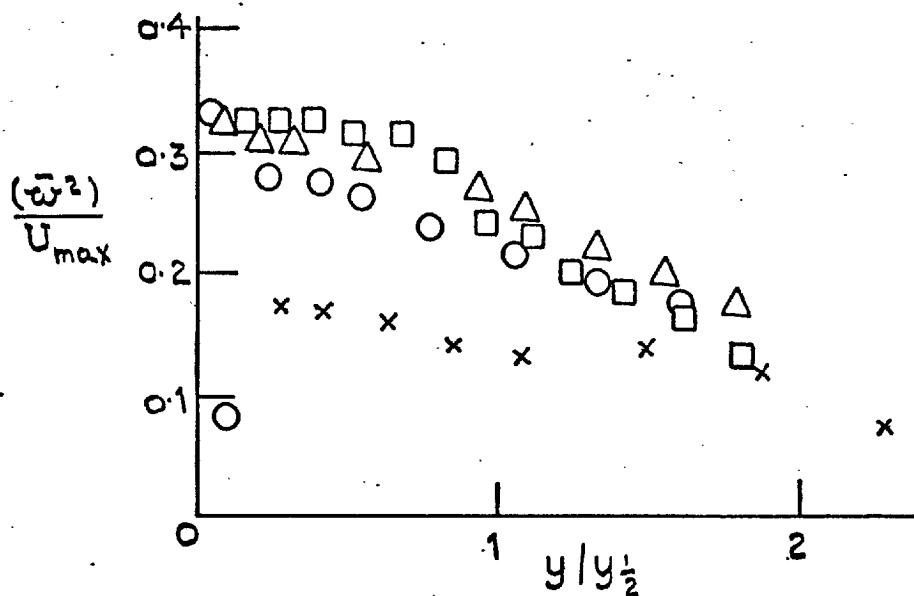
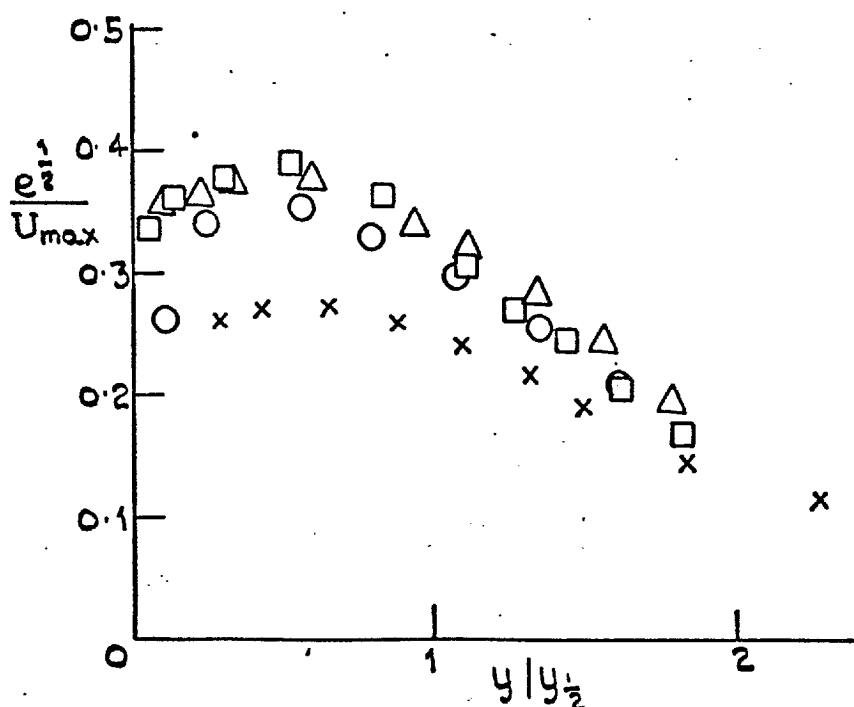


FIG. 7.13 (CONTINUED)

e).  $\bar{w}^2$  DISTRIBUTION

f). e' DISTRIBUTIONS

FIG. 7.13: MEASURED MEAN VELOCITY AND  
TURBULENCE PROFILES OF CASE (b)

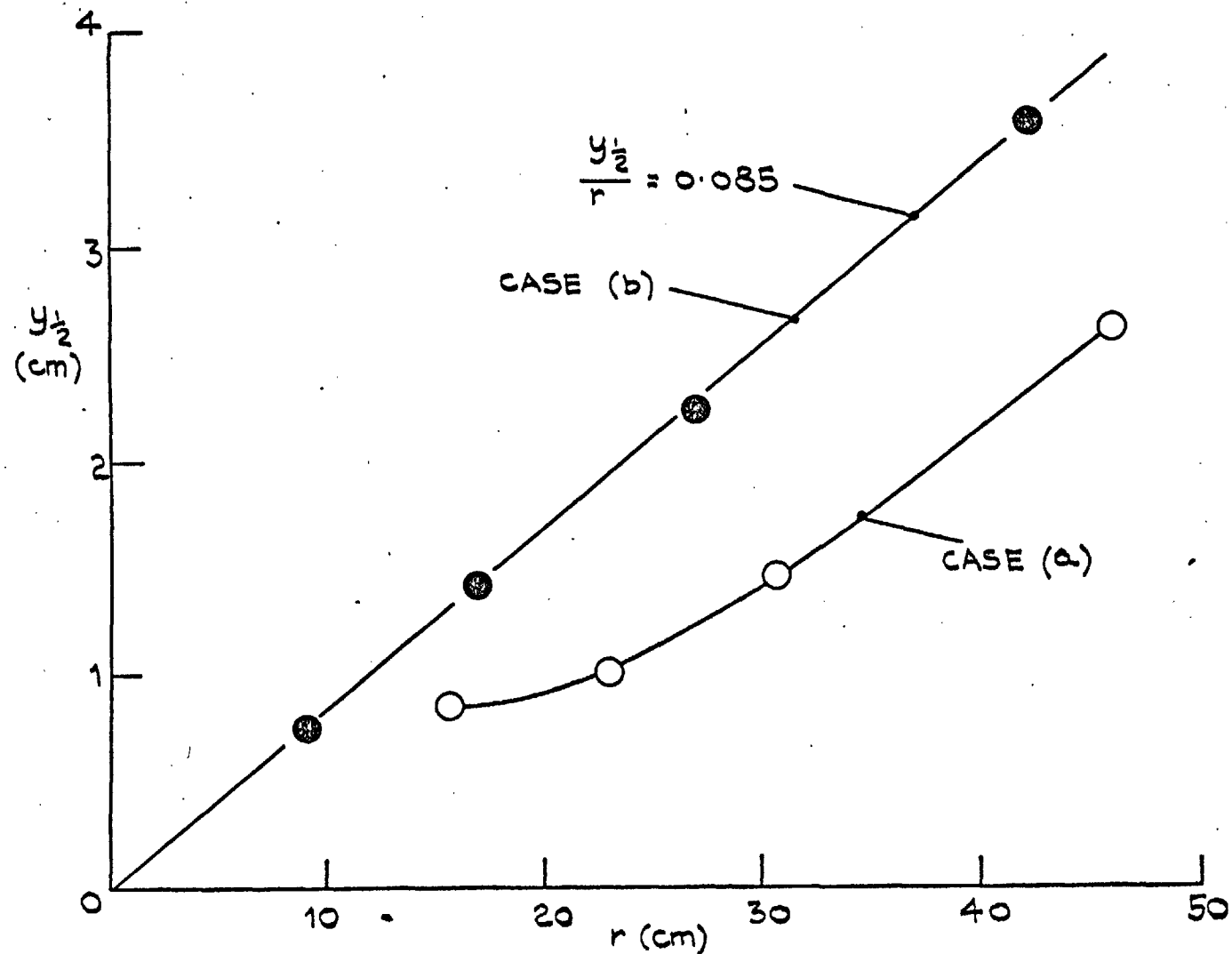


FIG. 7.14: GROWTH OF RADIAL WALL JETS.

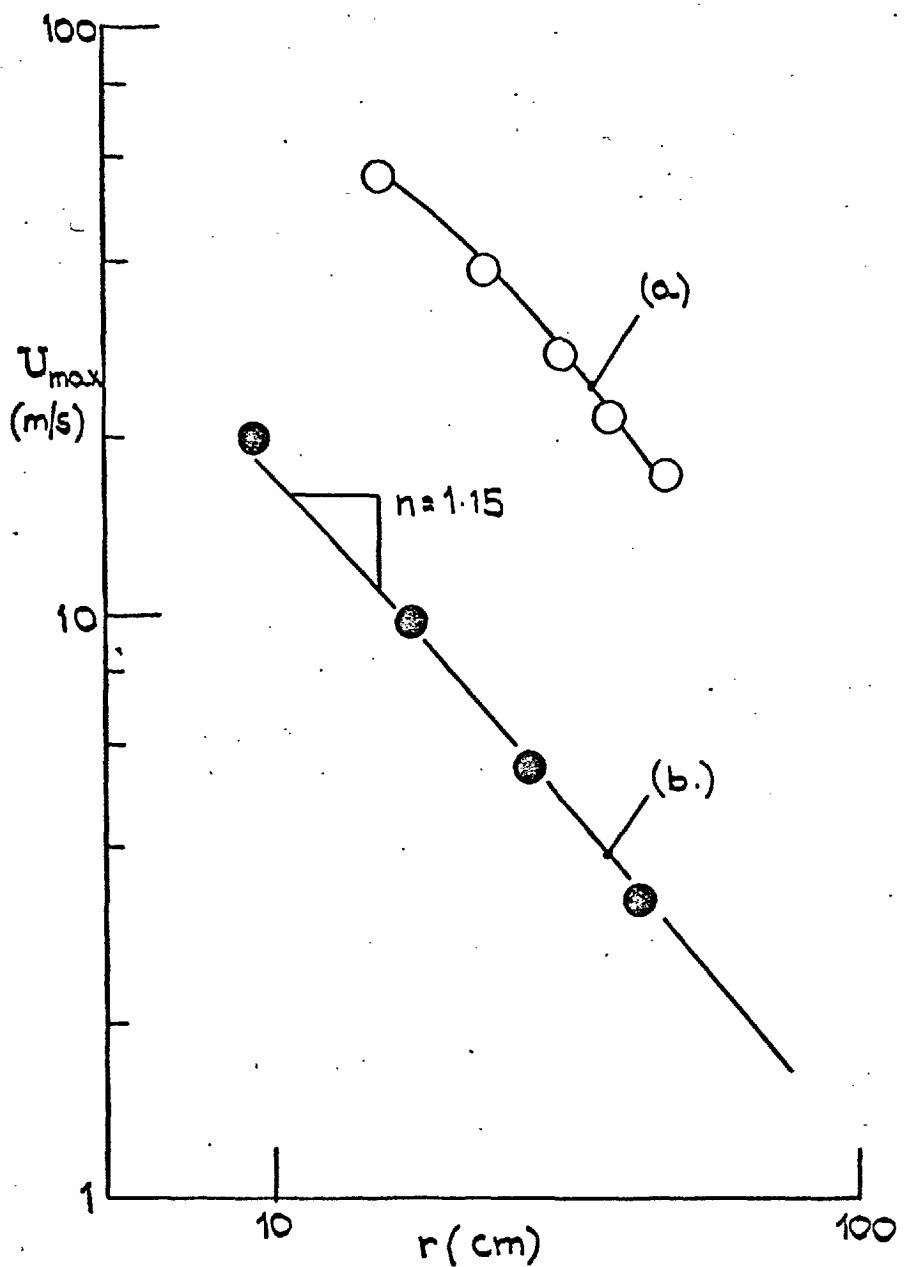


FIG. 7.15 : DECAY VELOCITY MAXIMUM  
FOR CASES (a) AND (b)

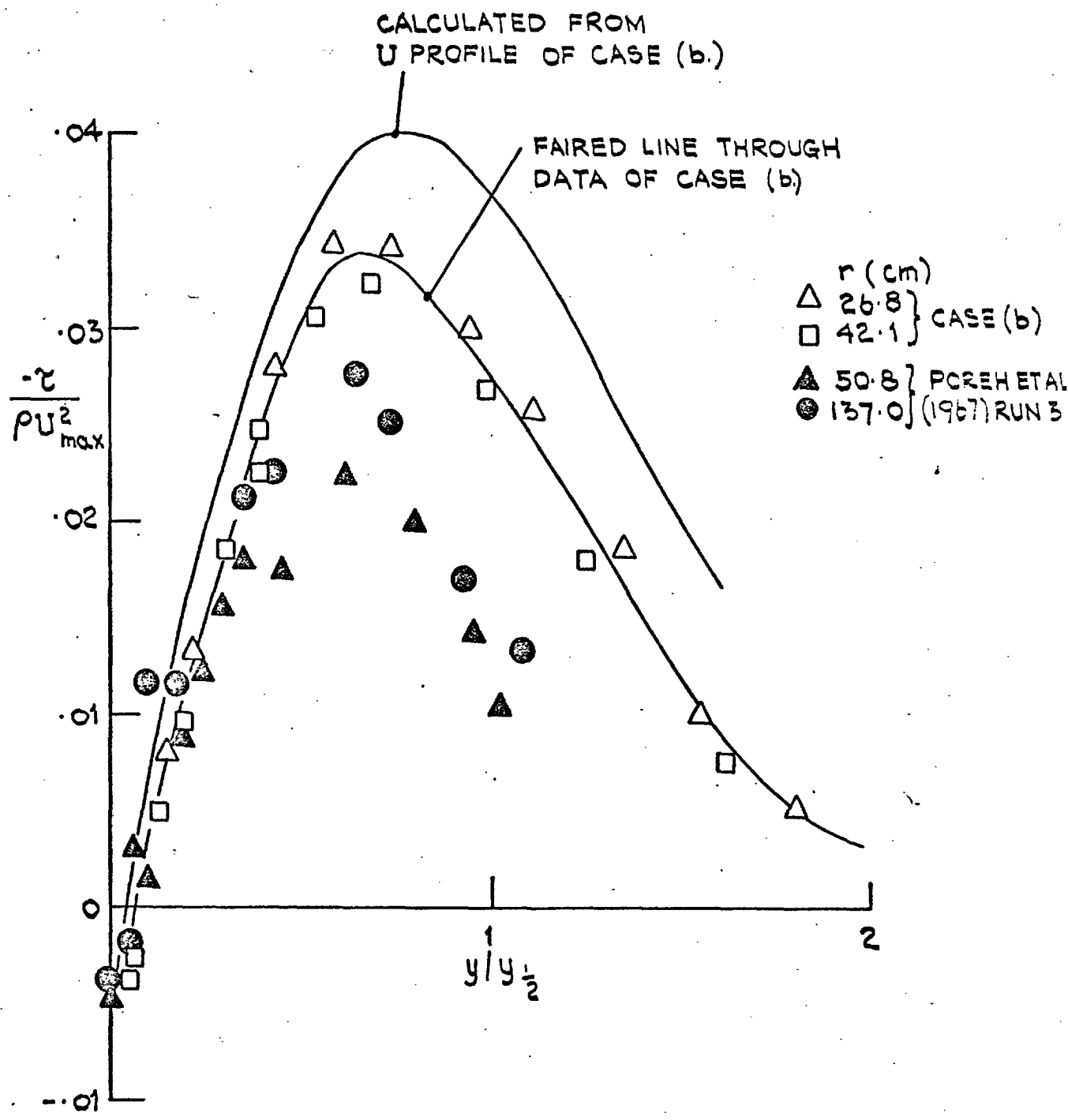


FIG. 7.16: COMPARISON OF THE SHEAR-STRESS PROFILES  
MEASURED IN THE PRESENT INVESTIGATION  
WITH DATA OF POREH ET AL (1967)

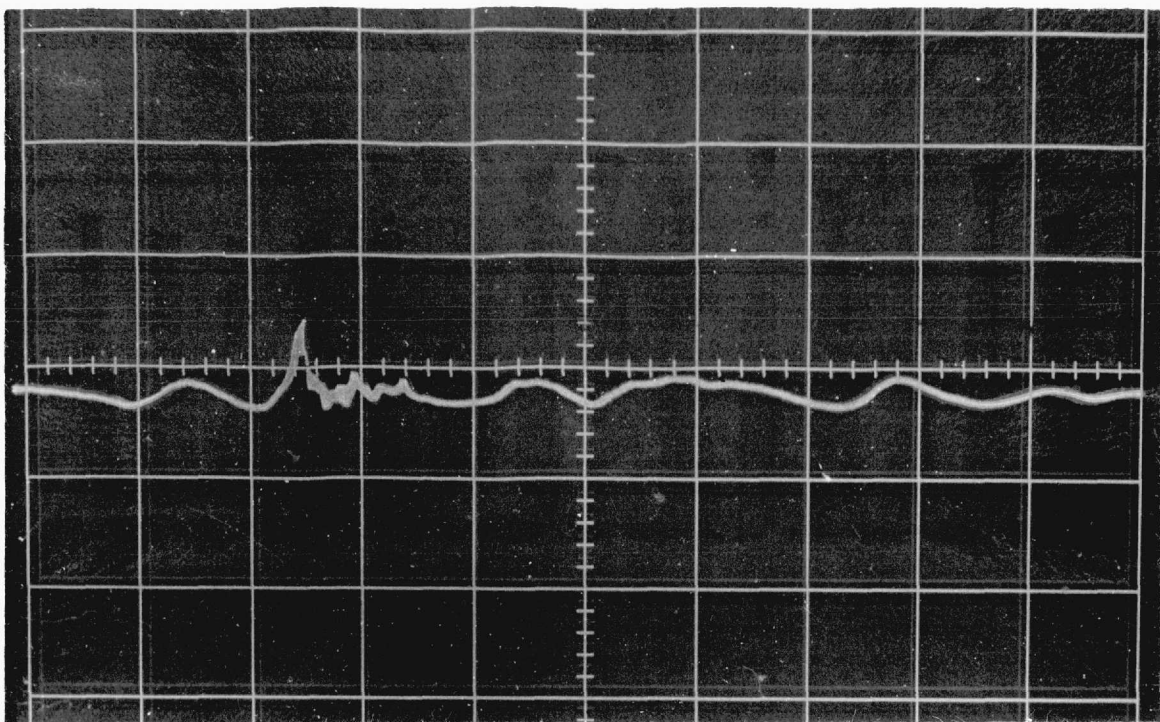
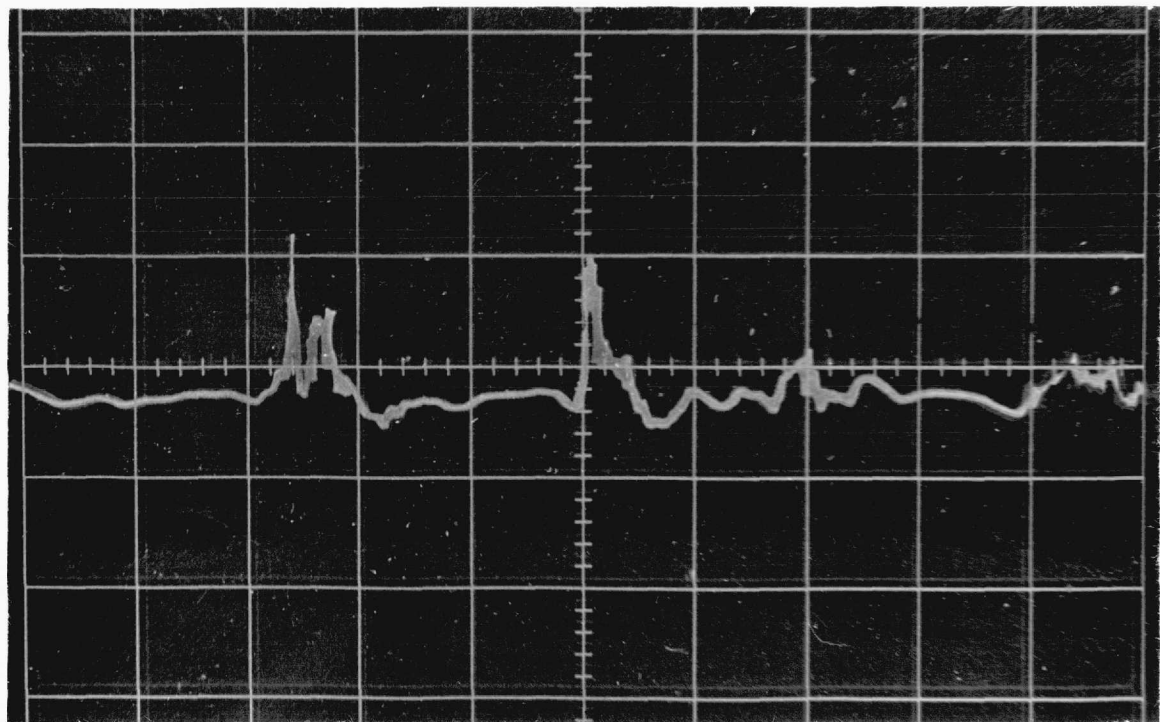
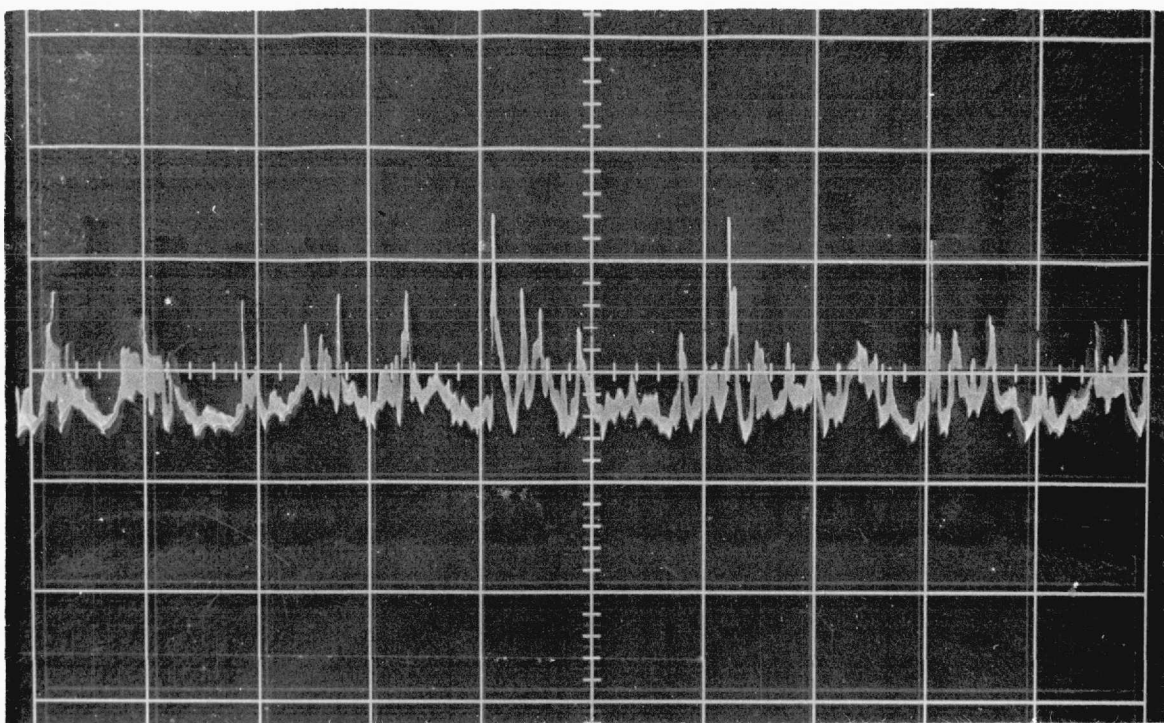
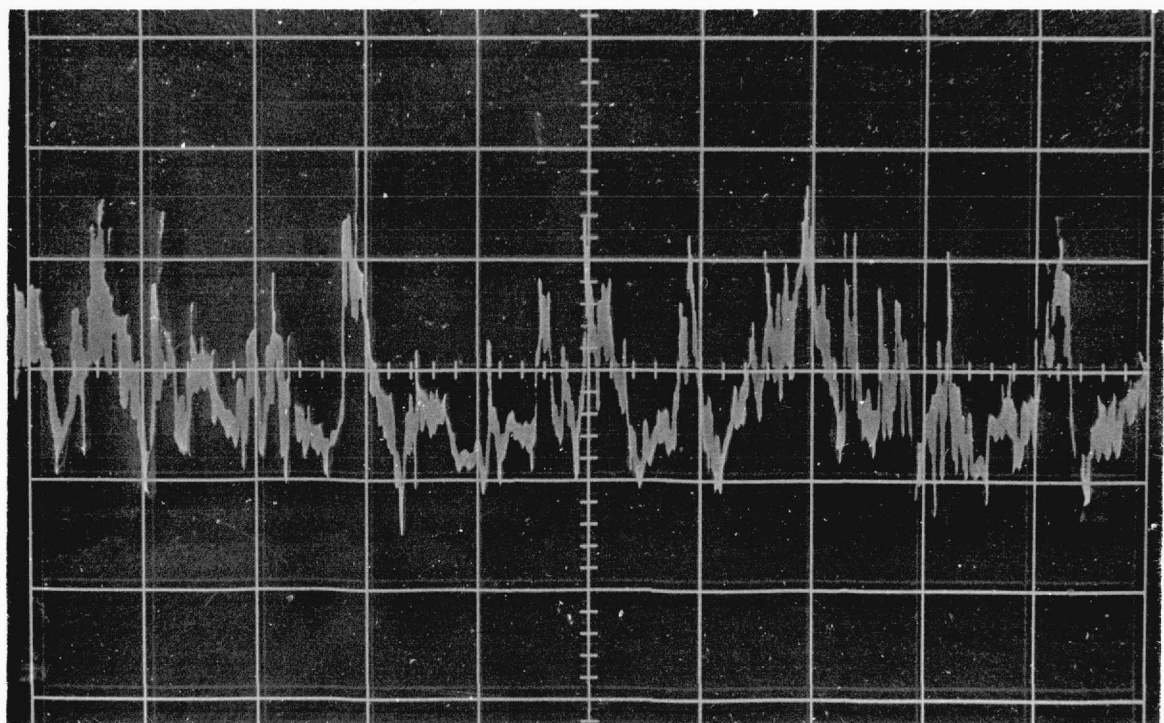
(a)  $\gamma/\Gamma = 0.305$ ;  $y/y_{\frac{1}{2}} = 2.74$ (b)  $\gamma/\Gamma = 0.690$ ;  $y/y_{\frac{1}{2}} = 1.84$ 

Figure 7.17 (contd.)



(c)  $\gamma/\Gamma = 0.528$ ;  $y/y_{\frac{1}{2}} = 0.85$



(d)  $\gamma/\Gamma = 0.510$ ;  $y/y_{\frac{1}{2}} = 0.014$

Figure 7.17 Hot-wire traces over the duration of 1 s. of a radial wall jet (case b); signals from a 55F04 probe at  $r = 42.1$  cm.